Spring 1-1-2012

Elucidating Zinc Distribution In Cancerous Prostate Cells Using Novel FRET Sensors

Jose Guadalupe Miranda
University of Colorado at Boulder, jose.miranda@colorado.edu

ELUCIDATING ZINC DISTRIBUTION IN CANCEROUS PROSTATE CELLS USING NOVEL FRET SENSORS

by

JOSE GUADALUPE MIRANDA

B.S., University of California at Irvine, 2004

A thesis submitted to the

Faculty of the Graduate School of the

University of Colorado in partial fulfillment

of the requirement for the degree of

Doctor of Philosophy

Department of Chemistry and Biochemistry

2012

This thesis entitled:

Elucidating Zinc Distribution In Cancerous Prostate Cells Using Novel FRET Sensors

written by José Guadalupe Miranda

has been approved for the Department of Chemistry and Biochemistry

_____
Associate Professor Amy E. Palmer, Ph.D.

_____
Profressor Natalie G. Ahn, Ph.D.

Date:_____

The final copy of this thesis has been examined by the signatories, and we
Find that both the content and the form meet acceptable presentation standards
Of Scholarly work in the above mentioned discipline.

Miranda, José Guadalupe (Ph.D., Biochemistry)

Elucidating Zinc Distribution In Cancerous Prostate Cells Using Novel FRET Sensors

Thesis directed by Associate Professor Amy E. Palmer, Ph.D.

Zinc (Zn^{2+}) is an important trace element that is found throughout the human body and plays essential roles in proteins to ensure structural integrity and catalytic activity. It is the second most abundant transition metal in the body. Transition metals are required for numerous enzymes, proteins, and cellular processes. It is important for cells to regulate distribution of metals because numerous enzymes and cellular processes depend on transition metals, yet metal imbalance leads to a wide range of diseases. Prostate tissue has the highest Zn^{2+} concentration in the body compared to other tissues but Zn^{2+} is significantly depleted upon onset of malignancy. Numerous studies have revealed that cancerous prostate tissue exhibits dramatically reduced levels of Zn^{2+} and that the levels of Zn^{2+} appear to correlate with progression from benign to invasive and metastatic cancer. The mechanistic correlation between malignancy and Zn^{2+} levels is not well understood and in particular, it is not clear whether Zn^{2+} depletion contributes to or is a consequence of disease progression. Although the majority of Zn^{2+} found in cells in bound by proteins, enzymes, and cellular ligands, pools of free Zn^{2+} have been identified in pancreatic islet cells, brain, and prostate. In this current study we used normal and cancerous prostate cells as a model system to map free Zn^{2+} levels in the nucleus, cytosol, endoplasmic reticulum, and mitochondria to identify the differences in Zn^{2+} at the subcellular level. This was accomplished by using novel Zn^{2+} sensors based on fluorescence resonance energy transfer (FRET) targeted to each

organelle compartment and carrying out live cell imaging experiments. FRET sensors are powerful tools to monitor Zn^{2+} dynamics in cells. This type of probes gives us the ability to monitor Zn^{2+} in multiple cellular compartments or simultaneously track two cellular signals using orthogonal FRET sensors. Such studies allow us to precisely correlate the timing of two interdependent cellular events or to track the movement of ions or molecules from one compartment to another. We discovered that the free Zn^{2+} pool in the nucleus and cytosol is higher in our prostate cancer cell line models compared to normal cell line. In the ER we observed that the free Zn^{2+} level in normal prostate cells is about 4 times higher than all three prostate cancer cell lines models used. Similar results were observed in mitochondria, revealing 3-4 times higher Zn^{2+} in the normal cells compared to all three prostate cancer cell lines. Although all three prostate cancer cell lines used in this study were characterized by over 50% reduction in total cellular Zn^{2+}, surprisingly we discovered this reduction did not translate into across-the-board deficiency in intracellular Zn^{2+} stores, but rather there was substantial redistribution of Zn^{2+} between subcellular locations. In an effort to define how and why Zn^{2+} pools are redistributed in prostate cancer, we measured the changes in expression levels of key Zn^{2+} regulatory proteins such as transporters (hZIP1, hZIP2, hZIP3, ZnT1, ZnT2, ZnT4, and ZnT7). Our results suggest that there is a dysregulation of the Zn^{2+} transporters in cancerous prostate cells and there is some heterogeneity between the prostate carcinoma cell lines. To complement existing tools, we developed a suite of sensors using alternately colored FRET pairs using tSapphire/TagRFP, tSapphire/mKO, Clover/mRuby2, mOrange2/mCherry, and mOrange2/mKATE that were used simultaneously with CFP-YFP sensors. Using these combinations of FRET sensors we

were able to monitor Zn^{2+} uptake simultaneously in two compartments, revealing that nuclear Zn^{2+} rises quickly, whereas the ER, Golgi, and mitochondria all sequester Zn^{2+} more slowly and with a delay of 600-700 sec. These new green-red sensors provided the starting point for developing vesicle-targeted sensors. In summary, this thesis details efforts to develop new fluorescent sensors for defining free Zn^{2+} in cells and applies these sensors to quantify free Zn^{2+} in normal prostate and cancerous cells at the subcellular level. We discovered unprecedented redistribution of Zn^{2+} stores in all three cancer cell lines and discovered this correlates, at least in part, to alteration of Zn^{2+} transporters. This work not only provides the first quantitative maps of Zn^{2+} distribution in cells, it also provides a critical glimpse of how Zn^{2+} is altered with disease progression.

This thesis is dedicated to my supportive and loving family

Rosa, Kassandra, Leonardo, and Christina.

Acknowledgements:

I would like to thank all the people who pushed me and told me I could get a Ph.D., even when I doubted myself. Dr. Lydia Yoshida at the University of California, Irvine who believed in me and gave me advice. My undergraduate advisor, Dr. Ricardo Miledi at the University of California, Irvine who always had the time to sit and have a conversation and guiding me into science. As well as Dr. Ataulfo Matinez-Torres for everything he thought me and all the good times amongst good friends at the Miledi Lab at the University of California, Irvine. Dr. Carlos Gutierrez at California State University, Los Angeles who after I finished undergraduate gave me a change when nobody else believed in me. I will never forget what he told me the first day I met him, "Don't be embarrassed of your past academic achievements this is the present and look to the future." Thank you all for everything.

One million thanks to my advisor Dr. Amy Palmer for letting me do research in her laboratory and for taking the time to teach me Chemistry, Physical Chemistry, and Biochemistry without her guidance throughout the years I would not have accomplished this. Dr. Palmer is a true inspiration for saying the right thing when nothing is working. I hope that I can grow as a scientist to be a fourth of what she is.

A special thank to Dr. Deborah Wuttke who let me sit in her Honors General Chemistry class and answering my questions as well as helping me at a time when I needed to know the subject. I would also like to thank Dr. Natalie Ahn, for all the help she has given me since I rotated in her lab. Especially when I was feeling I couldn't do this anymore and gave me advice by taking the time to analyze what was wrong, Thank you.

To Dr. Joseph Falke, whom I met at California State University, Los Angeles during a research seminar. Thank you for dinner and giving me a chance to come to this department.

To my family Rosa who has put-up with me my three beautiful and wonderful children Kassandra, Leonardo, and Christina, I love you guys very much. My children were my inspiration for everything. To my parents, Miguel and Josefina, who have supported me in

many ways as well as my brothers Miguel Jr., Jaime, and Alejandro. Thank you all for believing in me.

Finally, a special thanks to Dr. Olester and Sharmae Benson for the Adopt-A-Student award that I got throughout my graduate career.

Table of Contents **Page Number**

Table of Contents.....ix

List of Table.....xiii

List of Illustrations.....xiv

Equations.....xvi

Chapter I: Introduction.....1

1.1 Zinc Homeostasis.....2

1.2 Zinc and Prostate Cancer.....3

1.3 Prostate Cancer Cell Line Models.....7

1.4 Genetically Encoded FRET Sensors to Monitor Zinc.....7

1.5 Significance.....16

1.6 Conclusion.....18

1.7 References.....19

Chapter II: Redistribution of Free Zinc in Prostate Cancer.....32

2.1 Abstract.....31

2.2 Introduction.....33

2.3 Experimental Methods.....35

Cell Culture.....35

Inductively Coupled Plasma Mass Spectrometry.....35

X-Ray Fluorescence Microscopy.....36

Fractionation of Nucleus and Cytosol for ICP-MS.....37

FRET-based Zn^{2+} Sensors.....39

Cell Culture and Microscopy.....39

In situ FRET Sensor Calibration.....41

Table of Contents **Page Number**

2.4 Results....42

2.4.1 Identification of Total Cellular Zinc in Normal vs. Cancerous Prostate cells....42

2.4.2 Mapping of free Zinc in living cells....46

2.5 Discussion....52

2.6 References....55

Chapter III: Profiling Expression Levels and Localization of Zinc Transporters in Prostate Cancer....62

3.1 Abstract....63

3.2 Introduction....63

3.3 Experimental Methods....67

Chemicals and Reagents....68

Microscopy....68

Cell Culture....69

Zinc Chloride Incubation....69

Immunohistochemistry....69

Total RNA Isolation and Quantitative Reverse Transcription Polymerase Chain Reaction (qRT-PCR)....70

Melt Curve Analysis and PCR Percent Efficiency....70

Protein Isolation and Western Blotting....74

3.4 Results....77

3.4.1 Decreased Cellular Zinc in Prostate Cancer Cell Lines....77

3.4.2 Expression Levels and Localization of hZIP1 Zinc Transporter....77

3.4.3 Expression Levels and Localization of hZIP2 Zinc Transporter.....78

3.4.4 Expression Levels and Localization of hZIP3 Zinc Transporter.....82

3.4.5 Expression Levels and Localization of ZnT1 Zinc Transporter.....86

3.4.6 mRNA Expression Levels of ZnT2 Zinc Transporter.....87

3.4.7 Expression Levels and Localization of ZnT4 Zinc Transporter.....90

3.4.8 Expression Levels and Localization of ZnT7 Zinc Transporter.....91

3.5 Discussion.....96

3.6 References.....100

Chapter IV: New Alternately Colored FRET Sensors for Simultaneous Monitoring of Zinc in Multiple Cellular Location.....108

4.1 Abstract.....109

4.2 Introduction.....109

4.3 Experimental Methods.....111

FRET Sensor Cloning.....111

Cell Culture and Microscopy.....113

Live Cell Imaging Experiments.....114

Simultaneous Monitoring of Zinc Uptake Into Multiple Compartments.....115

4.4 Results.....115

4.4.1 Measurement of Spectral Bleedthrough.....115

4.4.2 Generation of Nuclear and Cytosol Localized Constructs.....117

4.4.3 Characterization of Sensors in HeLa Cells.....123

4.4.4 Zinc Uptake Into the Cytosol and Nucleus.....130

4.4.5 Simultaneous Monitoring of Nuclear and Organelle Zinc Uptake.....134

Table of Contents **Page Number**

4.5 Discussion....136

4.6 Acknowledgements....138

4.7 References....138

Chapter V: Vesicular Targeted FRET Sensor To Monitor Zinc....143

5.1 Abstract....144

5.2 Introduction....144

5.3 Experimental Methods....146

VAMP2 and FRET Sensor Cloning....146

Cell Culture and Microscopy....146

Live Cell Imaging Experiments....149

5.4 Results....150

5.4.1 VAMP2 and FluoZin3-AM Colocalization....150

5.4.2 VAMP2-ZapCmR1.1 *in vivo* Calibration....151

5.5 Discussion....154

5.6 References....155

Chapter VI: Conclusions and Future Directions....161

6.1 Zinc Dysregulation....162

6.2 Zinc Transporter Expression....163

6.3 Conclusion....164

6.4 References....165

Tables **Page Number**

1.1 Cation Diffusion Facilitator (ZnT) physiological expression.....5

1.2 *Z*rt-,*I*rt-like *P*rotein (ZIP) physiological expression.....5

1.3 mRNA and protein expression of specific zinc transporters

in prostate cancer cell lines and tissue samples.....8-9

1.4 List of prostate cancer cell lines.....10

1.5 Small molecule fluorescent zinc sensors.....16

2.1 Amino acid sequence of Zap zinc binding domain

(ZDB) in the ZapCY1 and ZapCY2 sensors.....41

3.1 Quantitative polymerase chain reaction primers.....71

3.2 Reference gene primer matrix.....72

4.1 Amino acid sequence of Zap zinc binding domains (ZDB).....113

4.2 Filter sets and dichroic mirrors used for cellular imaging.....115

4.3 Fluorescent protein excitation and emission.....117

4.4 Percent bleedthrough of fluorescent proteins.....118

4.5 Percent bleedthrough of sensor into FRET channels.....122

4.6 Comparison of sensors with different fluorescent proteins.....129

Figures **Page Number**

1.1 Schematic representation of cellular zinc.....4

1.2 *In vitro* fluorescence spectra of a ratiometric FRET sensor.....12

1.3 *In vitro* Zinc titration of FRET sensors.....13

1.4 Percent saturation of a FRET sensor and FluoZin3-AM as a function of the sensor concentration.....14

2.1 X-Ray Fluorescence Microscopy (XRFM) for measuring total Zinc.....38

2.2 Schematic diagram of a FRET Sensor.....40

2.3 ICP-MS of normal and cancerous prostate cells.....44

2.4 XRFM of RWPE1 and LNCaP cells.....45

2.5 ICP-MS of nucleus fractions.....47

2.6 Representative images of FRET sensor localization in VCaP cells.....48

2.7 Representative *in situ* calibration of localized sensors in VCaP.....50

2.8 Free zinc concentrations in nucleus, cytosol, ER, and Mitochondria in normal versus cancerous cell lines.....51

3.1 Schematic of a cell showing zinc transporters examined in this chapter.....65

3.2 Melt curve analysis confirms gene specificity.....73

3.3 Standard curve of qPCR to calculate percent efficiency of reaction.....75

3.4 qRT-PCR, western blot, and immunofluorescence of hZIP1.....79

3.5 qRT-PCR, western blot, and immunofluorescence of hZIP2.....80-81

3.6 qRT-PCR and western blot of hZIP3a and hZIP3b.....84

3.7 Immunofluorescence of hZIP3.....85

3.8 qRT-PCR, western blot, and immunofluorescence of ZnT1.....88-89

3.9 qRT-PCR of ZnT2.....90

3.10 qRT-PCR, western blot, and immunofluorescence of ZnT4.....93-94

3.11 qRT-PCR and western blot of ZnT7.....95

Figures **Page Number**

4.1 Nuclear localization and nuclear exclusion signal sequence constructs.....112

4.2 Bleed-through of fluorescent proteins.....119

4.3 Bleed-through of fluorescent proteins.....120

4.4 Cross-talk of FRET sensors.....121

4.5 FRET sensor calibration in the nucleus.....125-126

4.6 FRET sensor calibration in the cytosol.....127-128

4.7 Zinc uptake into cytosol.....131

4.8 Zinc uptake into nucleus.....131

4.9 Simultaneous monitoring of cytosolic and nuclear zinc uptake.....133

4.10 Simultaneous monitoring of zinc uptake into the nucleus and either the ER, Golgi apparatus, or mitochondria.....135

5.1 Schematic diagram of FRET sensor.....147

5.2 Schematic diagram of Vesicle-Associated Membrane Protein-2 (VAMP2) with ZapCmR1.1 FRET sensor.....148

5.3 Fluorescence images of FluoZin3 and VAMP2-mCherry.....152

5.4 Calibration of VAMP2-ZapCmR1.1 in HeLa cells.....153

Equation **Page Number**

2.1 Equation for converting R into $[Zn^{2+}]$.....42

Chapter I

Introduction

1.1 Zinc Homeostasis

In biological organisms, Zinc (Zn^{2+}) is the second most abundant transition metal and is critical to proteins, transcription factors, immune function, and neurotransmission (*1-3*). Zn^{2+} deficiency claims many lives per year worldwide (*5*) underscoring the importance of understanding how organisms take up and distribute Zn^{2+} within the cell. Zn^{2+} is an essential cofactor for numerous proteins and enzymes such as acetylcholinesterase (*6*), alcohol dehydrogenase, DNA and RNA polymerases, Nerve Growth Factor (NGF) (*7*), and finally transcription factors such as Zif268 (*8*) and MTF-1 (*9*). About half of all transcription factors in the human genome contain Zn^{2+} finger motifs and hence require this metal to function (*10*). This shows the importance of Zn^{2+} at the genome wide level and how it is essential for gene production. For example, nuclear receptors, such as retinoic acid, vitamin D, thyroid hormone, glucocorticoids, and estrogen, are all Zn^{2+} finger proteins (*11, 12*). In neurogenesis, cellular proliferation, and brain development the receptors mentioned are important gene regulators (*12*).

Mammalian cells contain high levels of Zn^{2+} (~ 0.1 - 0.5 mM) (*13, 14*), but the majority is bound to enzymes, proteins, and other low molecular weight species. Excess Zn^{2+} is buffered by cellular ligands because too much Zn^{2+} within the cell is toxic (*15*). The primary protein responsible for Zn^{2+} buffering is metallothionein (MT), which is itself regulated by Zn^{2+} (*16, 17*). The free (i.e. unbound) Zn^{2+} concentration has been estimated to be in the pM to nM range (*18, 19*) , but there is general agreement based on more recent estimates that free Zn^{2+} in the cytosol ranges from ~ 100pM – 400 pM in many different cell types (*18, 19*). There is far less information about the level of free Zn^{2+} in organelles. Recent studies from our group have used newly developed probes to measure free Zn^{2+} in organelles in HeLa cells, resulting in estimates of free Zn^{2+} pools in the endoplasmic reticulum (0.9 pM), Golgi apparatus (0.6 pM), and mitochondria (0.14 pM) (*18, 20*). Although resting levels of free Zn^{2+} in the cytosol are low, recent studies demonstrate that Zn^{2+} can be released from MT by a variety of cellular signals

(*21, 22*), indicating that Zn^{2+} levels may be highly variable. For example, the Zn^{2+} finger transcription factor Egr-1 signals MT to release Zn^{2+} (*23*) and metal transcription factor-1 (MTF-1) is activated by the release of Zn^{2+} from MT (*24*). Because Zn^{2+} can be mobilized, it strongly suggests that the levels of Zn^{2+} are dynamic and this mobilized Zn^{2+} may be transported between different organelles particularly given the large number of Zn^{2+} transporters on organelles. **Figure 1.1** is schematic summary of how much Zn^{2+} is within the cell and how it is distributed.

Zn^{2+} is regulated a number of ways within cells via transporters that are localized both in the membrane and organelles. These transporters are known to move Zn^{2+} from outside of the cell into the cytoplasm as well as store it in different compartments. The two types of Zn^{2+} transporters are the *Z*rt-, *I*rt-like *P*roteins (ZIP) and *C*ation *D*iffusion *F*acilitators (CDP) also referred to as ZnTs (*25*). The ZIP family Zn^{2+} transporters move Zn^{2+} from the extracellular space into the cytosol and from inside organelles to the cytosol (*26*). On the other hand, the ZnT family transporters move Zn^{2+} from the cytosol to the extracellular space as well as from the cytosol into organelles (*27*). To date there have been **10 ZnTs** and **14 ZIP** transporters identified. **Table 1.1 and Table 1.2** represent a complete list of these Zn^{2+} importers and exporters as well as their tissue specificity. In addition to these transporters, two other proteins are known to be fundamental regulators of Zn^{2+} homeostasis, metallothionein (the cellular buffer mentioned above) and the transcription factor MTF-1, which regulates both metallothionein and ZnT1 levels in response to Zn^{2+} (*9, 17*).

1.2 Zinc and Prostate cancer

Among all the tissues in the body, the prostate has the highest levels of Zn^{2+} per gram of tissue (*28, 29*). When normal prostate cells become malignant they lose over 50% of total

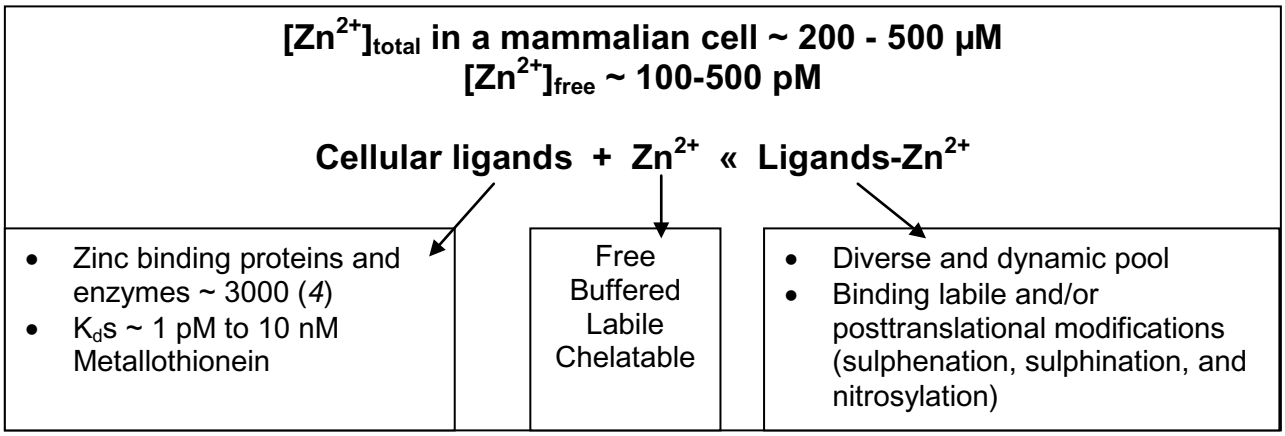

Figure 1.1. Schematic representation of cellular Zn^{2+}.

Table 1.1 Cation Diffusion Facilitator (ZnT) Physiological Expression

Zn^{2+} Transporter	Tissue (Localization)	Ref
ZnT1	Ubiquitous (Plasma membrane, vesicles)	(*15*)
ZnT2	Small Intestine, kidney, mammary glands (vesicles, secretory vesicles)	(*30*)
ZnT3	Neurons (vesicles)	(*31*)
ZnT4	Small Intestine, vesicles (vesicles, endosomes)	(*32*)
ZnT5	Small Intestine, secretory vesicles (secretory granules)	(*33*)
ZnT6	Small Intestine (TGN)	(*33*)
ZnT7	Lung, Small Intestine (Golgi apparatus, vesicles)	(*34*)
ZnT8	Pancreas (secretory vesicles)	(*25*)
ZnT9	Lung	(*35*)
ZnT10	Homologous to ZnT1 (no known tissue of localization)	(*36*)

Table 1.2 *Z*rt-, *I*rt-like *P*rotein (ZIP) Physiological Expression

Zn^{2+} Transporter	Tissue (Localization)	Ref
hZIP1	Ubiquitous (plasma membrane)	(*37*)
hZIP2	Liver, ovary	(*38*)
hZIP3	Blood Cells	(*31*)
hZIP4	Small Intestine, Colon (apical, plasma membrane)	(*39*)
hZIP5	Liver, kidney, pancreas	(*39*)
hZIP6	Lung, breast (plasma membrane)	(*40*)
hZIP7	Ubiquitous (Golgi apparatus)	(*40, 41*)
hZIP8	Kidney, liver, testis, brain, small intestine	(*42*)
hZIP9	No known function	Unknown
hZIP10	Liver, Brain, Erythroid Progenitor Cells (plasma membrane)	(*43*)
hZIP11	Member of gufA subfamily of ZIP transporters	(*25*)
hZIP12	Brain	(*25*)
hZIP13	Golgi apparatus	(*44*)
hZIP14	Liver, kidney, testis	(*45*)

cellular Zn^{2+} (*46, 47*). The depletion of Zn^{2+} in prostate cancer cells has been shown to be an important factor in the development and progression of metastasis of prostate cancer (*46*). The primary region of the prostate that undergoes metastasis is the peripheral zone and cancers derived from this zone are known to be more invasive than transition zone cancers (*48*). The peripheral zone is also the region that contains the highest levels of Zn^{2+} (*49*). The majority of the studies done to date have shown that there is marked depletion of Zn^{2+} in the prostate upon onset of malignancy, observed in cell lines, tissue samples, and mouse studies. In cells the most common cell lines used have been LNCaP, DU-145, and PC-3 prostate cancer cell lines and each study has shown that prostate cancer cell lines are depleted of Zn^{2+} (*46, 50-53*). In tissue samples from human patients with benign prostate hyperplasia (BPH) and prostate cancer, the levels of Zn^{2+} are also depleted (*54-58*). Tissue studies to determine Zn^{2+} content were elucidated by atomic absorption spectroscopy, electrothermal atomizeratomic absorption spectrometry (ETA-AAS), or Inductively coupled plasma mass spectrometry (ICP-MS). Moreover, studies have demonstrated that mice with prostate cancer lose a large percentage of total Zn^{2+} as well (*59-62*). In mice, similar to human cells or tissue samples, the low Zn^{2+} levels have been correlated with the downregulation of Zn^{2+} transporters such as hZIP1 (*59*). Additionally, in a transgenic adenocarcinoma of the prostate mouse models a ZnT7 null-mutation leads to low levels of Zn^{2+} and is associated with aggressive development of prostate cancer (*62*). These studies demonstrate that Zn^{2+} is markedly decreased whether the scientific group chooses to study cells, tissue, or mice. To date it is still not clear why cancer cells have lower Zn^{2+} content than normal cells, nor is it established from what areas of the cell Zn^{2+} is missing. Therefore, it is important to define why and from what regions of the cell Zn^{2+} is reduced as a first step in elucidating the consequence of depletion.

There is some evidence for changes in expression levels of Zn^{2+} transporters in cell lines and tumor samples, but many reports are incomplete. For example, numerous studies examine mRNA but not protein levels, or focus one specific transporter instead of a suite of transporters.

Additionally, there are inconsistencies in the literature, i.e. the reports directly disagree with one another (*32, 47, 52, 53*). The expression of Zn^{2+} transporters studies in prostate samples that have been carried out to date is presented in **Table 1.3**.

1.3 Prostate Cancer Cell Line Models

The focus of this thesis is to characterize the Zn^{2+} distribution in cancerous and noncancerous prostate cell lines. Prostate cancer is a complex and heterogeneous disease characterized by a wide diversity of molecular markers. **Table 1.4** summarizes a number of prostate cancer cell lines as well as tissue origin. For our current studies we chose two newly established prostate cancer cell lines; Dura matter Cancer of the Prostate (DuCaP) and Vertebral column Cancer of the Prostate (VCaP) cells that were immortalized by Pienta and colleagues (*63, 64*). DuCaP and VCaP prostate cancer cell lines were chosen because they exhibit molecular diversity not currently represented in the commonly used cell lines (*65, 66*). In addition to these features, these prostate cancer cell lines were karyotyped to contain many abnormalities characteristic of metastatic prostate cancer (*65, 66*). In addition, we used Lymph Node Cancer of the Prostate (LNCaP) cells (*67*), a well-established cell line. LNCaP is characterized by androgen responsiveness, expression of a mutated form of androgen receptor (AR) and wild type p53. Finally, to compare our results we used RWPE1, a standard noncancerous prostate cell line (*68*). From the large repertoire of prostate cancer cell lines we chose the above cell lines because of their key characteristics. Other cell line models such as the widely used DU-145 and PC-3 cells do not express the androgen receptor, produce PSA, or are sensitive to hormones (*69, 70*).

1.4 Genetically Encoded FRET Sensors to Monitor Zinc

Genetically encoded sensors are broadly defined as sensors that are encoded by a sequence of DNA that is genetically incorporated into cells and subsequently translated into functional sensor protein in live organisms. Our laboratory has created a family of genetically

Table 1.3. mRNA and Protein Expression of Specific Zn^{2+} transporters in prostate cancer cell lines and tissue samples

Transporter	Detection Method	Origin	Result	Reference
hZIP1	RT-PCR	LNCaP & PC3 Cells (Human)	• Upregulated with prolactin • Down-regulated when exposed to Zn^{2+}	(*71*)
hZIP1 & hZIP2	RT-PCR & Western	PC3 and LNCaP	• Transfected pCMV & pCMV-hZIP1; down-regulation of hZIP1 in pCMV only (empty vector) transfected cells at the mRNA and protein level; over-expressing cells with pCMV-hZIP1 show more Zn^{2+} uptake (PC3 only) • RT-PCR show a down-regulation of mRNA in PC-3 compared to LNCaP • Sense and anti-sense oligonucleotides were used to partially knock-down hZIP1 and anti-sense decrease the expression of hZIP1 and Zn^{2+} uptake as measured by ^{65}Zn; (RT-PCR & Western) • hZIP2 undetectable	(*72*)
ZnT1	RT-PCR & Western	PC3 and LNCaP	• ZnT1 expression levels increased after zinc and cadmium in PC3 but not LNCaP (Western & RNA) • RNA levels significantly decreased in prostate cells compared to Benign Prostate Hyperplasia (BPH) by semi-qPCR	(*73*)
ZnT4	Immunofluorescence & Western	Mouse Fibroblast Cells, NIH3T3 Cells (mouse), LNCaP, & PC3	• ZnT4 detected in transfected MFC, NIH3T3, and PC3 with ZnT4-HA • Whole Cell Lysate and surface biotinylated ZnT4-HA detected in MFC & 3T3 cells by western • ZnT4 protein found in LNCaP not PC3 cells (Western)	(*32*)
hZIP1, hZIP2, ZnT1, ZnT3, ZnT4	RT-PCR	LNCaP	• LNCaP cells were deprived of Zinc called AIDL • ZnT1 and ZnT3 down-regulated in LNCaP vs. AIDL cells • ZnT4 upregulated in LNCaP vs. AIDL cells • No significant change in hZIP1 and hZIP3 in both cell lines	(*53*)
hZIP1	RT-PCR and Immunofluorescence	LNCaP & PC3	• mRNA decreased in prostate cancer cells compared to BPH • PC3 & LNCaP show similar distribution of hZIP1	(*52*)
hZIP1 & hZIP2	RT-PCR	Rat—ventral, lateral, and dorsal	• Down regulation on all three anatomical sections of the prostate for hZIP1 • hZIP2 not detected in ventral or dorsal prostate ONLY in lateral; down-regulated	(*74*)

hZIP2 & hZIP3	Immunofluorescence	Human tissue samples	• both down-regulated in adenocarcinoma glands • function in the re-uptake and conservation of zinc from prostatic fluid • hZIP1 functions in the accumulation of zinc from circulation	(*55*)
ALL ZnT's and hZIPs	qRT-PCR	RWPE-1, LNCaP, PC3, & DU-145	• Detected mostly all in all cell lines, EXCEPT ZnT3, ZnT10, hZIP2, hZIP4, & hZIP5 • NO significant difference in mRNA levels between cell lines for ZnT2 & ZnT5-7 between all cell lines • ZnT1 and hZIP10 levels were elevated in RWPE1 • ZnT4 elevated in LNCaP compared to other cell lines • hZIP1 elevated in DU-145 compared to other cell lines • Exposure to Zn^{2+} had no effect on the mRNA levels of all cell lines EXCEPT; increased ZnT1-2 in RWPE1 and decreased ZnT7, hZIP7 and hZIP10 • ZnT1 levels increased in PC3 cells but to a lower magnitude that of RWPE1	(*50*)
ZnT1 – ZnT7	Immunohistochemistry	Mouse Tissue	• ZnTs were differentially expressed in prostate during sexual maturation • ZnT1 detected on lateral membrane • ZnT2/ZnT5 detected in the ER • ZnT3 not detected • ZnT4 detected in luminal border • ZnT6/7 across lobes of all ages	(*75*)

Table 1.4 List of Prostate Cancer Cells

Cell Line	Site of Origin	Reference
DuCaP	Dura matter	(*64*)
VCaP	Spinal cord	(*63*)
DU-145	Brain	(*76, 77*)
PC-3	Bone	(*78*)
LNCaP	Lymph Node	(*67*)
ARCaP	Ascites	(*79*)
NCI-H660	Lymph Node	(*80, 81*)
ALVA-101	Bone	(*82*)
ALVA-55	Lymph Node	(*83*)
LAPC-4	Lymph Node	(*84*)
MDA PCa 2a	Ascites	(*85*)
MDA PCa 2b	Bone	(*85*)
CTPE	Lung	(*86*)

encoded sensors which contain a Zn^{2+} binding domain with a donor cyan fluorescent protein (CFP) and acceptor yellow fluorescent protein (Citrine or circular permuted Venus) with apparent disassociation constants (K_d') that range from pM to μM (*18, 20, 87*). These sensors undergo a conformational change upon binding Zn^{2+} resulting in an increase in fluorescence energy transfer (FRET) from the donor to the acceptor. **Figure 1.2** depicts the changes in the emission spectrum of one sensor as the concentration of Zn^{2+} is increased. **Figure 1.3** shows representative Zn^{2+} binding curves of some of the FRET sensors created and characterized in our laboratory. These sensors have been expressed in mammalian cells and have been targeted to the cytosol, nucleus, mitochondria, ER, and Golgi and have proven to be an effective and powerful tool in monitoring Zn^{2+} homeostasis in HeLa and neuronal cells (*18, 20, 87*).

Although genetically encoded FRET sensors are powerful tools to monitor ions such as Zn^{2+} or Ca^{2+}, it is imperative that the sensor does not alter or perturb the cellular environment (*88*). This is important because the majority of Zn^{2+} binding domains that we use in FRET sensors are naturally occurring domains such as the Zif268 transcription factor (*8, 87*). It was previously shown that analogous Ca^{2+} sensors (cameleons) which are based on the ubiquitous calmodulin protein were perturbed in some cellular environments (*89, 90*). Redesign of the calmodulin within the sensor so that it could not bind endogenous effectors led to improved responses, suggesting that sensors have the potential to interact with other cellular constituents (*91*).

In our laboratory, Dr. Yan Qin, has performed extensive studies that demonstrate that, to the best of our detection, our sensors are not perturbing the cellular environment. **Figure 1.4a** shows that the level of measured Zn^{2+} does not depend on the sensor concentration, suggesting that at the concentrations present in these experiments, the incorporation of sensor into cells does not alter the resting Zn^{2+} levels. On the other hand, small molecule fluorescent Zn^{2+} sensors, such as FluoZin3-AM were observed to be highly perturbing to the cellular environment at high concentrations as depicted in **Figure 1.4b**.

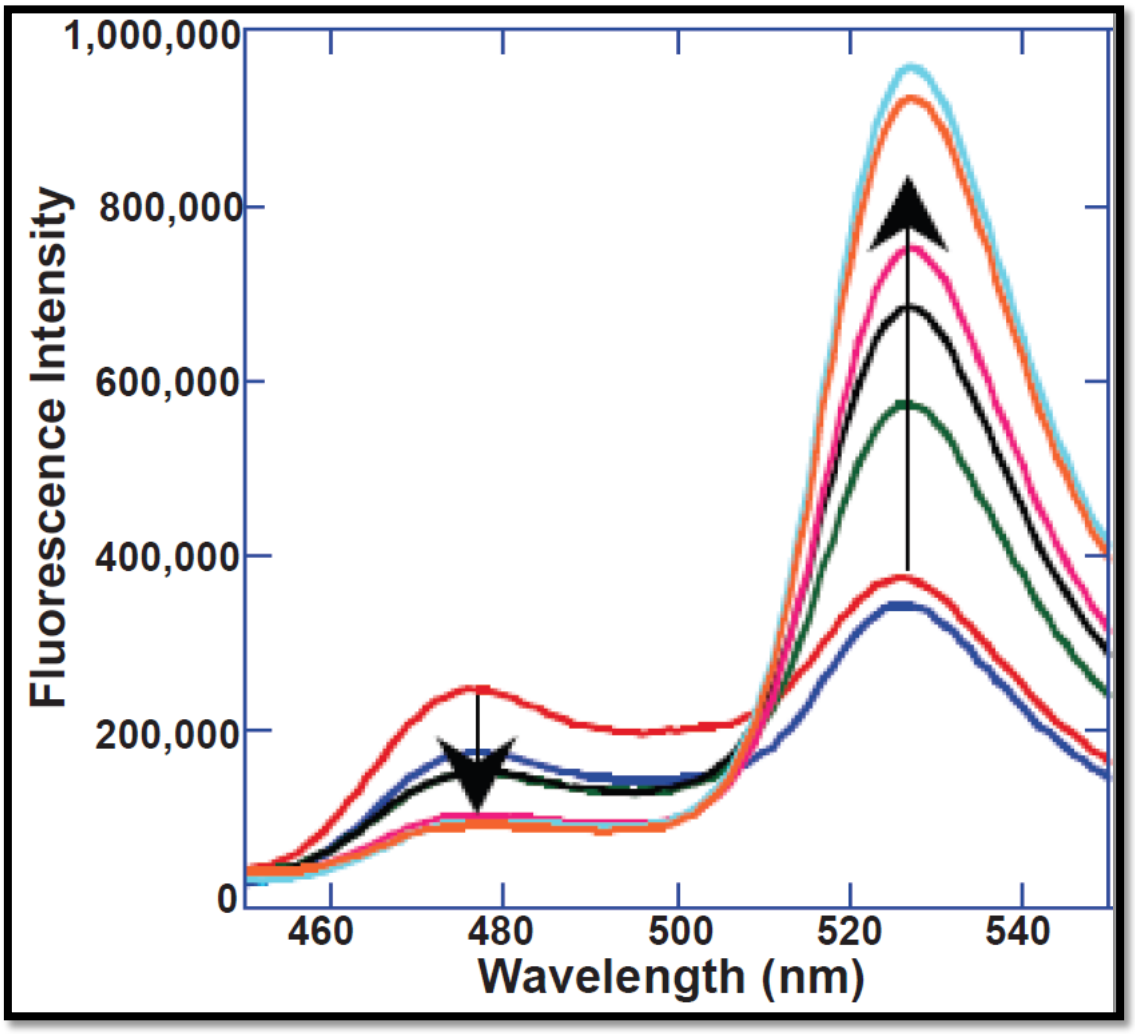

Figure 1.2. *In vitro* Fluorescence Spectra of a Ratiometric FRET Sensor. Representation of a FRET sensor changes in the emission spectra upon increasing [Zn^{2+}]. Arrows indicate a decrease in the donor fluorescence and an increase in the acceptor emission.

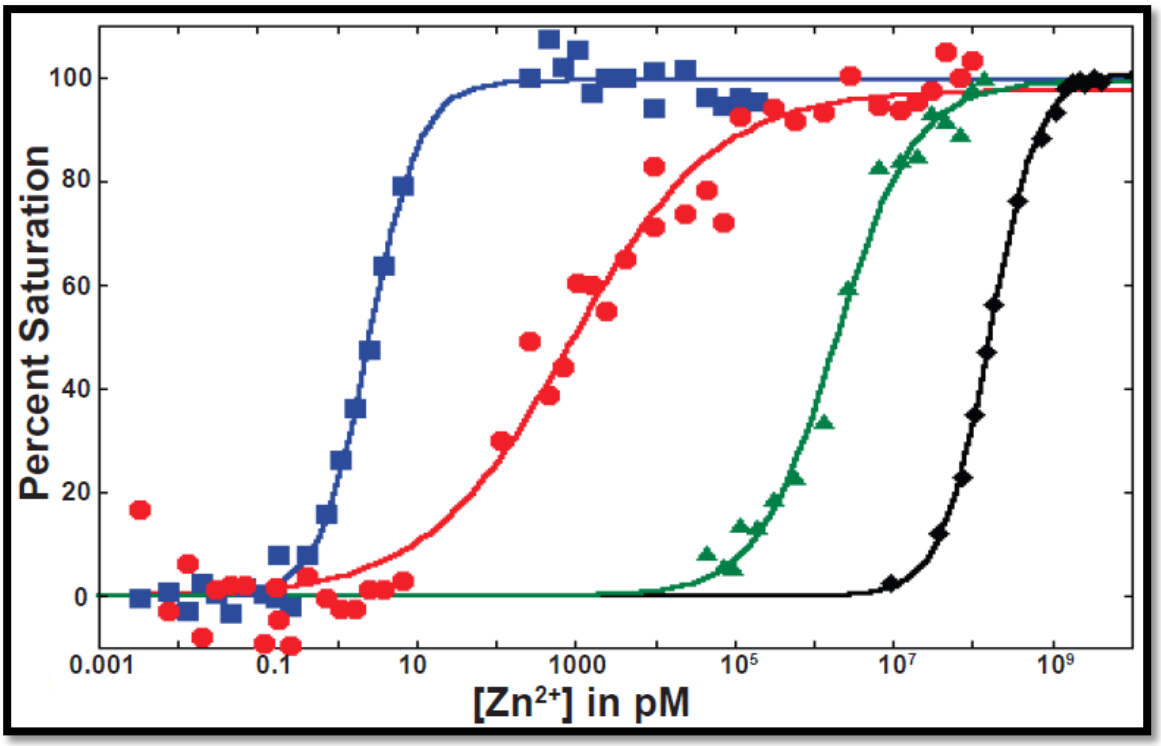

Figure 1.3 *In vitro* Zn^{2+} titration of FRET sensors. Data (symbols) are represented as the percent saturation of each sensor as a function of Zn^{2+} concentration. Each data trace is fit to binding model (solid line) in order to determine the Kd'. Blue trace represents ZapCY1 (K_d' - 2.5 pM), red trace ZapCY2 (K_d' - 811 pM), green trace ZifCY1 (K_d' - 1 µM), and black trace ZifCY2 (K_d' - 150 µM) (*18, 87*).

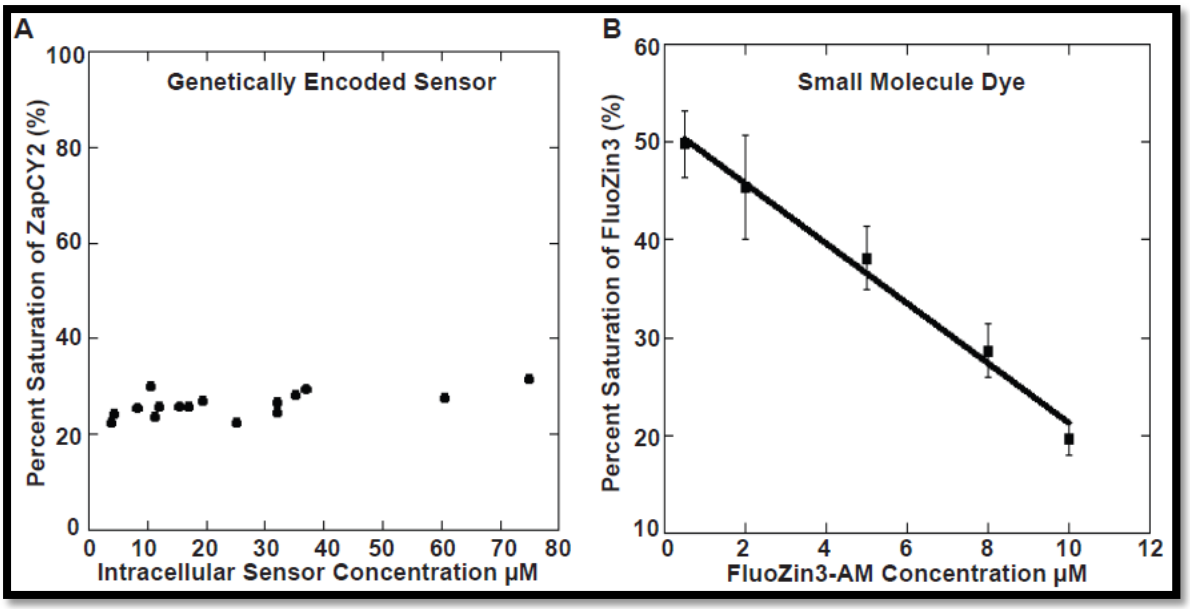

Figure 1.4. Percent saturation of a FRET sensor and FluoZin3-AM as a function of the sensor concentration. The percent saturation of either ZapCY2 or FluoZin3-AM was calculated at rest by obtaining Resting Ratio (R), R_{TPEN}, and R_{Zn}. These ratios are then converted into a percent using the following equation: % = $(R - R_{TPEN})/(R_{Zn} - R_{TPEN})$. A) The percent saturation of the sensor at rest as a function of sensor concentration, each point in the graph represents a region of interest in a single cell. B) The percent saturation of the small molecule dye at rest as a function of dye concentration. Estimate of free Zn^{2+} is more reliable with a genetically encoded sensor versus FluoZin3-AM because for the dye the estimated free Zn^{2+} is dependent of sensor concentration. Graphs are courtesy of Dr. Yan Qin.

In addition to genetically encoded sensors, there are a large number of small molecule sensors for Zn^{2+}. Great strides have been made over the years to increase the repertoire of small molecule fluorescent indicators for Zn^{2+}. **Table 1.5** lists the main small molecule indicators developed to date. There are many differences between small molecule and genetically encoded sensors and each class of indicators has notable strengths and weaknesses. One of the primary strengths of small molecule sensors is that they tend to have larger dynamic ranges than genetically encoded sensors (i.e. the change in signal upon Zn^{2+} binding is greater than for genetically encoded sensors). One of the primary reasons for this is that the vast majority of small molecule sensors are "intensiometric", i.e. Zn^{2+} binding induces a change in fluorescence intensity and intensiometric sensors can typically achieve higher dynamic ranges than "ratiometric" sensors, where Zn^{2+} binding induces a shift in the excitation or emission spectrum. High dynamic range intensiometric sensors are valuable for measuring Zn^{2+} dynamics, particularly when the change in Zn^{2+} levels might be small. However, these sensors pose problems for precise quantification of Zn^{2+}, because the intensity depends not only on Zn^{2+} but also the concentration of sensor (as discussed above) and the pathlength (i.e. cell thickness). In addition, small molecule sensors lack the capacity to be explicitly targeted to organelles, whereas genetically encoded sensors can be targeted to different compartments of the cell by attaching a signal sequence. Small molecule dyes are extruded from the cell after a couple of hours (*92*). On the other hand, genetically encoded sensors can easily be incorporated into cells and imaged over long periods of time (days to weeks). Lastly, the concentration of a genetically encoded sensor can be controlled if it is placed under an inducible promoter such as Tet-promoter in which the ligand can be titrated to induce sensor production. Because the goal of this thesis is to define Zn^{2+} levels in different cellular locations, I focused on the development and use of genetically encoded sensors.

Table 1.5 Small molecule fluorescent Zn^{2+} sensors

Sensor Name	Structure	K_d' (nM)	Ratiometric	References
Zinpyr (ZP) ZP1 ZP2 ZP3 ZP4 ZP5 ZP6 ZP7	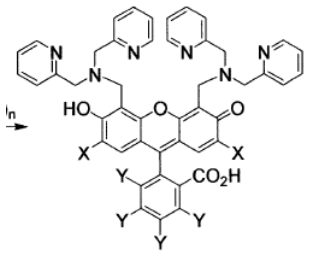	 0.7 0.5 0.7 0.9 1.1 0.9 0.8	 No No No No No No No	(*93*)
FluoZin-3	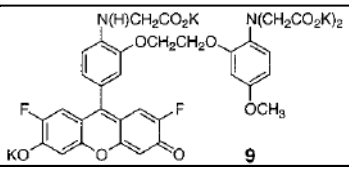	15	No	(*94*)
Zinbo-5	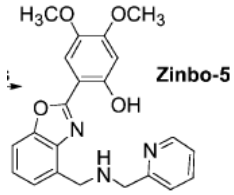	2.2	Yes	(*95*)
Zinspy-5	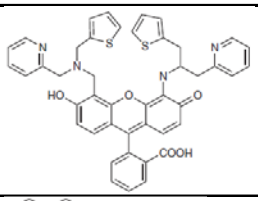	Low μM	No	(*96, 97*)
Quinozin	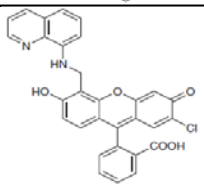	30,000 μM	No	(*98*)
IndoZin	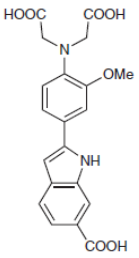	3,000 μM	Yes	(*99*)
Zin-naphthopyr-1	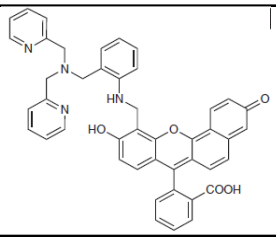	0.55	No	(*99*)

1.5 Significance

It is important for cells to regulate the distribution of metals because numerous enzymes and cellular processes depend on transition metals, yet metal imbalance leads to a wide range of diseases. Our current knowledge of metal homeostasis is limited because we are barely scratching the surface of metal distribution in living cells. Homeostasis is generally defined as the ability of a cell to regulate internal conditions through feedback controls to maintain stability independent of the outside conditions. Understanding metal homeostasis involves establishing where metals are located and tracking the movement of metals from one compartment to another. For example, Inositol 1,4,5-trisphosphate (IP3) receptor signaling causes a redistribution of Ca^{2+} stores from the ER to the cytosol and perturbations of this pathway may play a role in Huntington's and Alzheimer's disease (*100*). Therefore, in order to understand how metals move throughout the cell it is important to acquire the necessary tools to monitor these dynamics, and identify the proteins that regulate these actions.

Zn^{2+} is an important transition metal and is required in many processes of the cell from cell cycle regulation (*101*), gene regulation (*102*), and cell death (*103*). In addition, Zn^{2+} deficiency has been known to impair the immune system by lowering the number of T-cells (*104*). In pancreatic islet cells (*105*), brain (*2, 29*), and prostate (*28*), Zn^{2+} dysregulation has been linked to human disease. In the pancreas an upregulation of hZIP4 at the membrane increases the Zn^{2+} concentration contributing to tumor progression (*106*).

Although there is no mechanistic information on how Zn^{2+} perturbations contribute to prostate cancer, study after study done in prostate cancer cells and tissues demonstrate low levels of Zn^{2+} compared to normal prostate. Among all the tissues in the body, the prostate has the highest levels of Zn^{2+} per gram of tissue (*28, 29*). Moreover, when normal prostate cells become malignant they lose over 50% of total cellular Zn^{2+} (*46, 47*). According to the American Cancer Society, prostate cancer claims the lives of approximately 30,000 men a year in the United States (http://www.cancer.org/Cancer/ProstateCancer/DetailedGuide/prostate-cancer-

key-statistics and (*107*)) In addition to the high number of lives claimed per year due to prostate cancer, it is estimated that 1 out 6 men will be diagnosed with this disease during his lifetime (*108*). A significant problem with this disease is the lack of appropriate biomarkers for different stages of cancer progression. Understanding Zn^{2+} dysregulation in prostate cells is important for establishing the role of Zn^{2+} in disease progression.

Given the importance of Zn^{2+}, it is surprising how few robust quantitative tools we have to look at this important ion in cell. As explained earlier in this chapter, small molecule fluorescent dyes lack the capacity to localize to organelles and consequently are unable to identify and track critical pools of Zn^{2+}. Genetically encoded FRET sensors have the capacity and potential to fill this gap, as these sensors enable us to track Zn^{2+} using fluorescence microscopy techniques over long periods of time whereas small molecules are removed from the cell in a matter of hours. While we have made great strides in moving this field forward, we are stuck in one place in the sense that we are able to monitor Zn^{2+} in one compartment at a time in a single cell. To date most FRET sensors made, either to monitor Zn^{2+}, Ca^{2+}, or monitor protein-protein interactions have utilized the CFP-YFP FRET pair (*109*). In order to observe Zn^{2+} dynamics, orthogonal sensors need to be generated to be used alongside CFP-YFP to dissect Zn^{2+} movement in cells. Therefore one of the primary focuses of this thesis was to develop FRET sensors using alternate fluorescent proteins in the hopes that such sensors could be used alongside CFP-YFP sensors to track metal movements in cells.

1.6 Conclusion

Zn^{2+} is the second most abundant transition metal in the body and the highest concentrations of Zn^{2+} in the body are found in the prostate gland. The goal of this study has been to reveal the differences in Zn^{2+} distribution at the subcellular level in noncancerous compared to cancerous cells. Our study was focused on using novel tools (genetically encoded FRET sensors) to monitor Zn^{2+} distribution in cells (**Chapter 2**) and to correlate this with changes in expression levels of mRNA and proteins that regulate Zn^{2+} homeostasis (**Chapter**

3). By demonstrating which compartments have Zn^{2+} pools, we can further understand the fundamental role of Zn^{2+} in the cell and be able to define how Zn^{2+} is dysregulated in prostate cancer cells. The changes that occur in proteins that regulate Zn^{2+} homeostasis will provide a complete picture of how and why Zn^{2+} is altered in cancerous prostate cells. This is an important first step in defining the role of Zn^{2+} dysregulation in tumor progression.

The generation of new alternate colored Zn^{2+} sensors (**Chapter 4**) will represent a marked advance in our ability to monitor Zn^{2+} dynamics, will have more versatile optical properties, and will be pH insensitive. Because these new sensors will be pH insensitive, they will be instrumental in developing tools to monitor metal homeostasis in places like vesicles were the pH is low. This would be a major advance as there is currently no reliable way to measure vesicular Zn^{2+}. Very little is known about the concentrations of metal within acidic places and these new sensors will open up areas of research that may elucidate the signal mechanisms of metal storage. Preliminary work (**Chapter 5**) suggests that FRET sensors can indeed be targeted to vesicular pools and are sensitive to Zn^{2+} perturbations in these locations.

1.7 References

1. Auld, D. S. (2001) Zinc coordination sphere in biochemical zinc sites, *Biometals 14*, 271-313.
2. Frederickson, C. J., Koh, J. Y., and Bush, A. I. (2005) The neurobiology of zinc in health and disease, *Nat Rev Neurosci 6*, 449-462.
3. Nies, D. H. (2007) Biochemistry. How cells control zinc homeostasis, *Science 317*, 1695-1696.
4. Andreini, C., Banci, L., Bertini, I., and Rosato, A. (2006) Counting the zinc-proteins encoded in the human genome, *J Proteome Res 5*, 196-201.
5. Maret, W., and Sandstead, H. H. (2006) Zinc requirements and the risks and benefits of zinc supplementation, *J Trace Elem Med Biol 20*, 3-18.

6. Rajesh, R. V., Balasubramanian, A. S., and Boopathy, R. (2009) Evidence for presence of Zn+2-binding site in acetylcholinesterase, *Biochimie 91*, 526-532.

7. Mocchegiani, E., Muzzioli, M., Cipriano, C., and Giacconi, R. (1998) Zinc, T-cell pathways, aging: role of metallothioneins, *Mech Ageing Dev 106*, 183-204.

8. Pavletich, N. P., and Pabo, C. O. (1991) Zinc finger-DNA recognition: crystal structure of a Zif268-DNA complex at 2.1 A, *Science 252*, 809-817.

9. Laity, J. H., and Andrews, G. K. (2007) Understanding the mechanisms of zinc-sensing by metal-response element binding transcription factor-1 (MTF-1), *Arch Biochem Biophys 463*, 201-210.

10. O'Green, H., Frietze, S., and Rarnham, P. J. (2010) Using ChIP-seq technology to identify targets of zinc finger transcription factors, *Methods Mol Biol 649*, 437-455.

11. Freedman, L. P., and Luisi, B. F. (1993) On the mechanism of DNA binding by nuclear hormone receptors: a structural and functional perspective, *J Cell Biochem 51*, 140-150.

12. Levenson, C. W., and Morris, D. (2011) Zinc and neurogenesis: making new neurons from development to adulthood, *Adv Nutr 2*, 96-100.

13. Eide, D. J. (2006) Zinc transporters and the cellular trafficking of zinc, *Biochim Biophys Acta 1763*, 711-722.

14. Outten, C. E., and O'Halloran, T. V. (2001) Femtomolar sensitivity of metalloregulatory proteins controlling zinc homeostasis, *Science 292*, 2488-2492.

15. Palmiter, R. D., and Findley, S. D. (1995) Cloning and functional characterization of a mammalian zinc transporter that confers resistance to zinc, *EMBO J 14*, 639-649.

16. Krezel, A., and Maret, W. (2008) Thionein/metallothionein control Zn(II) availability and the activity of enzymes, *J Biol Inorg Chem 13*, 401-409.

17. Thirumoorthy, N., Shyam Sunder, A., Manisenthil Kumar, K., Senthil Kumar, M., Ganesh, G., and Chatterjee, M. (2011) A review of metallothionein isoforms and their role in pathophysiology, *World J Surg Oncol 9*, 54.

18. Qin, Y., Dittmer, P. J., Park, J. G., Jansen, K. B., and Palmer, A. E. (2011) Measuring steady-state and dynamic endoplasmic reticulum and Golgi Zn2+ with genetically encoded sensors, *Proc Natl Acad Sci U S A 108*, 7351-7356.

19. Vinkenborg, J. L., Nicolson, T. J., Bellomo, E. A., Koay, M. S., Rutter, G. A., and Merkx, M. (2009) Genetically encoded FRET sensors to monitor intracellular Zn2+ homeostasis, *Nat Methods 6*, 737-740.

20. Park, J. G., Qin, Y., Galati, D. F., and Palmer, A. E. (2012) New Sensors for Quantitative Measurement of Mitochondrial Zn(2+), *ACS Chem Biol*.

21. Inoue, K., Takano, H., Shimada, A., and Satoh, M. (2009) Metallothionein as an anti-inflammatory mediator, *Mediators Inflamm 2009*, 101659.

22. Maret, W. (2009) Molecular aspects of human cellular zinc homeostasis: redox control of zinc potentials and zinc signals, *Biometals 22*, 149-157.

23. Barbato, J. C., Catanescu, O., Murray, K., DiBello, P. M., and Jacobsen, D. W. (2007) Targeting of metallothionein by L-homocysteine: a novel mechanism for disruption of zinc and redox homeostasis, *Arterioscler Thromb Vasc Biol 27*, 49-54.

24. Stitt, M. S., Wasserloos, K. J., Tang, X., Liu, X., Pitt, B. R., and St Croix, C. M. (2006) Nitric oxide-induced nuclear translocation of the metal responsive transcription factor, MTF-1 is mediated by zinc release from metallothionein, *Vascul Pharmacol 44*, 149-155.

25. Lichten, L. A., and Cousins, R. J. (2009) Mammalian zinc transporters: nutritional and physiologic regulation, *Annu Rev Nutr 29*, 153-176.

26. Guerinot, M. L. (2000) The ZIP family of metal transporters, *Biochim Biophys Acta 1465*, 190-198.

27. Delhaize, E., Kataoka, T., Hebb, D. M., White, R. G., and Ryan, P. R. (2003) Genes encoding proteins of the cation diffusion facilitator family that confer manganese tolerance, *Plant Cell 15*, 1131-1142.

28. Franklin, R. B., and Costello, L. C. (2007) Zinc as an anti-tumor agent in prostate cancer and in other cancers, *Arch Biochem Biophys 463*, 211-217.

29. Sorensen, M. B., Stoltenberg, M., Juhl, S., Danscher, G., and Ernst, E. (1997) Ultrastructural localization of zinc ions in the rat prostate: an autometallographic study, *Prostate 31*, 125-130.

30. Palmiter, R. D., Cole, T. B., and Findley, S. D. (1996) ZnT-2, a mammalian protein that confers resistance to zinc by facilitating vesicular sequestration, *EMBO J 15*, 1784-1791.

31. Perez-Clausell, J., and Danscher, G. (1985) Intravesicular localization of zinc in rat telencephalic boutons. A histochemical study, *Brain Res 337*, 91-98.

32. Henshall, S. M., Afar, D. E., Rasiah, K. K., Horvath, L. G., Gish, K., Caras, I., Ramakrishnan, V., Wong, M., Jeffry, U., Kench, J. G., Quinn, D. I., Turner, J. J., Delprado, W., Lee, C. S., Golovsky, D., Brenner, P. C., O'Neill, G. F., Kooner, R., Stricker, P. D., Grygiel, J. J., Mack, D. H., and Sutherland, R. L. (2003) Expression of the zinc transporter ZnT4 is decreased in the progression from early prostate disease to invasive prostate cancer, *Oncogene 22*, 6005-6012.

33. Kambe, T., Narita, H., Yamaguchi-Iwai, Y., Hirose, J., Amano, T., Sugiura, N., Sasaki, R., Mori, K., Iwanaga, T., and Nagao, M. (2002) Cloning and characterization of a novel mammalian zinc transporter, zinc transporter 5, abundantly expressed in pancreatic beta cells, *J Biol Chem 277*, 19049-19055.

34. Kirschke, C. P., and Huang, L. (2003) ZnT7, a novel mammalian zinc transporter, accumulates zinc in the Golgi apparatus, *J Biol Chem 278*, 4096-4102.

35. Sim, D. L., and Chow, V. T. (1999) The novel human HUEL (C4orf1) gene maps to chromosome 4p12-p13 and encodes a nuclear protein containing the nuclear receptor interaction motif, *Genomics 59*, 224-233.

36. Seve, M., Chimienti, F., Devergnas, S., and Favier, A. (2004) In silico identification and expression of SLC30 family genes: an expressed sequence tag data mining strategy for the characterization of zinc transporters' tissue expression, *BMC Genomics 5*, 32.

37. Gaither, L. A., and Eide, D. J. (2001) The human ZIP1 transporter mediates zinc uptake in human K562 erythroleukemia cells, *J Biol Chem 276*, 22258-22264.

38. Dufner-Beattie, J., Langmade, S. J., Wang, F., Eide, D., and Andrews, G. K. (2003) Structure, function, and regulation of a subfamily of mouse zinc transporter genes, *J Biol Chem 278*, 50142-50150.

39. Wang, K., Zhou, B., Kuo, Y. M., Zemansky, J., and Gitschier, J. (2002) A novel member of a zinc transporter family is defective in acrodermatitis enteropathica, *Am J Hum Genet 71*, 66-73.

40. Taylor, K. M., and Nicholson, R. I. (2003) The LZT proteins; the LIV-1 subfamily of zinc transporters, *Biochim Biophys Acta 1611*, 16-30.

41. Huang, L., Kirschke, C. P., Zhang, Y., and Yu, Y. Y. (2005) The ZIP7 gene (Slc39a7) encodes a zinc transporter involved in zinc homeostasis of the Golgi apparatus, *J Biol Chem 280*, 15456-15463.

42. Ryu, M. S., Lichten, L. A., Liuzzi, J. P., and Cousins, R. J. (2008) Zinc transporters ZnT1 (Slc30a1), Zip8 (Slc39a8), and Zip10 (Slc39a10) in mouse red blood cells are differentially regulated during erythroid development and by dietary zinc deficiency, *J Nutr 138*, 2076-2083.

43. Kagara, N., Tanaka, N., Noguchi, S., and Hirano, T. (2007) Zinc and its transporter ZIP10 are involved in invasive behavior of breast cancer cells, *Cancer Sci 98*, 692-697.

44. Giunta, C., Randolph, A., and Steinmann, B. (2005) Mutation analysis of the PLOD1 gene: an efficient multistep approach to the molecular diagnosis of the kyphoscoliotic type of Ehlers-Danlos syndrome (EDS VIA), *Mol Genet Metab 86*, 269-276.

45. Nemeth, E., Rivera, S., Gabayan, V., Keller, C., Taudorf, S., Pedersen, B. K., and Ganz, T. (2004) IL-6 mediates hypoferremia of inflammation by inducing the synthesis of the iron regulatory hormone hepcidin, *J Clin Invest 113*, 1271-1276.

46. Franklin, R. B., Milon, B., Feng, P., and Costello, L. C. (2005) Zinc and zinc transporters in normal prostate and the pathogenesis of prostate cancer, *Front Biosci 10*, 2230-2239.

47. Huang, L., Kirschke, C. P., and Zhang, Y. (2006) Decreased intracellular zinc in human tumorigenic prostate epithelial cells: a possible role in prostate cancer progression, *Cancer Cell Int 6*, 10.

48. Sakai, I., Harada, K., Hara, I., Eto, H., and Miyake, H. (2005) A comparison of the biological features between prostate cancers arising in the transition and peripheral zones, *BJU Int 96*, 528-532.

49. Costello, L. C., and Franklin, R. B. (2006) The clinical relevance of the metabolism of prostate cancer; zinc and tumor suppression: connecting the dots, *Mol Cancer 5*, 17.

50. Albrecht, A. L., Somji, S., Sens, M. A., Sens, D. A., and Garrett, S. H. (2008) Zinc transporter mRNA expression in the RWPE-1 human prostate epithelial cell line, *Biometals 21*, 405-416.

51. Costello, L. C., Franklin, R. B., Feng, P., Tan, M., and Bagasra, O. (2005) Zinc and prostate cancer: a critical scientific, medical, and public interest issue (United States), *Cancer Causes Control 16*, 901-915.

52. Franklin, R. B., Feng, P., Milon, B., Desouki, M. M., Singh, K. K., Kajdacsy-Balla, A., Bagasra, O., and Costello, L. C. (2005) hZIP1 zinc uptake transporter down regulation and zinc depletion in prostate cancer, *Mol Cancer 4*, 32.

53. Iguchi, K., Otsuka, T., Usui, S., Ishii, K., Onishi, T., Sugimura, Y., and Hirano, K. (2004) Zinc and metallothionein levels and expression of zinc transporters in androgen-independent subline of LNCaP cells, *J Androl 25*, 154-161.

54. Christudoss, P., Selvakumar, R., Fleming, J. J., and Gopalakrishnan, G. (2011) Zinc status of patients with benign prostatic hyperplasia and prostate carcinoma, *Indian J Urol 27*, 14-18.

55. Desouki, M. M., Geradts, J., Milon, B., Franklin, R. B., and Costello, L. C. (2007) hZip2 and hZip3 zinc transporters are down regulated in human prostate adenocarcinomatous glands, *Mol Cancer 6*, 37.

56. Feng, P., Li, T. L., Guan, Z. X., Franklin, R. B., and Costello, L. C. (2002) Direct effect of zinc on mitochondrial apoptogenesis in prostate cells, *Prostate 52*, 311-318.

57. Gomez, Y., Arocha, F., Espinoza, F., Fernandez, D., Vasquez, A., and Granadillo, V. (2007) [Zinc levels in prostatic fluid of patients with prostate pathologies], *Invest Clin 48*, 287-294.

58. Kelleher, S. L., McCormick, N. H., Velasquez, V., and Lopez, V. (2011) Zinc in specialized secretory tissues: roles in the pancreas, prostate, and mammary gland, *Adv Nutr 2*, 101-111.

59. Costello, L. C., Franklin, R. B., Zou, J., Feng, P., Bok, R., Mark, G. S., and Kurhanewicz, J. (2011) Human prostate cancer ZIP1/zinc/citrate genetic/metabolic relationship in the TRAMP prostate cancer animal model, *Cancer Biol Ther 12*.

60. Feng, P., Li, T. L., Guan, Z. X., Franklin, R. B., and Costello, L. C. (2003) Effect of zinc on prostatic tumorigenicity in nude mice, *Ann N Y Acad Sci 1010*, 316-320.

61. Prasad, A. S., Mukhtar, H., Beck, F. W., Adhami, V. M., Siddiqui, I. A., Din, M., Hafeez, B. B., and Kucuk, O. (2010) Dietary zinc and prostate cancer in the TRAMP mouse model, *J Med Food 13*, 70-76.

62. Tepaamorndech, S., Huang, L., and Kirschke, C. P. (2011) A null-mutation in the Znt7 gene accelerates prostate tumor formation in a transgenic adenocarcinoma mouse prostate model, *Cancer Lett 308*, 33-42.

63. Korenchuk, S., Lehr, J. E., L, M. C., Lee, Y. G., Whitney, S., Vessella, R., Lin, D. L., and Pienta, K. J. (2001) VCaP, a cell-based model system of human prostate cancer, *In Vivo 15*, 163-168.

64. Lee, Y. G., Korenchuk, S., Lehr, J., Whitney, S., Vessela, R., and Pienta, K. J. (2001) Establishment and characterization of a new human prostatic cancer cell line: DuCaP, *In Vivo 15*, 157-162.

65. van Bokhoven, A., Caires, A., Maria, M. D., Schulte, A. P., Lucia, M. S., Nordeen, S. K., Miller, G. J., and Varella-Garcia, M. (2003) Spectral karyotype (SKY) analysis of human prostate carcinoma cell lines, *Prostate 57*, 226-244.

66. van Bokhoven, A., Varella-Garcia, M., Korch, C., Johannes, W. U., Smith, E. E., Miller, H. L., Nordeen, S. K., Miller, G. J., and Lucia, M. S. (2003) Molecular characterization of human prostate carcinoma cell lines, *Prostate 57*, 205-225.

67. Horoszewicz, J. S., Leong, S. S., Kawinski, E., Karr, J. P., Rosenthal, H., Chu, T. M., Mirand, E. A., and Murphy, G. P. (1983) LNCaP model of human prostatic carcinoma, *Cancer Res 43*, 1809-1818.

68. Bello, D., Webber, M. M., Kleinman, H. K., Wartinger, D. D., and Rhim, J. S. (1997) Androgen responsive adult human prostatic epithelial cell lines immortalized by human papillomavirus 18, *Carcinogenesis 18*, 1215-1223.

69. Sobel, R. E., and Sadar, M. D. (2005) Cell lines used in prostate cancer research: a compendium of old and new lines--part 2, *J Urol 173*, 360-372.

70. Sobel, R. E., and Sadar, M. D. (2005) Cell lines used in prostate cancer research: a compendium of old and new lines--part 1, *J Urol 173*, 342-359.

71. Costello, L. C., Liu, Y., Zou, J., and Franklin, R. B. (1999) Evidence for a zinc uptake transporter in human prostate cancer cells which is regulated by prolactin and testosterone, *J Biol Chem 274*, 17499-17504.

72. Franklin, R. B., Ma, J., Zou, J., Guan, Z., Kukoyi, B. I., Feng, P., and Costello, L. C. (2003) Human ZIP1 is a major zinc uptake transporter for the accumulation of zinc in prostate cells, *J Inorg Biochem 96*, 435-442.

73. Hasumi, M., Suzuki, K., Matsui, H., Koike, H., Ito, K., and Yamanaka, H. (2003) Regulation of metallothionein and zinc transporter expression in human prostate cancer cells and tissues, *Cancer Lett 200*, 187-195.

74. Iguchi, K., Otsuka, T., Usui, S., Sugimura, Y., and Hirano, K. (2006) Correlation between ZIP2 messenger RNA expression and zinc level in rat lateral prostate, *Biol Trace Elem Res 112*, 159-167.

75. Kirschke, C. P., and Huang, L. (2008) Expression of the ZNT (SLC30) family members in the epithelium of the mouse prostate during sexual maturation, *J Mol Histol 39*, 359-370.

76. Mickey, D. D., Stone, K. R., Wunderli, H., Mickey, G. H., Vollmer, R. T., and Paulson, D. F. (1977) Heterotransplantation of a human prostatic adenocarcinoma cell line in nude mice, *Cancer Res 37*, 4049-4058.

77. Stone, K. R., Mickey, D. D., Wunderli, H., Mickey, G. H., and Paulson, D. F. (1978) Isolation of a human prostate carcinoma cell line (DU 145), *Int J Cancer 21*, 274-281.

78. Kaighn, M. E., Narayan, K. S., Ohnuki, Y., Lechner, J. F., and Jones, L. W. (1979) Establishment and characterization of a human prostatic carcinoma cell line (PC-3), *Invest Urol 17*, 16-23.

79. Zhau, H. Y., Chang, S. M., Chen, B. Q., Wang, Y., Zhang, H., Kao, C., Sang, Q. A., Pathak, S. J., and Chung, L. W. (1996) Androgen-repressed phenotype in human prostate cancer, *Proc Natl Acad Sci U S A 93*, 15152-15157.

80. Carney, D. N., Gazdar, A. F., Bepler, G., Guccion, J. G., Marangos, P. J., Moody, T. W., Zweig, M. H., and Minna, J. D. (1985) Establishment and identification of small cell lung cancer cell lines having classic and variant features, *Cancer Res 45*, 2913-2923.

81. Johnson, B. E., Whang-Peng, J., Naylor, S. L., Zbar, B., Brauch, H., Lee, E., Simmons, A., Russell, E., Nam, M. H., and Gazdar, A. F. (1989) Retention of chromosome 3 in extrapulmonary small cell cancer shown by molecular and cytogenetic studies, *J Natl Cancer Inst 81*, 1223-1228.

82. Plymate, S. R., Loop, S. M., Hoop, R. C., Wiren, K. M., Ostenson, R., Hryb, D. J., and Rosner, W. (1991) Effects of sex hormone binding globulin (SHBG) on human prostatic carcinoma, *J Steroid Biochem Mol Biol 40*, 833-839.

83. Mehta, P. P., Lokeshwar, B. L., Schiller, P. C., Bendix, M. V., Ostenson, R. C., Howard, G. A., and Roos, B. A. (1996) Gap-junctional communication in normal and neoplastic prostate epithelial cells and its regulation by cAMP, *Mol Carcinog 15*, 18-32.

84. Klein, K. A., Reiter, R. E., Redula, J., Moradi, H., Zhu, X. L., Brothman, A. R., Lamb, D. J., Marcelli, M., Belldegrun, A., Witte, O. N., and Sawyers, C. L. (1997) Progression of metastatic human prostate cancer to androgen independence in immunodeficient SCID mice, *Nat Med 3*, 402-408.

85. Navone, N. M., Olive, M., Ozen, M., Davis, R., Troncoso, P., Tu, S. M., Johnston, D., Pollack, A., Pathak, S., von Eschenbach, A. C., and Logothetis, C. J. (1997) Establishment of two human prostate cancer cell lines derived from a single bone metastasis, *Clin Cancer Res 3*, 2493-2500.

86. Achanzar, W. E., Diwan, B. A., Liu, J., Quader, S. T., Webber, M. M., and Waalkes, M. P. (2001) Cadmium-induced malignant transformation of human prostate epithelial cells, *Cancer Res 61*, 455-458.

87. Dittmer, P. J., Miranda, J. G., Gorski, J. A., and Palmer, A. E. (2009) Genetically encoded sensors to elucidate spatial distribution of cellular zinc, *J Biol Chem 284*, 16289-16297.

88. Palmer, A. E., Qin, Y., Park, J. G., and McCombs, J. E. (2011) Design and application of genetically encoded biosensors, *Trends Biotechnol 29*, 144-152.

89. Miyawaki, A., Llopis, J., Heim, R., McCaffery, J. M., Adams, J. A., Ikura, M., and Tsien, R. Y. (1997) Fluorescent indicators for Ca2+ based on green fluorescent proteins and calmodulin, *Nature 388*, 882-887.

90. Palmer, A. E., and Tsien, R. Y. (2006) Measuring calcium signaling using genetically targetable fluorescent indicators, *Nat Protoc 1*, 1057-1065.

91. Palmer, A. E., Giacomello, M., Kortemme, T., Hires, S. A., Lev-Ram, V., Baker, D., and Tsien, R. Y. (2006) Ca2+ indicators based on computationally redesigned calmodulin-peptide pairs, *Chem Biol 13*, 521-530.

92. Kao, J. P. (1994) Practical aspects of measuring [Ca2+] with fluorescent indicators, *Methods Cell Biol 40*, 155-181.

93. Chang, C. J., Nolan, E. M., Jaworski, J., Burdette, S. C., Sheng, M., and Lippard, S. J. (2004) Bright fluorescent chemosensor platforms for imaging endogenous pools of neuronal zinc, *Chem Biol 11*, 203-210.

94. Gee, K. R., Zhou, Z. L., Qian, W. J., and Kennedy, R. (2002) Detection and imaging of zinc secretion from pancreatic beta-cells using a new fluorescent zinc indicator, *J Am Chem Soc 124*, 776-778.

95. Taki, M., Wolford, J. L., and O'Halloran, T. V. (2004) Emission ratiometric imaging of intracellular zinc: design of a benzoxazole fluorescent sensor and its application in two-photon microscopy, *J Am Chem Soc 126*, 712-713.

96. Nolan, E. M., and Lippard, S. J. (2004) The zinspy family of fluorescent zinc sensors: syntheses and spectroscopic investigations, *Inorg Chem 43*, 8310-8317.

97. Nolan, E. M., Ryu, J. W., Jaworski, J., Feazell, R. P., Sheng, M., and Lippard, S. J. (2006) Zinspy sensors with enhanced dynamic range for imaging neuronal cell zinc uptake and mobilization, *J Am Chem Soc 128*, 15517-15528.

98. Nolan, E. M., Jaworski, J., Okamoto, K., Hayashi, Y., Sheng, M., and Lippard, S. J. (2005) QZ1 and QZ2: rapid, reversible quinoline-derivatized fluoresceins for sensing biological Zn(II), *J Am Chem Soc 127*, 16812-16823.

99. Domaille, D. W., Que, E. L., and Chang, C. J. (2008) Synthetic fluorescent sensors for studying the cell biology of metals, *Nat Chem Biol 4*, 168-175.

100. Kawaai, K., Hisatsune, C., Kuroda, Y., Mizutani, A., Tashiro, T., and Mikoshiba, K. (2009) 80K-H interacts with inositol 1,4,5-trisphosphate (IP3) receptors and regulates IP3-induced calcium release activity, *J Biol Chem 284*, 372-380.

101. MacDonald, R. S. (2000) The role of zinc in growth and cell proliferation, *J Nutr 130*, 1500S-1508S.

102. Tan, S., Guschin, D., Davalos, A., Lee, Y. L., Snowden, A. W., Jouvenot, Y., Zhang, H. S., Howes, K., McNamara, A. R., Lai, A., Ullman, C., Reynolds, L., Moore, M., Isalan, M., Berg, L. P., Campos, B., Qi, H., Spratt, S. K., Case, C. C., Pabo, C. O., Campisi, J., and Gregory, P. D. (2003) Zinc-finger protein-targeted gene regulation: genomewide single-gene specificity, *Proc Natl Acad Sci U S A 100*, 11997-12002.

103. Sunderman, F. W., Jr. (1995) The influence of zinc on apoptosis, *Ann Clin Lab Sci 25*, 134-142.

104. Honscheid, A., Rink, L., and Haase, H. (2009) T-lymphocytes: a target for stimulatory and inhibitory effects of zinc ions, *Endocr Metab Immune Disord Drug Targets 9*, 132-144.

105. Zalewski, P. D., Millard, S. H., Forbes, I. J., Kapaniris, O., Slavotinek, A., Betts, W. H., Ward, A. D., Lincoln, S. F., and Mahadevan, I. (1994) Video image analysis of labile zinc in viable pancreatic islet cells using a specific fluorescent probe for zinc, *J Histochem Cytochem 42*, 877-884.

106. Zhang, Y., Bharadwaj, U., Logsdon, C. D., Chen, C., Yao, Q., and Li, M. (2010) ZIP4 regulates pancreatic cancer cell growth by activating IL-6/STAT3 pathway through zinc finger transcription factor CREB, *Clin Cancer Res 16*, 1423-1430.

107. Karan, D., Thrasher, J. B., and Lubaroff, D. (2008) Prostate cancer: genes, environment, immunity and the use of immunotherapy, *Prostate Cancer Prostatic Dis 11*, 230-236.

108. Troyer, D. A., Mubiru, J., Leach, R. J., and Naylor, S. L. (2004) Promise and challenge: Markers of prostate cancer detection, diagnosis and prognosis, *Dis Markers 20*, 117-128.

109. Ding, Y., Ai, H. W., Hoi, H., and Campbell, R. E. (2011) Forster resonance energy transfer-based biosensors for multiparameter ratiometric imaging of Ca2+ dynamics and caspase-3 activity in single cells, *Anal Chem 83*, 9687-9693.

Chapter II

Redistribution of Free Zinc in Prostate Cancer

2.1 Abstract

Prostate tissue is characterized by high levels of Zn^{2+} compared to other soft tissues in the human body. Upon malignant transformation, the prostate gland loses over 50% of its total Zn^{2+}. The mechanism of Zn^{2+} depletion has not been defined, nor is it established from which compartment of the cell Zn^{2+} is lost. While Zn^{2+} is an important transition metal necessary for many cellular functions, it has not been determined whether this reduction in Zn^{2+} is a cause or consequence of the malignancy. In this study we use Inductively Coupled Plasma Mass Spectrometry (ICP-MS) to quantify total cellular Zn^{2+}, X-Ray Fluorescence Microscopy (XRFM) to examine the distribution of total Zn^{2+}, and genetically encoded fluorescence resonance energy transfer (FRET)-based Zn^{2+} sensors with specific localization sequences to map out free Zn^{2+} levels in the nucleus, cytosol, endoplasmic reticulum, and mitochondria. These techniques enabled us to compare the Zn^{2+} levels between a normal prostate and three prostate cancer cell lines to define the changes in Zn^{2+} between normal and malignant cells. Using XRFM and FRET sensors we identified a massive redistribution of Zn^{2+} from the normal to the cancerous prostate cell lines.

2.2 Introduction

The prostate consists of the dorsal, lateral, and ventral lobes (*1*). The peripheral zone of the prostate is known to contain the highest levels of Zn^{2+}, and this is also the zone that contributes to the majority of malignancies (*2*). It is also been postulated that another function of Zn^{2+} in prostate is its role in inhibiting m-aconitase in the Krebs Cycle, preventing the oxidation of citrate to aconitase which causes citrate to accumulate before it is secreted, and influences the bioenergetics of cells (*2*).

Zinc is the second most abundant transition metal in the human body and is critical for proteins, transcription factors, immune function, and neurotransmission (*3-5*). Although the

majority of Zn^{2+} found in cells is bound by proteins, enzymes, and cellular ligands, pools of free Zn^{2+} have been indentified in pancreatic islet cells (*6*), brain (*4*), and prostate (*7*). Numerous studies have revealed that cancerous prostate tissue exhibits dramatically reduced levels of Zn^{2+} and that the levels of Zn^{2+} appear to correlate with progression from benign to invasive and metastatic cancer (*8-11*). The mechanistic correlation between malignancy and Zn^{2+} levels is not well understood and in particular, it is not clear whether Zn^{2+} depletion contributes to or is a consequence of disease progression.

To date there have been no studies that define the subcellular distribution of Zn^{2+} in prostate cancer cells that would allow us to determine whether Zn^{2+} is missing from a particular compartment or whether prostate cancer is characterized by a systematic depletion of Zn^{2+} throughout the cell. In this study we set out to elucidate differences in Zn^{2+} levels and distribution between two newly established prostate cancer cell lines and compare them to a normal prostate cell line and a widely-used traditional cancer cell line model.

Like all cancers, prostate cancer is a complex and heterogeneous disease characterized by a wide diversity in molecular markers, thus complicating efforts to identify an appropriate *in vitro* model system. We chose to characterize two newly established prostate cancer cell lines: dura matter cancer of the prostate (DuCaP) and vertebral cancer of the prostate (VCaP), which derive from metastases to distinct locations within the same patient (*12, 13*) because they exhibit molecular diversity not currently represented in the commonly used cell lines (*14, 15*). Both cell lines express normal androgen receptor (AR), mutant p53, are androgen sensitive, produce large quantities of prostate specific antigen (PSA), and are tumorigenic in mice without the need to coinject with stroma (*12, 13*). Spectral karyotyping of these cell lines revealed a large number of complex chromosomal abnormalities, consistent with their derivation from late-state tumors (*14*). In contrast, the traditional prostate cancer cell line model that has been used for the past 30 years, lymph node cancer of the prostate (LNCaP) (*16*), is characterized by

androgen responsiveness, expression of a mutated form of AR and wild type p53. However LNCaP cells are not tumorigenic in mice unless coinjected with stroma. To compare differences between cancerous and normal we used RWPE1 normal prostate cell line (*17*).

Using a combination of techniques that measure total Zn^{2+} and free Zn^{2+} levels, we identified systematic differences in Zn^{2+} homeostasis in all three cancer cell lines compared to the normal cell line. In particular, we discovered that while total Zn^{2+} is substantially depleted in prostate cancer cells, at the subcellular level, there is a redistribution of free Zn^{2+} among the various compartments of the cell, such that in some locations free Zn^{2+} is actually elevated in the cancer cells. This study will open up new areas of research to get closer to the question of why Zn^{2+} is markedly depleted by studying specific compartments and proteins that channel this metal in and out of them.

2.3 Experimental Methods

Cell Culture. RWPE1 (normal prostate cell line), VCaP (prostate cancer cell line), and LNCaP (prostate cancer cell line) were obtained from the American Type Cell Collection (ATCC). DuCaP was a kind gift from Dr. Scott M. Lucia at the University of Colorado Anschutz Medical Campus (Denver, CO). RWPE1 cells were cultured in *K*eratynocyte-*S*erum *F*ree *M*edia (KSFM) supplemented with 0.05 mg/mL bovine pituitary extract, 5 ng/mL epithelial growth factor (Life Sciences), 100 U/mL penicillin and 100 µg/mL streptomycin. DuCaP, VCaP, and LNCaP cell lines were cultured in *R*oswell *P*ark *M*emorial *I*nstitute (RPMI) media (Life Sciences) supplemented with 10% (v/v) fetal bovine serum (Atlanta Biologicals), L-glutamine, 100 U/mL penicillin, and 100 µg/mL streptomycin. All cell lines were incubated at 37ºC with 5% CO_2, changing the media every 2-3 days.

Inductively Coupled Plasma Mass Spectrometry. RWPE1, DuCaP, VCaP, and LNCaP cell lines were grown to 80-90% confluency in their respective media. Cells were collected by

adding 4 mL of trypsin to cells and incubating them at 37°C with 5% CO_2 for 5 minutes. After the incubation period, 8 mL of media were added to quench the trypsin activity and dislodge cells from plate. Cells were placed onto 15 mL conical tubes and centrifuged for 5 minutes at 1200 rpm. The centrifugation step was followed by aspiration of the media out of tube and resuspension in 3-6 mL of media. 20 µL of cells were removed and placed in a 1.5 mL tube. Cells were counted using Trypan Blue (Life Technologies) in a hemocytometer. Approximately 400,000 cells were placed into 15 mL metal-free conical tubes (Life Sciences Products), spun down at 5000 rpm for 2 minutes, and the supernatant was removed. To each tube 200 µL of low grade nitric acid (Fisher Scientific) was added followed by 3 minutes of continuous vortexing. Following the vortex period, tubes were placed in ice for 2 hours, and subsequently 5 mL of Chelex-100 (Sigma Aldrich) treated water was added. Tubes were mixed well and 300 µL of each sample was removed to perform a bicinchoninic *a*cid (BCA) assay to quantify the protein concentration for each sample. Samples were taken to The Laboratory for Environmental and Geological Studies (LEGS) ICP-MS facility for analysis.

X-Ray Fluorescence Microscopy. XRFM studies were performed in collaboration with Dr. Samuel Webb at the Stanford Linear Accelerator Center (SLAC, Palo Alto, CA). Cells were grown in 12-well plates with 100 mesh gold plated formvars (Electron Microscopy Sciences) until cells were close to 100% confluency. Cell coated formvars were then plunged into liquid ethane for approximately 10 seconds followed by storage in a cryogrid with liquid nitrogen. During the time period when formvars with cells were in liquid nitrogen, cyrovials were prepared in liquid nitrogen with 1 mL of 2% anhydrous EM Grade glutaraldehyde diluted in acetone (Electron Microscopy Sciences) and stored at -70°C in liquid nitrogen for 48 hours. After 48 hour incubation, glutaraldehyde was removed from cryovials and formvars were washed with 1 mL of acetone followed by an incubation period of acetone.

To dry samples, the pressure chamber of a *C*ritical *P*oint *D*rying (CPD) apparatus was frozen down to 0°C using short bursts of CO_2(g). After the chamber reached 0°C it was filled to its midpoint with acetone and the element specimen holder with formvars was placed in there. Once formvars were in the chamber, exhaust of CPD was closed and CO_2(g) was turned on for about 3 minutes followed by opening the exhaust, this step was done 3x. This was followed by heating the pressure chamber to 42°C for 5 minutes. After the 5 minute incubation period the exhaust was opened slightly until it reached 200 psi and then the exhaust was fully opened. Samples were taken from the specimen holder and placed in a grid box which was then sealed in a jar with desiccant until samples were taken to the linear accelerator. Schematic of x-ray beam and sample is presented in **Figure 2.1**.

Before taking samples to the linear accelerator we used our Zeiss Axiovert 200M microscope to map out bright field images of the formvars to enable overlay of the x-ray fluorescence image with bright field ones. The XRFM Zn^{2+}-map was collected using the x-ray source on Beam Line 2-3 at the Stanford Synchrotron Radiation Laboratory. The x-ray energy was tuned to 14.2 keV to detect Zn^{2+} and focused on the sample using Kirkpatrick-Baez mirrors. The sample was scanned in the beam using a step size of 1 μm x 1 μm. Zinc was quantified using a strip of high resolution Zinc Telluride (ZT).

Fractionation of Nucleus and Cytosol for ICP-MS. Cells were grown to approximately 90% confluency. Media was removed and cells were briefly washed in 2 mL cold phosphate buffered saline (PBS) pH 7.4 and scrapped off the plate in 2 mL PBS pH 7.4 and placed in ice chilled 2 mL eppendorf tubes. Cells were centrifuged for 5 minutes at 3000 rpm at 4°C, discarding the supernatant. The cell pellet was resuspended in Buffer 1 (0.33M sucrose, 10 mM HEPES pH 7.4, 1.5 mM $MgCl_2$, 10 mM KCl, 0.1% NP-40, protease inhibitor cocktail) and incubated in ice for 30 minutes with occasional pipeting using P200 tips. After ice incubation, tubes were centrifuged at 3000 rpm for 5 minutes at 4°C, and the supernatant (Cytosolic Fraction) was

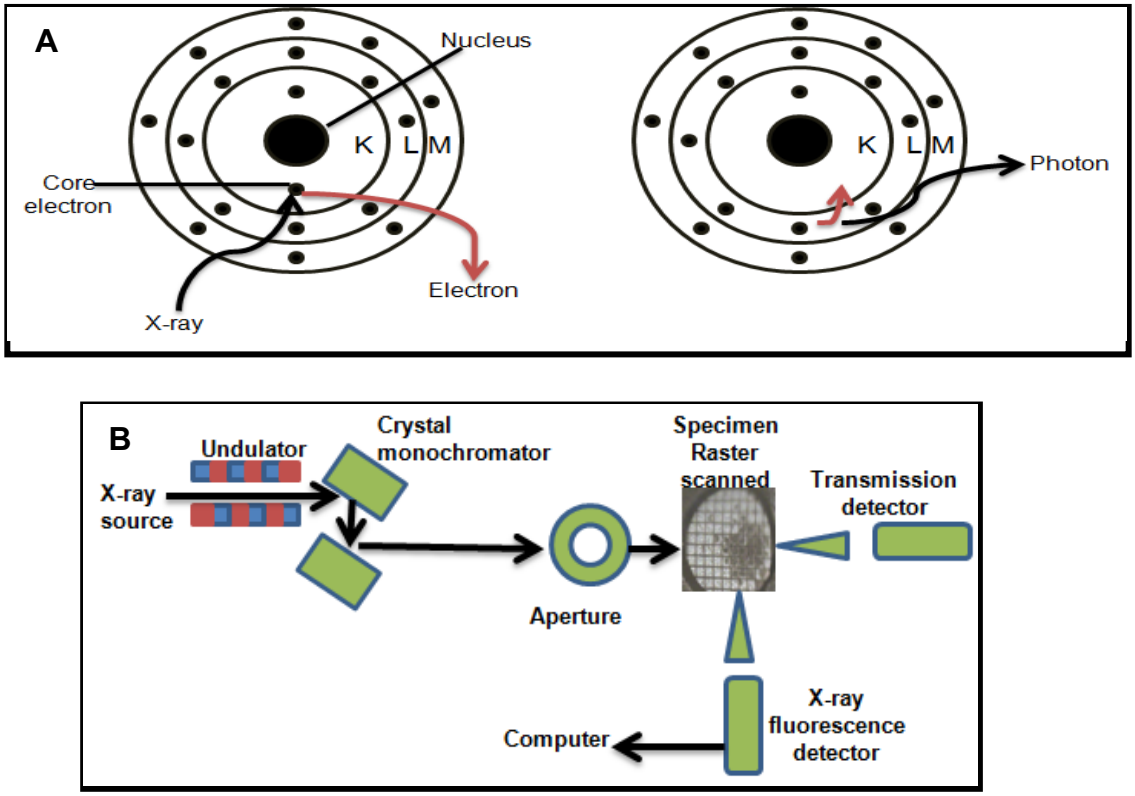

Figure 2.1. X-Ray Fluorescence Microscopy (XRFM) for Measuring Total Zn^{2+}. A) A high energy x-ray beam is tuned to the K-edge shell of Zn^{2+} ejecting a core electron and resulting in emission of a photon of light when an electron from the L-edge shell relaxes to the K-edge. B) Schematic diagram representing how XRFM uses an x-ray source that is focused to a spot on a macroscopic sample. The sample can be moved within the beam resulting in scanning of the beam across the sample to generate a map or image.

collected without disturbing the pellet. The pellet was resuspended in 300 µL of Buffer 1 and placed in ice for 20 minutes, centrifuged at 3000 rpm for 5 minutes at 4°C, discarding the supernatant leaving the pellet as dry as possible. The pellet was resuspended in 300 µL of Buffer 2 (0.45 M NaCl, 10 mM HEPES pH 7.4, 1.5 mM $MgCl_2$, 0.2 mM EDTA pH 8.0, 25% glycerol) and incubated in ice for 1 hour. After incubation tubes were centrifuged at 14,000 rpm for 20 minutes at 4°C, collecting the supernatant (Nuclear Fraction).

For ICP-MS preparation details please refer to above section entitled Inductively Coupled Plasma Mass Spectrometry.

FRET-based Zn^{2+} Sensors. A schematic representation of the type of FRET sensor used in this study is depicted in **Figure 2.2**. **Table 2.1** represents the dual Zn^{2+}-finger amino acid sequence of Zap1 and Zap2. All FRET sensors used to define the free Zn^{2+} concentrations in the cytosol, ER, Golgi, and mitochondria are described in Dittmer *et al.*, Qin *et al.*, and Park *et al.*, (*18-20*). Nuclear localization was accomplished by fusion of the signal sequence (PKKKRKVEDA) to the carboxy terminal end of the ZapCY2 sensor.

Cell Culture and Microscopy. RWPE1, DuCaP, VCaP, and LNCaP cell lines were seeded onto 3.5 cm glass bottom imaging dishes with their respective media and incubated at 37°C with 5% CO_2 until cells were 40-50% confluent. 1 µg of sensor cDNA was transiently transfected using TransIT®-LT1 (Mirus) as specified by manufacturer instructions.

Forty-eight hours after transfection, cells were imaged using phosphate, calcium, and magnesium free HEPES-buffered Hanks' balanced salt solution (HHBSS) media (5.36 mM KCl, 137 mM NaCl, 16.65 mM D-Glucose, and 30 mM HEPES) pH 7.4. This buffer is made in our laboratory because phosphates are known to precipitate Zn^{2+}. Buffer was generated with Chelex-100-treated water (Sigma Aldrich). Cell imaging was performed on a Zeiss Axiovert 200 M microscope with a Cascade 512B CCD camera (Roper Scientific) and xenon arc lamp

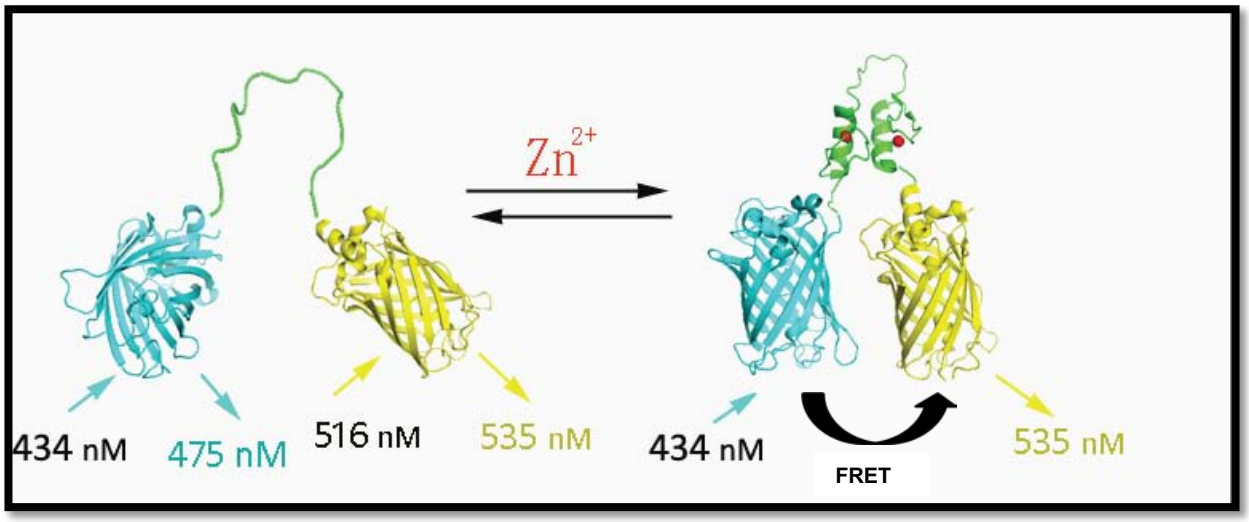

Figure 2.2. Schematic Diagram of a FRET Sensor. The sensor is composed a Cyan Fluorescent Protein (CFP) and the citrine variant of the Yellow Fluorescent Protein (YFP). The Zn^{2+} binding domain is relatively unstructured in the absence of Zn^{2+} and undergoes a conformational change upon Zn^{2+} binding leading to an increase in FRET from the donor CFP to the acceptor YFP.

ZBD	Amino Acid Sequence
Zap1	Zinc Finger1 = KNNDLK**C**KWKE**C**PESCSSLFDLQR**H**LLKD**H**VSQDFKHP Zinc Finger2 = MEPLA**C**NWED**C**DFLGDDTCSIVN**H**INCQ**H**GI
Zap2	Zinc Finger1 = KNNDLK**H**KWKE**C**PESCSSLFDLQR**H**LLKD**H**VSQDFKHP Zinc Finger2 = MEPLA**H**NWED**C**DFLGDDTCSIVN**H**INCQ**H**GI

Table 2.1. Amino acid sequence of Zap Zinc Binding Domains (ZBD) in the ZapCY1 and ZapCY2 sensors

(XBO75) using MetaFluor software (Universal Imaging) to operate the system. CFP (430/24 excitation, 455 dichroic, 470/24 emission), YFP (495/10 excitation, 515 dichroic, 535/25 emission), and YFP FRET (430/24 excitation, 515 dichroic, 535/25 emission) filters were used for the CFP, YFP, and FRET optical channels. All excitation filters, dichroic mirrors, and emission filters were from Chroma Technology or Semrock.

The following settings were used: exposure time 400-600 msec, 20-30 second acquisition rate, 1.3NA 40x oil immersion objective, and excitation light was attenuated with a 10% neutral density filter.

***In situ* FRET Sensor Calibrations.** To calibrate the sensors in cells, a region of interest (ROI) was placed on an individual cell and on an untransfected cell or a region in the field of view with no cells as a measure of the background fluorescence. The FRET channel is defined as the emission intensity in the acceptor fluorescent protein (FP) channel, upon excitation of the donor. The FRET ratio (R) is defined as the background corrected intensity in the FRET channel divided by the background corrected intensity in the donor channel, i.e. $(I_{FRET} - I_{FRETbackground})/(I_{Donor} - I_{donorbackground})$. For imaging experiments, media was removed and cells

were washed twice with HHBSS buffer followed by the addition of 1 mL HHBSS. ROIs were followed for 300 seconds to establish a resting R followed by the addition of 150 μM TPEN (N,N,N',N'-tetrakis-(2-pyridylmethyl)-ethylenediamine) to chelate Zn^{2+} and obtain the FRET ratio of the unbound sensor (R_{TPEN}). Once R_{TPEN} was established, cells were washed 3-times with the HHBSS solution to remove residual TPEN followed by addition of 1 mL of fresh HHBSS. Subsequently, 10 μM $ZnCl_2$ and 7.5 μM digitonin were added to saturate the sensors localized to the nucleus and cytosol and establish the FRET ratio of the Zn^{2+} bound sensor (R_{Zn}). Alternatively, 10 μM $ZnCl_2$ and 750 nM pyrithione were added to saturate the sensors localized to the ER, Golgi, and mitochondria and establish the FRET ratio of the Zn^{2+} bound sensor (R_{Zn}). Data were collected at a 30 sec acquisition rate until Zn^{2+} and digitonin/pyrithione were added, at this point the acquisition rate was changed to 20 sec.

For all experiments the resting R was converted to a Zn^{2+} concentration using the following equation (*21*) and the experimentally derived R, R_{TPEN}, R_{Zn}, and the published K_d' and n values:

$$[Zn^{2+}] = K_{d'} \left(\frac{R - R_{TPEN}}{R_{Zn} - R} \right)^{1/n}$$

Equation 2.1: Equation for converting R into $[Zn^{2+}]$, where 'n' represents the Hill coefficient. For the data reported here, the published values for ZapCY1 (K_d' = 2.5 pM, n = 1.37) and ZapCY2 (K_d' = 811 pM, n = 0.44) were used.

For each experiment, R_{TPEN} and R_{Zn} were determined for each individual cell in the field of view of the microscope.

2.4 Results

2.4.1 Identification of Total Cellular Zinc in Normal vs. Cancerous Prostate Cells

There is a growing consensus that prostate carcinoma is marked by a significant reduction in Zn^{2+} levels. The majority of studies done to date have revealed that prostate cancer exhibits a greater than 50% reduction in total Zn^{2+} (*8-10*). To determine total Zn^{2+} in the recently established prostate cancer cell lines DuCaP and VCaP, we performed ICP-MS to compare the differences between RWPE1 normal prostate cell line and LNCaP, a long traditional cancer cell line model. ICP-MS is a technique that measures total ions, in this case Zn^{2+}, based on a charge to mass ratio (*22, 23*). **Figure 2.3** reveals that DuCaP and VCaP exhibit a marked reduction in Zn^{2+} (ng Zinc/mg protein) by well over 50%. In addition, LNCaP also exhibited a significant depletion in Zn^{2+}, consistent with previous studies (*10*).

To continue characterizing total Zn^{2+} in these cell lines, we performed X-Ray Fluorescence Microscopy (XRFM). This technique detects total Zn^{2+} in fixed cells (i.e. free plus bound Zn^{2+}), but can do so in a spatially resolved manner. In XRFM, a high energy x-ray beam from a synchrotron source is tuned to the K-edge shell of Zn^{2+}, the x-ray beam ejects an electron from the core, resulting in release of a photon of light upon relaxation of an L-edge electron to the K-edge (*24*) as depicted in **Figure 2.1a**. A schematic representation of instrumentation for this experiment is depicted in **Figure 2.1b**. Briefly, the X-ray beam is rastered across the sample to obtain a map of Zn^{2+} across a cell. Zinc in cells was quantified using a strip of high resolution Zinc-Telluride, which is a standard used to compare samples.

To obtain a distribution map of total Zn^{2+} in normal and cancerous prostate cells, cells were grown on gold formvars, flash frozen and freeze dried to preserve cellular structures. After imaging the cells with light microscopy, samples were subjected to XRFM. **Figure 2.4** depicts representative images obtained for LNCaP and RWPE1 cell lines. Unfortunately, DuCaP and VCaP, did not adhere well to formvars and cells were dislodged during the initial plunge freeze. On beam line 2-3 the x-ray beam is focused to a 1µm x 1µm spot and hence is not high enough resolution to distinguish specific organelles, but rather we were able to observe hot spots

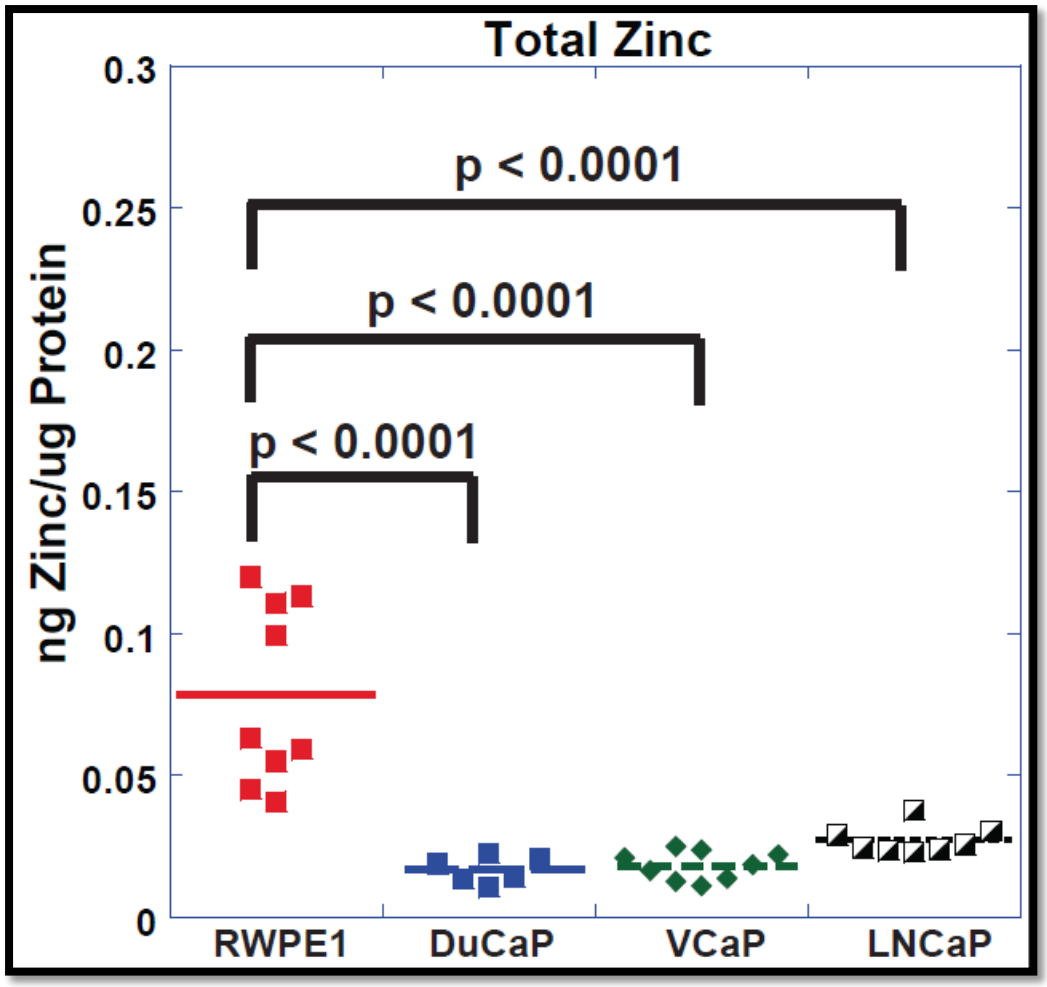

Figure 2.3. ICP-MS of Normal and Cancerous Prostate Cells. Relative levels of total Zn^{2+} (ng Zn^{2+}/µg protein) in prostate cells. Cells were digested in low grade nitric acid and Zn^{2+} was measured by ICP-MS. RWPE cells have significantly higher total Zn^{2+} than cancer cells (ANOVA with Tukey HSD post hoc test). Each data point represents an individual experiment consisting of approximately 400,000 cells per one 10 cm dish of cells.

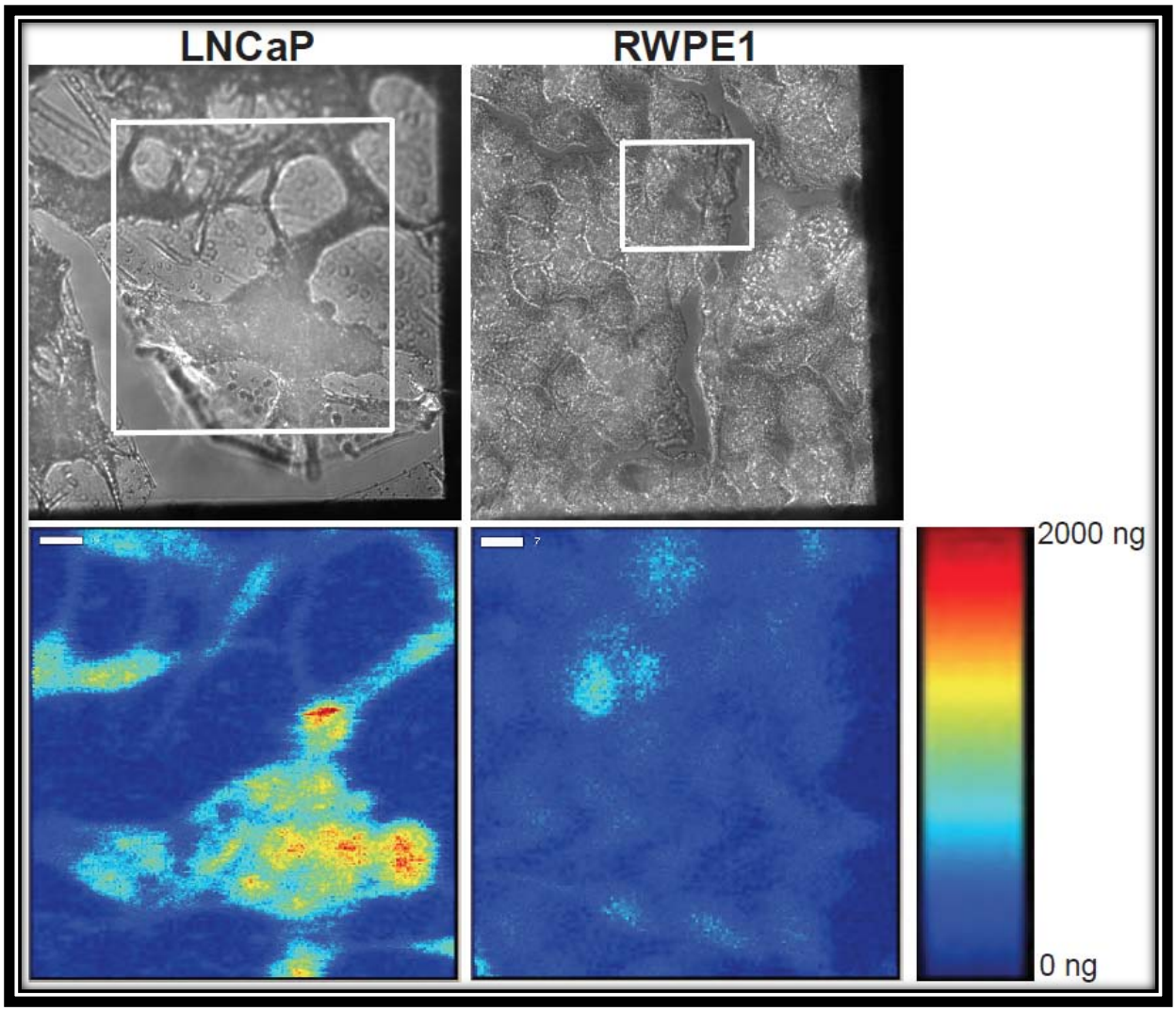

Figure 2.4. XRFM of RWPE1 and LNCaP Cells. Cells were grown on gold formvar and bright field images were taken on a Zeiss Axiovert 200M microscope (top panel). The white box identifies the region over which XRFM data were collected. High energy x-ray source is tuned and focused on sample and rastered across to obtain an elemental map. As depicted in the figure legend to the right, the warmer the color (red) the higher the Zn^{2+} in the area that the x-ray has rastered. Scale bar represents 10 μm.

throughout the cell. Overall, it appeared that LNCaP cells contained higher levels of total Zn^{2+}, but it is important to note that some cellular organelles, such as Zn^{2+} containing vesicles, could not be resolved with this technique. A zoom-in of some LNCaP cells (lower image, **Figure 2.4**) suggested that perhaps the higher Zn^{2+} observed in the prostate cancer cell line was concentrated in the nucleus.

To determine if the LNCaP prostate cancer cell line contained more nuclear Zn^{2+} than RWPE1, cells were fractionated and the nuclear fraction was isolated and subjected to ICP-MS. **Figure 2.5** demonstrates that the nucleus of LNCaP cancer cell line contains higher total Zn^{2+} than that of RWPE1 normal cell line, corroborating the XRFM results. To our knowledge this is the first study in which total nuclear Zn^{2+} has been measured and compared amongst a normal and cancerous cell line. Intriguingly, although the cancer cell line exhibits a significant reduction in total Zn^{2+}, the nucleus contains elevated Zn^{2+}, indicating that prostate cancer is not simply marked by Zn^{2+} depletion, but rather there is redistribution of Zn^{2+}, suggested more widespread dysregulation of Zn^{2+} homeostasis.

2.4.2 Mapping of free Zn^{2+} in living cells

To quantify and map out the differences in free Zn^{2+} between normal and cancerous prostate cells, high affinity FRET sensors that target specific compartments in the cell were used. The overall FRET sensor schematic is depicted in **Figure 2.2**. This model consists of a Zn^{2+}-binding domain (Zap1 or Zap2, **Table 2.1**) and two fluorescent proteins, cyan fluorescent protein (CFP) and citrine fluorescent protein (YFP). Zn^{2+} binding to the Zap domain leads to an increase in energy transfer from CFP to YFP, thereby increasing the FRET ratio ($\frac{YFP\ FRET_{Em}}{CFP_{Em}}$). To map Zn^{2+} in distinct locations, the ZapCY1 or ZapCY2 sensor was genetically targeted to organelles as described previously (*18, 19*). **Figure 2.6** demonstrates nucleus, cytosol, ER, and mitochondria sensor localization in the VCaP cell line. Because ZapCY1 was saturated at rest

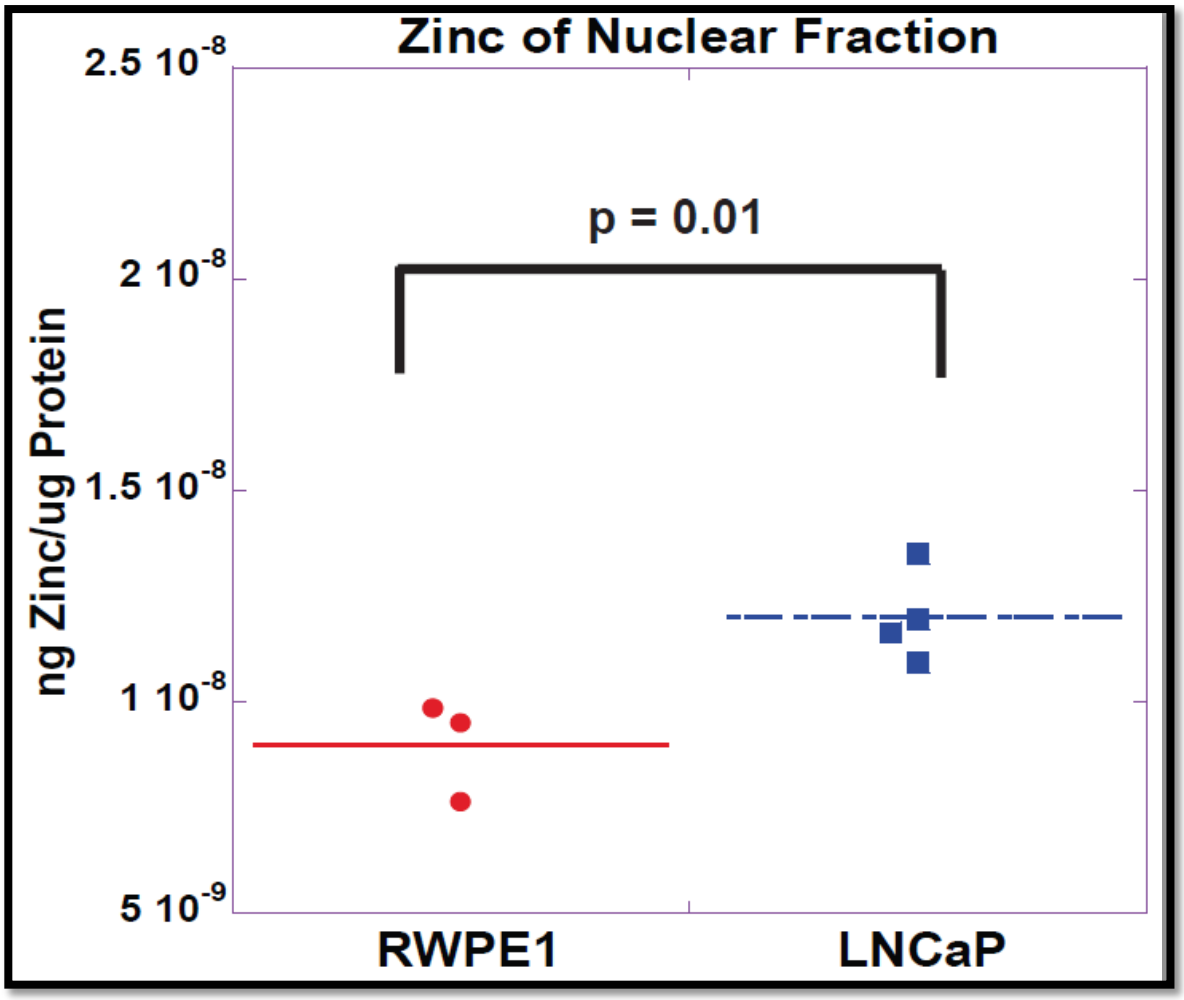

Figure 2.5. ICP-MS of Nuclear Fractions. Cells were fractionated to separate the nucleus and the cytosol to measure the total nuclear Zn^{2+} content by ICP-MS. Total Zn^{2+} as reported by ng Zn^{2+}/µg protein, is shown in figure and this data corroborates with XRFM data in which nucleus of LNCaP contains more Zn^{2+} compared to RWPE1 cell line. Each data point represents an individual experiment and ANOVA with Tukey HSD post hoc test was performed.

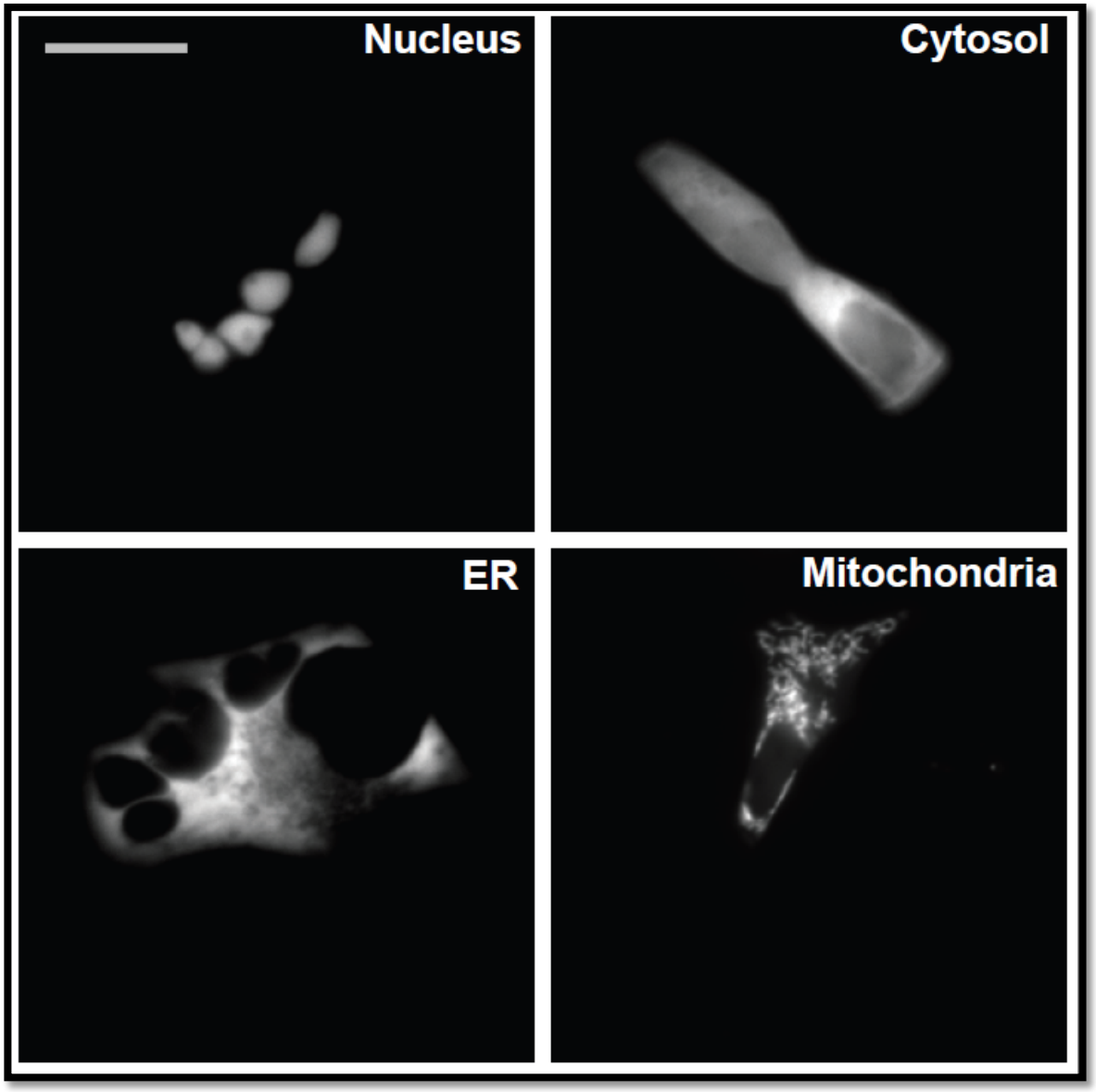

Figure 2.6. Representative Images of FRET Sensor Localization in VCaP Cells. The following sensors were used: NLS-ZapCY2 (nucleus), NES-ZapCY2 (cytosol), ER-ZapCY1 (ER), and mitoZapCY1 (mitochondria). All images depict the FRET channel. Scale Bar = 25 μm.

in the cytosol (*19*), we used the lower affinity ZapCY2 in the nucleus and cytosol. For the ER, Golgi, and mitochondria we used the high affinity ZapCY1 (*18, 19*). The sensors exhibited similar localization in the other cell lines (data not shown).

To quantify free Zn^{2+} in cellular compartments, sensors were calibrated in situ using the approach outlined in Experimental Methods. **Figure 2.7** depicts representative calibrations for the VCaP cell line, demonstrating that treatment with a Zn^{2+} chelator led to a decrease in the FRET ratio, while elevating Zn^{2+} with a membrane permeabilization agent or an ionophore led to an increase in the FRET ratio, as expected. Other cell lines exhibited analogous behavior when subjected to *in situ* calibrations (data not shown).

Using our panel of genetically targeted sensors, we quantified the concentration of free Zn^{2+} in the nucleus, cytosol, ER, and mitochondria using Equation 2.1 and the experimentally determined R, R_{TPEN}, and R_{Zn}, and the published $K_{d'}$ and n values. The results are presented in **Figure 2.8**. Our data reveal that in the cytosol of DuCaP, VCaP, and LNCaP cancer cell lines free Zn^{2+} is 100-300 pM compared to 60 pM in normal RWPE1 cell lines. There results demonstrate that the free Zn^{2+} levels in the cytosol of all three prostate cancer cell line models is about 2-5 times higher compared to normal cell line. The nucleus of DuCaP, VCaP, and LNCaP cancer cell lines free Zn^{2+} is 250-400 pM compared to the RWPE1 normal cell line which is 97 pM. Therefore in the nucleus we observed that in all three prostate cancer cell lines the free Zn^{2+} levels are 2.5-4 times higher than the normal cell line.

Quantification of the free Zn^{2+} in the ER revealed that the free Zn^{2+} content is 5.4 pM in normal cell line compared to DuCaP (1.1 pM), VCaP (0.7 pM), and LNCaP (0.9 pM). Thus, the free Zn^{2+} level in RWPE1 is about 4 times higher than all three prostate cancer cell line models. In addition, mitochondria of the normal RWPE1 cells contain 4.6 pM free Zn^{2+} versus DuCaP

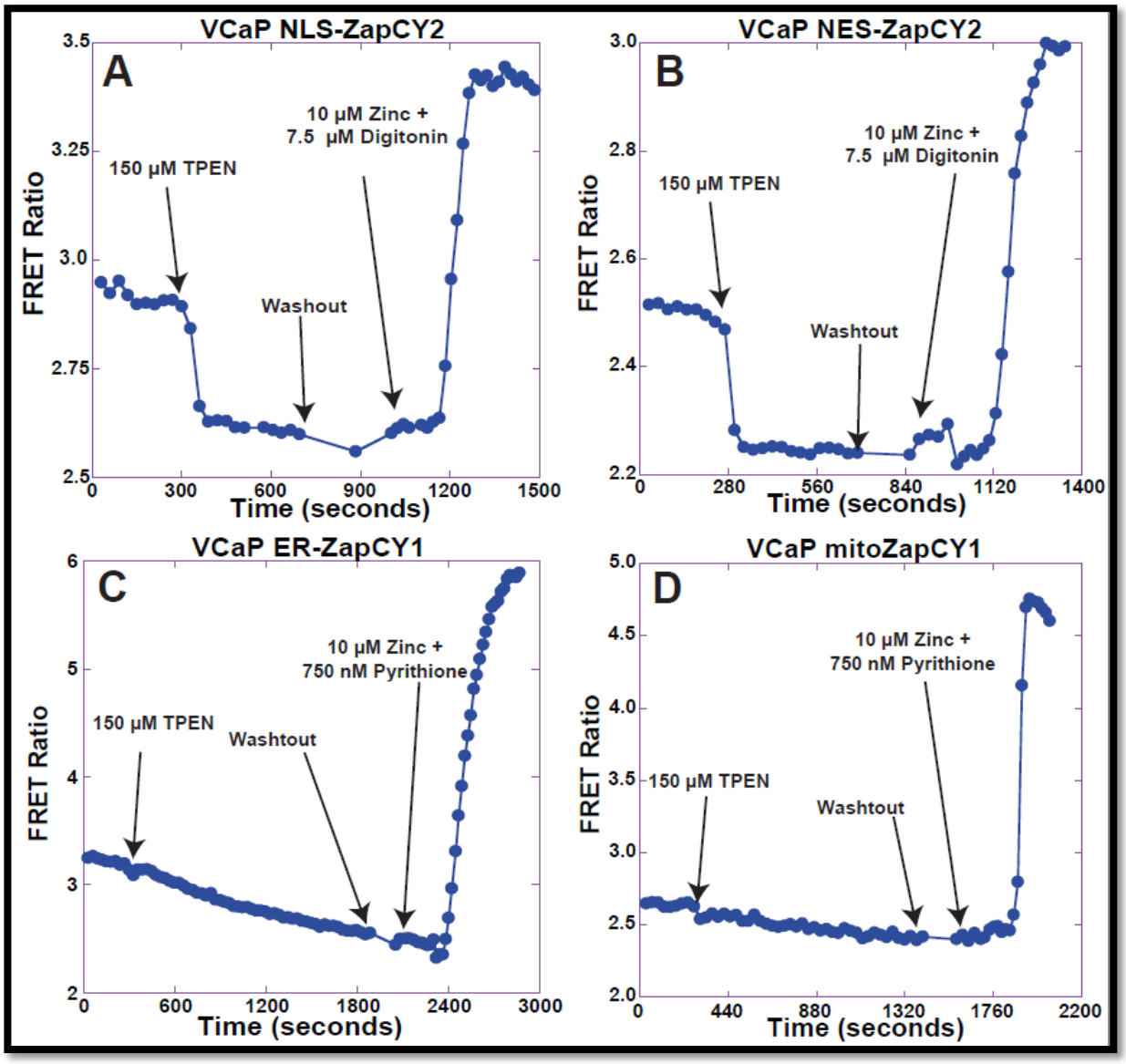

Figure 2.7. Representative *in situ* Calibration of Localized Sensors in VCaP. A) Nuclear Zn^{2+} measured using NLS-ZapCY2, B) Cytosolic Zn^{2+} measure using NES-ZapCY2, C) ER Zn^{2+} measured using ER-ZapCY1, D) Mitochondria Zn^{2+} measured using ER-ZapCY1. To calibrate these sensors the region of interest is followed for 300 seconds followed by the addition of 150 μM TPEN to chelate Zn^{2+}. Once minimum FRET ratio is established TPEN is washed out and subsequently 10 μM Zn^{2+} with 7.5 μM Digitonin (for nucleus and cytosol) or 750 nM Pyrithione (ER and mitochondria) permeant is added to saturate the sensor and obtain a maximum FRET ratio.

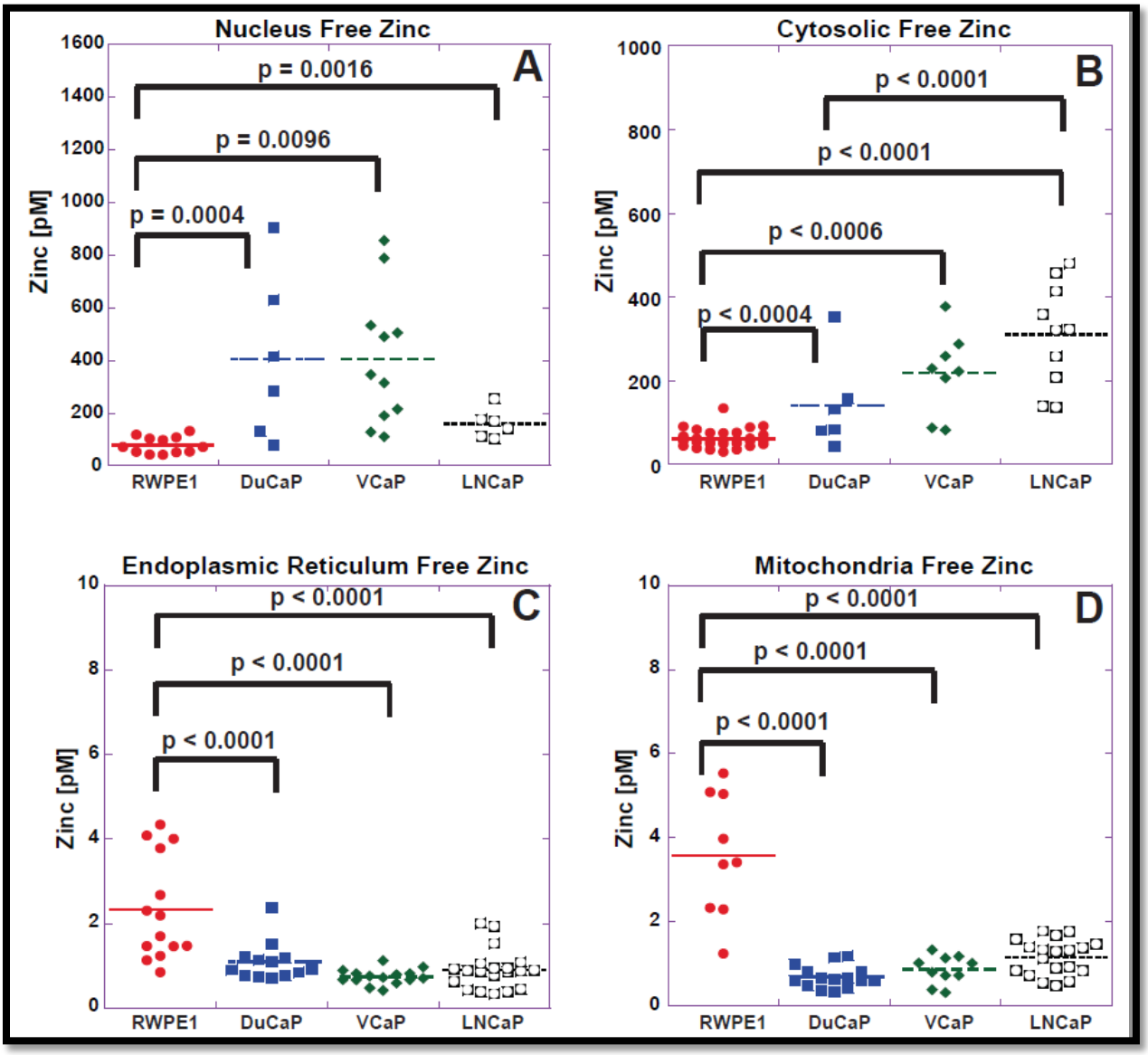

Figure 2.8. Free Zinc Concentration in Nucleus, Cytosol, ER, and Mitochondria In Normal Versus Cancerous Cell Lines. A) Concentration of free Zn^{2+} in the nucleus, B) Concentration of free Zn^{2+} in the cytosol, C) Concentration of free Zn^{2+} in the ER, D) Concentration of free Zn^{2+} the mitochondria. In the nucleus and cytosol the free Zn^{2+} concentration is higher in the prostate cancer cell lines (DuCaP, VCaP, and LNCaP) compared to normal prostate RWPE1 cell line. In the ER and mitochondria the free Zn^{2+} concentration is lower in all three prostate cancer cell lines in comparison to RWPE1. Each data point represents an individual cell and the data were compiled from a minimum of 4 separate experiments. ANOVA with Tukey HSD post hoc test was performed.

(0.8 pM), VCaP (0.8 pM), and LNCaP (1.2 pM) cancer cells, revealing 3-4 times higher Zn^{2+} in the normal cells compared to all three prostate cancer cell lines.

We attempted to quantify Zn^{2+} in the Golgi using Golgi-ZapCY1, but our calibrations revealed that the sensor was saturated at rest in all four cell lines (data not shown). As an alternate approach the lower affinity ZapCY2 was targeted to the Golgi but transfections routinely failed to result in Golgi-localized fluorescence.

2.5 Discussion

Prostate cancer is one of the most common cancers in men (*25*) and it is accompanied by a high degree of metastasis to bone (*25, 26*), which correlate with DuCaP and VCaP cancer cell line site of metastasis. Malignant cells in the prostate begin to migrate after matrix metalloproteases degrade the extracellular matrix in localized prostate cancer, allowing cells to travel through the blood stream invading bone and metastising (*25-28*). However, the exact molecular mechanism of how prostate cancer arises is still unknown, and clinical diagnostic and prognostic markers are flawed. Diagnostic detection is primarily based on regular examinations in which the patient undergoes blood treatment to detect PSA levels. However, over the last few years the value of PSA as a screening method for prostate cancer has diminished due to the over diagnosis of this disease (*29*). In the last 15 years, more and more studies have revealed that there is a significant reduction of Zn^{2+} that may correlate with disease progression (*11, 30, 31*). But to evaluate Zn^{2+} as a potential diagnostic or prognostic marker, it is important to have a better understanding of how and why Zn^{2+} is altered in prostate cancer. To date it is still unclear how prostate cells lose their Zn^{2+} and most importantly it is still unclear whether the reduction has consequences for cancer progression.

In this study we set out to define the nature of Zn^{2+} dysregulation in prostate cancer by measuring total Zn^{2+} and generating quantitative maps of the distribution of free Zn^{2+} amongst

intracellular pools. In addition, we characterized two recently developed prostate cancer cell lines DuCap and VCaP. These cell lines were chosen because of the high degree chromosomal and structural abnormalities, comparable to those observed in late-stage metastatic tumors, thus adding a more diverse molecular profile to the repertoire of prostate cancer cell lines. In addition, our initial studies revealed that they were depleted of over 50% total Zn^{2+}, suggesting they would be good models to study the cellular and molecular mechanisms for Zn^{2+} dysregulation in prostate cancer.

Although all three prostate cancer cell lines used in this study were characterized by over 50% reduction in total cellular Zn^{2+}, surprisingly we discovered this reduction did not translate into across-the-board deficiency in intracellular Zn^{2+} stores, but rather there was substantial redistribution of Zn^{2+} between subcellular locations. XRFM provided the first initial suggestion that total nuclear Zn^{2+} might be higher in the LNCaP cancer cell line compared to the normal RWPE1 cell line and this was corroborated by ICP-MS on nuclear fractions. In addition, live cell imaging of free Zn^{2+} revealed that the nucleus and the cytosol of the DuCaP, VCaP, and LNCaP cancer cell lines have 2-5x and 0.5-2.5x, respectively higher Zn^{2+} levels than the RWPE1 normal cell line.

To date there have been few studies that have revealed or quantified Zn^{2+} in either the nucleus and cytosol. In our current studies we have elucidated that prostate cancer cell lines are depleted of total Zn^{2+} but free Zn^{2+} levels in these cell lines is elevated in the cytosol and nucleus. In the cytosol there are a large number of proteins that buffer Zn^{2+} such as metallothionein, which has 17 mammalian isoforms (*32*). Some of these isoforms may be over-expressed in DuCaP, VCaP, and LNCaP cancer cell lines leading to the high free Zn^{2+} concentration in prostate cancer compared to normal cell line RWPE1. In addition, elevated Zn^{2+} has been proposed to inhibit apoptosis thereby increasing the proliferation rate of cells (*33,*

34). Elucidating the expression levels of metallothionein between normal and prostate cancer cell lines could explain the difference in a higher Zn^{2+} pool in the cytosol of these cells.

We revealed a similar scenario in the nucleus of these prostate cancer cell lines in which the free Zn^{2+} pool is higher compared to RWPE1 normal cell line. This could be because Zn^{2+} handling and buffering might be different in the nucleus versus the cytosol. In the nucleus there is a large repertoire of transcription factors that bind Zn^{2+} (*5*). Previous studies have shown that approximately 25% of total Zn^{2+} is found in the nuclei of rat liver cells (*35*). In addition, Zn^{2+} is bound to chromatin which is the stable complex of DNA and plays a role in DNA replication, transcription, and repair (*36*). One possible consequence of elevated pools of Zn^{2+} found in the nucleus is that it ensures metallation of the nuclear machinery to aid uncontrolled division.

In the ER and mitochondria all three prostate cancer cell lines have a significant reduction in the free Zn^{2+} pool compared to the RWPE1 normal cell line. The mitochondria is the power house of the cell and the site for synthesis of adenosine triphosphate (ATP) (*37*). In a previous study, mitochondria of prostate cells were isolated using a sucrose gradient and it was revealed that Zn^{2+} was able to inhibit m-aconitase. Because m-aconitase converts citrate to isocitrate, producing more ATP per each Krebs cycle (*2, 38*), it was suggested that depletion of Zn^{2+} in the mitochondria would lead to more efficient energy generation, thus fueling cancer cells. In our current studies we determined that the free Zn^{2+} pool is in the low pM range, which is well below to estimated K_I for inhibition of m-aconitase. To assess whether Zn^{2+} depletion indeed impacts energy production, it will be necessary to determine the amount of ATP production in these cells and compare the results among all four cell lines. While the free Zn^{2+} pool is low in the prostate cancer cell line models very little is known about how Zn^{2+} enters the mitochondria. In a more recent study Zn^{2+} was shown to inhibit cytochrome *c* release from the mitochondria by the direct binding of Zn^{2+} to H_2O_2 (Zn^{2+}-H_2O_2) (*39*).

In the ER we observed that there is a 2-3 fold reduction in Zn^{2+} from normal to cancer cells which may lead to the improper folding of some proteins. In the ER it has been found that

the Zn^{2+} is transported into the compartment via the ZnT5 importer while it is exported via the hZIP7 transporter (*40, 41*). However, very little is known about Zn^{2+} in the ER of prostate cells. To determine if either ZnT5 or hZIP7 are connected with the low levels of Zn^{2+} in the ER of prostate cancer cells it would be necessary to over-express ZnT5 and test whether this manipulation causes Zn^{2+} to be elevated to similar levels of normal prostate cancer cell line. Stress to cells induces the unfolded protein response (UPR) in the ER and this has been implicated to tumor progression as well as inflammatory bowel disease, bacterial translocation, and inflammatory response (*42-45*). The UPR and tumor progression could be directly correlated with the low Zn^{2+} in our prostate cancer cell lines models because in HeLa cell line chelating Zn^{2+} with 4-5 μM TPEN for 12 hours induced the UPR response (*46*).

The current study has revealed significant perturbations in Zn^{2+} between normal and cancerous prostate cells. But it is still unclear how or why these changes arise and what implications they have for cancer progression. The widespread redistribution in Zn^{2+} suggests substantial changes in Zn^{2+} homeostasis and therefore likely are targets are Zn^{2+} regulatory proteins such as transporters, buffers, and Zn^{2+}-binding proteins. Indeed, there are a number of studies suggesting systematic alterations in Zn^{2+} transporter levels in prostate cancer (*9, 10, 47-50*). But how such changes influence total and free Zn^{2+} has yet to be defined.

2.6 References

1. Kelleher, S. L., McCormick, N. H., Velasquez, V., and Lopez, V. (2011) Zinc in specialized secretory tissues: roles in the pancreas, prostate, and mammary gland, *Adv Nutr 2*, 101-111.
2. Costello, L. C., and Franklin, R. B. (1998) Novel role of zinc in the regulation of prostate citrate metabolism and its implications in prostate cancer, *Prostate 35*, 285-296.

3. Auld, D. S. (2001) Zinc coordination sphere in biochemical zinc sites, *Biometals 14*, 271-313.

4. Frederickson, C. J., Koh, J. Y., and Bush, A. I. (2005) The neurobiology of zinc in health and disease, *Nat Rev Neurosci 6*, 449-462.

5. Nies, D. H. (2007) Biochemistry. How cells control zinc homeostasis, *Science 317*, 1695-1696.

6. Zalewski, P. D., Millard, S. H., Forbes, I. J., Kapaniris, O., Slavotinek, A., Betts, W. H., Ward, A. D., Lincoln, S. F., and Mahadevan, I. (1994) Video image analysis of labile zinc in viable pancreatic islet cells using a specific fluorescent probe for zinc, *J Histochem Cytochem 42*, 877-884.

7. Sorensen, M. B., Stoltenberg, M., Juhl, S., Danscher, G., and Ernst, E. (1997) Ultrastructural localization of zinc ions in the rat prostate: an autometallographic study, *Prostate 31*, 125-130.

8. Feustel, A., and Wennrich, R. (1984) Determination of the distribution of zinc and cadmium in cellular fractions of BPH, normal prostate and prostatic cancers of different histologies by atomic and laser absorption spectrometry in tissue slices, *Urol Res 12*, 253-256.

9. Franklin, R. B., Feng, P., Milon, B., Desouki, M. M., Singh, K. K., Kajdacsy-Balla, A., Bagasra, O., and Costello, L. C. (2005) hZIP1 zinc uptake transporter down regulation and zinc depletion in prostate cancer, *Mol Cancer 4*, 32.

10. Huang, L., Kirschke, C. P., and Zhang, Y. (2006) Decreased intracellular zinc in human tumorigenic prostate epithelial cells: a possible role in prostate cancer progression, *Cancer Cell Int 6*, 10.

11. Rosoff, B. (1981) Studies of zinc in normal and neoplastic prostatic tissues, *Prog Clin Biol Res 75A*, 447-457.

12. Korenchuk, S., Lehr, J. E., L, M. C., Lee, Y. G., Whitney, S., Vessella, R., Lin, D. L., and Pienta, K. J. (2001) VCaP, a cell-based model system of human prostate cancer, *In Vivo 15*, 163-168.

13. Lee, Y. G., Korenchuk, S., Lehr, J., Whitney, S., Vessela, R., and Pienta, K. J. (2001) Establishment and characterization of a new human prostatic cancer cell line: DuCaP, *In Vivo 15*, 157-162.

14. van Bokhoven, A., Caires, A., Maria, M. D., Schulte, A. P., Lucia, M. S., Nordeen, S. K., Miller, G. J., and Varella-Garcia, M. (2003) Spectral karyotype (SKY) analysis of human prostate carcinoma cell lines, *Prostate 57*, 226-244.

15. van Bokhoven, A., Varella-Garcia, M., Korch, C., Johannes, W. U., Smith, E. E., Miller, H. L., Nordeen, S. K., Miller, G. J., and Lucia, M. S. (2003) Molecular characterization of human prostate carcinoma cell lines, *Prostate 57*, 205-225.

16. Horoszewicz, J. S., Leong, S. S., Kawinski, E., Karr, J. P., Rosenthal, H., Chu, T. M., Mirand, E. A., and Murphy, G. P. (1983) LNCaP model of human prostatic carcinoma, *Cancer Res 43*, 1809-1818.

17. Bello, D., Webber, M. M., Kleinman, H. K., Wartinger, D. D., and Rhim, J. S. (1997) Androgen responsive adult human prostatic epithelial cell lines immortalized by human papillomavirus 18, *Carcinogenesis 18*, 1215-1223.

18. Park, J. G., Qin, Y., Galati, D. F., and Palmer, A. E. (2012) New Sensors for Quantitative Measurement of Mitochondrial Zn(2+), *ACS Chem Biol*.

19. Qin, Y., Dittmer, P. J., Park, J. G., Jansen, K. B., and Palmer, A. E. (2011) Measuring steady-state and dynamic endoplasmic reticulum and Golgi Zn2+ with genetically encoded sensors, *Proc Natl Acad Sci U S A 108*, 7351-7356.

20. Dittmer, P. J., Miranda, J. G., Gorski, J. A., and Palmer, A. E. (2009) Genetically encoded sensors to elucidate spatial distribution of cellular zinc, *J Biol Chem 284*, 16289-16297.

21. Grynkiewicz, G., Poenie, M., and Tsien, R. Y. (1985) A new generation of Ca2+ indicators with greatly improved fluorescence properties, *J Biol Chem 260*, 3440-3450.

22. Ammann, A. A. (2007) Inductively coupled plasma mass spectrometry (ICP MS): a versatile tool, *J Mass Spectrom 42*, 419-427.

23. Moor, C., Devos, W., Guecheva, M., and Kobler, J. (2000) Inductively coupled plasma mass spectrometry: a versatile tool for a variety of different tasks, *Fresenius J Anal Chem 366*, 159-164.

24. Fahrni, C. J. (2007) Biological applications of X-ray fluorescence microscopy: exploring the subcellular topography and speciation of transition metals, *Curr Opin Chem Biol 11*, 121-127.

25. Dasgupta, S., Srinidhi, S., and Vishwanatha, J. K. (2012) Oncogenic activation in prostate cancer progression and metastasis: Molecular insights and future challenges, *J Carcinog 11*, 4.

26. Ye, L., Kynaston, H. G., and Jiang, W. G. (2007) Bone metastasis in prostate cancer: molecular and cellular mechanisms (Review), *Int J Mol Med 20*, 103-111.

27. Cooper, C. R., Chay, C. H., Gendernalik, J. D., Lee, H. L., Bhatia, J., Taichman, R. S., McCauley, L. K., Keller, E. T., and Pienta, K. J. (2003) Stromal factors involved in prostate carcinoma metastasis to bone, *Cancer 97*, 739-747.

28. Raubenheimer, E. J., and Noffke, C. E. (2006) Pathogenesis of bone metastasis: a review, *J Oral Pathol Med 35*, 129-135.

29. Etzioni, R., Penson, D. F., Legler, J. M., di Tommaso, D., Boer, R., Gann, P. H., and Feuer, E. J. (2002) Overdiagnosis due to prostate-specific antigen screening: lessons from U.S. prostate cancer incidence trends, *J Natl Cancer Inst 94*, 981-990.

30. Costello, L. C., and Franklin, R. B. (2011) Zinc is decreased in prostate cancer: an established relationship of prostate cancer!, *J Biol Inorg Chem 16*, 3-8.

31. Liang, J. Y., Liu, Y. Y., Zou, J., Franklin, R. B., Costello, L. C., and Feng, P. (1999) Inhibitory effect of zinc on human prostatic carcinoma cell growth, *Prostate 40*, 200-207.

32. Coyle, P., Philcox, J. C., Carey, L. C., and Rofe, A. M. (2002) Metallothionein: the multipurpose protein, *Cell Mol Life Sci 59*, 627-647.

33. Zalewski, P. D., Forbes, I. J., and Betts, W. H. (1993) Correlation of apoptosis with change in intracellular labile Zn(II) using zinquin [(2-methyl-8-p-toluenesulphonamido-6-quinolyloxy)acetic acid], a new specific fluorescent probe for Zn(II), *Biochem J 296 (Pt 2)*, 403-408.

34. Zalewski, P. D., Forbes, I. J., and Giannakis, C. (1991) Physiological role for zinc in prevention of apoptosis (gene-directed death), *Biochem Int 24*, 1093-1101.

35. Cousins, R. J. (1998) A role of zinc in the regulation of gene expression, *Proc Nutr Soc 57*, 307-311.

36. Falchuk, K. H. (1998) The molecular basis for the role of zinc in developmental biology, *Mol Cell Biochem 188*, 41-48.

37. Finkel, T., and Hwang, P. M. (2009) The Krebs cycle meets the cell cycle: mitochondria and the G1-S transition, *Proc Natl Acad Sci U S A 106*, 11825-11826.

38. Costello, L. C., Liu, Y., Franklin, R. B., and Kennedy, M. C. (1997) Zinc inhibition of mitochondrial aconitase and its importance in citrate metabolism of prostate epithelial cells, *J Biol Chem 272*, 28875-28881.

39. Liang, D., Yang, M., Guo, B., Cao, J., Yang, L., Guo, X., Li, Y., and Gao, Z. (2012) Zinc inhibits H(2)O(2)-induced MC3T3-E1 cells apoptosis via MAPK and PI3K/AKT pathways, *Biol Trace Elem Res 148*, 420-429.

40. Lichten, L. A., and Cousins, R. J. (2009) Mammalian zinc transporters: nutritional and physiologic regulation, *Annu Rev Nutr 29*, 153-176.

41. Thornton, J. K., Taylor, K. M., Ford, D., and Valentine, R. A. (2011) Differential subcellular localization of the splice variants of the zinc transporter ZnT5 is dictated by the different C-terminal regions, *PLoS One 6*, e23878.

42. Diehl, J. A., Fuchs, S. Y., and Koumenis, C. (2011) The cell biology of the unfolded protein response, *Gastroenterology 141*, 38-41, 41 e31-32.

43. Grootjans, J., Hodin, C. M., de Haan, J. J., Derikx, J. P., Rouschop, K. M., Verheyen, F. K., van Dam, R. M., Dejong, C. H., Buurman, W. A., and Lenaerts, K. (2011) Level of activation of the unfolded protein response correlates with Paneth cell apoptosis in human small intestine exposed to ischemia/reperfusion, *Gastroenterology 140*, 529-539 e523.

44. Kaser, A., Lee, A. H., Franke, A., Glickman, J. N., Zeissig, S., Tilg, H., Nieuwenhuis, E. E., Higgins, D. E., Schreiber, S., Glimcher, L. H., and Blumberg, R. S. (2008) XBP1 links ER stress to intestinal inflammation and confers genetic risk for human inflammatory bowel disease, *Cell 134*, 743-756.

45. Kaser, A., Tomczak, M., and Blumberg, R. S. (2011) "ER stress(ed out)!": Paneth cells and ischemia-reperfusion injury of the small intestine, *Gastroenterology 140*, 393-396.

46. Ellis, C. D., Wang, F., MacDiarmid, C. W., Clark, S., Lyons, T., and Eide, D. J. (2004) Zinc and the Msc2 zinc transporter protein are required for endoplasmic reticulum function, *J Cell Biol 166*, 325-335.

47. Albrecht, A. L., Somji, S., Sens, M. A., Sens, D. A., and Garrett, S. H. (2008) Zinc transporter mRNA expression in the RWPE-1 human prostate epithelial cell line, *Biometals 21*, 405-416.

48. Chen, Q. G., Zhang, Z., Yang, Q., Shan, G. Y., Yu, X. Y., and Kong, C. Z. (2011) The role of zinc transporter ZIP4 in prostate carcinoma, *Urol Oncol*.

49. Henshall, S. M., Afar, D. E., Rasiah, K. K., Horvath, L. G., Gish, K., Caras, I., Ramakrishnan, V., Wong, M., Jeffry, U., Kench, J. G., Quinn, D. I., Turner, J. J.,

Delprado, W., Lee, C. S., Golovsky, D., Brenner, P. C., O'Neill, G. F., Kooner, R., Stricker, P. D., Grygiel, J. J., Mack, D. H., and Sutherland, R. L. (2003) Expression of the zinc transporter ZnT4 is decreased in the progression from early prostate disease to invasive prostate cancer, *Oncogene 22*, 6005-6012.

50. Tepaamorndech, S., Huang, L., and Kirschke, C. P. (2011) A null-mutation in the Znt7 gene accelerates prostate tumor formation in a transgenic adenocarcinoma mouse prostate model, *Cancer Lett 308*, 33-42.

Chapter III

Profiling Expression Levels and Localization of Zinc Transporters in Prostate Cancer Cells

3.1 Abstract

The prostate has the highest concentration of Zn^{2+} in the human body compared to other tissues and transformation from normal to cancerous prostate tissue is marked by a significant depletion in total Zn^{2+}. The mechanistic correlation between malignancy and Zn^{2+} levels is not well understood. To date 24 Zn^{2+} transporters have been identified. The two classes of transporters are the *Z*rt-, *I*rt-like *P*roteins (ZIP) and *C*ation *D*iffusion *F*acilitators (CDF) also referred to as ZnTs. The ZIP family Zn^{2+} transporters move Zn^{2+} from the extracellular space into the cytosol and from inside organelles to the cytosol. On the other hand, the ZnT family transporters move Zn^{2+} from the cytosol to the extracellular space as well as from the cytosol into organelles. In an effort to define how and why Zn^{2+} is depleted in prostate cancer, we establish the changes in expression levels of hZIP1, hZIP2, hZIP3, ZnT1, ZnT2, ZnT4, and ZnT7 Zn^{2+} transporters in a normal prostate cell line (RWPE1) and three prostate cancer cell lines (DuCaP, VCaP, and LNCaP). DuCaP and VCaP are newly established prostate carcinoma cell lines with different molecular characteristics than LNCaP and significant chromosomal abnormalities that resemble metastatic prostate carcinoma. We examined the mRNA and protein expression levels of the Zn^{2+} transporters mentioned above by quantitative RT-PCR and western blotting respectively, and defined their localization by immunofluorescence. Our data suggest that the regulation of these Zn^{2+} transporters is altered from normal to cancerous cell lines.

3.2 Introduction

Zinc is the second most abundant transition metal in the human body and is critical for transcription factors, immune function, and neurotransmission (*1-3*). It is estimated that the total concentration of Zn^{2+} in mammalian cells is about 0.1-0.5 mM (*4, 5*). Although the majority of

cellular Zn^{2+} is bound by proteins, enzymes, and cellular ligands, labile pools have been identified in pancreatic islets cells (*6*), brain (*2*), and prostate (*7*).

Peripheral zone prostate tissue accumulates the highest Zn^{2+} levels in the body compared to other soft tissues (*7-9*). This zone is also the primary region that undergoes malignant transformation and peripheral zone carcinomas are more invasive than those originating from the transition zone (*10*). Numerous studies have revealed that cancerous prostate tissue exhibits dramatically reduced levels of Zn^{2+} (60-70% lower than in the normal peripheral zone) and that the levels of Zn^{2+} appear to track with progression from benign to invasive and metastatic cancers (*8, 11-13*). The mechanistic correlation between malignancy and Zn^{2+} levels is not well understood and in particular, it is not clear whether Zn^{2+} depletion contributes to or is a consequence of disease progression.

Cellular Zn^{2+} is regulated in part via transporters that are localized both in the plasma membrane and organelles. These transporters, which include the *Z*rt-, *I*rt-like *P*roteins (ZIP) and *C*ation *D*iffusion *F*acilitators (CDF, also referred to as ZnT) move Zn^{2+} in and out of the cell as well as store it in different compartments (*5, 14*). Zinc transporters maintain Zn^{2+} at constant homeostatic levels and hence have been the target of a handful of studies to identify the origin of Zn^{2+} depletion in prostate cancer. To date 24 Zn^{2+} transporters have been identified, including 10 ZnTs and 14 ZIPs. Some transporters are found in all tissues, while others are tissue specific (*5, 14, 15*). A schematic representation of some Zn^{2+} transporter localization is depicted in **Figure 3.1** In this work we focus on a subset of these transporters (ZnT1, ZnT2, ZnT4, ZnT7, hZIP1, hZIP2, hZIP3a, and hZIP3b) which have been implicated in or suggested to be involved in Zn^{2+} regulation in prostate cells. The rationale for selecting these transporters is highlighted below.

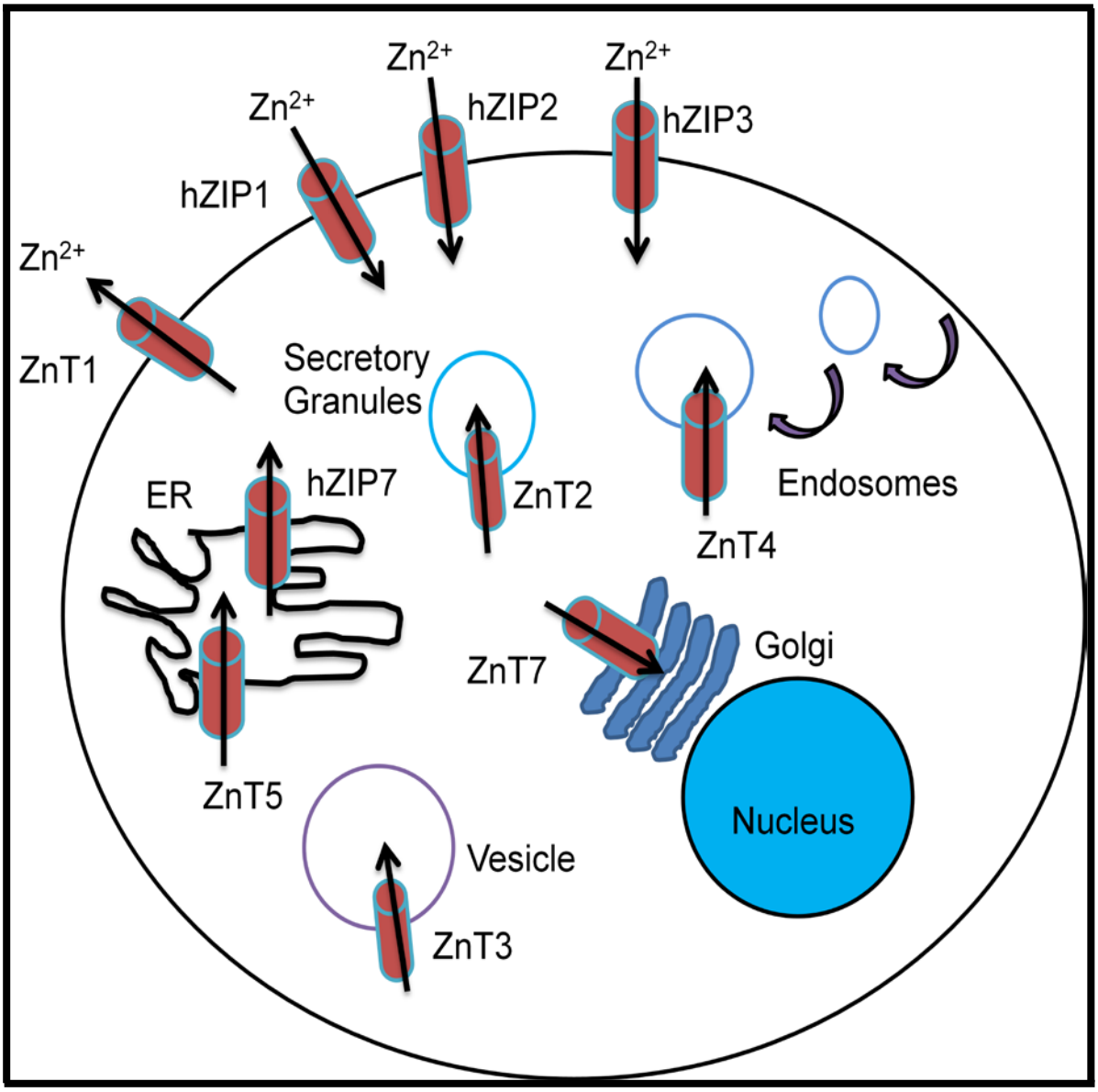

Figure 3.1. Schematic of a Cell Showing Zinc Transporters Examined in this Chapter. Localization of transporters is specific to each organelle and tissue. The ZIP family transporters move Zn^{2+} into the cytosol from the extracellular space and organelles while the ZnT family transporters move Zn^{2+} from the cytosol into organelles and export it out of the cell.

The primary importer of Zn^{2+} for all cell types is hZIP1, but others such as hZIP2 and hZIP3 has been suggested to import Zn^{2+} in prostate cells (*14, 16-19*). Comparison of mRNA levels of the primary Zn^{2+} importer in human cells, hZIP1, in two model prostate cancer cell lines (LNCaP and PC-3) revealed a decrease in hZIP1 in PC-3 compared to LNCaP, suggesting heterogeneity among prostate cancer cell lines (*12, 17, 20-22*). Comparison of hZIP1 levels in a panel of normal and malignant prostate tissue samples revealed a high degree of heterogeneity in hZIP1 immunoreactivity, but in general the malignant samples exhibited lower hZIP1 immunoreactivity, suggesting lower hZIP1 protein levels (*12*). hZIP2 and hZIP3 function for the re-uptake and conservation of Zn^{2+} from the prostate fluid and were shown to be down-regulated in adenocarcinomatous glands, which have lost the ability to accumulate Zn^{2+} (*16*).

Expression levels of the primary Zn^{2+} exporter (ZnT1) have also been characterized in PC-3 and LNCaP cells, revealing differential regulation of ZnT1 in these two cell lines (*23*). The ZnT2 transporter is believed to store Zn^{2+} in lysosomal like compartments of lateral and dorsal prostate sections of mice (*24, 25*). In the previous two studies quantitative PCR revealed that ZnT2 is over-expressed in mouse tissue but no studies have been done using human prostate cells to identify the expression level. While most studies on ZnT2 have been done on mice, the prostate gland between mice and humans is different because have humans have three distinct tissue sections while mice have four (*26*). In addition to ZnT2 storing Zn^{2+} into lysosomal like organelles, ZnT4 has also been proposed to be responsible for concentrating Zn^{2+} into prostatic secretory vesicles and expression levels of this transporter decreased from normal to cancerous prostate tissue (*27*). ZnT7 Zn^{2+} transporter is expressed in the intestinal tract, lung, and the prostate and is localized to the Golgi apparatus as well as vesicles (*28*). This transporter has been identified to have a null mutation which leads a decrease in total cellular Zn^{2+} (*29*). These studies suggest that dysregulation of Zn^{2+} transporters may be a consistent feature of prostate carcinoma, however it is not clear if a single transporter is primarily responsible for the changes

in Zn^{2+} physiology or whether different prostate cancer cell lines and tumors may be characterized by a different perturbation in Zn^{2+} transporters.

One challenge in studying the cellular and molecular characteristics of prostate cancer is the limited number of *in vitro* models (i.e., cell lines) that reflect the diversity of characteristics associated with prostate carcinoma (*30*). These characteristics include a range of sensitivity to hormones (androgen sensitive, responsive, or insensitive), expression of the androgen receptor (AR), secretion of prostate specific antigen (PSA), normal and mutated p53 tumor suppressor gene, the ability to establish tumors in mice, and the level and complexity of chromosomal abnormalities (*31*). DU-145, PC-3, and LNCaP prostate cancer cell lines are widely used, yet DU-145 and PC-3 do not produce PSA, are androgen insensitive, and do not express AR (*31*). On the other hand, LNCaP produces PSA, expresses a mutated form of AR, expresses wild type p53, and is androgen responsive, making it a closer model of prostate carcinoma (*32*). Yet, LNCaP does not develop tumors in mice unless co-injected with stroma (*33*).

Two newly developed prostate cancer cell lines, established from dura matter (DuCaP) and vertebra (VCaP) metastases to distinct locations within the same patient (*34, 35*), have recently been characterized (*31, 36*). Both cell lines express normal AR, mutant p53, are androgen sensitive, produce large quantities of PSA, and are tumorigenic in mice without the need to co-inject with stroma (*34, 35*). Spectral karyotyping of these lines revealed a large number of complex chromosomal abnormalities, consistent with their derivation from late-state tumors (*36*). To gain insight into the molecular origin of the decreased levels of total Zn^{2+} between normal and prostate cancer cell lines, and the redistribution of free Zn^{2+} observed with organelle-targeted FRET-based sensors, we began establishing how Zn^{2+} is dysregulated in these cell lines, and characterize potential heterogeneity between the diverse cell line models. To accomplish this, we measured the mRNA and protein expression levels as well as the localization of the Zn^{2+} transporters mentioned above. Our results suggest that there is a

dysregulation the Zn^{2+} transporters analyzed in cancerous prostate cells and there is some heterogeneity between the prostate carcinoma cell lines.

3.3 Experimental Methods

Chemicals and Reagents. Keratinocyte-serum free media (KSFM), Roswell Park memorial Institute (RPMI) 1640 media, and Alexa-Fluor 568 were purchased from Invitrogen-Life Sciences (Carlsbad, CA). ZnT1, ZnT4, ZnT7, hZIP1, hZIP2, and hZIP3 goat-polyclonal antibodies and donkey anti-goat IgG-HRP were obtained from Santa Cruz Biotechnology (Santa Cruz, CA). RNeasy Mini Kit and Omniscript Reverse Transcriptase Kit were obtained from Qiagen (Valencia, CA). SYBR Green PCR Master Mix was purchased by Applied Biosystems. Zinc chloride, low metal grade nitric acid, and β-actin mouse monoclonal antibody were purchased from Sigma Aldrich. Amersham ECL Plus™ Western Blotting Detection Reagent and Polyvinylidene Fluoride (PVDF) membrane were obtained from GE Amersham. Ready 4-20% gradient Tris-HCl Gels and 10X Tris/Glycine/SDS premixed electrophoresis buffer were obtained from Bio-Rad. Bicinchoninic acid assay protein kit and Surfact-Amps* NP-40 Detergent Solution were purchased from Pierce (Rockford, IL). Electron Microscopy grade paraformaldehyde and Fluoromount-G (for immunofluorescence) were purchased from Electron Microscopy Sciences (Hatfield, PA).

Microscopy. Fixed samples stained with antibody-Alexa-Fluor 568 were imaged using on a Nikon A1-R Confocal system on an Eclipse Ti-E PFS Microscope using a 60X Plan Apo VC, numerical aperture of 1.4. Nikon images were analyzed with NIS-Elements software. In addition we also used a Zeiss Laser Scanning Microscope (LSM) 510 confocal with 3 photon-multiplier tubes, 60X oil objective, and a numerical aperture of 1.4. Zeiss LSM images were analyzed with ZEN 2009 software. All fluorescent images obtained on a given microscope

system were thresholded to the same intensity in order to highlight the relative fluorescent intensity unless indicated.

Cell Culture. RWPE1 (normal prostate cell line), VCaP, and LNCaP (prostate cancer cell lines) were obtained from the American type Cell Collection (ATCC). DuCaP was a kind gift from Dr. Scott M Lucia at the University of Colorado Health Sciences Center (Denver, CO). RWPE1 cells were culture in *K*eratynocyte-*S*erum *F*ree *M*edia (KSFM) supplemented with 0.05 mg/mL bovine pituitary extract, 5 ng/mL epithelial growth factor (Life Sciences), 100 U/mL penicillin and 100 µg/mL streptomycin. DuCaP, VCaP, and LNCaP cell lines were cultured in *R*oswell *P*ark *M*emorial *I*nstitute (RPMI) media (Life Sciences) supplemented with 10% (v/v) fetal bovine serum (Atlanta Biologicals), L-glutamine, 100 U/mL penicillin, and 100 µg/mL streptomycin. All cell lines were incubated at 37ºC with 5% CO_2, changing the media every 2-3 days.

Zinc Chloride Incubation. Because the presence of phosphates causes Zn^{2+} to precipitate out of solution, all Zn^{2+} incubation studies were done in phosphate free HEPES-Hanks' Balanced Salt Solution (HHBSS) (1.26 mM $CaCl_2$, 5.36 mM KCl, 984 µM $MgCl_2$, 137 mM NaCl, 16.65 mM D-Glucose, and 30 mM HEPES). Buffers were generated with Chelex-100 treated water (Sigma Aldrich). Incubations were done at 37°C with 5% CO_2 for 2 hours prior to imaging and mRNA or protein extraction.

Immunohistochemistry. To observe localization of ZnT1, ZnT4, hZIP1, hZIP2, and hZIP3 Zn^{2+} transporters, cells were grown to approximately 70% confluency on cover slips in 12-well plates. A set of cells was grown in normal media conditions and another set incubated with Zn^{2+} prior to fixation as mentioned above. Cells were briefly washed with Phosphate Buffered Saline (PBS) pH 7.4 and fixed with 3.7% paraformaldehyde in PBS for 20 minutes followed by permeabilization using 0.1% Triton X-100 in PBS for 20 minutes. Blocking was done using 3% BSA in PBS for 1 hour at room temperature. Primary antibodies were diluted in blocking buffer

50-fold (1:50) and incubated for 1 hour followed by 2-3 PBS washes. Secondary AlexaFluor conjugated antibody was diluted 1000-fold (1:1000) in blocking buffer. After secondary antibody incubation, cells were washed with PBS two times and mounted onto cover slides using Fluoromount-G and left in a dark environment at room temperature overnight.

Total RNA Isolation and Quantitative Reverse Transcription Polymerase Chain Reaction (qRT-PCR). To measure mRNA levels of each transporter under normal growth conditions and Zn^{2+} incubation, cells were grown to 90% confluency and collected by scraping cells and placing them into a 15 mL conical tube followed by a 5 minute spin at 5000 rpm at room temperature. Following spin, supernatant was removed carefully without disturbing cell pellet and total RNA was extracted using RNeasy Kit supplemented with RNase-free DNase solution as per manufacturers' instructions. DNase was added to ensure pure total RNA sample. Total RNA was quantified by diluting RNA 10-fold (1:10) in 10 mM Tris•Cl, pH 7.5 and the absorbance at 260 nm and 280 nm was measured. Blank measurements were performed using 10 mM Tris•Cl, pH 7.5. The ratio of (A_{260}/A_{280}) was calculated to ensure a pure RNA sample with a ratio between 1.9-2.1. After RNA quantification, 100 ng of total RNA was used to perform RT-PCR and obtain the cDNA of each cell line using QIAGENs Omniscript RT Kit. The RT-PCR step consisted of a 10 minute incubation at 25°C to allow proper annealing of a random primer followed by a 70 minute incubation at 37°C, and finally a 5 minute incubation at 95°C to inactivate the polymerase. For primers, annealing temperature, and size of fragment refer to **Table 3.1**.

Melt Curve Analysis and PCR Percent Efficiency. To characterize the integrity of the primers of the cDNA for each cell line, the Melt Curve of the reference genes (Homo sapiens tubulin, alpha 1b (**K-ALPHA-1**) and Homo sapiens hypoxanthine phosphoribosyltransferase 1 (**HPRT1**)) was done by performing a primer matrix reaction. K-ALPHA-1 and HPRT1 were chosen because studies have revealed that housekeeping genes such as GAPDH, β-actin, and 18S-

Table 3.1. Quantitative Polymerase Chain Reaction Primers.

Transporter	Primer Sequence	Annealing Temperature (°C)	Size (bp)
ZnT1	CCTCGTCGCTGGCGATGCTC (FWD) TTTCTGGGTCTGCGGGGTCCAA (REV)	60	537
ZnT2	AGTCCCGCGCGCAACTTTCA (FWD) TGTGCCAGGTACCCACCAACGA (REV)	60	360
ZnT4	CTAGAAGGTGTGCCAAGCCATTTGA (FWD) GCACTGTCAGGCTGGGGCAA (REV)	59	449
ZnT7	TCAGAGGGTACAGCAGTTGCAAGG (FWD) AACGGCTGACTCTACCCCGT (REV)	58	348
hZIP1	GCACGTGACGCTCCAGTTCCC (FWD) GAGCTGCACCCAGCCCGATG (REV)	60	470
hZIP2	AGCCAGAGGTCATCACCGGCTA (FWD) AGCAAGGCAGAGCTGCACGG (REV)	59	487
hZIP3a	AGCCAGAGGTCATCACCGGCTA (FWD) AGCAAGGCAGAGCTGCACGG (REV)	59	487
hZIP3b	CCCCCGGGAGTTGCTGGACTGAG (FWD) GGCCATAAGGTGCCAAGGGCTG (REV)	61	389
Reference Gene			
Kβ1	GGCCCCGCCCTAGTGCGTTA (FWD) GGTGCACTGGTCAGCCAGCTT (REV)	60	496
HRTP1	GCAGCCCTGGCGTCGTGATTA (FWD) CGTGGGGTCCTTTTCACCAGCA (REV)	60	499

*Primers were designed in our laboratory using NCBI Primer-Blast and selection included the criterion that the primers span Exon-Exon junctions.

Table 3.2. Reference Gene Primer Matrix

	Forward Primer (nM)		
Reverse Primer (nM)	**50**	**300**	**900**
50	50/50	300/50	900/50
300	50/300	300/300	900/300
900	50/900	300/900	900/900

RNA demonstrate different behavior in various tissue types as well as treatments within the same tissue (*37, 38*). Both, K-ALPHA-1 and HPRT1, reference genes have been shown to not change from normal to cancerous prostate cells (*39*) making them ideal reference genes to normalize the expression of the Zn^{2+} transporters being studied. Briefly a series of qPCR reactions were performed using different forward and reverse primer concentrations (**Table 3.2**). To perform qPCR a CFX96 BioRad Thermocycler was used with the following conditions: Initial 95°C for 10 minutes to start polymerase, denaturation at 95°C for 30 seconds, annealing at 55°C for 40 seconds, and extension at 72°C for 35 seconds. PCR was set for 65 cycles followed by a Melt Curve Analysis from 55-95°C with 0.5°C increments for 5 seconds incubation per increment. Analysis is plotted as fluorescence output of SYBR Green as a function of temperature increase as illustrated in **Figure 3.2**. **Figure 3.2** represents the K-ALPHA-1 reference gene using DuCaP prostate cancer cell line and demonstrates a single peak, indicating that the reaction yielded one product, and hence the reaction demonstrates good gene specificity. Both, K-ALPHA-1 and HPRT1, yielded similar results on all four cell lines using

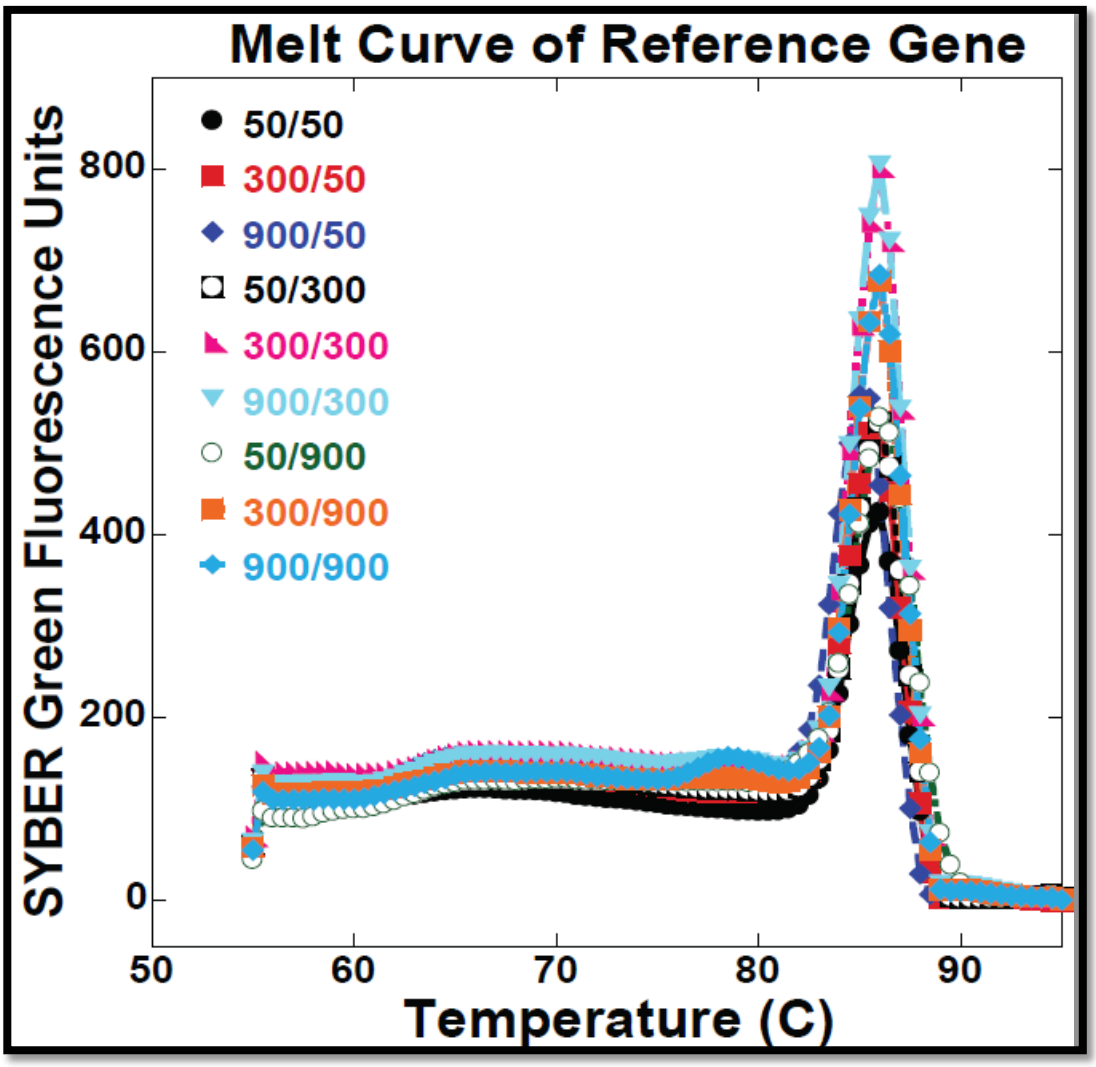

Figure 3.2. Melt Curve Analysis Confirms Gene Specificity. The primer matrix yielded a peak that demonstrates robust amplification of desired product as detailed by the single peak at approximately 85°C. The DuCaP prostate cancer cell line was used in this representation and qPCR was performed on an CFX96 BioRad Thermocycler. The legend within the graph represents forward and reverse primer concentrations in nM.

900 nM forward and 300 nM reverse primers concentration. After analyzing all data sets we decided to use 900 nM forward and 300 nM reverse primer concentrations because the primer matrix using all cell lines with the reference genes yielded best specificity with these primer concentrations, because other combinations of concentrations yielded multiple peaks, indicative of non-specificity or primer-dimer products.

Once forward and reverse primer concentrations were determined, a PCR percent efficiency was carried out to ensure that the amount of DNA is doubled per cycle. A serial dilution of cDNA of all cell lines was done from 1:10 to 1:10,000. This serial dilution ensures that there is equal coverage of the range of quantification being performed and ensures that there are no pipeting errors. In addition we need to ensure that we obtain a linear relationship between the amount of template and the C_t-value to ensure accurate and reproducible quantification of all samples. The C_t-value is defined in a quantitative PCR as the number of cycles needed for the SYBR Green fluorescent output to cross the threshold (i.e., background levels). These experiments utilized a hard-shell thin-wall 96-well skirted PCR plate and 3 µL of template cDNA was used per reaction. The C_t-value was plotted as function of serial dilution, as depicted in **Figure 3.2**, generating a standard curve. **Figure 3.3** shows a slope of -3.4504 which is used to calculate the amplification efficiency using $\mathbf{E = 10^{(-1/slope)}}$ or denoted as **% Efficiency = (E-1) x 100%**. For the representative plot the efficiency of amplification is 1.95 which means that for every cycle of the PCR the template number is increased by 1.95 fold or 95% of the template was amplified. Optimal qPCR conditions should have between 90-105% amplification efficiency and using both reference genes and all four cell lines we were able to obtain this range of efficiency.

Protein Isolation and Western Blotting. Cells were grown to 90% confluency in normal media conditions. One set of cells was grown under normal media conditions and another set was incubated with 50 µM $ZnCl_2$ for 2 hours prior to collecting cells. Cells were briefly washed with

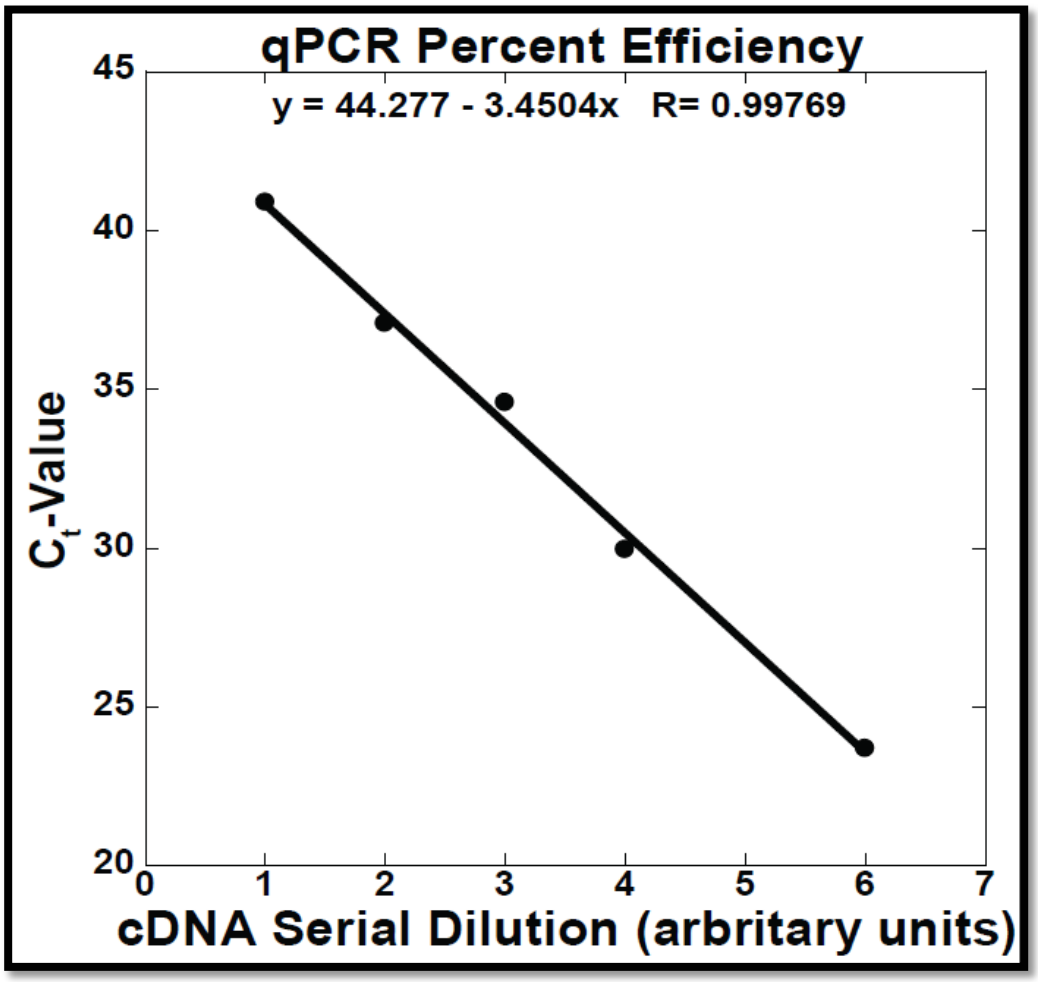

Figure 3.3. Standard Curve of qPCR to Calculate Percent Efficiency of Reaction. This application defines the efficiency of a qPCR based on a serial dilution of cDNA. Homo sapiens tubulin, alpha 1b (TUBA1B), **Kα1 Reference Gene** is shown. Serial dilution was done from 1:10 to 1:10,000. Amplification efficiency is calculated from the slope of the line using: $E = 10^{(-1/slope)}$. The amount of DNA should double with every cycle in the PCR and the amplification efficiency will denote this. The efficiency for a good PCR should be within 90-105%. In this example the percent efficiency is 95%.

ice-cold PBS pH 7.4, followed by scraping the cells with 2 mL of PBS onto 2 mL eppendorf tubes. Cells were then centrifuged for 5000 rpm for 5 minutes at 4°C. Approximately 400-900 µL of Lysis buffer (150 mM Tris-HCl pH 7.4, 150 mM NaCl, 2 mM EDTA pH 8.0, 1% Triton X-100, and 0.2% NP040 plus protease inhibitor cocktail) was used to extract proteins. Following lysis, tubes were incubated in ice for 20 minutes, centrifuged for 20 minutes at 14,000 rpm at 4°C, and supernatant was collected. A BCA assay was performed to quantify protein and 90 µg of protein was loaded per lane to resolve on acrylamide Tris-HCl gel.

For resolution and detection of each Zn^{2+} transporter, a 4-20% gradient gel was used and resolved at 130 Volts until the dye front ran out of the gel, followed by transfer onto a PVDF membrane at 300 mA for 90 minutes in 10% methanol transfer buffer at 4°C. Following transfer, the PVDF membrane was washed in TBS-Tween (TBST, 0.05% Tween-20) for 15 minutes in the cold room, and incubated in blocking buffer containing 5% dry milk in TBST overnight at 4°C. Each membrane was then incubated with ZnT1, ZnT4, ZnT7, hZIP1, hZIP2, or hZIP3 goat-polyclonal antibody at a 1:200 fold dilution in 1% milk-TBST for 1 hour at room temperature followed by 3-washes with TBST. Donkey anti-goat IgG-HRP secondary antibody at a 1:10,000 fold dilution was incubated in 1% milk-TBST for 1 hour at room temperature followed by 3-washes with TBST. The ECL reagent was used as specified by manufacturers' instructions and blots exposed.

Once detection of specified protein was observed, blots were stripped using 67.5 mM Tris-HCl pH 6.8, 2% SDS, and 100 mM DTT. Blots were placed in shaker using gentle agitation for 10-15 minutes at room temperature followed by 15-20 minute TBST wash. Blots were blocked as specified above and β-actin probing done using a 1:6000 fold dilution and rabbit anti-mouse IgG-HRP secondary antibody at a 1:20,000 fold dilution. Both primary and secondary antibodies were diluted in 1% milk-TBST.

3.4 Results

3.4.1 Decreased Cellular Zinc in Prostate Cancer Cell Lines

There is a growing consensus that prostate carcinoma is marked by a significant reduction in Zn^{2+} levels. While LNCaP, PC-3, DU-145, and RWPE2 cells lines have been extensively examined (*12, 13, 21, 23*), Zn^{2+} levels and regulatory proteins have not been characterized for the newly developed DuCaP and VCaP cell lines. Therefore we sought to define these parameters and compare the results with the more commonly used LNCaP, and a normal prostate cell line RWPE1. In **Chapter II**, we defined total cellular Zn^{2+} in all four cell lines by ICP-MS and found that DuCaP and VCaP are significantly reduced of Zn^{2+} compared to the normal cell line. Similar results have been observed for other prostate cancer cell lines such as PC-3 and RWPE2 (*13, 21*).

3.4.2 Expression Levels and Localization of hZIP1 Zn^{2+} Transporter

hZIP1 is a 36 kDa protein, ubiquitously expressed at the membrane and is primarily responsible for import of Zn^{2+} from the extracellular matrix into the cytoplasm of prostate cells (*17*). **Figure 3.4.A** shows no difference in the mRNA level of hZIP1 in cancerous vs. noncancerous cell lines grown under normal media conditions, as measured by qPCR. However, western blot analysis shows an increase in hZIP1 protein levels in the cancerous cell lines (**Figure 3.4.B**), suggesting that in these cancer cell lines perhaps hZIP1 protein is up-regulated to compensate for the loss of Zn^{2+}. Comparable levels of hZIP1 were observed in DuCaP, VCaP, and LNCaP.

hZIP1 expression has been shown to be regulated by Zn^{2+}, where high extracellular Zn^{2+} leads to a decrease in protein expression, perhaps to minimize accumulation of excess Zn^{2+} (*13*). To explore whether Zn^{2+} regulation of hZIP1 differs in normal vs. cancerous cell lines, cells were incubated with 50 μM $ZnCl_2$ for 2 hours prior to mRNA and protein extraction. Under

these conditions there was a decrease in mRNA expression level for RWPE1 and DuCaP post-Zn^{2+} incubation (18% and 52% decrease in mRNA expression, respectively), while no change was observed for VCaP and LNCaP. On the other hand, a significant decrease in hZIP1 protein level was observed in RWPE1 cells, consistent with the finding of Huang *et al.*, (*13*). Conversely, the cancer cell lines exhibited an increase in hZIP1 protein levels in response to Zn^{2+} treatment (**Figure 3.4.B**), suggesting aberrant Zn^{2+}-dependent transporter regulation in all three cancerous cell lines. The increase in hZIP1 protein level was greatest in the LNCaP cell line.

Given the altered level of hZIP1 protein and perturbed regulation by extracellular Zn^{2+}, we examined hZIP1 localization by immunofluorescence. As shown in **Figure 3.4.C**, under normal growth conditions hZIP1 is primarily localized to the plasma membrane in all four cell lines, consistent with previous studies on RWPE1, LNCaP, and PC-3 cell lines (*12, 13*). There is also some localization to fluorescent punctae, consistent with vesicular localization, primarily at the cell periphery. The images in **Figure 3.4.C** are thresholded to the same intensity level, revealing the greater expression of hZIP1 in the prostate cancer cell lines, consistent with the western blotting results. Treatment of cells with extracellular Zn^{2+} did not give rise to a significant change in hZIP1 localization (Data Not Shown).

3.4.3 Expression Levels and Localization of hZIP2 Zn^{2+} Transporter

hZIP2 is a 33kDa protein and is expressed at the membrane of specific cell types such as prostate, uterus, cervical epithelium, monocytes, and optic nerve (*16, 40*). It has been found to bring Zn^{2+} into the cell by measuring uptake of ^{65}Zn in transfected K562 erythroleukemia cells expressing hZIP2 (*18*). **Figure 3.5.A** shows that under normal growth conditions in DuCaP and VCaP prostate cancer cells hZIP2 mRNA is elevated compared to RWPE1 by1176% and 1000%, respectively, and no difference is observed in the LNCaP cell line compared to normal

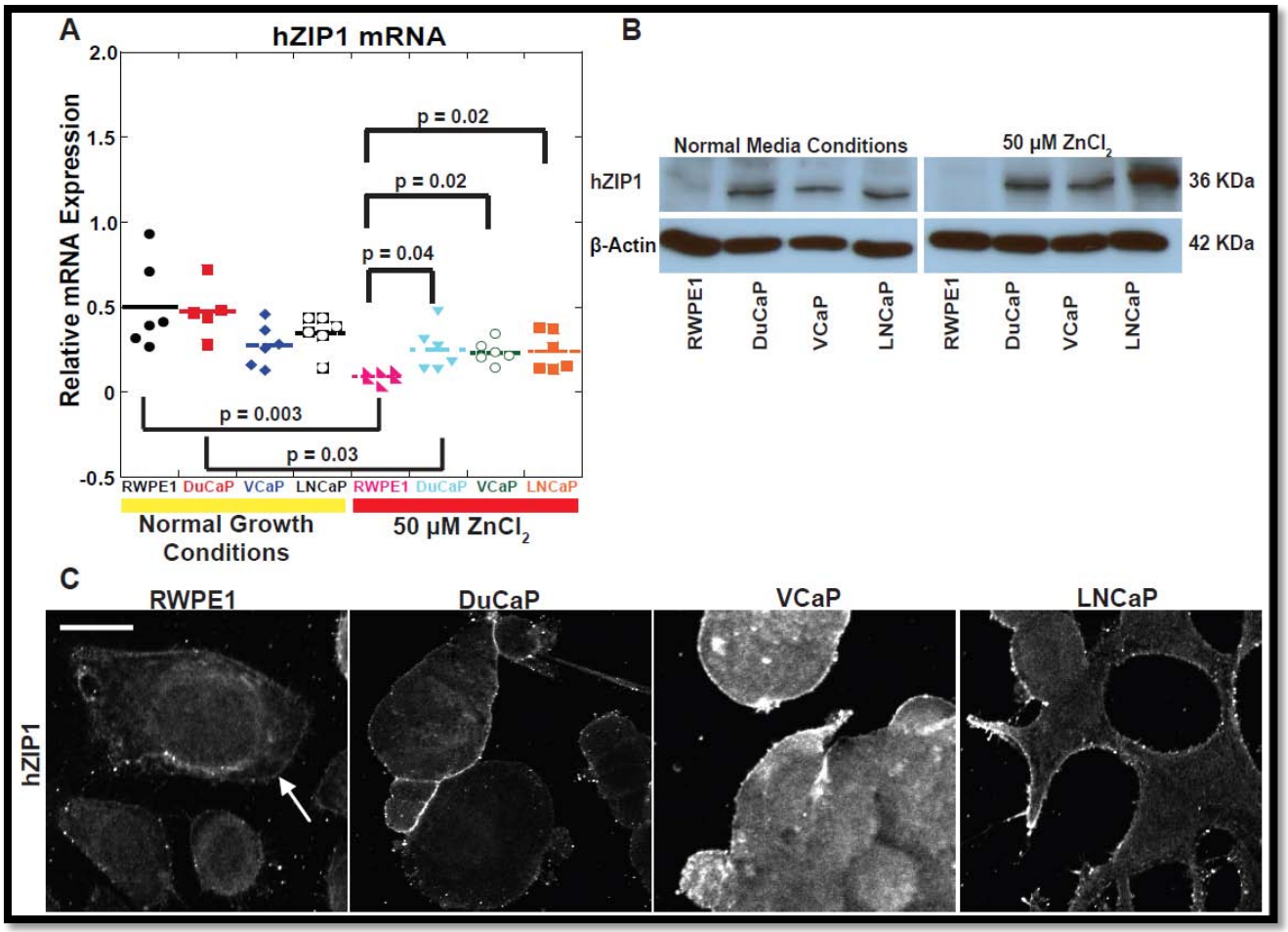

Figure 3.4. qRT-PCR, Western Blot, and Immunofluorescence of hZIP1. A) Quantitative RT-PCR analysis reveals that there is no difference in the mRNA level of hZIP1 between RWPE1 and the three cancer cell lines, when cells are grown under normal growth conditions. After incubating the cells with Zn^{2+} for 2h prior to total RNA extraction, hZIP1 mRNA is down-regulated in RWPE1 and DuCaP cell lines by 138% and 63%, respectively. Each qRT-PCR data point represents one 10 cm dish of cells. Relative mRNA levels were corrected to the Kβ1 reference gene B) Western blot analysis reveals that all three prostate cancer cell lines have higher hZIP1 expression compared to RWPE1 normal cell line. After incubating cells with Zn^{2+}, there is a decrease in expression in RWPE1, but an increase in all three cancer cell lines. C) Immunofluorescence reveals that hZIP1 localizes to the plasma membrane. All fluorescent images were thresholded to the same intensity, scale Bar = 25 μm, and arrow denotes localization on cell. ANOVA with Tukey HSD post hoc test was performed for qRT-PCR.

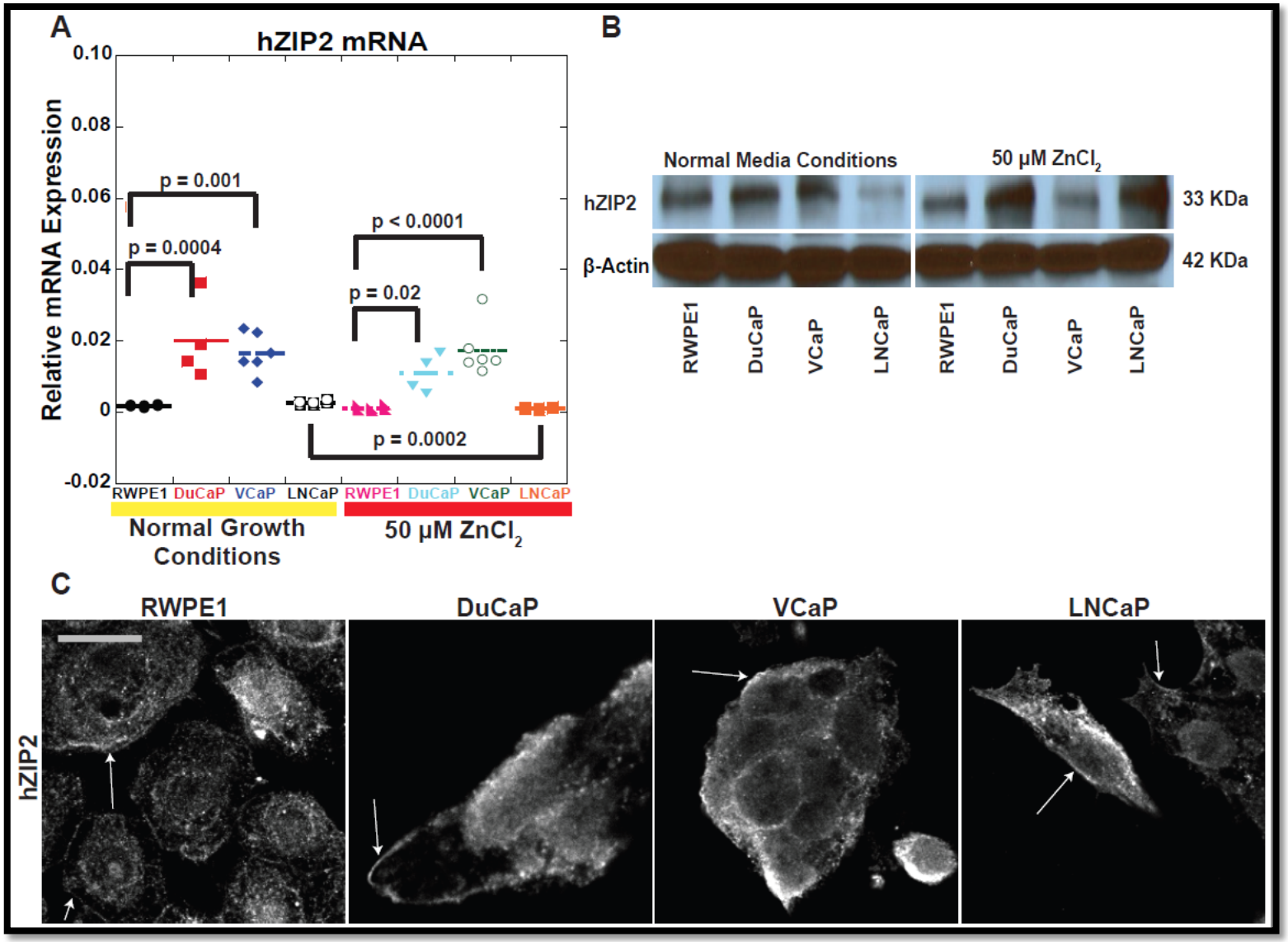
A
hZIP2 mRNA
Relative mRNA Expression
0.10
0.08
0.06
0.04
0.02
0
-0.02
p = 0.001
p = 0.0004
p < 0.0001
p = 0.02
p = 0.0002
RWPE1 DuCaP VCaP LNCaP RWPE1 DuCaP VCaP LNCaP
Normal Growth Conditions
50 μM ZnCl2
B
Normal Media Conditions
50 μM ZnCl2
hZIP2
β-Actin
33 KDa
42 KDa
RWPE1
DuCaP
VCaP
LNCaP
C
RWPE1
DuCaP
VCaP
LNCaP
hZIP2

Figure 3.5. qRT-PCR, Western Blot, and Immunofluorescence of hZIP2. A) Quantitative RT-PCR analysis reveals that hZIP2 mRNA expression is low in RWPE1 and LNCaP cell lines compared to DuCaP and VCaP. DuCaP and VCaP cancer cell lines express 168% and 163% more mRNA compared to RWPE1. After incubating the cells with Zn^{2+} for 2h prior to total RNA extraction, there is no change in mRNA levels for RWPE1, DuCaP, and VCaP cell lines but a 81% decrease in LNCaP. Each qRT-PCR data point represents one 10 cm dish of cells. Relative mRNA levels corrected to Kβ1 reference gene. B) Western blot analysis reveals that RWPE1, DuCaP, and LNCaP cell lines express similar levels of hZIP2 protein and a higher level than the LNCaP cell line. After incubating cells with Zn^{2+}, the hZIP2 protein levels in DuCaP and LNCaP increase while the expression levels of RWPE1 and VCaP remain the same. C) Immunofluorescence analysis reveals that hZIP2 protein localizes to the plasma membrane. Incubating cells with Zn^{2+} did not reveal that transporter localizes to another region of the cell but is retained at the membrane (Data Not Shown). All fluorescent images were thresholded to the same intensity, scale Bar = 25 μm, and arrow denotes localization on cell. ANOVA with Tukey HSD post hoc test was performed for qRT-PCR.

cell line RWPE1. Under the same conditions, Western blot analysis (**Figure 3.5.B**) revealed that RWPE1, DuCaP, and VCaP cell lines express comparable amounts of protein which is consistently higher than the LNCaP cell line. These results confirm that hZIP2 is present in the prostate lines and reveals that there is some heterogeneity in expression. There is not a consistent trend between the cancerous and noncancerous cells.

Very little is known about whether hZIP2 mRNA expression or localization is regulated by Zn^{2+}. There was no change in mRNA expression level for RWPE1, DuCaP, and VCaP cell lines, but a decrease of 42% in for LNCaP upon treatment with Zn^{2+}. Conversely, at the protein expression level DuCaP and LNCaP protein levels increased while VCaP exhibited a decrease and RWPE1 did not change. These results suggest that while Zn^{2+} does not substantially affect the expression level of mRNA, it affects the protein expression levels of all three cancer cell lines and again heterogeneity is observed in how Zn^{2+} elevation impacts protein expression levels.

Given the altered expression level of hZIP2 mRNA and protein level we examined the localization of hZIP2 localization by immunofluorescence. As shown in **Figure 3.5.C** under normal growth conditions hZIP2 is primarily localized at the plasma membrane of all four cell lines, as well as in punctae at the cell periphery. All images in this panel are thresholded to the same intensity level, revealing greater expression of hZIP2 in the prostate cancer cell lines, similar to hZIP1. Treatment of cells with extracellular Zn^{2+} did not give rise to a significant change in hZIP2 localization (Data Not Shown).

3.4.4 Expression Levels and Localization of hZIP3 Zn^{2+} Transporter

hZIP3 is a 34 kDa protein and in human prostate tissue is localized at the plasma membrane (*16*) but has not been characterized to a great extent other than identifying that it is responsible for Zn^{2+} accumulation in K562 erythroleukemia cells using ^{65}Zn (*18*). When primers

were designed for quantitative analysis of the mRNA in our cell line, two alternatively spliced isoforms were predicted by the NCBI Nucleotide-BLAST. These two isoforms, hZIP3a and hZIP3b, have a distinct C-terminus and hZIP3b is shorter compared to hZIP3b by 212 amino acids, giving rise to a 34 kDa and 11 kDa protein respectively. Due to this we decided to measure and quantify the mRNA expression levels of both if detectable. **Figure 3.6.A** and **3.6.B** reveal marked differences in the expression level of both isoforms. For hZIP3a, DuCaP and VCaP mRNA is higher compared to RWPE1, 1176% and 1000%, respectively and for the hZIP3b isoform, DuCaP and VCaP prostate cancer cell lines express lower levels of mRNA than RWPE1 (46% and 75%decrease, respectively). Our current antibody detects only the 34 kDa protein (hZIP3a isoform) (**Figure 3.6.C)**. Western blot analysis reveals that hZIP3 protein is expressed higher in RWPE1 compared to the cancer cell lines, this band has been consistent with the 34 kDa isoform.

To explore whether Zn^{2+} regulation of hZIP3 differs in normal compared to cancerous cell lines, cells were incubated with 50 μM $ZnCl_2$ for 2 hours prior to mRNA and protein extraction. **Figure 3.6.A** reveals that hZIP3a mRNA expression is not altered by Zn^{2+} for RWPE1, DuCaP, and VCaP cell lines but it decreases mRNA expression in LNCaP cell line by32%. On the other hand, hZIP3b expression decreases for RWPE1 (22%), DuCaP (59%), and LNCaP (44%) while no change is observed for VCaP cell line.

Given the difference in expression level of hZIP3 between mRNA and protein in all four cell lines we examined the localization of this transporter in our cell lines by immunofluorescence. As observed in **Figure 3.7** under normal growth conditions hZIP3 is located at the plasma membrane of all four cell lines. But similar to hZIP1 and hZIP2 a fluorescent signal is observed in punctae as well. In RWPE1 and VCaP cell lines the fluorescent signal is uniform at the membrane and very few punctae are visible.

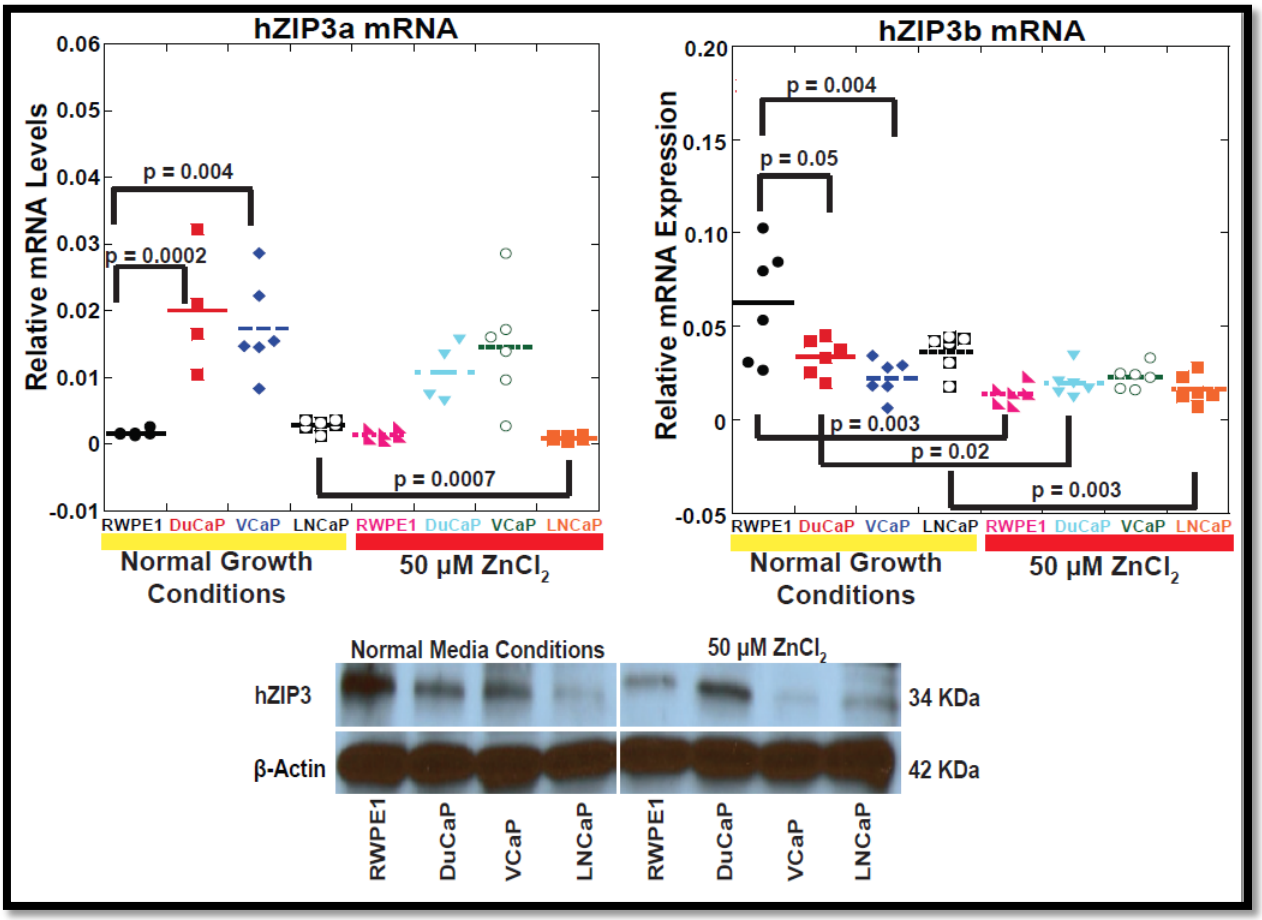

Figure 3.6. qRT-PCR and Western Blot of hZIP3a and hZIP3b. A) Quantitative RT-PCR analysis reveals that mRNA expression of hZIP3a is low in RWPE1 and LNCaP cell lines while expression is higher in DuCaP and VCaP by 168% and 163%, respectively. Incubating cells with Zn^{2+} for 2 hours prior to total RNA extraction revealed that hZIP3a mRNA expression levels did not change for RWPE1, DuCaP, and VCaP cell line while mRNA levels decreased by 100% for the LNCaP cell line. B) qRT-PCR of hZIP3b demonstrates that mRNA expression level is lower in DuCaP and VCaP compared to RWPE1. After incubating the cells with Zn^{2+} for 2h prior to total RNA extraction mRNA expression levels for hZIP3b decreased in RWPE1, DuCaP, and LNCaP but not for VCaP cell line. Each qRT-PCR data point represents one 10 cm dish of cells. Relative mRNA levels were corrected to the Kβ1 reference gene. C) Western blot analysis shows that RWPE1 cell lines exhibit higher protein expression compared to DuCaP, VCaP and LNCaP. After incubating cells with Zn^{2+} we observe that hZIP3 protein expression is regulated by Zn^{2+}. DuCaP protein expression increases, while in RWPE1 and VCaP there is a decrease in expression. ANOVA with Tukey HSD post hoc test was performed for qRT-PCR.

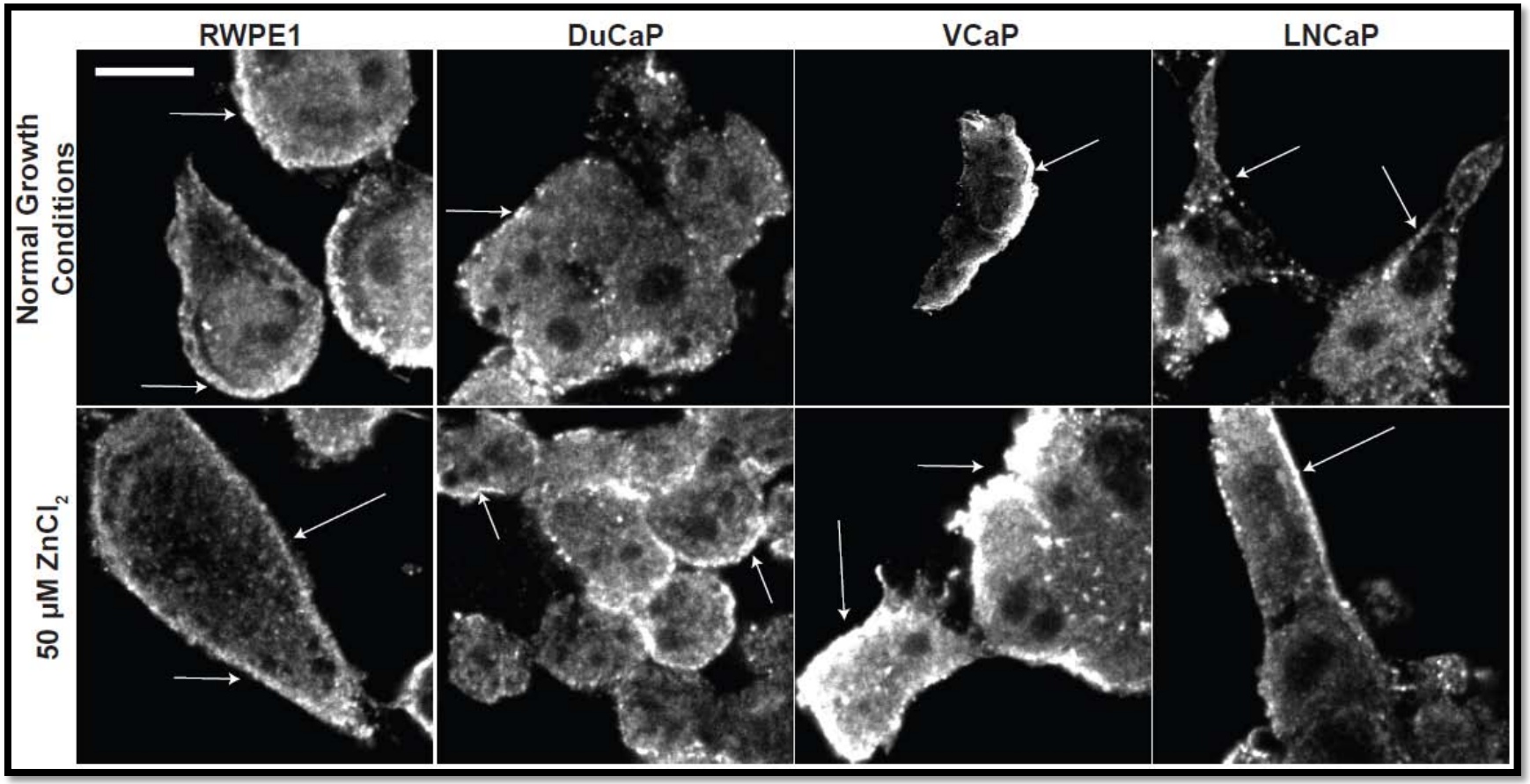

Figure 3.7. Immunofluorescence of hZIP3. hZIP3 is primarily localized to the plasma membrane. Under normal media conditions most hZIP3 is found at the periphery of the cell but there is some staining of punctae. In particular DuCaP and LNCaP puncta are found at the membrane. After incubating cells with Zn^{2+} hZIP3 is more uniform along the membrane and less puncta are observed at the periphery as well. hZIP3 localization is altered after Zn^{2+} from puncta to more membrane localization. Scale Bar = 25 µm, and arrow denotes localization on cell. All images were thresholded to the same intensity.

3.4.5 Expression Levels and Localization of ZnT1 Zn^{2+} Transporter

ZnT1 is a 60 kDa Zn^{2+} transporter located at the plasma membrane and on vesicles (*41*) which functions in exporting Zn^{2+} out of the cell. As observed in **Figure 3.8.A**, about the cancer cells exhibit decreased ZnT1 mRNA levels compared to RWPE(71% for DuCaP, 64% for VCaP and LNCaP). While qPCR reveals that mRNA expression is low in all three cancer cell lines the protein expression does not correlate with mRNA and in all three cancer cell lines the protein expression level is higher than RWPE1, as shown in **Figure 3.8.B**. DuCaP and LNCaP express higher levels of ZnT1 than VCaP signifying heterogeneity within cancer cell lines. Because ZnT1 exports Zn^{2+} from the cell, the higher levels in cancer cells could signify one mechanism for reducing Zn^{2+} levels in cancer cell lines.

To determine whether Zn^{2+} regulates the mRNA and protein expression of ZnT1, cells were treated with 50 μM extracellular Zn^{2+} for 2 hours prior to extractions. **Figure 3.8.A** shows that Zn^{2+} treatment changes the mRNA expression level of RWPE1, DuCaP, and VCaP by decreasing expression in normal cell line by 19% and increasing expression in DuCaP (275%) and VCaP (700%). There were no significant mRNA expression changes in LNCaP cell line, consistent with previous studies (*20, 23*). Because of slight variations in protein loading, it is harder to discern a pattern for ZnT1 protein levels, but it appears there may be subtle increases in ZnT1 protein levels upon Zn^{2+} treatment. There was no significant difference in Zn^{2+} regulation between the normal and cancerous cell lines.

To examine whether the localization of ZnT1 was altered in prostate cancer cell lines, transporter localization was examined by immunofluorescence. In all three cancer cell lines, ZnT1 was observed on the membrane and intracellular vesicles as observed in **Figure 3.8.C**. Subtle differences were observed in the localization in cancer cell lines. In DuCaP and VCaP, the majority of ZnT1 was found at the membrane and vesicles located at the cell periphery,

whereas LNCaP showed a much greater portion of vesicular localization, perhaps because LNCaP exhibits the highest ZnT1 protein expression of all the cell lines. These results suggest heterogeneity in the prostate cancer cell lines. It was difficult to detect plasma membrane or vesicular localization in RWPE1 cells, perhaps because of the lower ZnT1 protein expression levels. Addition of extracellular Zn^{2+} did not cause a significant change in localization (Data Not Shown).

3.4.6 mRNA Expression Levels of ZnT2 Zn^{2+} Transporter

ZnT2 is thought to have two splice isoforms which produce two different protein species with molecular weights 42 and 35 kDa (*42*). The 35 kDa Zn^{2+} transporter lacks part of the N-terminus producing a shorter isoform of ZnT2. It has been proposed that these two isoforms of ZnT2 may have different physiological functions, because one isoform localizes to the plasma membrane and the other to secretory compartments (*42, 43*). But because we were interested in defining the mRNA of ZnT2 localized to vesicles we decided to quantify the 42 kDa isoform. Many studies have measured the mRNA expression level of ZnT2 in mouse or rat prostate (*24, 25, 44, 45*), but no studies have examined the mRNA or protein expression in human cells. The tissue specificity of ZnT2 is restricted to small intestine, liver, pancreatic acinar cells, kidney, and mammary gland with subcellular localization in vesicles and secretory granules (*14*). Because ZnT2 lacks a good specific antibody we decided to only measure the mRNA expression level.

Figure 3.9 reveals that the mRNA expression in DuCaP and VCaP cancer cell lines is higher than RWPE1 and LNCaP. The increase in mRNA expression for DuCaP is 500% and VCaP is 400% higher than RWPE1. Although we were able to detect mRNA coding for ZnT2, the relative mRNA expression is significantly lower compared to other transporters studied. To determine whether Zn^{2+} regulates the mRNA and protein expression of ZnT2, cells were treated

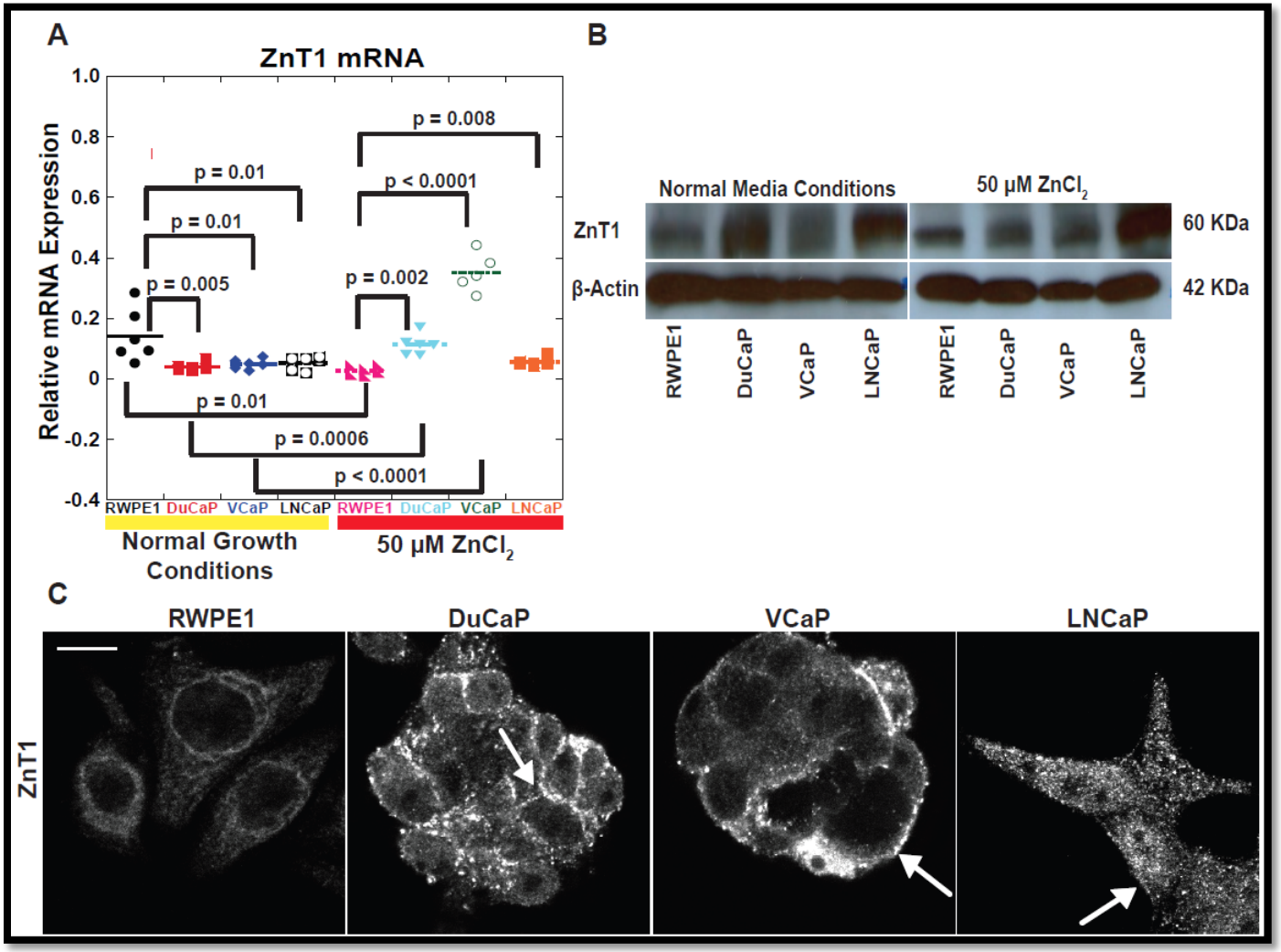
A
ZnT1 mRNA
Relative mRNA Expression
1.0
0.8
0.6
0.4
0.2
0
-0.2
-0.4
p = 0.01
p = 0.01
p = 0.005
p = 0.01
p = 0.0006
p < 0.0001
p = 0.008
p < 0.0001
p = 0.002
RWPE1 DuCaP VCaP LNCaP RWPE1 DuCaP VCaP LNCaP
Normal Growth Conditions
50 μM ZnCl2
B
Normal Media Conditions
50 μM ZnCl2
ZnT1
β-Actin
60 KDa
42 KDa
RWPE1
DuCaP
VCaP
LNCaP
RWPE1
DuCaP
VCaP
LNCaP
C
RWPE1
DuCaP
VCaP
LNCaP
ZnT1

Figure 3.8. qRT-PCR, Western Blot, and Immunofluorescence of ZnT1. A) Quantitative RT-PCR analysis reveals that mRNA expression is high in RWPE1 compared to DuCaP, VCaP, and LNCaP by 111% for DuCaP and 94% for VCaP and LNCaP. After incubating the cells with Zn^{2+} for 2h prior to total RNA extraction, in RWPE1 there is a 135% decrease in mRNA expression while in DuCaP and VCaP mRNA levels increase by 93% and 150%, respectively. Each qRT-PCR data point represents one 10 cm dish of cells. Relative mRNA levels were corrected to Kβ1 reference gene. B) Western blot analysis reveals that DuCaP, VCaP, and LNCaP cell lines exhibit higher protein levels than RWPE1. After incubating cells with Zn^{2+}, ZnT1 protein expression does not change. C) Immunofluorescence analysis reveals that ZnT1 localizes to the plasma membrane. Incubating cells with Zn^{2+} did not reveal that transporter localizes to another region of the cell but is retained at the membrane (Data Not Shown). All fluorescent images were thresholded to the same intensity, scale Bar = 25 μm, and arrow denotes localization on cell. ANOVA with Tukey HSD post hoc test was performed for qRT-PCR.

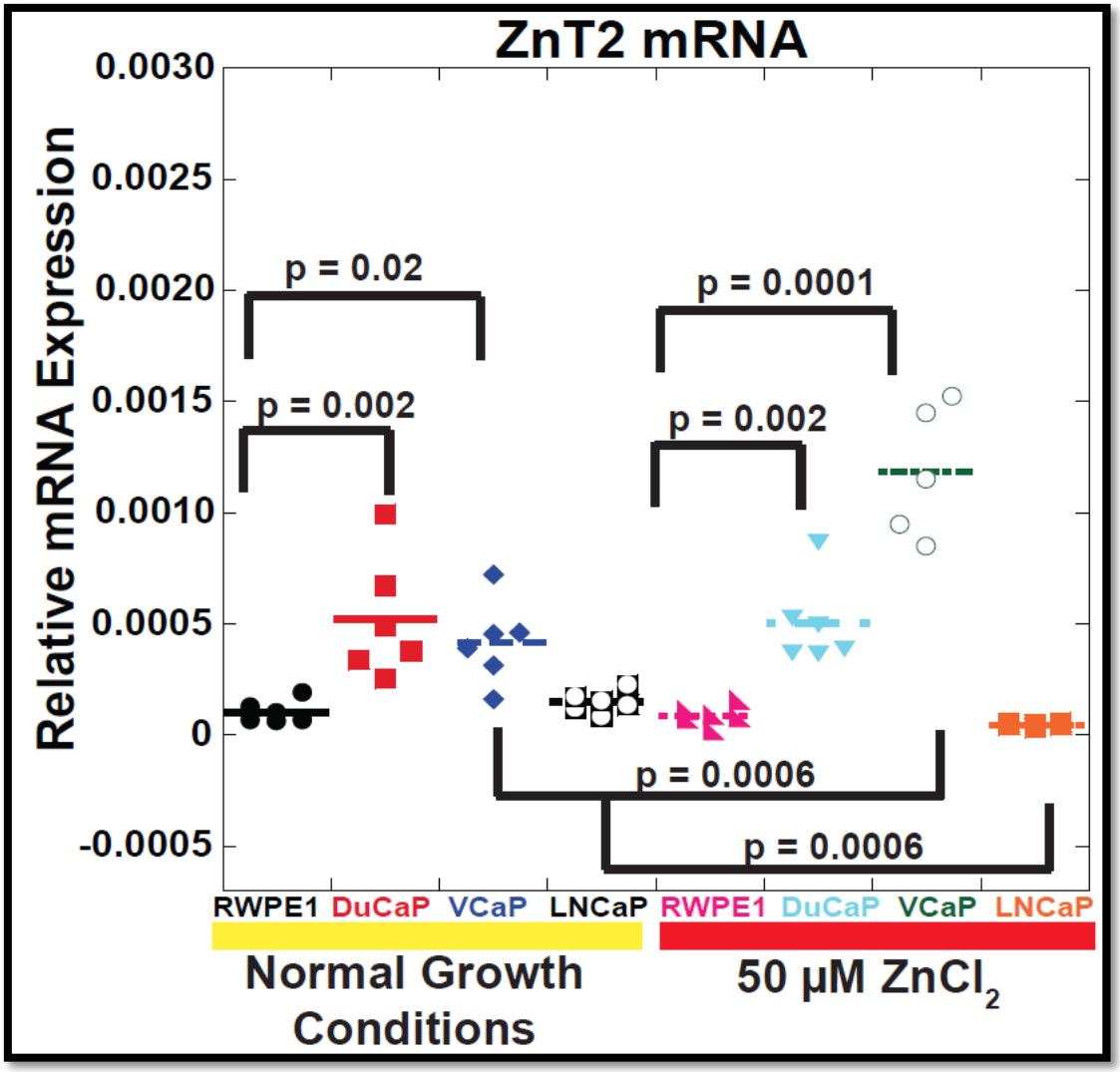

Figure 3.9. qRT-PCR Analysis of ZnT2. qRT-PCR revealed that ZnT2 mRNA expression levels are low in RWPE1 and LNCaP compared to DuCaP and VCaP. DuCaP mRNA is 133% and VCaP mRNA is 120% higher compared to RWPE1. Incubating the cells with Zn^{2+} for 2h prior to total RNA extraction revealed no change in ZnT2 mRNA expression level for RWPE1 and DuCaP but a 100% increase for VCaP and 100% decrease for LNCaP. Each qRT-PCR data point represents one 10 cm dish of cells. Relative mRNA levels corrected to Kβ1 reference gene. ANOVA with Tukey HSD post hoc test was performed for qRT-PCR.

with 50 μM extracellular Zn^{2+} for 2 hours prior to extractions. **Figure 3.9** shows that Zn^{2+} treatment increases the expression level in VCaP (by 300%), but decreases the expression level in LNCaP (by 33%). For RWPE1 and DuCaP there was no significant change in expression post-Zn^{2+} treatment.

3.4.7 Expression Levels and Localization of ZnT4 Zn^{2+} Transporter

ZnT4 is a 47 kDa protein that is primarily localized to intracellular vesicles of prostate, mammary, and small intestine cells (*14, 27, 46*). Henshall and coworkers (*27*) measured ZnT4 protein levels in prostate tumor samples of over 100 patients, and found decreased ZnT4 protein levels in malignant tissues. **Figure 3.10.A** and **3.10.B** demonstrate that the mRNA level is higher in VCaP (1389%) and LNCaP (1667%) and the protein level is higher in all 3 cancer cell lines compared to the normal RWPE1 cells, with LNCaP exhibiting the highest protein levels of all cell lines. Incubation of cells with Zn^{2+} for 2 hours did not yield significant changes in the protein levels, suggesting that ZnT4 expression levels are not regulated by Zn^{2+} during the time frame examined. However, DuCaP mRNA expression level decreased by 43%, post-Zn^{2+}. ZnT4 has been shown to be associated with vesicles and membrane, similar to ZnT2 and ZnT3 Zn^{2+} transporters that are associated with vesicles in the small intestine and neurons, respectively (*14, 27, 46*). In all prostate cell lines, there was a strong ZnT4 fluorescent signal associated with punctae, consistent with vesicular localization as demonstrated in **Figure 3.10.C** (top panel). The levels of ZnT4 protein were higher in all three cancer cell lines.

To explore whether localization was regulated by Zn^{2+}, we observed ZnT4 localization 2 hours after incubating the cells with 50 μM $ZnCl_2$. **Figure 3.10.C** (lower panel) demonstrates that RWPE1 cells show a decrease in vesicular localization and an increase in membrane localization. Conversely DuCaP and VCaP show very little change upon incubation with Zn^{2+}, while LNCaP displays an increase in vesicular localization. Combined these results suggests

aberrant Zn^{2+}-dependent regulation of ZnT4 (cancer cells respond differently than the noncancerous cell line) and differential regulation in the prostate carcinoma lines.

3.4.8 Expression Levels of ZnT7 Zn^{2+} Transporter

ZnT7 is a 42 kDa protein that is primarily localized to the Golgi apparatus and vesicles in prostate, lung and small intestine and highly expressed in the proximal segment of the small intestine facilitating Zn^{2+} transport from the cytoplasm to the Golgi (*28, 29*). **Figure 3.11.A** and **3.11.B** show that the mRNA of ZnT7 is expressed at similar levels in all cell lines. However, western blot analysis shows an increase in ZnT7 protein levels in RWPE1 (**Figure 3.11.B**), while all cancer cell lines express lower levels of protein with LNCaP expressing the least amount. Incubation of cells with Zn^{2+} for 2 hours did not yield significant changes in the mRNA in RWPE1, DuCaP, and VCaP cell line, but gave rise to a small decrease in expression in LNCaP of 31%. Western blot analysis reveals that aberrant Zn^{2+}-dependent regulation of ZnT7 occurs in all four cell lines. In **Figure 3.11.B** protein levels are highly regulated by Zn^{2+} because in RWPE1, DuCaP, and VCaP protein expression levels decrease, while in cancer cell line LNCaP ZnT7 is slightly up-regulated from endogenous levels. Given the drastic changes in protein expression we sought to perform immunofluorescence to observe its localization but experiments were futile because we did not clearly observe Golgi localization (Data Not Shown).

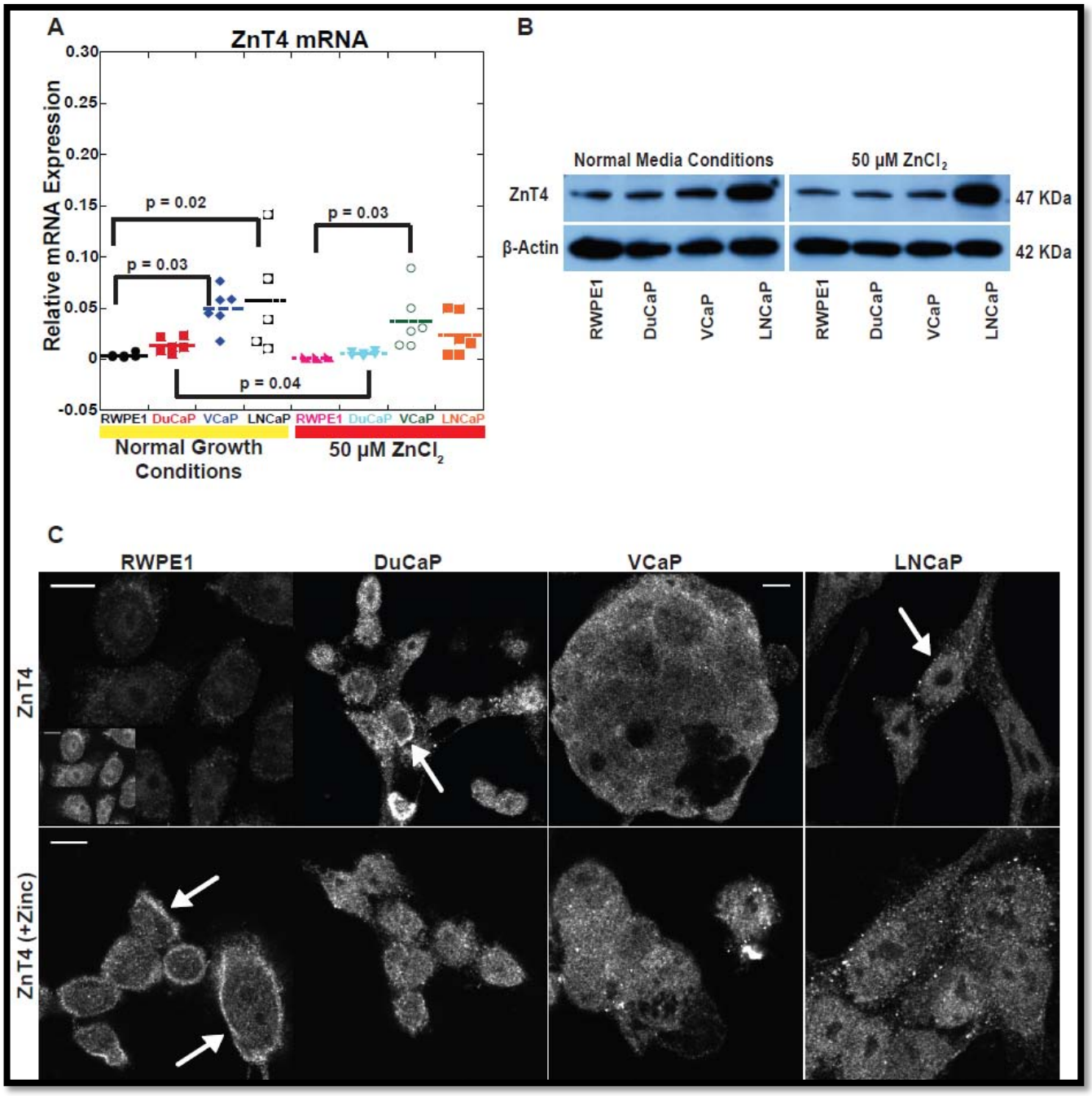
A
ZnT4 mRNA
Relative mRNA Expression
0.30
0.25
0.20
0.15
0.10
0.05
0
-0.05
p = 0.02
p = 0.03
p = 0.03
p = 0.04
RWPE1 DuCaP VCaP LNCaP RWPE1 DuCaP VCaP LNCaP
Normal Growth Conditions
50 μM ZnCl2
B
Normal Media Conditions
50 μM ZnCl2
ZnT4
β-Actin
47 KDa
42 KDa
RWPE1
DuCaP
VCaP
LNCaP
RWPE1
DuCaP
VCaP
LNCaP
C
RWPE1
DuCaP
VCaP
LNCaP
ZnT4
ZnT4 (+Zinc)

Figure 3.10. qRT-PCR, Western Blot, and Immunofluorescence of ZnT4. A) Quantitative RT-PCR analysis reveals that mRNA expression is low in RWPE1 compared to VCaP, and LNCaP by 173% and 177%, respectively. After incubating the cells with Zn^{2+} for 2h prior to total RNA extraction there is no change in mRNA expression level in RWPE1, VCaP, and LNCaP while there is a 80% decrease in mRNA expression in DuCaP. Each qRT-PCR data point represents one 10 cm dish of cells. Relative mRNA levels corrected to Kβ1 reference gene. B) Western blot analysis reveals RWPE1, DuCaP and, VCaP cell lines have similar protein levels while LNCaP expresses more protein. After incubating cells with Zn^{2+}, ZnT4 protein expression does not change. C) Immunofluorescence analysis reveals that most of the ZnT4 localizes to vesicles in RWPE1 while in DuCaP, VCaP and LNCaP prostate cancer cell lines it localized at the plasma membrane and some vesicles. Incubating cells with Zn^{2+} reveals changes in ZnT4 localization. Lower panel demonstrates that plasma membrane localization of ZnT4 increases for RWPE1 but decreases for DuCaP, VCaP, and LNCaP which show more vesicular staining. Image within RWPE1 (normal growth condition) fluorescence was increase to demonstrate vesicle signal. All fluorescent images were thresholded to the same intensity, scale Bar = 25 μm, and arrow denotes localization on cell. ANOVA with Tukey HSD post hoc test was performed for qRT-PCR.

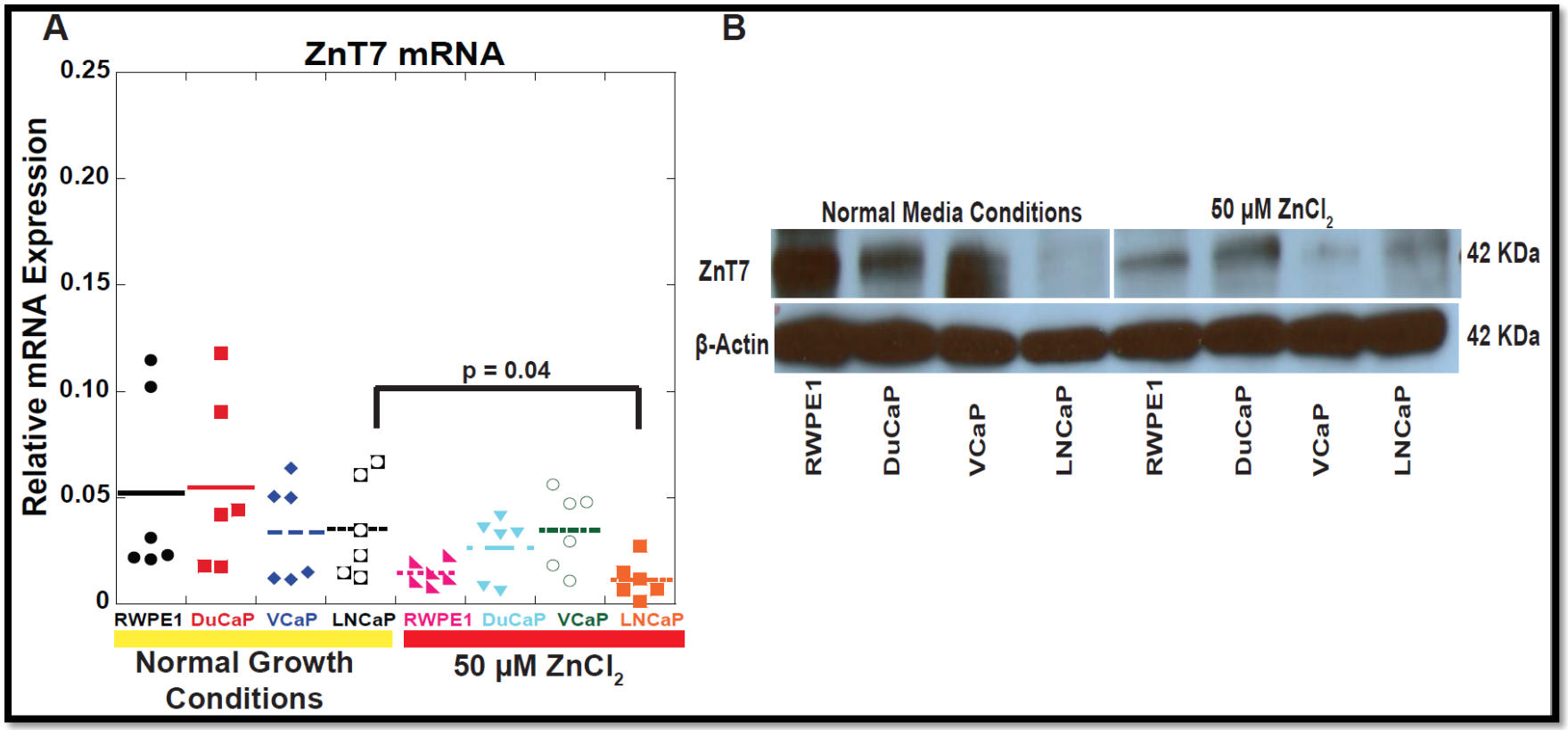

Figure 3.11. qRT-PCR and Western Blot of ZnT7. A) Quantitative RT-PCR analysis reveals no differences between the cell lines. Incubating the cells with Zn^{2+} for 2h prior to total RNA extraction does not lead to any changes in RWPE1, DuCaP, and VCaP while there is a 104% decrease in LNCaP cell line. Each qRT-PCR data point represents one 10 cm dish of cells. Relative mRNA levels corrected to Kβ1 reference gene. B) Western blot analysis reveals that in RWPE1 ZnT7 protein expression is higher compared to DuCaP and VCaP cell lines while LNCaP expression was undetectable. After incubating cells with Zn^{2+}, RWPE1 protein expression decreases, DuCaP appears to have no change, VCaP protein expression decreases, and LNCaP protein expression increases slightly. ANOVA with Tukey HSD post hoc test was performed for qRT-PCR.

3.5 Discussion

The American Cancer Society estimates that there are 241,740 new cases of prostate cancer per year in the United States, approximately 28,170 of which result in death (http://www.cancer.org/Cancer/ProstateCancer/OverviewGuide/prostate-cancer-overview-key-statistics). Early detection of prostate cancer requires regular examinations along with blood work to detect serum prostate specific antigen (PSA) (*47*). Elevation of serum PSA, also known as human kallikrein 3, is a widely used marker to monitor prostate health and malignancy. Unfortunately, benign tumors and some forms of inflammatory prostate disease can lead to elevated serum PSA and may result in false positive diagnosis of prostate cancer (*48-50*), conversely PSA levels can appear normal in patients with prostate cancer. Moreover, PSA levels do not correlate with the aggressiveness of the cancer and hence are not always reliable predictors of prognosis (*51, 52*).

Due to the need for more reliable diagnostic and prognostic prostate cancer markers, a growing number of studies have suggested the use of Zn^{2+} as a potential biomarker in the progression of this disease (*22, 53-55*). To evaluate this possibility, it is essential to better characterize Zn^{2+} levels and regulation in cell lines (*in vitro* models), animals models, and tissue samples from patients at different stages of malignancy. Because prostate cancer is characterized by a high degree of heterogeneity at the molecular level, we set out to define the levels of Zn^{2+} as well as key regulatory proteins in two newly developed prostate cancer cell lines that derived from different metastases from the same patient.

In previous Chapters we report that DuCaP, VCaP, and LNCaP prostate cancer cell lines are depleted of over 50% total cellular Zn^{2+} compared to normal cell line. While these cell lines are markedly depleted of cellular Zn^{2+} it did not translate across the board in all organelle but rather we found a redistribution of Zn^{2+}. Both nucleus and cytosol in the prostate cancer cell

line models contain a higher pool of free Zn^{2+} compared to normal cell line. On the other hand, the ER and mitochondria were markedly depleted of free Zn^{2+} in all three prostate cancer cell line models compared to normal cell line RWPE1. These differences in Zn^{2+} suggest that the Zn^{2+}-regulatory proteins might be expressed differently between our cell line models.

Examination of the mRNA levels, proteins, and protein localization of six Zn^{2+} transporters revealed significant differences between the cancer and noncancerous cell lines, suggesting widespread dysregulation of Zn^{2+} homeostasis in prostate carcinoma. In this study we examined 7 out of 24 known Zn^{2+} transporters and we suspect examination of a broader spectrum of Zn^{2+} regulatory proteins will yield further differences between normal and cancer cells. These 7-Zn^{2+} transporters (hZIP1, hZIP2, hZIP3, ZnT1, ZnT2, ZnT4, and ZnT7) were chosen because they all have been suggested to be regulated differently in either prostate tissue or cell carcinoma, but there are no comprehensive studies that compare mRNA levels, protein levels, localization, and dependence of expression on Zn^{2+} treatment. Moreover, few studies examine multiple cell lines, making it difficult to assess whether observed differences reflect heterogeneity in transporter expression or a systematic change associated with the cancer phenotype.

Very little is known about regulation of Zn^{2+} transporter expression levels. Our results show substantial differences between the mRNA expression levels measured by qRT-PCR and protein levels measure by western blotting. In fact, for six of the seven transporters analyzed we did not observe a direct correlation of mRNA and protein expression levels, suggesting that expression must be regulated post transcriptionally and/or post-translationally and revealing that relative mRNA levels tell us little about the relative levels of protein in cells. There is some evidence that some Zn^{2+} transporters are glycosylated. For example, in mammary gland tissues ZnT1 has two N-linked and two O-linked glycosylations (*43*). But otherwise there is very little information on post-translational modifications that might be present that could influence levels

of stability. As noted below, for many transporters we observed modulation of protein levels upon treatment of cells with Zn^{2+} for two hours, suggesting that transporter expression may be altered by Zn^{2+} status and environmental conditions. There is precedent for this in the literature as in the intestine of mice hZIP4 is internalized and degraded in response to Zn^{2+} (*56*).

Our initial intent in pursuing these studies was to answer two questions: 1) do cancer cells yield a consistent "Zn^{2+} dysregulation phenotype" or is there substantial heterogeneity among the Zn^{2+} regulatory proteins and 2) do changes in Zn^{2+} transporters track with changes in the free or total Zn^{2+} levels observed in normal versus cancerous cells. With regard to the first question, there are some systematic differences in transporters across all cancer cell lines, but there is also substantial heterogeneity. For example, both hZIP1 and ZnT1, the primary importer and exporter, respectively, are expressed higher in DuCaP, VCaP and LNCaP cancer cell lines compared to RWPE1. The increased expression of ZnT1 protein in prostate cancer cell lines could lead to enhanced extrusion of Zn^{2+} and hence lower total cellular Zn^{2+} levels. On the other hand, the high protein expression of hZIP1 in the prostate cancer cell lines suggests that perhaps hZIP1 is upregulated to compensate for the low Zn^{2+} levels. hZIP3 protein levels are lower in all three cancer lines compared to RWPE1. Similarly, the ZnT4 protein expression level is elevated in all three cancer cell lines. ZnT4 is primarily localized to vesicles and the plasma membrane. Qualitatively, it appeared as if ZnT4 exhibited increased plasma membrane localization in the cancer cell lines, but this needs to be explored more systematically and quantitatively. If this turns out to be the case, perhaps increased levels of ZnT4 facilitate extrusion of Zn^{2+} from cells, lowering total Zn^{2+} levels.

Because little is known about regulation of Zn^{2+} transporters in mammalian cells, at the outset of the study we weren't sure whether transporters would be sensitive to levels of free Zn^{2+} or total Zn^{2+}. Our observation of ZnT1 protein in the prostate cancer cell lines could be interpreted two ways. One interpretation is that increased ZnT1 may lead to enhanced

extrusion of Zn^{2+}, which would correlate with the lower total Zn^{2+} observed in cancer cell lines. Alternatively, ZnT1 expression levels may be regulated by Metal Transcription Factor-1 (MTF-1) "sensing" free Zn^{2+} in the cytosol. Studies have shown that MTF-1 is regulated by high levels of Zn^{2+} in the cytosol to increase ZnT1 expression as well as expression of the buffer regulatory protein metallothionein (MT) (*57-59*). While we observe high Zn^{2+} content in the cytosol of these prostate cancer cell lines using FRET sensors it could be possible that high Zn^{2+} is affecting MTF-1 hence leading to the high expression ZnT1 that we observe in all three prostate cancer cell lines.

We also observe substantial differences among the cancer cell lines. For example hZIP2 expression is higher in DuCaP and VCaP compared to RWPE1, but there is almost no protein detected in LNCaP cells, demonstrating heterogeneity between these cancer cell lines. ZnT7 localizes to Golgi and the protein expression varies in all four cell lines. In the last chapter we tried to quantify the free Zn^{2+} levels in the Golgi but found that our sensor was saturated in this compartment in normal and cancer cell lines. This may signify that the Zn^{2+} levels in the Golgi are not controlled by ZnT7.

Finally, complicating analysis of transporter expression is the fact that that Zn^{2+} transporters may be influenced by environmental Zn^{2+} levels. In this study when cells were treated with Zn^{2+} for 2 hrs, we saw many changes in protein levels, although often we did not observe a consistent trend amongst the prostate cancer cell lines. For example, Zn^{2+} treatment led to changes in protein levels for ZnT7, hZIP2, and hZIP3, but there was no consistent trend between the cancerous and noncancerous cell lines. Alternatively, for ZnT4 there was no change in expression upon treatment and for ZnT1, the blots were difficult to interpret because of differential loading. However, an interesting trend was observed for hZIP1 in RWPE1 Zn^{2+} caused a dramatic down-regulation of the this transporter similar to previous observations (*13*),

whereas protein levels actually increased in all three cancer cell lines, suggesting overall dysregulation of Zn^{2+} homeostasis..

In conclusion, our results demonstrate marked differences in mRNA and protein expression levels and localization of 7-Zn^{2+} transporters. While some of the differences occur systematically across all cancer cell lines, others don't. Although all three prostate cancer cell lines exhibit a similar Zn^{2+} phenotype (depletion of total Zn^{2+} and redistribution of free Zn^{2+}), it is hard to determine which Zn^{2+} transporter may be responsible for the altered Zn^{2+} levels, particularly when we have only profiled a subset of the transporters. This is perhaps not surprising given the heterogeneity in molecular characteristics of these cell lines. Heterogeneity in Zn^{2+} transporters has also be observed in studies characterizing hZIP1 and ZnT4 in a panel of tumor cells Costello and coworkers observed a high degree of heterogeneity in hZIP1 in 22 prostate tissue samples although malignant samples generally showed lower levels of hZIP1 tan normal samples (*12*). Moreover, a study characterizing hZIP2 and hZIP3 in normal and benign prostate hyperplasia (BPH) demonstrates that these transporters are downregulated in malignant cells (*16*), consistent in our observation for hZIP2 in LNCaP cancer cell line and hZIP3 in DuCaP and VCaP. In order to fully probe the mechanistic correlation of these transporters to Zn^{2+} levels and distribution in these cell lines, functional assays are required to determine whether the explicit changes observed in transporter expression lead to changes in Zn^{2+}.

3.6 References

1. Auld, D. S. (2001) Zinc coordination sphere in biochemical zinc sites, *Biometals 14*, 271-313.
2. Frederickson, C. J., Koh, J. Y., and Bush, A. I. (2005) The neurobiology of zinc in health and disease, *Nat Rev Neurosci 6*, 449-462.

3. Nies, D. H. (2007) Biochemistry. How cells control zinc homeostasis, *Science 317*, 1695-1696.

4. Outten, C. E., and O'Halloran, T. V. (2001) Femtomolar sensitivity of metalloregulatory proteins controlling zinc homeostasis, *Science 292*, 2488-2492.

5. Eide, D. J. (2006) Zinc transporters and the cellular trafficking of zinc, *Biochim Biophys Acta 1763*, 711-722.

6. Zalewski, P. D., Millard, S. H., Forbes, I. J., Kapaniris, O., Slavotinek, A., Betts, W. H., Ward, A. D., Lincoln, S. F., and Mahadevan, I. (1994) Video image analysis of labile zinc in viable pancreatic islet cells using a specific fluorescent probe for zinc, *J Histochem Cytochem 42*, 877-884.

7. Sorensen, M. B., Stoltenberg, M., Juhl, S., Danscher, G., and Ernst, E. (1997) Ultrastructural localization of zinc ions in the rat prostate: an autometallographic study, *Prostate 31*, 125-130.

8. Rosoff, B. (1981) Studies of zinc in normal and neoplastic prostatic tissues, *Prog Clin Biol Res 75A*, 447-457.

9. Zaichick, V., Sviridova, T. V., and Zaichick, S. V. (1997) Zinc in the human prostate gland: normal, hyperplastic and cancerous, *Int Urol Nephrol 29*, 565-574.

10. Sakai, I., Harada, K., Hara, I., Eto, H., and Miyake, H. (2005) A comparison of the biological features between prostate cancers arising in the transition and peripheral zones, *BJU Int 96*, 528-532.

11. Feustel, A., and Wennrich, R. (1984) Determination of the distribution of zinc and cadmium in cellular fractions of BPH, normal prostate and prostatic cancers of different histologies by atomic and laser absorption spectrometry in tissue slices, *Urol Res 12*, 253-256.

12. Franklin, R. B., Feng, P., Milon, B., Desouki, M. M., Singh, K. K., Kajdacsy-Balla, A., Bagasra, O., and Costello, L. C. (2005) hZIP1 zinc uptake transporter down regulation and zinc depletion in prostate cancer, *Mol Cancer 4*, 32.

13. Huang, L., Kirschke, C. P., and Zhang, Y. (2006) Decreased intracellular zinc in human tumorigenic prostate epithelial cells: a possible role in prostate cancer progression, *Cancer Cell Int 6*, 10.

14. Lichten, L. A., and Cousins, R. J. (2009) Mammalian zinc transporters: nutritional and physiologic regulation, *Annu Rev Nutr 29*, 153-176.

15. Hennigar, S. R., and Kelleher, S. L. (2012) Zinc networks: the cell-specific compartmentalization of zinc for specialized functions, *Biol Chem 393*, 565-578.

16. Desouki, M. M., Geradts, J., Milon, B., Franklin, R. B., and Costello, L. C. (2007) hZip2 and hZip3 zinc transporters are down regulated in human prostate adenocarcinomatous glands, *Mol Cancer 6*, 37.

17. Franklin, R. B., Ma, J., Zou, J., Guan, Z., Kukoyi, B. I., Feng, P., and Costello, L. C. (2003) Human ZIP1 is a major zinc uptake transporter for the accumulation of zinc in prostate cells, *J Inorg Biochem 96*, 435-442.

18. Gaither, L. A., and Eide, D. J. (2000) Functional expression of the human hZIP2 zinc transporter, *J Biol Chem 275*, 5560-5564.

19. Gaither, L. A., and Eide, D. J. (2001) The human ZIP1 transporter mediates zinc uptake in human K562 erythroleukemia cells, *J Biol Chem 276*, 22258-22264.

20. Albrecht, A. L., Somji, S., Sens, M. A., Sens, D. A., and Garrett, S. H. (2008) Zinc transporter mRNA expression in the RWPE-1 human prostate epithelial cell line, *Biometals 21*, 405-416.

21. Costello, L. C., Liu, Y., Zou, J., and Franklin, R. B. (1999) Evidence for a zinc uptake transporter in human prostate cancer cells which is regulated by prolactin and testosterone, *J Biol Chem 274*, 17499-17504.

22. Iguchi, K., Otsuka, T., Usui, S., Ishii, K., Onishi, T., Sugimura, Y., and Hirano, K. (2004) Zinc and metallothionein levels and expression of zinc transporters in androgen-independent subline of LNCaP cells, *J Androl 25*, 154-161.

23. Hasumi, M., Suzuki, K., Matsui, H., Koike, H., Ito, K., and Yamanaka, H. (2003) Regulation of metallothionein and zinc transporter expression in human prostate cancer cells and tissues, *Cancer Lett 200*, 187-195.

24. Iguchi, K., Usui, S., Inoue, T., Sugimura, Y., Tatematsu, M., and Hirano, K. (2002) High-level expression of zinc transporter-2 in the rat lateral and dorsal prostate, *J Androl 23*, 819-824.

25. Song, Y., Elias, V., Wong, C. P., Scrimgeour, A. G., and Ho, E. (2010) Zinc transporter expression profiles in the rat prostate following alterations in dietary zinc, *Biometals 23*, 51-58.

26. Valkenburg, K. C., and Williams, B. O. (2011) Mouse models of prostate cancer, *Prostate Cancer 2011*, 895238.

27. Henshall, S. M., Afar, D. E., Rasiah, K. K., Horvath, L. G., Gish, K., Caras, I., Ramakrishnan, V., Wong, M., Jeffry, U., Kench, J. G., Quinn, D. I., Turner, J. J., Delprado, W., Lee, C. S., Golovsky, D., Brenner, P. C., O'Neill, G. F., Kooner, R., Stricker, P. D., Grygiel, J. J., Mack, D. H., and Sutherland, R. L. (2003) Expression of the zinc transporter ZnT4 is decreased in the progression from early prostate disease to invasive prostate cancer, *Oncogene 22*, 6005-6012.

28. Kirschke, C. P., and Huang, L. (2003) ZnT7, a novel mammalian zinc transporter, accumulates zinc in the Golgi apparatus, *J Biol Chem 278*, 4096-4102.

29. Tepaamorndech, S., Huang, L., and Kirschke, C. P. (2011) A null-mutation in the Znt7 gene accelerates prostate tumor formation in a transgenic adenocarcinoma mouse prostate model, *Cancer Lett 308*, 33-42.

30. Peehl, D. M. (2005) Primary cell cultures as models of prostate cancer development, *Endocr Relat Cancer 12*, 19-47.

31. van Bokhoven, A., Varella-Garcia, M., Korch, C., Johannes, W. U., Smith, E. E., Miller, H. L., Nordeen, S. K., Miller, G. J., and Lucia, M. S. (2003) Molecular characterization of human prostate carcinoma cell lines, *Prostate 57*, 205-225.

32. Webber, M. M., Bello, D., and Quader, S. (1997) Immortalized and tumorigenic adult human prostatic epithelial cell lines: characteristics and applications Part 2. Tumorigenic cell lines, *Prostate 30*, 58-64.

33. Webber, M. M., Bello, D., and Quader, S. (1997) Immortalized and tumorigenic adult human prostatic epithelial cell lines: characteristics and applications. Part 3. Oncogenes, suppressor genes, and applications, *Prostate 30*, 136-142.

34. Korenchuk, S., Lehr, J. E., L, M. C., Lee, Y. G., Whitney, S., Vessella, R., Lin, D. L., and Pienta, K. J. (2001) VCaP, a cell-based model system of human prostate cancer, *In Vivo 15*, 163-168.

35. Lee, Y. G., Korenchuk, S., Lehr, J., Whitney, S., Vessela, R., and Pienta, K. J. (2001) Establishment and characterization of a new human prostatic cancer cell line: DuCaP, *In Vivo 15*, 157-162.

36. van Bokhoven, A., Caires, A., Maria, M. D., Schulte, A. P., Lucia, M. S., Nordeen, S. K., Miller, G. J., and Varella-Garcia, M. (2003) Spectral karyotype (SKY) analysis of human prostate carcinoma cell lines, *Prostate 57*, 226-244.

37. Goidin, D., Mamessier, A., Staquet, M. J., Schmitt, D., and Berthier-Vergnes, O. (2001) Ribosomal 18S RNA prevails over glyceraldehyde-3-phosphate dehydrogenase and beta-actin genes as internal standard for quantitative comparison of mRNA levels in invasive and noninvasive human melanoma cell subpopulations, *Anal Biochem 295*, 17-21.

38. Schmittgen, T. D., and Zakrajsek, B. A. (2000) Effect of experimental treatment on housekeeping gene expression: validation by real-time, quantitative RT-PCR, *J Biochem Biophys Methods 46*, 69-81.

39. Ohl, F., Jung, M., Xu, C., Stephan, C., Rabien, A., Burkhardt, M., Nitsche, A., Kristiansen, G., Loening, S. A., Radonic, A., and Jung, K. (2005) Gene expression studies in prostate cancer tissue: which reference gene should be selected for normalization?, *J Mol Med (Berl) 83*, 1014-1024.

40. Eide, D. J. (2004) The SLC39 family of metal ion transporters, *Pflugers Arch 447*, 796-800.

41. Palmiter, R. D., and Findley, S. D. (1995) Cloning and functional characterization of a mammalian zinc transporter that confers resistance to zinc, *Embo J 14*, 639-649.

42. Lopez, V., and Kelleher, S. L. (2009) Zinc transporter-2 (ZnT2) variants are localized to distinct subcellular compartments and functionally transport zinc, *Biochem J 422*, 43-52.

43. Kelleher, S. L., and Lonnerdal, B. (2003) Zn transporter levels and localization change throughout lactation in rat mammary gland and are regulated by Zn in mammary cells, *J Nutr 133*, 3378-3385.

44. Iguchi, K., Morihara, N., Usui, S., Hayama, M., Sugimura, Y., and Hirano, K. (2011) Castration- and aging-induced changes in the expression of zinc transporter and metallothionein in rat prostate, *J Androl 32*, 144-150.

45. Kirschke, C. P., and Huang, L. (2008) Expression of the ZNT (SLC30) family members in the epithelium of the mouse prostate during sexual maturation, *J Mol Histol 39*, 359-370.

46. Huang, L., and Gitschier, J. (1997) A novel gene involved in zinc transport is deficient in the lethal milk mouse, *Nat Genet 17*, 292-297.

47. Franklin, R. B., and Costello, L. C. (2007) Zinc as an anti-tumor agent in prostate cancer and in other cancers, *Arch Biochem Biophys 463*, 211-217.

48. Bozeman, C. B., Carver, B. S., Eastham, J. A., and Venable, D. D. (2002) Treatment of chronic prostatitis lowers serum prostate specific antigen, *J Urol 167*, 1723-1726.

49. Emberton, M., Andriole, G. L., de la Rosette, J., Djavan, B., Hoefner, K., Vela Navarrete, R., Nordling, J., Roehrborn, C., Schulman, C., Teillac, P., Tubaro, A., and Nickel, J. C. (2003) Benign prostatic hyperplasia: a progressive disease of aging men, *Urology 61*, 267-273.

50. Polascik, T. J., Oesterling, J. E., and Partin, A. W. (1999) Prostate specific antigen: a decade of discovery--what we have learned and where we are going, *J Urol 162*, 293-306.

51. Bradford, T. J., Tomlins, S. A., Wang, X., and Chinnaiyan, A. M. (2006) Molecular markers of prostate cancer, *Urol Oncol 24*, 538-551.

52. Stamey, T. A., Caldwell, M., McNeal, J. E., Nolley, R., Hemenez, M., and Downs, J. (2004) The prostate specific antigen era in the United States is over for prostate cancer: what happened in the last 20 years?, *J Urol 172*, 1297-1301.

53. Cortesi, M., Fridman, E., Volkov, A., Shilstein, S., Chechik, R., Breskin, A., Vartsky, D., Raviv, G., and Ramon, J. New prospective for non-invasive detection, grading, size evaluation, and tumor location of prostate cancer, *Prostate 70*, 1701-1708.

54. Franklin, R. B., and Costello, L. C. (2009) The important role of the apoptotic effects of zinc in the development of cancers, *J Cell Biochem 106*, 750-757.

55. Ghosh, S. K., Kim, P., Zhang, X. A., Yun, S. H., Moore, A., Lippard, S. J., and Medarova, Z. A novel imaging approach for early detection of prostate cancer based on endogenous zinc sensing, *Cancer Res 70*, 6119-6127.

56. Weaver, B. P., Dufner-Beattie, J., Kambe, T., and Andrews, G. K. (2007) Novel zinc-responsive post-transcriptional mechanisms reciprocally regulate expression of the mouse Slc39a4 and Slc39a5 zinc transporters (Zip4 and Zip5), *Biol Chem 388*, 1301-1312.

57. Giedroc, D. P., Chen, X., and Apuy, J. L. (2001) Metal response element (MRE)-binding transcription factor-1 (MTF-1): structure, function, and regulation, *Antioxid Redox Signal 3*, 577-596.

58. Giedroc, D. P., Chen, X., Pennella, M. A., and LiWang, A. C. (2001) Conformational heterogeneity in the C-terminal zinc fingers of human MTF-1: an NMR and zinc-binding study, *J Biol Chem 276*, 42322-42332.

59. Laity, J. H., and Andrews, G. K. (2007) Understanding the mechanisms of zinc-sensing by metal-response element binding transcription factor-1 (MTF-1), *Arch Biochem Biophys 463*, 201-210.

Chapter IV

New alternately colored FRET sensors for simultaneous monitoring of Zn^{2+} in multiple cellular locations

Jose G. Miranda[1], Amanda L. Weaver[1], Yan Qin[1], J. Genevieve Park[1], Caitlin I. Stoddard[1], Michael Z. Lin[2], Amy E. Palmer[1*]

1 Department of Chemistry and Biochemistry and BioFrontiers Institute, UCB 596, University of Colorado, Boulder, CO 80309

2 Department of Pediatrics and Engineering, Stanford Medical School, Stanford, CA, 94305-5164

4.1 Abstract

Genetically encoded sensors based on fluorescence resonance energy transfer (FRET) are powerful tools for reporting on ions, molecules and biochemical reactions in living cells. Here we describe the development of new sensors for Zn^{2+} based on alternate FRET-pairs that do not involve the traditional CFP and YFP. Zn^{2+} is an essential micronutrient and plays fundamental roles in cell biology. Consequently there is a pressing need for robust sensors to monitor Zn^{2+} levels and dynamics in cells with high spatial and temporal resolution. All the existing sensors are comprised of CFP and YFP and hence have limited utility in acid compartments and don't permit simultaneous imaging of Zn^{2+} fluxes in multiple cellular locations. Here we develop a suite of sensors using alternate FRET pairs, including tSapphire/TagRFP, tSapphire/mKO, Clover/mRuby2, mOrange2/mCherry, and mOrange2/mKate. These sensors were targeted to both the nucleus and cytosol and characterized and validated in living cells. Sensors based on the new FRET pair Clover/mRuby2 displayed a higher dynamic range and better signal-to-noise ratio than the remaining sensors tested and were optimal for monitoring changes in cytosolic and nuclear Zn^{2+}. Using a green-red sensor targeted to the nucleus and cyan-yellow sensor targeted to either the ER, Golgi, or mitochondria, we were able to monitor Zn^{2+} uptake simultaneously in two compartments, revealing that nuclear Zn^{2+} rises quickly, whereas the ER, Golgi, and mitochondria all sequester Zn^{2+} more slowly and with a delay of 600-700 sec. Lastly, these studies provide the first glimpse of nuclear Zn^{2+} and reveal that nuclear Zn^{2+} is buffered at a higher level than cytosolic Zn^{2+}.

4.2 Introduction

Fluorescent proteins (FP) are powerful tools to monitor cellular signals. Since the initial development of GFP as a research tool for biological discovery, laboratories have diversified FP spectra through directed evolution, resulting in a plethora of probes across the visible spectrum (*1*). These FPs have been used in the generation of fluorescence resonance energy transfer

(FRET)-based sensors to report dynamic biochemistry in living cells (*2, 3*). Because FRET efficiency is sensitive to distance and orientation between the donor and acceptor fluorophore, conformational changes due to binding of a ligand to a protein of interest can form the basis of FRET-based biosensors. The most commonly used donor and acceptor FPs are variants of cyan FP (CFP) and yellow FP (YFP) (*2*).

In recent years the development of alternate color FRET sensors has enabled new avenues of research such as the ability to monitor a single signal in multiple cellular compartments or simultaneously track two cellular signals (*4*). For example, two complementary probes for caspase-3 activity based on mTFP1/mCitrine and mAmetrine/tdTomato were used to visualize caspase-3 activity in the nucleus and cytoplasm, revealing temporal differences in caspase-3 activation (*5*). The same FRET pairs were used to develop probes for monitoring both Ca^{2+} and caspase-3 in the same cell (*6*). Monomeric Teal FP (mTFP) is an FP version of the widely used CFP derived a s replacement for enhanced CFP because of its high quantum yield (*7*). Such studies allow researchers to precisely correlate the timing of two interdependent cellular events or to track the movement of ions or molecules from one compartment to another. An additional advantage of alternate color FRET sensors, particularly those that avoid using a variant of YFP which is quenched by acid (*8*), is that they are likely to be less sensitive to pH perturbations.

While in principle the concept of generating alternate color FRET sensors is attractive, in practice there are a number challenges that have limited availability of non-CFP/YFP biosensors. First and foremost, the vast majority of the > 120 FRET-based biosensors currently available are based on CFP/YFP and as noted in a recent publication (*6*), changing the FPs often requires extensive re-optimization of the sensor. Secondly, the biophysical (folding, maturation, oligomerization state) and photophysical properties (brightness) of red and orange FPs still lag behind those of the cyan-yellow counterparts (*9*), making it challenging to identify a

robust alternate FRET pair. Indeed of the non-CFP/YFP biosensors developed thus far, each research team chose a different combination of FRET partners (*5, 10-14*).

In this work, we developed alternately colored Zn^{2+} biosensors, testing a series of green-red and orange-red FP combinations. Because it is common for sensors to exhibit diminished responses in cells compared to *in vitro* (*15, 16*), we screened the panel of sensors in mammalian cells to assess whether they were capable to responding to manipulation of cellular Zn^{2+} levels. The sensors were then targeted to both the nucleus and cytosol and nuclear sensors were used in conjunction with an organelle-localized CFP-YFP-based Zn^{2+} sensor to monitor Zn^{2+} fluxes in two cellular compartments simultaneously. We believe these represent an important breakthrough in expanding the palette of Zn^{2+} sensors and developing sensors for use in acidic compartments.

4.3 Experimental Methods

FRET Sensor Cloning. A schematic of the general sensor construction is presented in **Figure 4.1a** and all sequences have been deposited in GenBank. **Table 4.1** summarizes the mutations in the zinc finger domain. For bacterial expression and sensor purification, sensor cDNA was cloned into pET302/NT-His (Life Technologies) in which the *Bam*HI and *Eco*RI restriction sites were reversed by site directed mutagenesis. For mammalian cell expression sensor cDNA was cloned into pcDNA3.1-(+) between *Bam*HI and *Eco*RI. To localize sensors to either the nucleus or the cytosol, a nuclear localization (NLS) or nuclear exclusion (NES) signal sequence was cloned upstream of *Bam*HI site, such that the signal sequence is at the N-terminus of the sensor. For nuclear or cytosolic localization the following primers were used: 5'-**ATG**CCTAAAAAAAAACGTAAAGTTGAAGATGCT**GGATCC**-3' (NLS) and 5'-**ATG**CTTCAACTTCCTCCTCTTGAACGTCTTACTCTT**GGATCC**-3' (NES). Sensors containing localization sequences for endoplasmic reticulum, Golgi apparatus, and mitochondria were developed previously (*15, 17*).

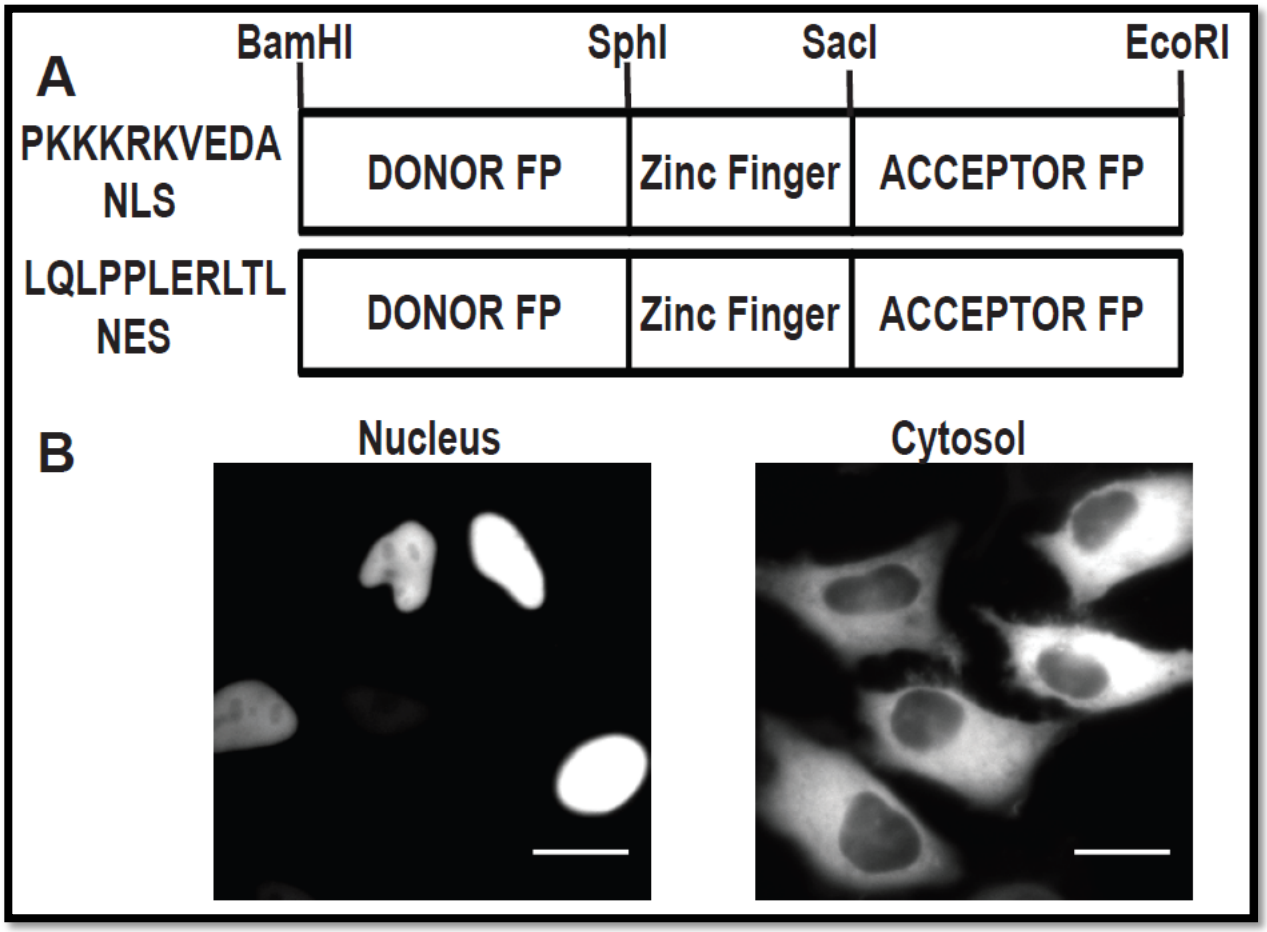

Figure 4.1. Nuclear Localization and Nuclear Exclusion Signal Sequence constructs. A NLS and NES signal sequence were cloned into pcDNA 3.1 (+) vector upstream *Bam*HI. A) Schematic of FRET sensor construct. B) Representative images of transfected sensor showing localization to either the nucleus or cytosol. Scale bar = 20 μm.

Table 4.1. Amino acid sequence of Zap Zinc Binding Domains (ZBD)

ZBD	Amino Acid Sequence
Zap1	KNNDLK**C**KWKE**C**PESCSSLFDLQR**H**LLKD**H**VSQDFKHPMEPLA**C**NWED**C**DFLGDDTCSIVN**H**INCQ**H**GI
Zap1.1	KNNDLK**H**KWKE**C**PESCSSLFDLQR**H**LLKD**H**VSQDFKHPMEPLA**C**NWED**C**DFLGDDTCSIVN**H**INCQ**H**GI
Zap2	KNNDLK**H**KWKE**C**PESCSSLFDLQR**H**LLKD**H**VSQDFKHPMEPLA**H**NWED**C**DFLGDDTCSIVN**H**INCQ**H**GI

Zap1 disassociation constant (K_d') = 2.53 pM; Zap2 (K_d') = 811 pM; Zap1.1 (K_d') = undetermined

Clover lacks the C-terminal residues GITLMDELYK that are present in other GFP-based proteins. During the initial cloning of ZapCmR1 there was an inadvertent addition of the linker MVSKGEEL to the N-terminus of mRuby2 so the sensor contains this additional linker.

Cell Culture and Microscopy. HeLa cells were grown in Dulbecco's Modified Eagle's Medium (DMEM) (Life Technologies) supplemented with 10% (v/v) fetal bovine serum (Atlanta Biologicals), 100 U/mL penicillin, and 100 µg/mL streptomycin. Cells were incubated at 37°C in 5% CO_2, changing the media every 3 days. Once cells were approximately 80-90% confluent they were split and seeded onto 3.5 cm imaging dishes until they were approximately 40-50% confluent. At this point 1 µg of sensor DNA was transiently transfected using TransIT®-LT1 (Mirus) as specified by manufacturer instructions.

Forty-eight hours after transfection, cells were imaged using phosphate, calcium, and magnesium free HEPES-buffered Hanks' balanced salt (HHBSS) media (5.36 mM KCl, 137 mM NaCl, 16.65 mM D-Glucose, and 30 mM HEPES) pH 7.4. This buffer is made in our laboratory because phosphates are known to precipitate Zn^{2+}. Buffer was generated with Chelex-100-treated water (Sigma Aldrich). Cell imaging was performed on a Zeiss Axiovert 200 M microscope with a Cascade 512B CCD camera (Roper Scientific) and Xenon arc lamp (XBO75)

using MetaFluor software (Universal Imaging) to operate the system. All excitation filters, dichroic mirrors, and emission filters (Chroma Technology or Semrock) are presented in **Table 4.2**. The following settings were used: exposure time 400 msec, 20-30 second acquisition rate, 1.3NA 40x oil immersion objective, and excitation light was attenuated with either a 10% neutral density filter for tSapphire paired with mKO or TagRFP as well as for Clover and mRuby2 and 5% neutral density filter for mOrange2 paired with mCherry or mKate as well as for CFP-YFP pair.

Live cell imaging experiments. To characterize sensors in cells, a region of interest (ROI) was placed on an individual cell and on an untransfected cell or a region in the field of view with no cells as a measure of the background fluorescence. The FRET channel is defined as the emission intensity in the acceptor FP channel, upon excitation of the donor. The FRET ratio is defined as the background corrected intensity in the FRET channel divided by the background corrected intensity in the donor channel, i.e. $(I_{FRET} - I_{FRETbackground})/(I_{Donor} - I_{donorbackground})$. For imaging experiments, DMEM media was removed and cells were washed twice with HHBSS buffer followed by the addition of 1 mL HHBSS. ROIs were followed for 300 seconds to establish a resting R followed by the addition of 150 μM TPEN (N,N,N',N'-tetrakis-(2-pyridylmethyl)-ethylenediamine) to chelate Zn^{2+} and obtain the FRET ratio of the unbound sensor (R_{TPEN}). Once R_{TPEN} was established, cells were washed 3-times with the HHBSS

Table 4.2. Filter sets and dichroic mirrors used for cellular imaging

FP	Excitation filter (nm/bandwidth)	Dichroic (nm)	Emission filter (nm/bandwidth)
CFP	430/24	455	470/24
YFP	495/10	515	535/20
tSapphire	390/22	495	510/20
mKO	540/25	565	595/50
TagRFP	540/25	565	595/50
mOrange2	540/25	565	595/50
mCherry	577/20	595	630/60
mKate	577/20	595	630/60
Clover	480/20	495	510/20
mRuby2	540/25	565	595/50

For FRET experiments, the donor excitation filter and dichroic mirror are used along with the emission filter of the acceptor FP.

solution to remove residual TPEN followed by addition of 1 mL of fresh HHBSS. Subsequently, 135 μM $ZnCl_2$ and 10 μM digitonin were added to saturate the sensor and establish the FRET ratio of the Zn^{2+} bound sensor (R_{Zn}). Data were collected at 20-30 sec acquisition rate. The dynamic range of each sensor was defined as the maximum FRET ratio divided by the minimum FRET ratio (R_{max}/R_{min}), and the percent saturation was calculated according to $[(|R-R_{TPEN}|)/(|R_{Zn}-R_{TPEN}|)]*100\%$.

Simultaneous monitoring of Zn^{2+} uptake into multiple compartments. In order to monitor Zn^{2+} in two compartments of a single cell, cells were transfected with both a cyan-yellow and green-red or red-orange FRET sensor. Zinc uptake was initiated by addition of 100 μM $ZnCl_2$ extracellularly without any ionophores or membrane permeabilization agents. Previous studies

in our lab have established that addition of 100 μM $ZnCl_2$ extracellularly leads to a rise in cytosolic Zn^{2+} from ~ 100 pM to ~ 6 nM (*15*). The background corrected FRET ratio was measured for each compartment as described above.

4.4 Results

4.4.1 Measurement of spectral bleedthrough. Given the lack of consensus on an optimal green-red or red-orange FRET pair, we decided to test 5 different alternate FRET pairs in the zinc sensor platform. **Table 4.3** summarizes the sensors generated using tSapphire, an ultra-violet (UV) excitable FP (*18*), Clover (*19*), mKO (*20*), mOrange2 (*21*), TagRFP (*22*), mCherry (*23*), mKate (*24*), or mRuby2 (*19*). An important consideration when evaluating whether multiple FRE sensors can be used simultaneously in cells is the extent of spectral crosstalk between individual FPs and FRET constructs. Spectral crosstalk generally refers to the presence of fluorescence signal from more than one species in a single optical channel. The extent of crosstalk is given by the percent bleedthrough (or contamination) of a given fluorescent species in an optical channel. Because FRET ratios are calculated using the FRET optical channel and the donor optical channel, we felt it was important to determine bleedthrough in both of these channels. For the donor channel, HeLa cells were transfected with cDNA encoding an individual FP and the fluorescence intensity was measured in all channels. **Table 4.4** and **Figure 4.2 and 4.3** present the percent bleedthrough in each of the donor channels (CFP, tSapphire, mOrange2, and Clover), which was less than 5% in all cases. For the FRET channel constructs in **Table 4.5** were transfected into cells and the intensity was measured in each of the FRET channels (**Figure 4.4**). When pairing CFP-YFP with a green-red sensor, there was substantial bleedthrough of Clover-mRuby2, tSapphire-TagRFP and tSapphire-mKO into the CFP-YFP FRET channel (50%, 96%, and 80%, respectively), and < 10% of CFP-YFP into the green-red channels. This indicates that if one of these green-red sensors is to be used alongside a CFY-YFP sensor, the sensors need to be in non-overlapping

Table 4.3. Fluorescent Protein Excitation and Emission

Donor FP	Acceptor FP	Sensor Name	Excitation max (nm)	Emission max (nm)
CFP	**Y**FP	Zap**CY**2	435	535
t**S**apphire	**m**KO	Zap**SM**2	399	559
t**S**apphire	Tag**R**FP	Zap**SR**2	399	580
m**O**range2	m**C**herry	Zap**OC**2	549	610
m**O**range2	m**K**ate	Zap**OK**2	549	633
Clover	**mR**uby2	Zap**CmR**1	486	605
Clover	**mR**uby2	Zap**CmR**1.1	486	605
Clover	**mR**uby2	Zap**CmR**2	486	605

Sensor nomenclature is as follows: Zap refers to the 1st two zinc fingers of the *Saccaromyces cerevisiae* Zap1 transcription factor that serves as the zinc binding domain, the next two letters refer to the donor and acceptor FPs, finally the "1" at the end of a sensor name indicates the wild type Zap1 domain was used, the "2" indicates that two mutations (Cys to His) were incorporated to lower the zinc affinity, as outlined in [15]. "1.1" indicates one mutation (Cys to His) was incorporated.

spatial locations. Spectral crosstalk was minimized by pairing CFP-YFP with an orange-red sensor (< 3% for all combinations).

4.4.2 Generation of nuclear and cytosol localized constructs

There are no published sensors for quantitatively measuring Zn^{2+} in the nucleus. Yet nuclear Zn^{2+} is an important component of cellular Zn^{2+} homeostasis. First, a large number of nuclear proteins, including polymerases, transcription factors, and DNA remodeling factors such as histone deacetylases require Zn^{2+} for proper function (*25, 26*). Second, there is evidence that the primary Zn^{2+} storage protein, metallothionein, shuttles into the nucleus during the G_1 to S phase transition, suggesting dynamic regulation of nuclear Zn^{2+} during cell division (*27*). Third, studies have reported the generation of transient nuclear Zn^{2+} signals (*28*). Therefore, we

Table 4.4. Percent Bleedthrough of Fluorescent Proteins

Transfected FP	Percent intensity in each channel[1]					
	Clover channel	CFP channel	YFP channel	tSapphire channel	mKO/mOrange2/TagRFP/mRuby2 channel	mCherry/mKATE channel
CFP	15 ± 0.06	100	0.06 ± 0.01	3 ± 0.03	0.09 ± 0.01	0.06 ± 0.01
YFP	41 ± 0.6	0.02 ± 0.003	100	0.06 ± 0.001	5 ± 0.3	0.01 ± 0.01
tSapphire	16 ± 0.06	4 ± 0.06	27 ± 0.2	100	0.01 ± 0.03	0.3 ± 0.03
mKO	2 ± 0.4	0.4 ± 0.05	4 ± 0.07		100	2 ± 0.08
mOrange2	0.2 ± 0.01	0.3 ± 0.01	4 ± 0.05	0.07 ± 0.01	100	4 ± 0.02
TagRFP	0.09 ± 0.01	0.6 ± 0.08	0.3 ± 0.03	0.1 ± 0.01	100	22 ± 0.04
mCherry	0.16 ± 0.02	0.4 ± 0.02	0.06 ± 0.01	0.08 ± 0.01	57 ± 0.1	100
mKate	0.35 ± 0.03	0.5 ± 0.02	2 ± 0.01	0.2 ± 0.01	43 ± 0.3	100
Clover	100	0.3 ± 0.03	84 ± 5.3	0.2 ± 0.01	0.3 ± 0.001	0.06 ± 0.004
mRuby2	3 ± 0.3	8 ± 1	2 ± 0.2	0.3 ± 0.07	100	44 ± 0.1

Each experiment was performed in triplicate and a minimum of 6-cells per field of view were observed. Values reported represent the mean ± SEM. Excitation filters, Dichroic mirrors, and Emission filters for each channel are given in **Table 4.2**. Percent intensity was calculated as follows: Intensity in the designated channel divided by Intensity in the channel of the transfected FP. Cross-talk between the donor channels is highlighted in gray.

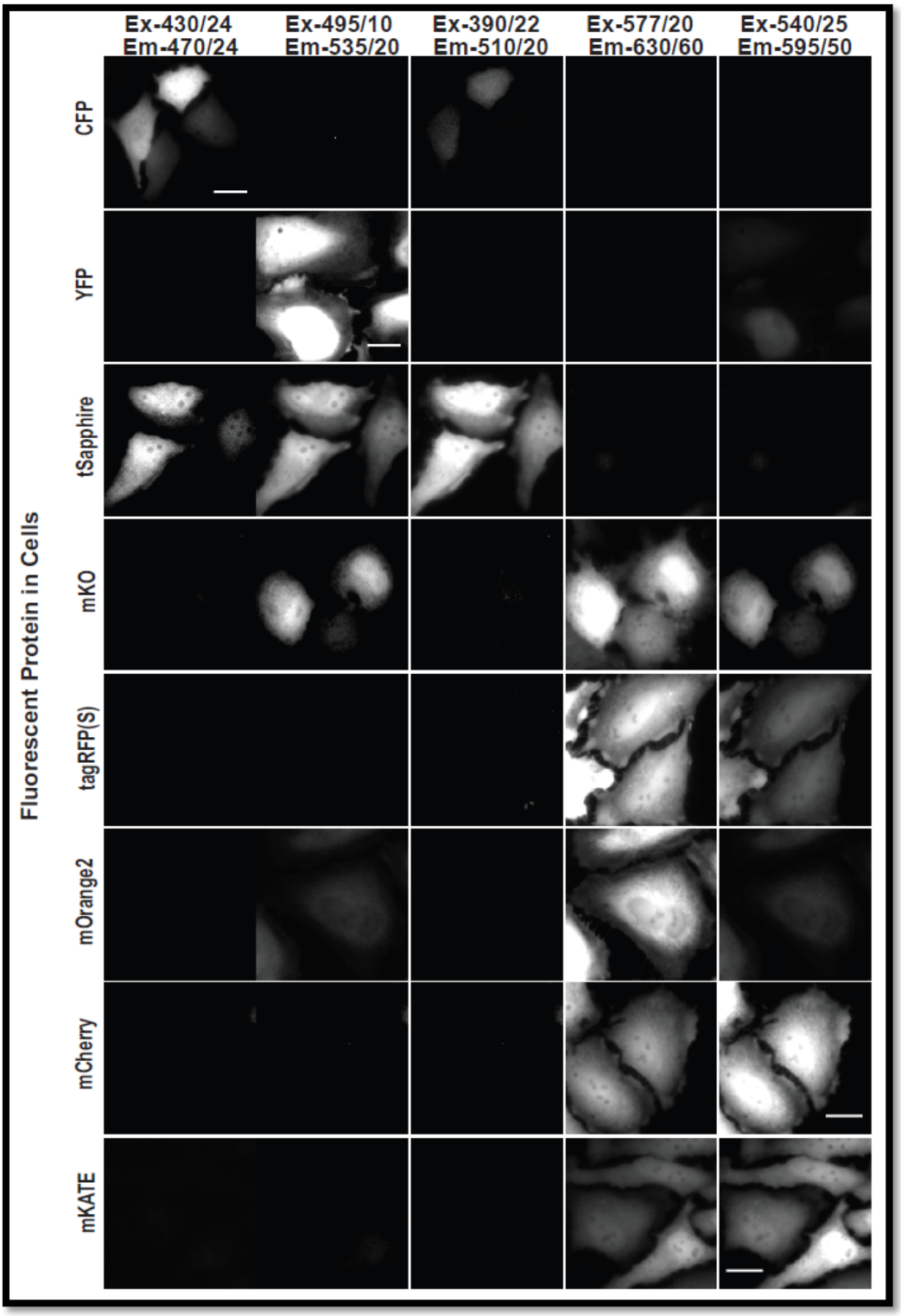

Figure 4.2. Bleed-through of fluorescent proteins. Representative images for bleedthrough measurements. Cells were transfected with the FP listed on the left hand side and the excitation and emission parameters used as shown on top. Ex = Excitation and Em = Emission and bandwidth in nanometers. Scale bar = 20 μm.

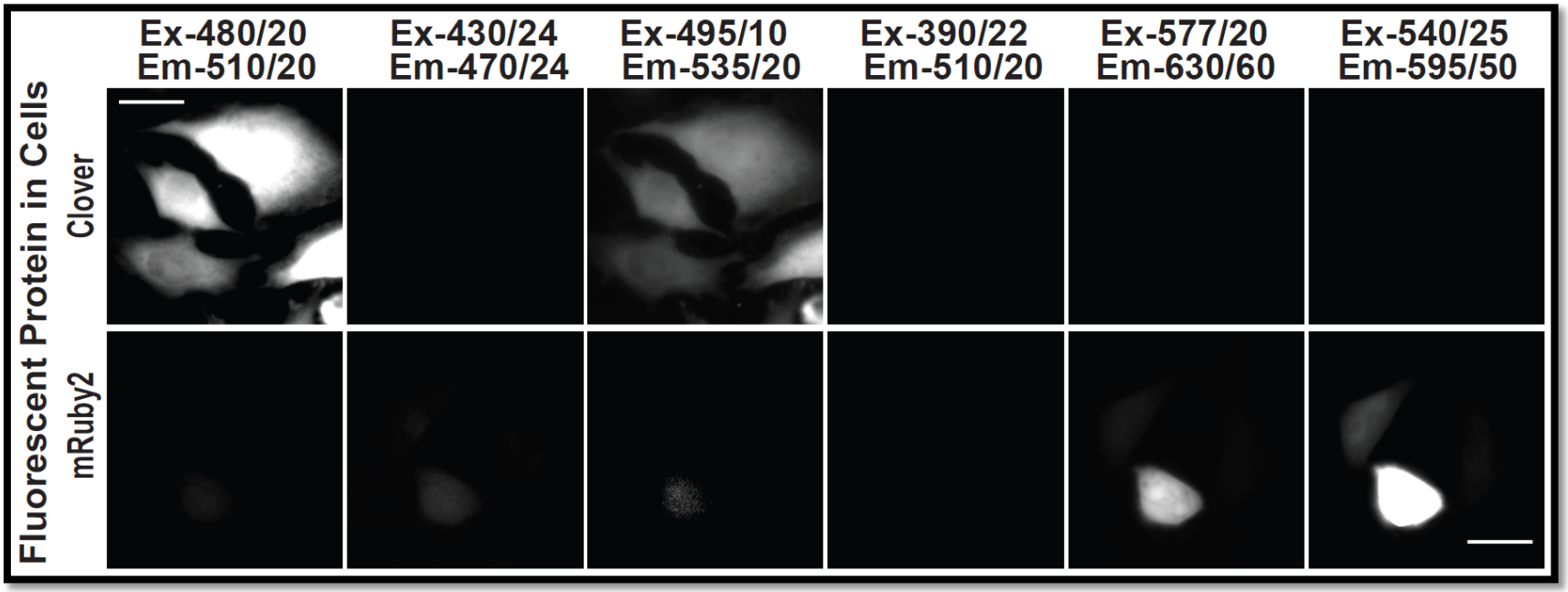

Figure 4.3. Bleed-through of fluorescent proteins. Representative images for bleedthrough measurements. Cells were transfected with the FP listed on the left hand side and the excitation and emission parameters used as shown on top. Ex = Excitation and Em = Emission and bandwidth in nanometers. Scale bar = 20 μm.

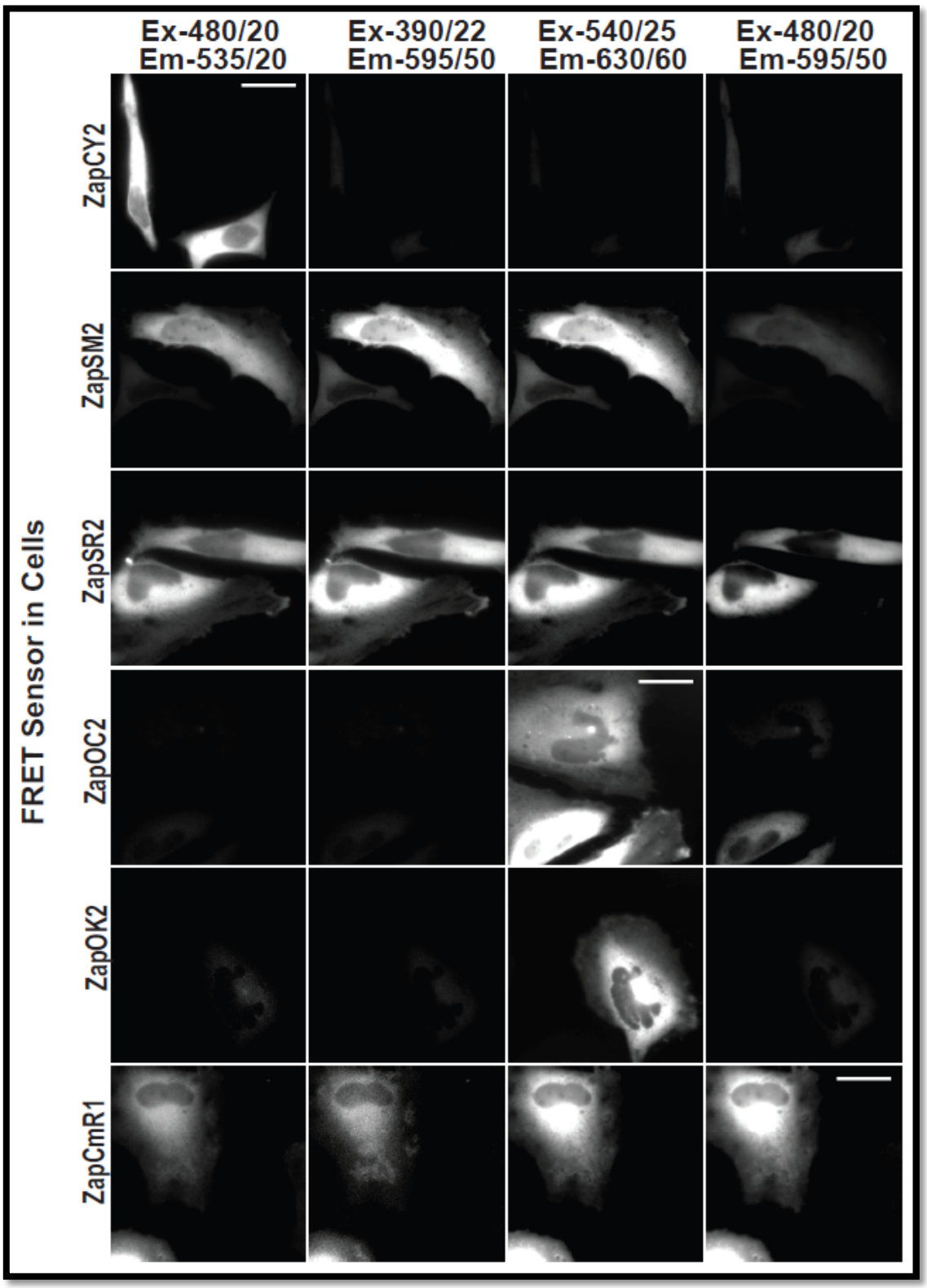

Figure 4.4. Cross-talk of FRET sensors. Representative images for bleedthrough measurements. Cells were transfected with the FRET sensor listed on the left hand side and the excitation and emission parameters used as shown on top. Ex = Excitation and Em = Emission and bandwidth in nanometers. Scale bar = 20 μm.

Table 4.5. Percent Bleedthrough of sensor into FRET channels

Transfected Sensor	Percent intensity in emission channels below upon direct excitation of the transfected FRET Sensor[1]			
	Cyan-yellow	tSapphire-mKO tSapphire-TagRFP	mOrange2-mCherry mOrange2-mKate	Clover-mRuby2
ZapCY2	100	4.7 ± 0.02	2.17 ± 0.01	9.4 ± 0.1
ZapSM2	80 ± 1	100	≥ 100	37 ± 0.3
ZapSR2	96 ± 2	100	≥ 100	31 ± 0.2
ZapOC2	2 ± 0.2	3.5 ± 0.1	100	17.5 ± 0.4
ZapOK2	2.3 ± 0.1	2.8 ± 0.1	100	17 ± 0.3
ZapCmR1	50 ± 1	11 ± 0.2	≥ 100	100

Each experiment was performed in triplicate and a minimum of 4-cells per field of view were observed. Values reported represent the mean ± SEM. Cells were transfected with FRET sensor listed in the left column. The sensors were excited with their respective excitation filters and the emission intensity in each of the channels on the right hand side was measured. Excitation filters, Dichroic mirrors, and Emission filters for each channel are given in **Table 4.2**. Percent intensity was calculated as follows: Intensity of the designated channel divided by Intensity in the channel of the transfected FRET sensor.

thought it would be valuable to generate both nuclear- localized and cytoplasmic Zn^{2+} sensors of the non-CFP/YFP variety. To localize sensors to either the nucleus or cytosol a nuclear localization signal (NLS) or nuclear exclusion signal (NES) was incorporated into the pcDNA 3.1 (+) mammalian expression vector upstream of the sensor. Both signal sequences were verified by sequence analysis followed by the direct observation of localization in cells. **Figure 4.1a** shows a schematic of the sensor construct illustrating the localization signals. **Figure 4.1b** shows a representative FRET sensor localized to either the nucleus or the cytosol. All sensors exhibited a similar localization pattern.

4.4.3 Characterization of sensors in HeLa Cells

There are many examples of genetically encoded biosensors exhibiting diminished responses in cells compared to in vitro (*16*), therefore we set out to screen all sensors in mammalian cells to verify functionality. All six sensors described in **Table 4.3** were transiently transfected into HeLa cells, expressed in either the nucleus or cytosol, and subjected to an in situ calibration to determine $R_{resting}$, R_{TPEN}, and R_{Zn}. This calibration involved treatment of cells with 150 μM TPEN to chelate Zn^{2+} and obtain the FRET ratio in the Zn^{2+}-free state (R_{TPEN}), followed by a washout and treatment with 10 μM digitonin to permeabilize the cell membrane and addition of 135 μM $ZnCl_2$ to saturate the sensor and obtain the FRET ratio of the Zn^{2+}-bound state (R_{Zn}). **Figure 4.5** shows that all nuclear-localized sensors responded to manipulation of cellular Zn^{2+}, with the majority of sensors exhibiting an increase in the FRET ratio for R_{Zn} and a decrease for R_{TPEN}. ZapCmR1 was the only sensor that displayed an inverted response ($R_{TPEN} > R_{Zn}$). It is not uncommon for sensors to exhibit inverted FRET responses when the relative orientation of the FPs is altered (*17*), particularly when the linkers are different as they are in the Clover-mRuby2 construct. Incorporation of mutations in the ZBD reverted the response to that of other sensors, and decreased the affinity for Zn^{2+} as observed by comparison of R_{TPEN} and R_{Zn} with other sensors. **Figure 4.6** shows that all sensors localized tot the cytosol responded to manipulation of cellular Zn^{2+}.

The dynamic range of a sensor provides a measure of the sensitivity is defined as R_{Zn}/R_{TPEN}. **Table 4.6** presents the dynamic range for each sensor, which varies from 1.1 to 1.2-fold for most of sensors with the exception of ZapCmR1.1 and ZapCmR2 which exhibit a 1.4-1.5 fold change. Two additional important parameters are the resting FRET ratio and the $R_{max} - R_{min}$ which help to define the signal-to-noise. For example if the dynamic range is 1.1 and the resting ratio is 0.5, this means the FRET ratio only changes from 0.5 to 0.55, i.e. $R_{max} - R_{min}$ is 0.05; whereas if the resting ratio is 1.0, the same dynamic range would yield a FRET ratio change from 1 to 1.1 and hence an $R_{max} - R_{min}$ of 0.1 and overall greater sensitivity. From **Table 4.6**, ZapSM2, ZapSR2, ZapOC2, and ZapCmR1 exhibit comparable sensitivity, whereas ZapOK2 displays lower sensitivity. Both ZapCmR1.1 and ZapCmR2 exhibit substantially greater sensitivity when compared to the other FRET sensors from **Table 4.6**.

The percent saturation is a measure of how much Zn^{2+} is bound to a sensor under resting conditions and provides a relative measure of Zn^{2+} levels in different locations. **Table 4.6** shows the resting percent saturation of each sensor in the nucleus and cytosol. Interestingly, all six sensors reveal a higher saturation percentage in the nucleus than the cytosol, suggesting that nuclear Zn^{2+} is buffered at a higher concentration than the cytosol. The final sensor, ZapOK2 demonstrated a similar resting percent saturation in both compartments, although as explained above, this sensor had the lowest sensitivity. Both ZapCmR1.1 and ZapCmR2 displayed low percent saturation compared to wild-type ZapCmR1, as expected due to the incorporation of mutations to weaken the Zn^{2+}-affinity.

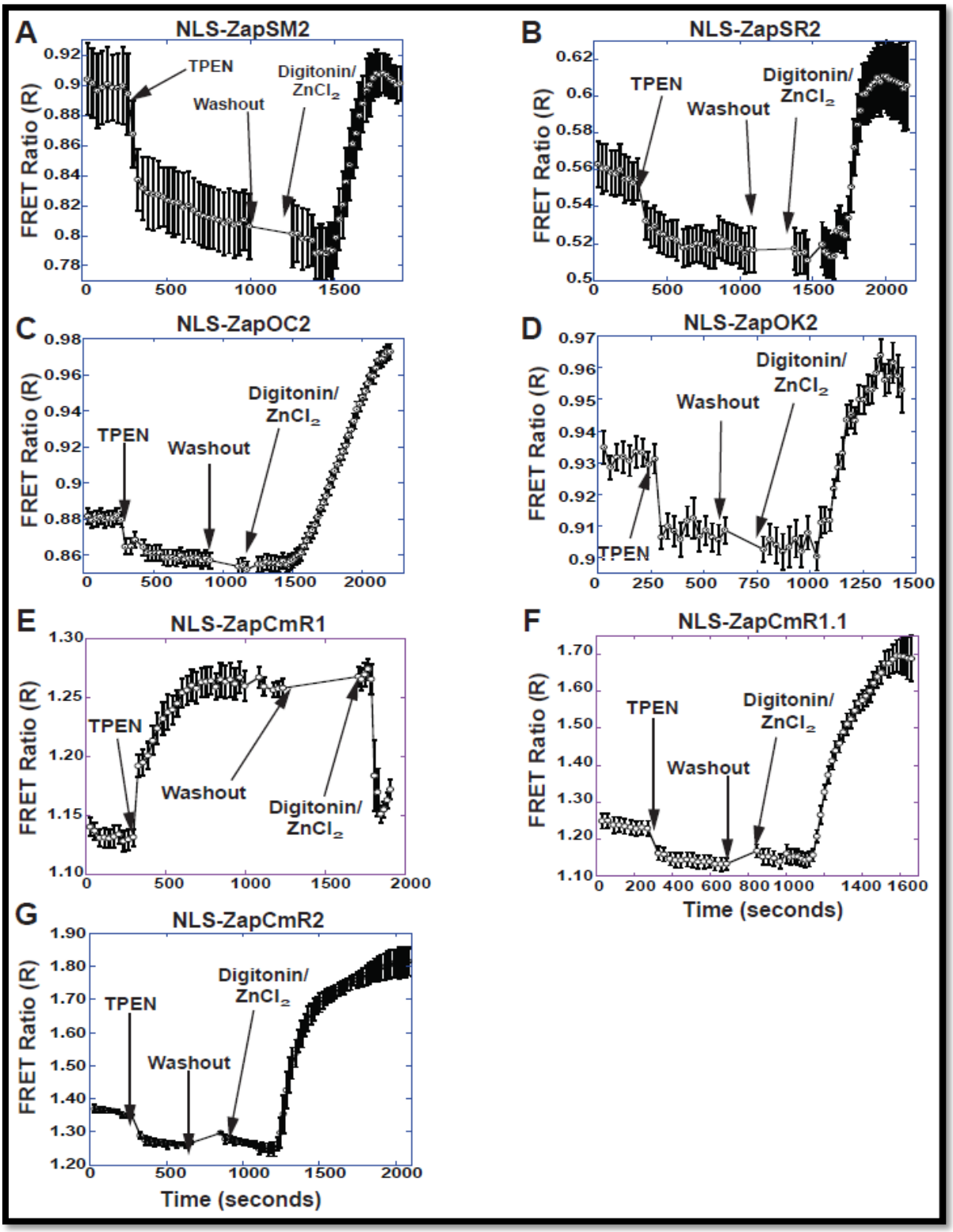
A
NLS-ZapSM2
FRET Ratio (R)
TPEN
Washout
Digitonin/
ZnCl2
B
NLS-ZapSR2
C
NLS-ZapOC2
D
NLS-ZapOK2
E
NLS-ZapCmR1
F
NLS-ZapCmR1.1
G
NLS-ZapCmR2
Time (seconds)

Figure 4.5. FRET Sensor calibration in the nucleus. Representative calibrations of each sensor localized to the nucleus. The background corrected FRET ratio (FRET Intensity ÷ Donor Intensity) is represented as a function of time. Calibrations were performed by adding 150 μM TPEN to achieve R_{TPEN}, followed by washing of residual TPEN and addition of 135 μM $ZnCl_2$ with 10 μM Digitonin to permeabilize the cell membrane and obtain R_{Zn}. A) NLS-ZapSM2 FRET ratio increases slightly above resting suggesting that it is close to saturation at rest; B) NLS-ZapSR2, FRET ratio goes above resting; C) NLS-ZapOC2 has a small decrease in FRET ratio after TPEN and a larger increase after treatment with Zn^{2+}; D) NLS-ZapOK2 exhibits a small change in FRET ratio after TPEN and Zn^{2+}; E) NLS-ZapCmR1 has an inverted response in which TPEN causes an increase in FRET ratio while Zn^{2+} with digitonin causes a decrease in the ratio; F) NLS-ZapCmR1.1 displays a decrease in the FRET ratio after TPEN and large increase with Zn^{2+} and digitonin; G) NLS-ZapCmR2 is similar to ZapCmR1.1. Representative traces are mean ± s.e.m. (n = 4 cells). Each experiment was repeated a minimum of three times.

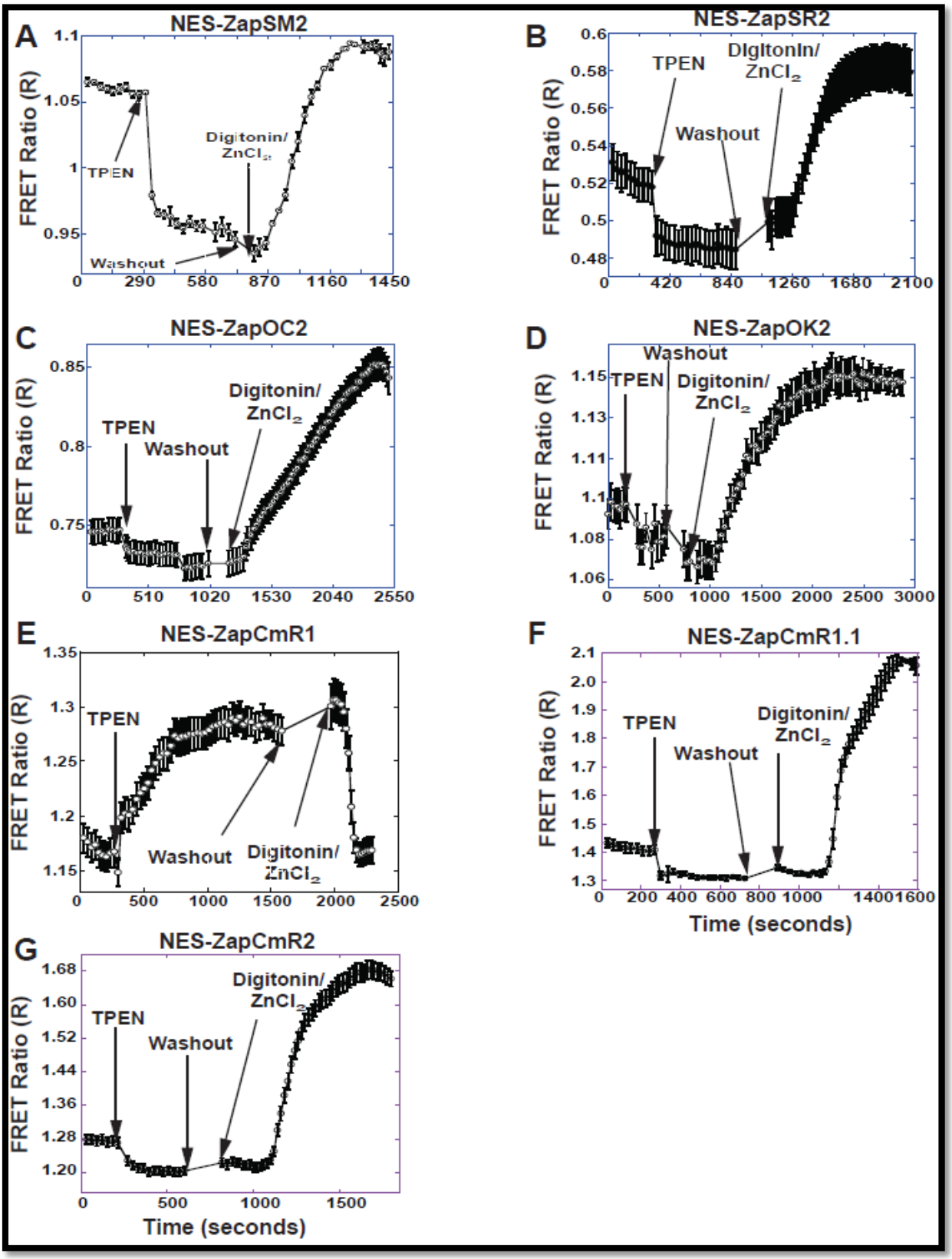
A
NES-ZapSM2
FRET Ratio (R)
TPEN
Digitonin/ ZnCl2
Washout
B
NES-ZapSR2
TPEN
Digitonin/ ZnCl2
Washout
C
NES-ZapOC2
TPEN
Washout
Digitonin/ ZnCl2
D
NES-ZapOK2
Washout
TPEN
Digitonin/ ZnCl2
E
NES-ZapCmR1
TPEN
Washout
Digitonin/ ZnCl2
F
NES-ZapCmR1.1
TPEN
Washout
Digitonin/ ZnCl2
Time (seconds)
G
NES-ZapCmR2
TPEN
Washout
Digitonin/ ZnCl2
Time (seconds)

Figure 4.6. FRET Sensor calibration in the cytosol. Representative calibrations of each sensor localized to the cytosol. The background corrected FRET ratio (FRET Intensity ÷ Donor Intensity) is represented as a function of time. Calibrations were performed by adding 150 μM TPEN to achieve R_{TPEN}, followed by washing of residual TPEN and addition of 135 μM $ZnCl_2$ with 10 μM Digitonin to permeabilize the cell membrane and obtain R_{Zn}. A) NES-ZapSM2, FRET ratio goes slightly above resting; B) NES-ZapSR2 has a similar response as observed in the nucleus, Figure 2B; C) NES-ZapOC2 demonstrates a small decrease after TPEN compared to the same sensor in the nucleus; D) NES-ZapOK2 is observed with small changes in FRET ratio after TPEN and Zn^{2+}/digitonin; E) NES-ZapCmR1 has an inverted response in which TPEN causes an increase in FRET ratio while Zn^{2+} with digitonin causes a decrease in the ratio; F) NES-ZapCmR1.1 and G) NES-ZapCmR2 exhibit a small decrease with TPEN and a larger increase in FRET ratio after addition of Zn^{2+} and digitonin. Representative traces are mean ± s.e.m. (n = 4 cells). Each experiment was repeated a minimum of three times.

Table 4.6. Comparison of sensors with different fluorescent proteins

Sensor Name	*In vivo* Dynamic Range (R_{max}/R_{min}) (Mean±SEM)	Percent Saturation at Rest [(R-R_{TPEN})/(R_{Zn}-$_{TPEN}$)x100% (Mean±SEM)	R_{rest}	R_{max}-R_{min}
NLSZapSM2	1.14 ± 0.003	91% ± 3%	0.89	0.11
NESZapSM2	1.13 ± 0.01	67 ± 5%	1.05	0.15
NLSZapSR2	1.18 ± 0.004	48 ± 3%	0.55	0.1
NESZapSR2	1.21 ± 0.01	38 ± 2%	0.52	0.1
NLSZapOC2	1.11 ± 0.01	22 ± 2%	0.88	0.12
NESZapOC2	1.13 ± 0.01	20 ± 2%	0.74	0.13
NLSZapOK2	1.1 ± 0.01	32 ± 4%	0.93	0.06
NESZapOK2	1.09 ± 0.004	35 ± 2%	1.09	0.08
NLSZapCmR1	1.15 ± 0.01	92 ± 2	1.02	0.15
NESZapCmR1	1.17 ± 0.04	88 ± 7	1.07	0.18
NLSZapCmR1.1	1.44 ± 0.5	22 ± 6	1.22	0.4
NESZapCmR1.1	1.52 ± 0.03	17 ± 1	1.43	0.6
NLSZapCmR2	1.38 ± 0.02	24 ± 1	1.38	0.4
NESZapCmR2	1.39 ± 0.02	17 ± 1	1.28	0.5

***Each experiment was performed in triplicate and a minimum of 3-4 cells per field of view were observed.**

4.4.4 Zinc uptake into the cytosol and nucleus

Extracellular Zn^{2+} levels are typically in the 1-10 μM range (*29-31*), but a number of cells contain high levels of Zn^{2+} in vesicles and secrete Zn^{2+} in response to stimulation (*32-35*). Therefore, there are physiological situations in which extracellular Zn^{2+} is transiently elevated. We have demonstrated that elevation of extracellular Zn^{2+} results in uptake of Zn^{2+} into the cytosol, increasing the level of free Zn^{2+} from approximately 100 pM to 6 nM (*15*), but it is unclear whether an increase in cytosolic Zn^{2+} leads into an increase in nuclear Zn^{2+}. Therefore we set out to monitor Zn^{2+} uptake in both the cytosol and nucleus with the new sensors. Sensor cDNA were transfected into each compartment and the FRET ratio was observed after the addition of 100 μM $ZnCl_2$. **Figure 4.7** depicts representative traces of each sensor in the cytosol upon elevation of extracellular Zn^{26+}, confirming with that the new sensors are sensitive enough for monitoring Zn^{2+} uptake. **Figure 4.8** demonstrates that all nuclear sensors exhibit an increase in the FRET ratio, indicating that nuclear Zn^{2+} also rises under this experimental paradigm. Because ZapCmR1 was close to saturated under resting conditions, we did not use this sensor for uptake studies.

While the clover-mRuby2 sensors clearly represent superior green-red sensors, we wanted to test the limits of responsiveness of the low dynamic range sensors. Therefore, we co-transfected NLS-ZapSM2, -ZapSR2, -ZapOC2, and -ZapOK2 sensors with a NES-ZapCY2 to simultaneously monitor Zn^{2+} uptake into the nucleus and cytosol. ZapCY2 was used in the cytosol due to its lower affinity (K_d' = 811 pM) for Zn^{2+} compared to ZapCY1 which is saturated at rest due to its high affinity (K_d' = 2.53 pM) (*15*). **Figure 4.9** reveals that two sensors (NLS-ZapSR2 and -ZapOC2) were sensitive enough to detect changes in nuclear Zn^{2+} when coupled with cytosolic ZapCY2. Moreover, under this experimental paradigm, the cytosol and nucleus accumulated Zn^{2+} with comparable rates, indicating that in defining the rate of Zn^{2+} uptake from the extracellular environment, localizing sensors to the nucleus could serve as a proxy for

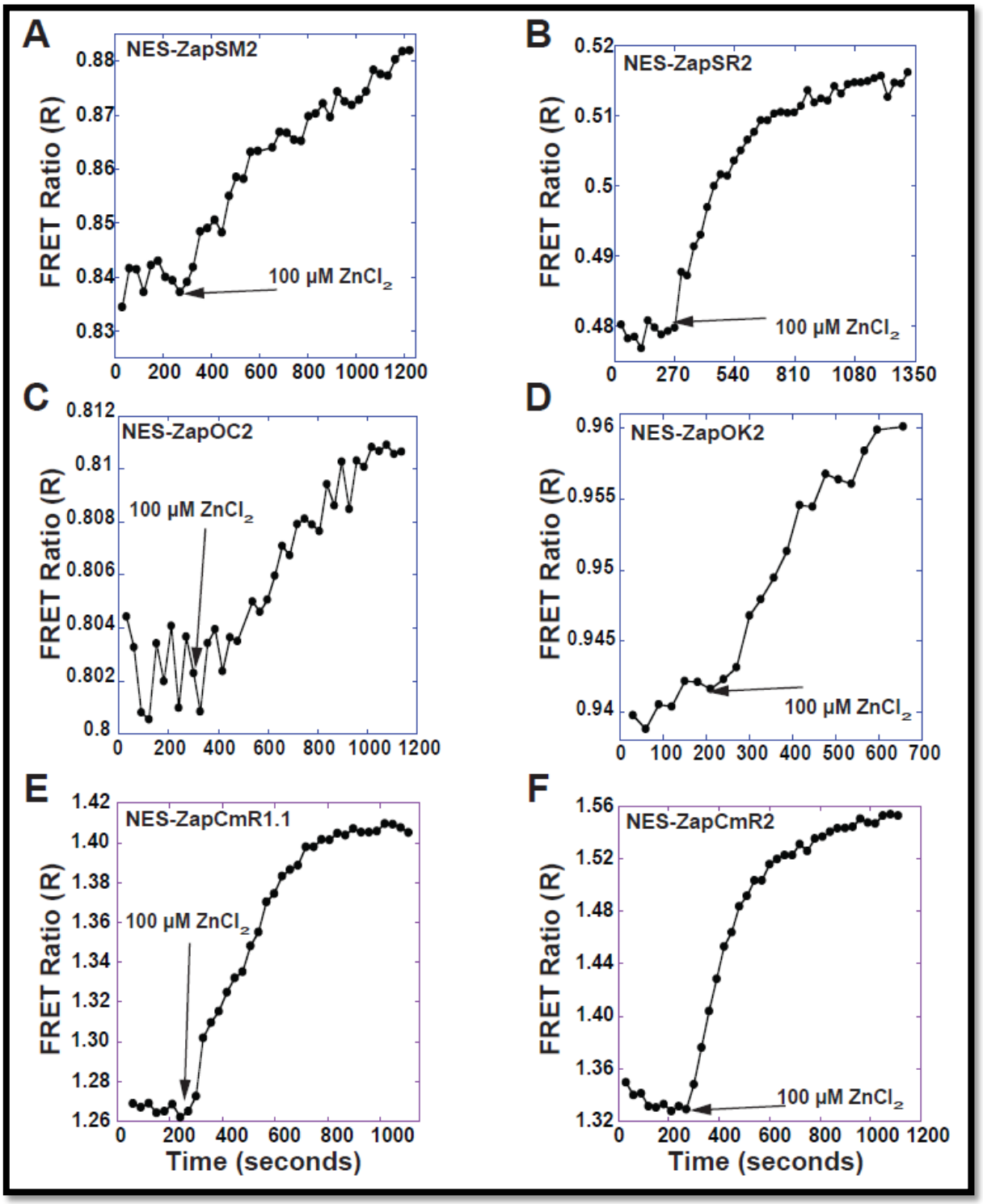

Figure 4.7. Zn^{2+} uptake into cytosol. Sensors were localized to nucleus to monitor uptake of extracellular Zn^{2+}. A) NLS-ZapSM2, B) NLS-ZapSR2, C) NLS-ZapOC2, D) NLS-ZapCmR1.1, E) NLS-ZapCmR2. Regions were imaged for approximately 300 seconds followed by the addition of 100 μM extracellular $ZnCl_2$ at the time indicated. Nuclear FRET ratios rose immediately after the addition of Zn^{2+}. The background corrected FRET ratio (FRET Intensity ÷ Donor Intensity) is represented as a function of time. Each experiment was repeated a minimum of three times with a minimum of 3-4 cells per field of view.

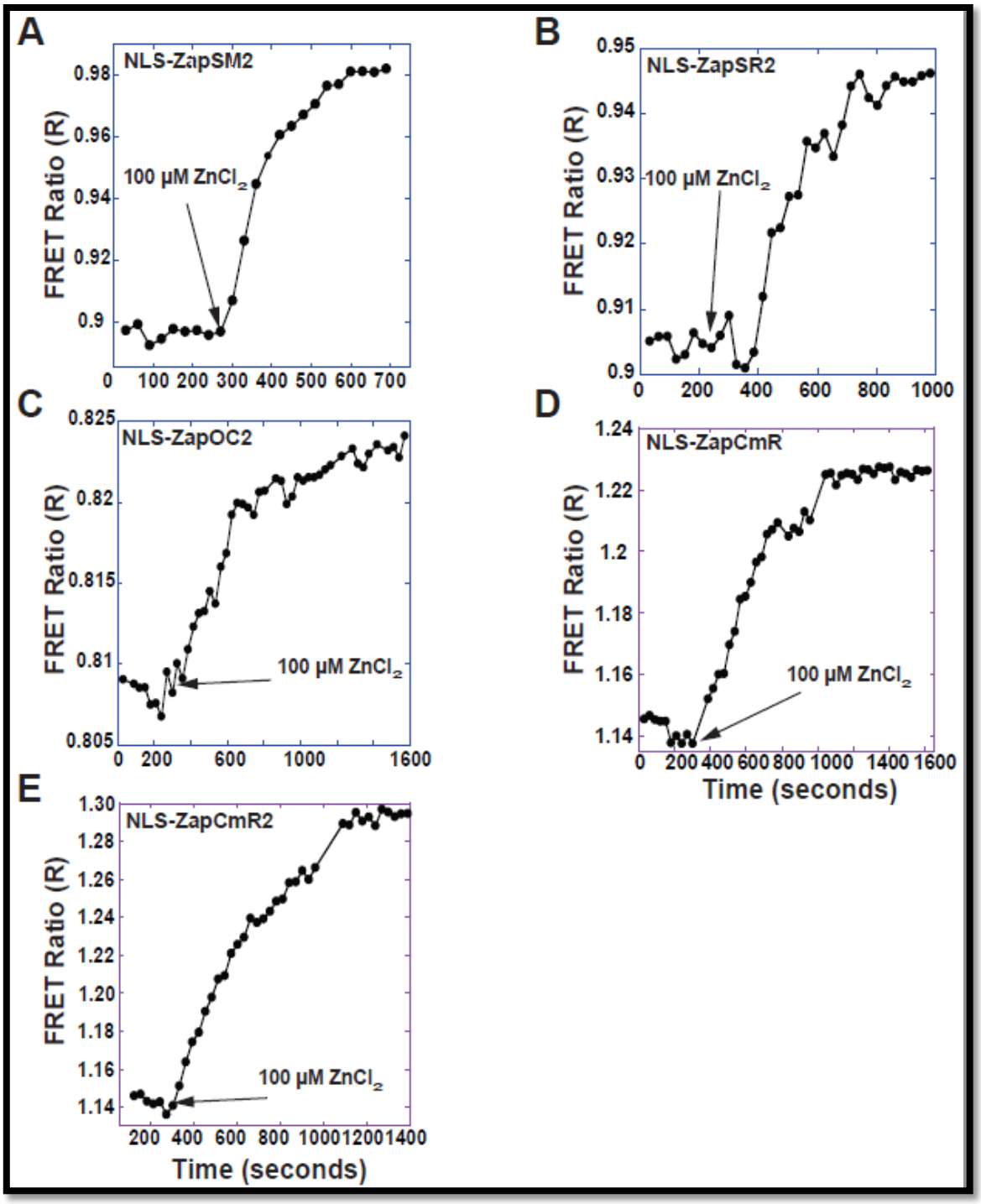

Figure 4.8. Zn^{2+} uptake into nucleus. Sensors were localized to nucleus to monitor uptake of extracellular Zn^{2+}. A) NLS-ZapSM2, B) NLS-ZapSR2, C) NLS-ZapOC2, D) NLS-ZapCmR1.1, E) NLS-ZapCmR2. Regions were imaged for approximately 300 seconds followed by the addition of 100 μM extracellular $ZnCl_2$ at the time indicated. Nuclear FRET ratios rose immediately after the addition of Zn^{2+}. The background corrected FRET ratio (FRET Intensity ÷ Donor Intensity) is represented as a function of time. Each experiment was repeated a minimum of three times with a minimum of 3-4 cells per field of view.

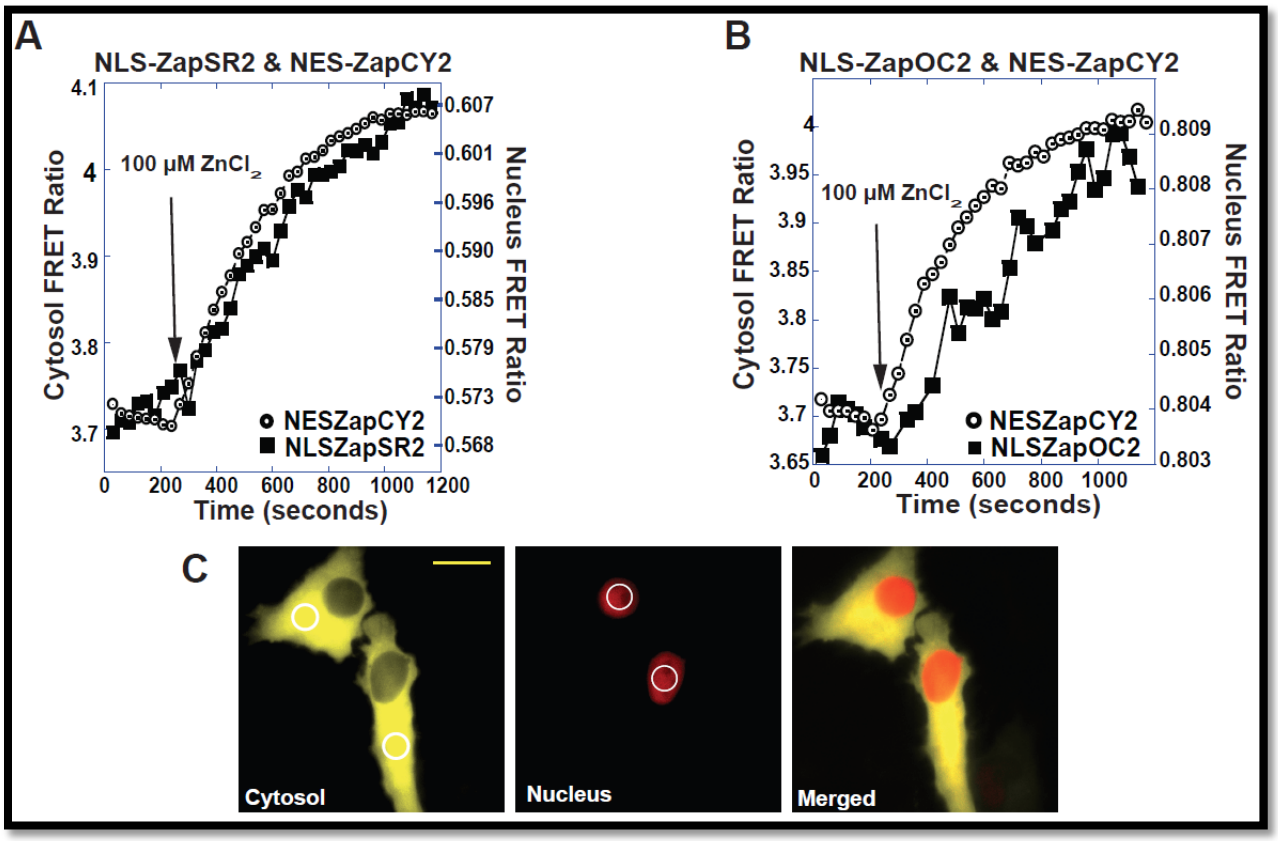

Figure 4.9. Simultaneous monitoring of cytosolic and nuclear Zn^{2+} uptake . (A) Simultaneous imaging of NLS-ZapSR2 and NES-ZapCY2 in the same cell. (B) Simultaneous imaging of NLS-ZapOC2 and NES-ZapCY2 in the same cell. In both experiments 100 μM $ZnCl_2$ was added at the time indicated. The rate of increase in the FRET ratio is essentially the same in both locations, suggesting similar rates for nuclear and cytosolic uptake. C) Left panel (cytosol) is NES-ZapCY2 and circles represent ROI followed throughout experiment, middle panel represents NLS-ZapSR2, circles represent ROI (NLS-ZapOC2 not shown), and right panel represents NLS-ZapSR2 and NES-ZapCY2 merged. Images were bleedthrough corrected. Experiments were repeated at least five times with a minimum of 1-2 cells per experiment. Scale bar = 20 μm.

monitoring the rate of change of cytosolic Zn^{2+}. NLS-ZapSR2 exhibited the largest FRET ratio change compared to NLS-ZapOC2, making it the preferable choice of low sensitivity sensors. Experiments in which NLS-ZapSM2 and NLS-ZapOK2 were used with NES-ZapCY2, only the cytosolic sensor exhibited an increase in FRET upon Zn^{2+} (Data Not Shown), suggesting these sensors had limited sensitivity to monitor physiological fluxes of cellular Zn^{2+}.

4.4.5 Simultaneous monitoring of nuclear and organelle Zn^{2+} uptake

Previous studies in our lab have demonstrated that intracellular organelles such the ER, Golgi, and mitochondria can accumulate Zn^{2+} when cytosolic Zn^{2+} levels become elevated, demonstrating these compartments play an important role in cytosolic clearance and maintenance of homeostasis (*15, 36*). However for these prior experiments accumulation of Zn^{2+} in the cytosol and intracellular organelles was measured in separate experiments making it impossible to directly compare the relative rate of uptake in individual cells. To observe Zn^{2+} uptake into the nucleus we continued to use NLS-ZapSR2 because it yielded the most robust signal compared to the other sensors and ZapCY1 was targeted to individual organelles. **Figure 4.10a,c,e** depicts representative images showing sensor localization. As observed in **Figure 4.10b,d,f**, addition of 100 μM $ZnCl_2$ to the extracellular milieu, gave rise to an immediate increase in nuclear Zn^{2+}, whereas organelle Zn^{2+} (ER, Golgi, and mitochondria,) increases approximately 600-700 seconds later, and only after the nuclear Zn^{2+} begins to decline.

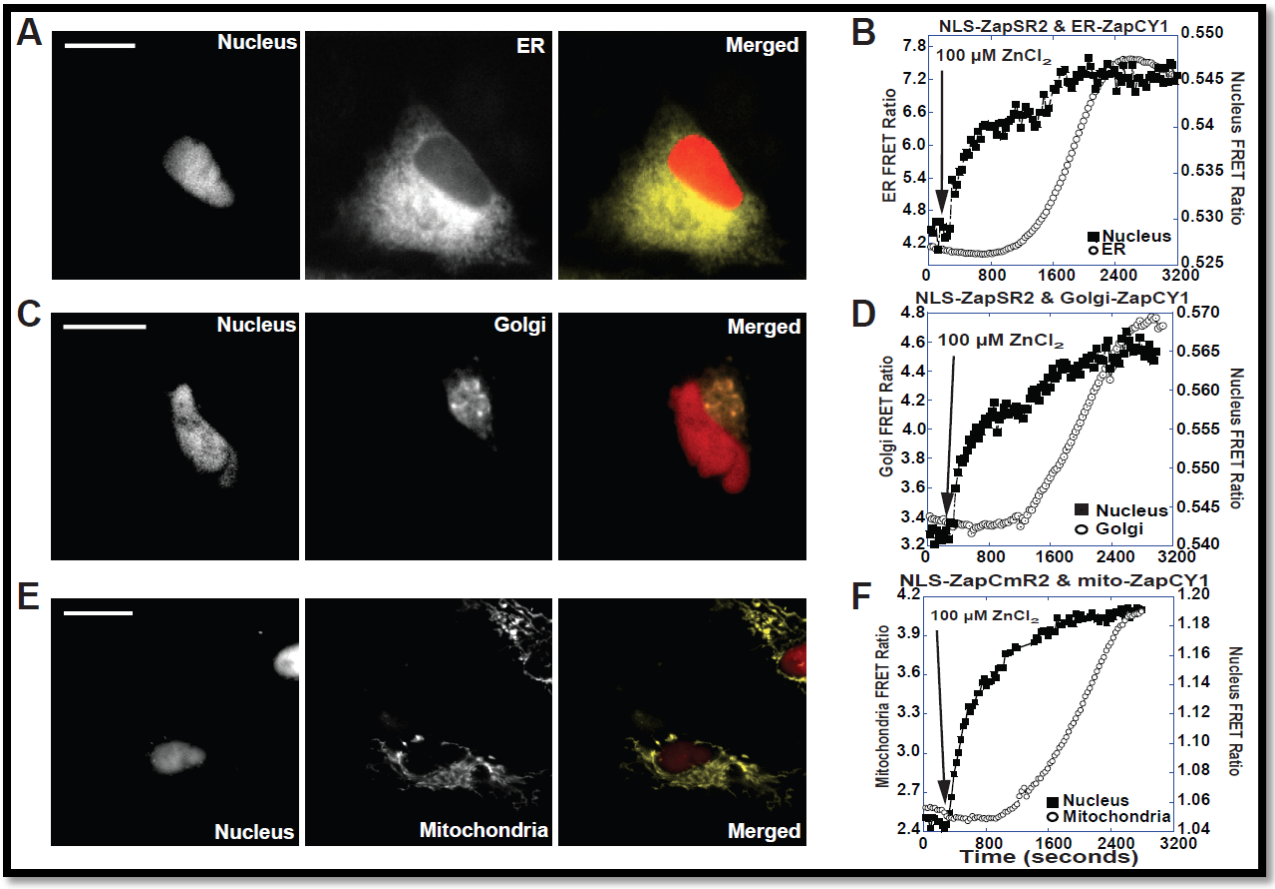

Figure 4.10. Simultaneous monitoring of Zn^{2+} uptake into the nucleus and either the ER, Golgi apparatus, or mitochondria. Representative images (FRET channel) and FRET ratio traces of Zn^{2+} uptake into the nucleus, ER, Golgi, or mitochondria are presented. A) Image of nuclear and ER FRET sensor, left panel illustrates NLS-ZapSR2, middle panel ER-ZapCY1 and right panel is a pseudo-color merged image of NLS-ZapSR2 and ER-ZapCY1. B) Image of nuclear and ER FRET sensor, left panel illustrates NLS-ZapSR2, middle panel Golgi-ZapCY1 and right panel is a pseudo- color merged image of NLS-ZapSR2 and Golgi-ZapCY1. C) Image of nuclear and mitochondrial FRET sensor, left panel illustrates NLS-ZapCmR2, middle panel mitochondria-ZapCY1 and right panel is a pseudo- color merged image of NLS-ZapCmR2 and mitochondria-ZapCY1. D-F) FRET ratio traces of NLS-ZapSR2 or NLS-ZapCmR2 with ER-, Golgi-, and mitochondrial-ZapCY1 upon addition of 100 μM extracellular $ZnCl_2$ at the time indicated. The nuclear FRET ratio rises more rapidly than organelle FRET ratio. The organelle FRET ratio begins to increase approximately 600 seconds post-Zn^{2+}. Experiments were repeated at least five times with a minimum of 1-2 cells per experiment. All images were bleedthrough corrected. Scale bar = 20 μm.

4.5 Discussion

Here we report the first alternatively colored Zn^{2+} sensors using FPs constructed from green, orange, and red FPs, that can be used simultaneously with a CFP-YFP sensor as the first step toward monitoring Zn^{2+} in multiple subcellular locations. Given the evidence that changes in cellular Zn^{2+} have been linked with changes in other ions such as Ca^{2+} (*15, 37*) and signaling pathways such as the MAPK pathway (*38*) and apoptotic cascades (*39, 40*) a broad palette of Zn^{2+} sensors that permits simultaneous monitoring of multiple events would be useful tools to provide mechanistic insight into these connections.

Sensors were targeted to both the cytosol and nucleus and intriguingly, 6 of the 7 sensors registered a higher fractional saturation in the nucleus compared to the cytosol, suggesting the possibility that nuclear Zn^{2+} may be buffered at a higher concentration than cytosolic Zn^{2+}. Although there are currently no estimates of nuclear Zn^{2+} levels, given the large number of transcription factors that bind Zn^{2+} (*41*) it seems reasonable to speculate the nuclear buffering system may differ from that in the cytosol.

The development of multi-color FRET sensors for Zn^{2+} allowed us to monitor Zn^{2+} simultaneously in the nucleus and other organelles, such as the ER, Golgi, or mitochondria. For these experiments we measured Zn^{2+} uptake or sequestration following acute elevation of extracellular Zn^{2+}. Extracellular Zn^{2+} levels are typically in the range of 1 to 10 μM. However there are a number of cell types (hippocampal neurons, prostate cells, and pancreatic cells) that are known to secrete Zn^{2+}. Although the amount of Zn^{2+} these cells secrete has not been rigorously quantified, estimates range from 1 μM to 2 mM (*32-35*). Therefore we believe the acute elevation of extracellular Zn^{2+} represents a physiologically relevant stimulus similar to Zn^{2+} secretion. Here we demonstrate that elevation of extracellular Zn^{2+} leads to immediate uptake of Zn^{2+} into the nucleus and much slower sequestration of Zn^{2+} into organelles after a lag time of ~ 600 seconds. The reason for organelle sequestration is unclear but it may represent a

detoxification mechanism, ensuring that cytosolic levels of Zn^{2+} don't get too high. The mechanism of sequestration and the reason for the delay are unclear. There are 24 mammalian Zn-transporters with varied subcellular distribution and it is possible that specific transporters are activated for Zn^{2+} transport into organelles (*42*). We believe these new tools (i.e. sensors targeted to multiple locations to simultaneously monitor Zn^{2+} flux) will allow us to dissect these fundamental questions about Zn^{2+} homeostasis.

In contrast to the robust signal that is observed using CFP and YFP as a FRET pair, alternate color FRET pairs often suffer from greatly reduced dynamic ranges. Additionally, because of the lower quantum yields of most red FPs compared to appropriate donor FPs and the relatively poor sensitized emission, FRET sensors with a red FP as the acceptor typically yield a resting FRET ratio less than 1 and a reduced ΔR, thus limiting their sensitivity. Not surprisingly the majority of sensors reported here exhibit modest FRET ratio changes. Of the 5 different FRET pairs explored, Clover-mRuby2 based sensors yielded the greatest sensitivity with a dynamic range of 1.4-1.5 and ΔR of 0.4-0.6. The other FRET sensors exhibited a lower ΔR making them less robust for monitoring cellular Zn^{2+} fluxes, although many were still sensitive enough to permit measurement of subtle changes in cellular Zn^{2+} levels. Still, ZapCmR1.1 and ZapCmR2 are clearly superior and even exhibit a slightly better dynamic range than their CFP-YFP counterpart, ZapCY2 (*15*).

In conclusion, we have established new genetically encoded Zn^{2+} sensors employing FRET pairs that are complementary to the traditional CFP-YFP pair that can help define Zn^{2+} dynamics in different compartments simultaneously. A limitation of some of these alternately colored biosensors is that their dynamic range is reduced compared to their CFP-YFP counterparts (1.1-1.2 versus 1.3-1.4). However, we did identify superior sensors based on the new FRET pair Clover and mRuby2, which have higher dynamic ranges than their CFP-YFP

counterparts. These green-red sensors should also be useful for monitoring Zn^{2+} levels alongside other signaling agents such as Ca^{2+} and therefore have the potential to be instrumental in dissecting crosstalk between these two ions. Given the lower pKa values of green and red FPs compared to YFP, we anticipate these sensors will be more resistant to quenching at lower pHs and hence may be particularly useful for quantifying Zn^{2+} when targeted to acidic compartments.

4.6 Acknowledgements

We would like to thank the following agencies for financial support: NIH Predoctoral Fellowship (F31 GM093443) to J.G.M., NIH GM084027 and GM084027-S1 to A.E.P. Research in the Palmer Lab is also supported by an Alfred P. Sloan Fellowship. This work was supported by a Burroughs Welcome Career Award for Medical Scientist and NIH grant to M.Z.L.

4.7 References

1. Shaner, N. C., Steinbach, P. A., and Tsien, R. Y. (2005) A guide to choosing fluorescent proteins, *Nat Methods 2*, 905-909.
2. Newman, R. H., Fosbrink, M. D., and Zhang, J. (2011) Genetically encodable fluorescent biosensors for tracking signaling dynamics in living cells, *Chem Rev 111*, 3614-3666.
3. VanEngelenburg, S. B., and Palmer, A. E. (2008) Fluorescent biosensors of protein function, *Curr Opin Chem Biol 12*, 60-65.
4. Carlson, H. J., and Campbell, R. E. (2009) Genetically encoded FRET-based biosensors for multiparameter fluorescence imaging, *Curr Opin Biotechnol 20*, 19-27.
5. Ai, H. W., Hazelwood, K. L., Davidson, M. W., and Campbell, R. E. (2008) Fluorescent protein FRET pairs for ratiometric imaging of dual biosensors, *Nat Methods 5*, 401-403.

6. Ding, Y., Ai, H. W., Hoi, H., and Campbell, R. E. (2011) Forster resonance energy transfer-based biosensors for multiparameter ratiometric imaging of Ca2+ dynamics and caspase-3 activity in single cells, *Anal Chem 83*, 9687-9693.

7. Ai, H. W., Henderson, J. N., Remington, S. J., and Campbell, R. E. (2006) Directed evolution of a monomeric, bright and photostable version of Clavularia cyan fluorescent protein: structural characterization and applications in fluorescence imaging, *Biochem J 400*, 531-540.

8. Miyawaki, A., Griesbeck, O., Heim, R., and Tsien, R. Y. (1999) Dynamic and quantitative Ca2+ measurements using improved cameleons, *Proc Natl Acad Sci U S A 96*, 2135-2140.

9. Davidson, M. W., and Campbell, R. E. (2009) Engineered fluorescent proteins: innovations and applications, *Nat Methods 6*, 713-717.

10. Grant, D. M., Zhang, W., McGhee, E. J., Bunney, T. D., Talbot, C. B., Kumar, S., Munro, I., Dunsby, C., Neil, M. A., Katan, M., and French, P. M. (2008) Multiplexed FRET to image multiple signaling events in live cells, *Biophys J 95*, L69-71.

11. Ni, Q., Ganesan, A., Aye-Han, N. N., Gao, X., Allen, M. D., Levchenko, A., and Zhang, J. (2011) Signaling diversity of PKA achieved via a Ca2+-cAMP-PKA oscillatory circuit, *Nat Chem Biol 7*, 34-40.

12. Niino, Y., Hotta, K., and Oka, K. (2009) Simultaneous live cell imaging using dual FRET sensors with a single excitation light, *PLoS One 4*, e6036.

13. Ouyang, M., Huang, H., Shaner, N. C., Remacle, A. G., Shiryaev, S. A., Strongin, A. Y., Tsien, R. Y., and Wang, Y. (2010) Simultaneous visualization of protumorigenic Src and MT1-MMP activities with fluorescence resonance energy transfer, *Cancer Res 70*, 2204-2212.

14. Piljic, A., and Schultz, C. (2008) Simultaneous recording of multiple cellular events by FRET, *ACS Chem Biol 3*, 156-160.

15. Qin, Y., Dittmer, P. J., Park, J. G., Jansen, K. B., and Palmer, A. E. (2011) Measuring steady-state and dynamic endoplasmic reticulum and Golgi Zn2+ with genetically encoded sensors, *Proc Natl Acad Sci U S A 108*, 7351-7356.

16. Vinkenborg, J. L., Nicolson, T. J., Bellomo, E. A., Koay, M. S., Rutter, G. A., and Merkx, M. (2009) Genetically encoded FRET sensors to monitor intracellular Zn2+ homeostasis, *Nat Methods 6*, 737-740.

17. Park, J. G., Qin, Y., Galati, D. F., and Palmer, A. E. (2012) New Sensors for Quantitative Measurement of Mitochondrial Zn(2+), *ACS Chem Biol*.

18. Zapata-Hommer, O., and Griesbeck, O. (2003) Efficiently folding and circularly permuted variants of the Sapphire mutant of GFP, *BMC Biotechnol 3*, 5.

19. Lam, A., St-Pierre, F., Gong, Y., Marshall, J. D., Cranfill, P. J., Baird, M. A., McKeown, M. R., Wiedenmann, J., Davidson, M. W., Schnitzer, M., Tsien, R. Y., Lin, M. Z. (2012) Improved dynamic range of genetically encoded FRET sensors with bright new green and red fluorescent proteins., *Nat Methods*.

20. Karasawa, S., Araki, T., Nagai, T., Mizuno, H., and Miyawaki, A. (2004) Cyan-emitting and orange-emitting fluorescent proteins as a donor/acceptor pair for fluorescence resonance energy transfer, *Biochem J 381*, 307-312.

21. Shaner, N. C., Lin, M. Z., McKeown, M. R., Steinbach, P. A., Hazelwood, K. L., Davidson, M. W., and Tsien, R. Y. (2008) Improving the photostability of bright monomeric orange and red fluorescent proteins, *Nat Methods 5*, 545-551.

22. Merzlyak, E. M., Goedhart, J., Shcherbo, D., Bulina, M. E., Shcheglov, A. S., Fradkov, A. F., Gaintzeva, A., Lukyanov, K. A., Lukyanov, S., Gadella, T. W., and Chudakov, D. M. (2007) Bright monomeric red fluorescent protein with an extended fluorescence lifetime, *Nat Methods 4*, 555-557.

23. Shaner, N. C., Campbell, R. E., Steinbach, P. A., Giepmans, B. N., Palmer, A. E., and Tsien, R. Y. (2004) Improved monomeric red, orange and yellow fluorescent proteins derived from Discosoma sp. red fluorescent protein, *Nat Biotechnol 22*, 1567-1572.

24. Shcherbo, D., Merzlyak, E. M., Chepurnykh, T. V., Fradkov, A. F., Ermakova, G. V., Solovieva, E. A., Lukyanov, K. A., Bogdanova, E. A., Zaraisky, A. G., Lukyanov, S., and Chudakov, D. M. (2007) Bright far-red fluorescent protein for whole-body imaging, *Nat Methods 4*, 741-746.

25. Andreini, C., Banci, L., Bertini, I., and Rosato, A. (2006) Zinc through the three domains of life, *J Proteome Res 5*, 3173-3178.

26. Andreini, C., Banci, L., Bertini, I., and Rosato, A. (2006) Counting the zinc-proteins encoded in the human genome, *J Proteome Res 5*, 196-201.

27. Tsujikawa, K., Imai, T., Kakutani, M., Kayamori, Y., Mimura, T., Otaki, N., Kimura, M., Fukuyama, R., and Shimizu, N. (1991) Localization of metallothionein in nuclei of growing primary cultured adult rat hepatocytes, *FEBS Lett 283*, 239-242.

28. Spahl, D. U., Berendji-Grun, D., Suschek, C. V., Kolb-Bachofen, V., and Kroncke, K. D. (2003) Regulation of zinc homeostasis by inducible NO synthase-derived NO: nuclear metallothionein translocation and intranuclear Zn2+ release, *Proc Natl Acad Sci U S A 100*, 13952-13957.

29. Gandhi, M. S., Deshmukh, P. A., Kamalov, G., Zhao, T., Zhao, W., Whaley, J. T., Tichy, J. R., Bhattacharya, S. K., Ahokas, R. A., Sun, Y., Gerling, I. C., and Weber, K. T. (2008) Causes and consequences of zinc dyshomeostasis in rats with chronic aldosteronism, *J Cardiovasc Pharmacol 52*, 245-252.

30. Gibson, R. S., Hess, S. Y., Hotz, C., and Brown, K. H. (2008) Indicators of zinc status at the population level: a review of the evidence, *Br J Nutr 99 Suppl 3*, S14-23.

31. Stoecker, B. J., Abebe, Y., Hubbs-Tait, L., Kennedy, T. S., Gibson, R. S., Arbide, I., Teshome, A., Westcott, J., Krebs, N. F., and Hambidge, K. M. (2009) Zinc status and cognitive function of pregnant women in Southern Ethiopia, *Eur J Clin Nutr 63*, 916-918.

32. Sorensen, M. B., Stoltenberg, M., Danscher, G., and Ernst, E. (1999) Chelation of intracellular zinc ions affects human sperm cell motility, *Mol Hum Reprod 5*, 338-341.

33. Takeda, A. (2012) Zinc signaling in the hippocampus and its relation to pathogenesis of depression, *J Trace Elem Med Biol 26*, 80-84.

34. Yoshida, K., Kawano, N., Yoshiike, M., Yoshida, M., Iwamoto, T., and Morisawa, M. (2008) Physiological roles of semenogelin I and zinc in sperm motility and semen coagulation on ejaculation in humans, *Mol Hum Reprod 14*, 151-156.

35. Zalewski, P. D., Millard, S. H., Forbes, I. J., Kapaniris, O., Slavotinek, A., Betts, W. H., Ward, A. D., Lincoln, S. F., and Mahadevan, I. (1994) Video image analysis of labile zinc in viable pancreatic islet cells using a specific fluorescent probe for zinc, *J Histochem Cytochem 42*, 877-884.

36. Dittmer, P. J., Miranda, J. G., Gorski, J. A., and Palmer, A. E. (2009) Genetically encoded sensors to elucidate spatial distribution of cellular zinc, *J Biol Chem 284*, 16289-16297.

37. Kim, A. M., Vogt, S., O'Halloran, T. V., and Woodruff, T. K. (2010) Zinc availability regulates exit from meiosis in maturing mammalian oocytes, *Nat Chem Biol 6*, 674-681.

38. Du, S., McLaughlin, B., Pal, S., and Aizenman, E. (2002) In vitro neurotoxicity of methylisothiazolinone, a commonly used industrial and household biocide, proceeds via a zinc and extracellular signal-regulated kinase mitogen-activated protein kinase-dependent pathway, *J Neurosci 22*, 7408-7416.

39. Perry, D. K., Smyth, M. J., Stennicke, H. R., Salvesen, G. S., Duriez, P., Poirier, G. G., and Hannun, Y. A. (1997) Zinc is a potent inhibitor of the apoptotic protease, caspase-3. A novel target for zinc in the inhibition of apoptosis, *J Biol Chem 272*, 18530-18533.

40. West, D. C., Qin, Y., Peterson, Q. P., Thomas, D. L., Palchaudhuri, R., Morrison, K. C., Lucas, P. W., Palmer, A. E., Fan, T. M., and Hergenrother, P. J. (2012) Differential effects of procaspase-3 activating compounds in the induction of cancer cell death, *Mol Pharm 9*, 1425-1434.

41. Andreini, C., Bertini, I., and Rosato, A. (2009) Metalloproteomes: a bioinformatic approach, *Acc Chem Res 42*, 1471-1479.

42. Lichten, L. A., and Cousins, R. J. (2009) Mammalian zinc transporters: nutritional and physiologic regulation, *Annu Rev Nutr 29*, 153-176.

Chapter V

Vesicular Targeted FRET Sensor To Monitor Zinc

5.1 Abstract

Zinc (Zn^{2+}) is important in many biological processes and it is an essential component throughout the cell. As evident from previous chapters we have observed Zn^{2+} pools in the ER, mitochondria, cytosol, and nucleus of our prostate cell line models with genetically encoded fluorescent sensors localized to each compartment. While we have almost obtained a full map of labile Zn^{2+} of prostate cells, we are lacking quantification of Zn^{2+} in the Golgi and vesicles. Therefore, we set out to develop a FRET-based sensor genetically targeted to vesicles. Initially, mCherry was fused to the C-terminus of Vesicle-Associated Membrane Protein 2 (VAMP2) , a single transmembrane domain protein, and transfected into cells as a positive control for vesicular localization. To observe if VAMP2-mCherry localized to Zn^{2+} containing vesicles, cells were transfected with VAMP2-mCherry and stained with FluoZin3-AM, a commonly used small molecule dye for visualizing vesicular Zn^{2+}. Subsequently, VAMP2 was fused to the N-terminus of the green-red sensor developed in Chapter IV, resulting in the first functional, vesicle-targeted, ratiometric Zn^{2+} sensor.

5.2 Introduction

Zinc is the second most abundant transition metal and is an essential cofactor for numerous proteins and enzymes such as acetylcholinesterase (*1*), alcohol dehydrogenase, DNA and RNA polymerases, Nerve Growth Factor (NGF) (*2*), and finally transcription factors such as Zif268 (*3*) and Metal Transcription Factor-1 (MTF1) (*4*). The total Zn^{2+} in mammalian cells is estimated to be 0.1 - 0.5 mM (*5, 6*). Most of this Zn^{2+} is bound by proteins, enzymes, and cellular ligands, however free Zn^{2+} has been identified in vesicles in brain (*7, 8*), prostate (*8*), and pancreatic islets cells (*9*). While we have developed tools to monitor Zn^{2+} in many different compartments of the cell, there are still no robust ratiometric sensors for defining the amount of free Zn^{2+} in vesicular compartments.

Zinc is known to be concentrated into secretory vesicles and this vesicular Zn^{2+} plays biological functions in the cells. In the brain, vesicular Zn^{2+} has been shown to regulate synaptic

transmission. Zinc is stored in vesicles that are assembled in the Golgi along with glutamate and are released upon electrical stimulation in glutamatergic neurons (*10*). Mice that cannot store Zn^{2+} in vesicles develop amyloid pathology (*11*). In addition, pancreatic β-islet cells contain vesicular Zn^{2+} which helps to stabilize insulin within vesicles (*12, 13*). It is evident that Zn^{2+} is a major signaling agent and may act in some major signaling pathways in the brain and pancreas (*14, 15*). In order to more thoroughly investigate vesicular Zn^{2+} we need to develop tools that are easily targeted to vesicles, unaffected by pH, and sensitive to Zn^{2+}.

Because of the importance of Zn^{2+} in vesicles we need to develop new tools to monitor and quantify the level of free Zn^{2+} in this specific compartment. Currently the only way to monitor vesicular Zn^{2+} in cells is to use an intensiometric small molecule dye and the most commonly used dye is the commercially available FluoZin3-AM (acetoxymethyl (AM) ester) (*16*). This dye is an intensity based dye, meaning the more Zn^{2+} it binds the higher the fluorescent output. A problem with this is that the fluorescence output is also determined by the amount of FluoZin3 in the cell. Additionally, the dye does not explicitly target vesicles, but rather is present in both the cytosol and vesicles, making it difficult to separate contributions from each of these locations. For this reason we need genetically encoded FRET sensors that are ratiometric and are specifically targeted to vesicles.

The vast majority of FRET sensors are comprised of CFP-YFP, as noted in a recent publication (*17*). A sensor comprised of a CFP-YFP would not be useful in vesicles because the pKa of the chromophore of YFP is about 6.0 (*18, 19*) and hence fluorescence would be quenched in vesicles where the pH between 4.5 - 6 (*20, 21*). Because of this we need to swap the CFP-YFP for a green-red sensor, because green and red fluorescent proteins have lower pKa's and would potentially respond in an acidic environment such as vesicles.

In Chapter IV, we describe a new FRET sensor based on Clover and mRuby2 (*22*) fluorescent proteins with a Zn^{2+} finger nested between them. To determine if we can monitor Zn^{2+} in vesicles we used the Vesicle-Associated Membrane Protein 2 (VAMP2) which is a single

transmembrane domain. This single transmembrane domain protein is useful because it is attached to early and late endosomes (*23*) and has its C-terminus localized in the luminal side of the vesicle for easily attaching a FRET sensor. In preliminary data we have targeted VAMP2-ZapCmR1.1 sensor to vesicles and have observed robust localization to vesicles in HeLa cell line.

5.3 Experimental Methods

VAMP2 and FRET Sensor Cloning. A schematic of the general sensor construct is presented in **Figure 5.1** and VAMP2 targeting domain in **Figure 5.2.** VAMP2 was obtained by polymerase chain reaction (PCR) and cloned into a mammalian expression vector pcDNA3.1 (+) (Life Technologies) between *Hind*III and *Bam*HI restriction sites and verified by sequence analysis. To create VAMP2-mCherry, the mCherry fluorescent protein DNA sequence was amplified by PCR and subcloned into pcDNA3.1 (+) using *Bam*HI and *Eco*RI restriction sites and verified by sequence analysis. VAMP2-mCherry was created to observe localization of a VAMP2-targeted construct alongside FluoZin3 to determine if indeed VAMP2 targeted Zn^{2+} containing vesicles. To generate a Zn^{2+} sensor targeted to vesicles, ZapCmR1.1 was removed from pET302/NT-His (Life Technologies) using *Bam*HI and *Eco*RI restriction sites and subcloned into pcDNA3.1 (+) VAMP2 and verified by sequence analysis.

Cell Culture and Microscopy. HeLa cells were grown in Dulbecco's Modified Eagle's Medium (DMEM) (Life Technologies) supplemented with 10% (v/v) fetal bovine serum (Atlanta Biologicals), 100 U/mL penicillin, and 100 µg/mL streptomycin. Cells were incubated at 37°C in 5% CO_2, changing the media every 3 days. Once cells were approximately 80-90% confluent they were split and seeded onto 3.5 cm imaging dishes until they were approximately 40-50% confluent. At this point 1 µg of VAMP2-mCherry or VAMP2-ZapCmR1.1 was transiently transfected using TransIT®-LT1 (Mirus) as specified by manufacturer instructions.

Forty-eight hours after transfection, cells were imaged using phosphate, calcium, and magnesium free HEPES-buffered Hanks' balanced salt (HHBSS) media (5.36 mM KCl, 137 mM

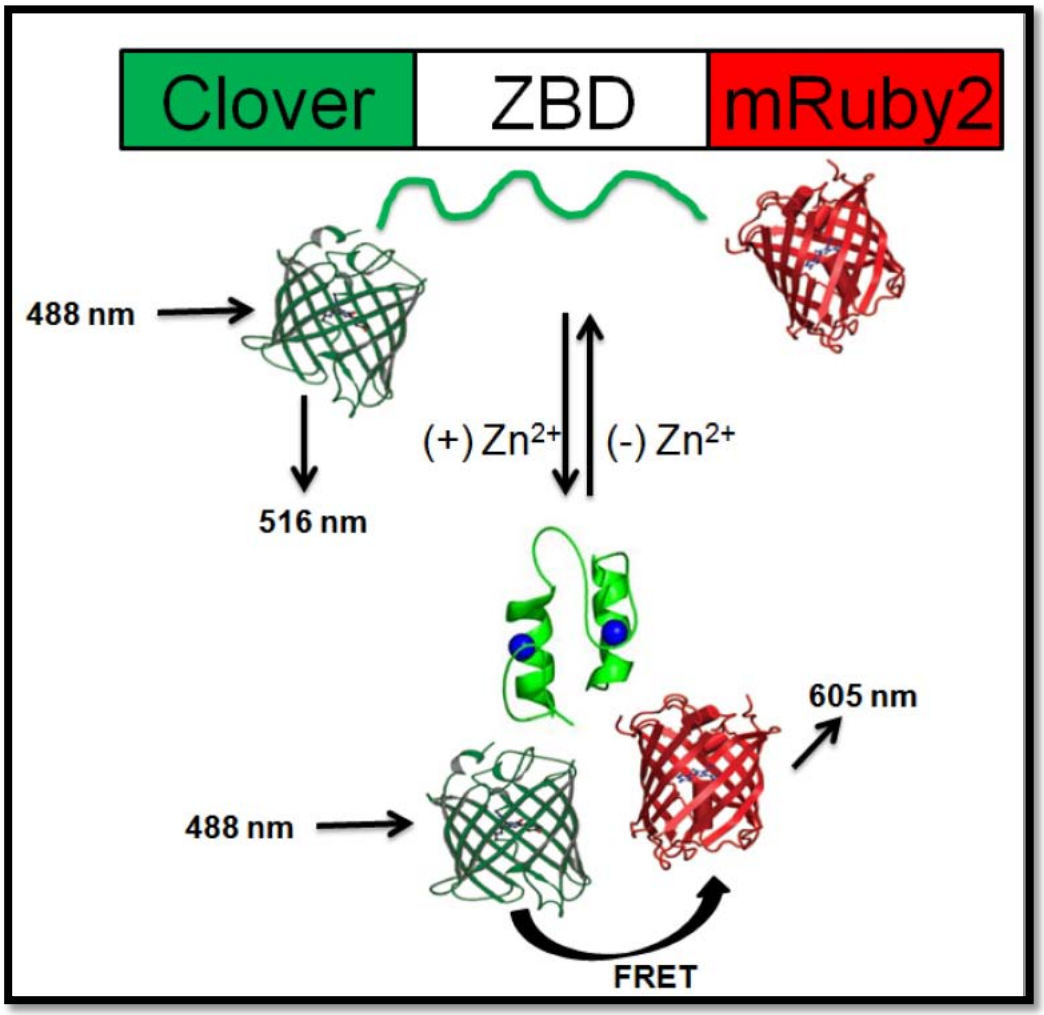

Figure 5.1. Schematic diagram of FRET Sensor. The sensor is composed a Clover Fluorescent Protein, mRuby2 Fluorescent Protein, and a Zn^{2+} binding domain derived from the first two zinc fingers of Zap1. The Zn^{2+} binding domain is relatively unstructured in the absence of Zn^{2+} and undergoes a conformational change upon Zn^{2+} binding leading to an increase in FRET from the donor Clover to the acceptor mRuby2.

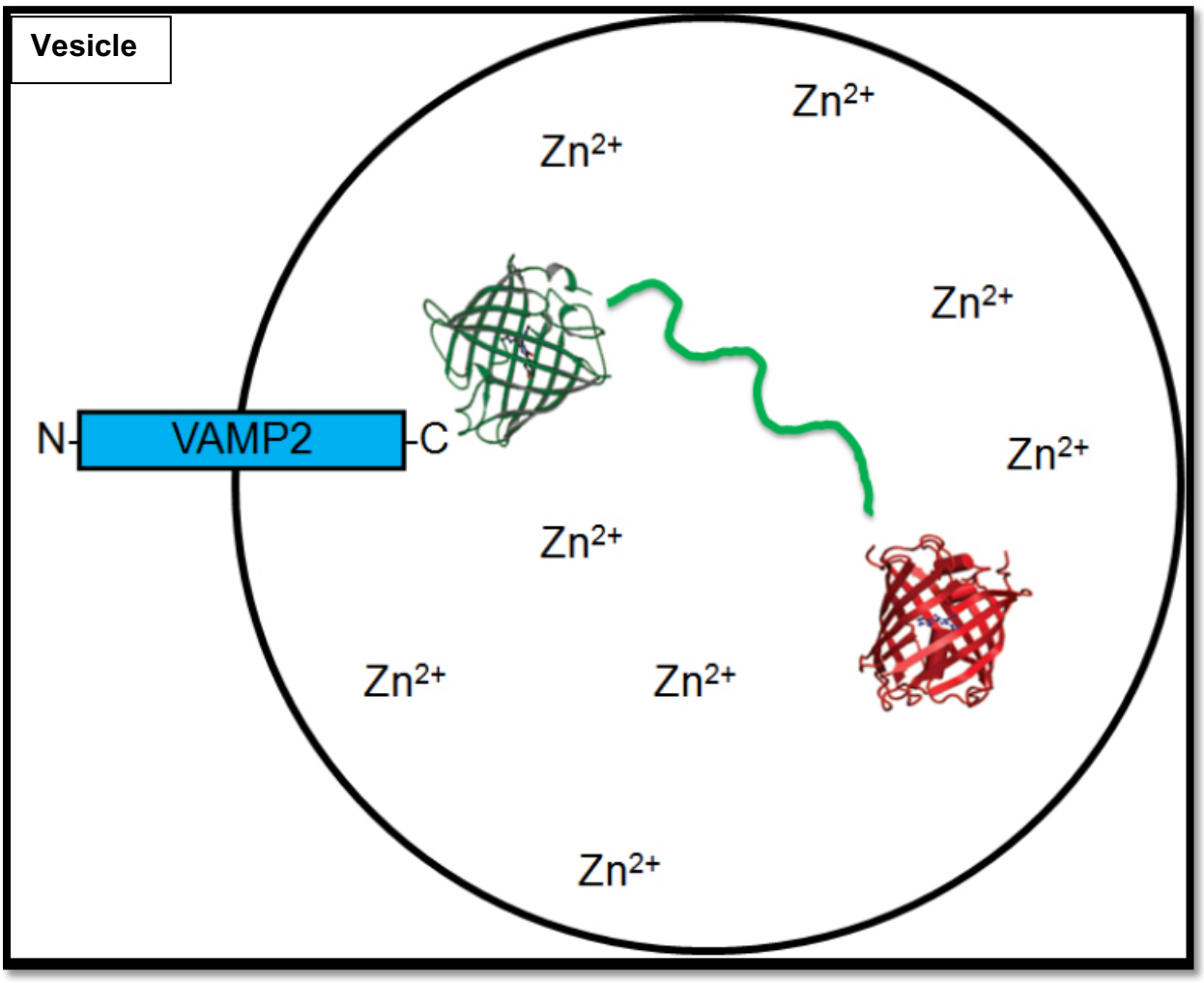

Figure 5.2. Schematic diagram Vesicle-Associated Membrane Protein 2 (VAMP2) with ZapCmR1.1 FRET sensor. VAMP2 is a single transmembrane protein that target vesicles and is a part of the SNARE machinery. ZapCmR1.1 was cloned onto the C-terminus of VAMP2 so that its spatial location resided in the luminal space of the vesicle to monitor Zn^{2+} content.

NaCl, 16.65 mM D-Glucose, and 30 mM HEPES) pH 7.4. This buffer is made in our laboratory because phosphates are known to precipitate Zn^{2+}. Buffer was generated with Chelex-100-treated water (Sigma Aldrich). Cell imaging was performed on a Zeiss Axiovert 200 M microscope with a Cascade 512B CCD camera (Roper Scientific) and Xenon arc lamp (XBO75) using MetaFluor software (Universal Imaging) to operate the system. The following settings were used: exposure time 600 msec, 20-30 second acquisition rate, 1.3NA 40x oil immersion objective, and excitation light was attenuated with a 5% neutral density filter for VAMP2-mCherry and VAMP2-ZapCmR1.1. mCherry fluorescent protein was excited with a 577/20 (nm/bandwidth) excitation filter, dichroic 595 nm, and 630/60 (nm/bandwidth) emission filter. FluoZin3 was excited with a 495/10 (nm/bandwidth) excitation filter, dichroic 515 nm, and 535/20 (nm/bandwidth) emission filter. Clover fluorescent protein was excited with a 480/20 (nm/bandwidth) excitation filter, dichroic 495 nm, and 510/20 (nm/bandwidth) emission filter. mRuby2 fluorescent protein was excited with a 540/25 (nm/bandwidth) excitation filter, dichroic 565 nm, and 595/20 (nm/bandwidth) emission filter. ZapCmR1.1 FRET sensor was excited with a 480/20 (nm/bandwidth) excitation filter, dichroic 565 nm, and 595/20 (nm/bandwidth) emission filter.

In addition to using a Zeiss Axiovert 200M microscope, we used a Nikon Ti-E microscope with a Perfect Focus System (PFS) for maintenance of sample focus, Differential Interference Contrast (DIC), Motorized XY stage with piezo Z-Drive insert for rapid multidimensional (XYZ) imaging and photomultiplier tubes (PMTs) to collect images. Images were analyzed using Nikon Elements software. A 100X objective was used with NA 1.4, 488 nm (FluoZin3), and 561 nm (mCherry) excitation laser light was used. A 525/50 (nm/bandwidth) and 650/50 (nm/bandwidth) confocal emission filters were used for FluoZin3 and mCherry, respectively.

Live Cell Imaging Experiments. To observe if VAMP2 localized to Zn^{2+} containing vesicles, VAMP2-mCherry transfected cultured cells were incubated with 2 μM FluoZin3 (K_d' = 15 nM;

Life Technologies) and 5 µL 20% Pluronic F-127 for 1 hour in phosphate free HHBSS buffer at room temperature in a dark place. Following incubation, the cells were washed with HHBSS two times to remove extracellular excess dye and 1 mL of HHBSS buffered was left with cells and placed in a dark environment to allow time for cleavage of the AM ester. Vesicles were followed for approximately 40 minutes with 30 second acquisition rate of FluoZin3 and mCherry channels.

To characterize VAMP2-ZapCmR1.1 in cells, a region of interest (ROI) was placed on an individual vesicle and on an untransfected cell or a region in the field of view with no cells as a measure of the background fluorescence. The FRET channel is defined as the emission intensity in the acceptor FP channel, upon excitation of the donor. The FRET ratio is defined as the background corrected intensity in the FRET channel divided by the background corrected intensity in the donor channel, i.e. $(I_{FRET} - I_{FRETbackground})/(I_{Donor} - I_{donorbackground})$. For imaging experiments, DMEM media was removed and cells were washed twice with HHBSS buffer followed by the addition of 1 mL HHBSS. ROIs were followed for 300 seconds to establish a resting R followed by the addition of 150 µM TPEN (N,N,N',N'-tetrakis-(2-pyridylmethyl)-ethylenediamine) to chelate Zn^{2+} and obtain the FRET ratio of the unbound sensor (R_{TPEN}). Once R_{TPEN} was established, cells were washed 3-times with the HHBSS solution to remove residual TPEN followed by addition of 1 mL of fresh HHBSS. Subsequently, 100 µM $ZnCl_2$ and 2 µM pyrithione was added to saturate the sensor and establish the FRET ratio of the Zn^{2+} bound sensor (R_{Zn}). Data were collected at 20-30 sec acquisition rate. The dynamic range of a sensor was defined as the maximum FRET ratio divided by the minimum FRET ratio (R_{max}/R_{min}), and the percent saturation was calculated according to $[(|R-R_{TPEN}|)/(|R_{Zn}-R_{TPEN}|)]*100\%$.

5.4 Results

5.4.1 VAMP2 and FluoZin3-AM Colocalization.

VAMP2 is a single pass transmembrane protein that is part of the ubiquitous SNARE complex involved in vesicle fusion. To assess whether VAMP2 colocalized with Zn^{2+}-containing vesicles, we created VAMP2-mCherry which can be imaged simultaneously with the green FluoZin3 small molecule dye. Although FluoZin3 targeting is inexact and in some cases ambiguous, it represents the current best way to visualize vesicular Zn^{2+}. As shown in **Figure 5.3a** VAMP2-mCherry robustly localizes to vesicles in HeLa cells. In some cells, there is co-localization with FluoZin3 (denoted by the arrow in **Figure 5.3a)**. However, the staining of vesicles by FluoZin3 was highly variable and vesicular localization of the dye was difficult to detect in many cells. For example, **Figure 5.3b** shows that HeLa cells stained with FluoZin3 exhibit poor illumination of vesicles, while VAMP2-mCherry robustly localizes to numerous vesicles throughout the cell. These results suggest that VAMP2 robustly targets vesicle populations in cells and looks to be a good targeting motif for a Zn^{2+} sensor.

5.4.2 VAMP2-ZapCmR1.1 *in vivo* Calibration

VAMP2 is localized to early and late endosomes (*23*) as well as localizing to exocytic vesicles that are sorted in the *trans*-Golgi network (TGN) (*24*). **Figure 5.4a** depicts HeLa cells transfected with the VAMP2-ZapCmR1.1 sensor and demonstrates localization of the sensor to puncta, consistent with localization to vesicles. The bright fluorescence intensity of the sensor indicates that the chromophore fluorescence is not quenched by the low pH of vesicles. To determine if the sensor responds to perturbations of cellular Zn^{2+} an in situ calibration was performed to measure the $R_{resting}$, R_{TPEN}, and R_{Zn}. This calibration involved treatment of cells with 150 μM TPEN to chelate Zn^{2+} and obtain the FRET ratio in the Zn^{2+}-free state (R_{TPEN}), followed by a washout and treatment with 2 μM pyrithione to permeabilize all cell membranes and addition of 100 μM $ZnCl_2$ to saturate the sensor and obtain the FRET ratio of the Zn^{2+}-bound state (R_{Zn}). **Figure 5.4b** shows two traces from two independent vesicles that VAMP2-ZapCmR1.1 responded to manipulation of cellular Zn^{2+} exhibiting an increase in the FRET ratio for R_{Zn} and a decrease for R_{TPEN}.

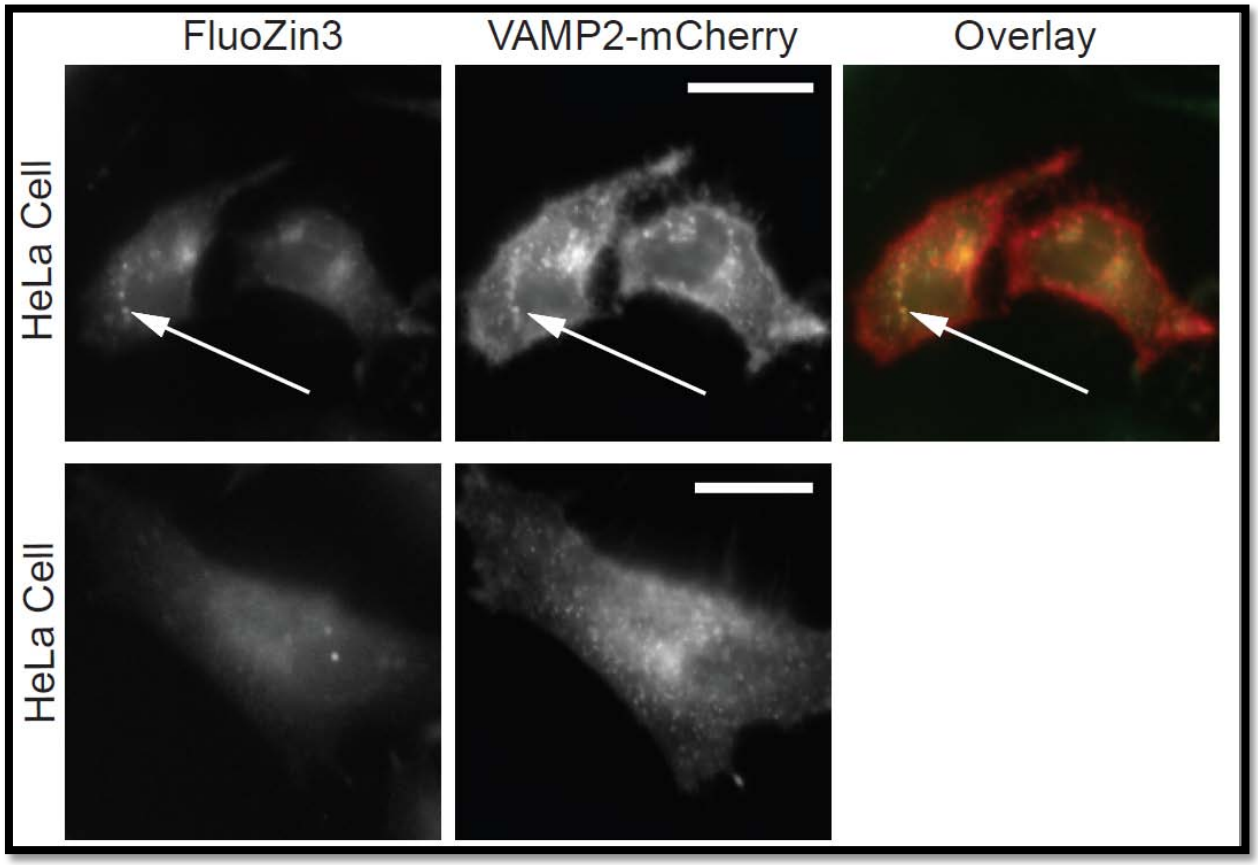

Figure 5.3. Fluorescence images of FluoZin3 and VAMP2-mCherry. A) Left image represents FluoZin3 stain, middle image is VAMP2-mCherry, and right image represents co-localization of FluoZin3 and VAMP2-mCherry. Arrow points to a vesicle containing FluoZin3 and VAMP2-mCherry. B) Left image demonstrates poor vesicular staining by FluoZin3 and right image demonstrates robust vesicular localization of VAMP2-mCherry. Scale bar = 20 μm.

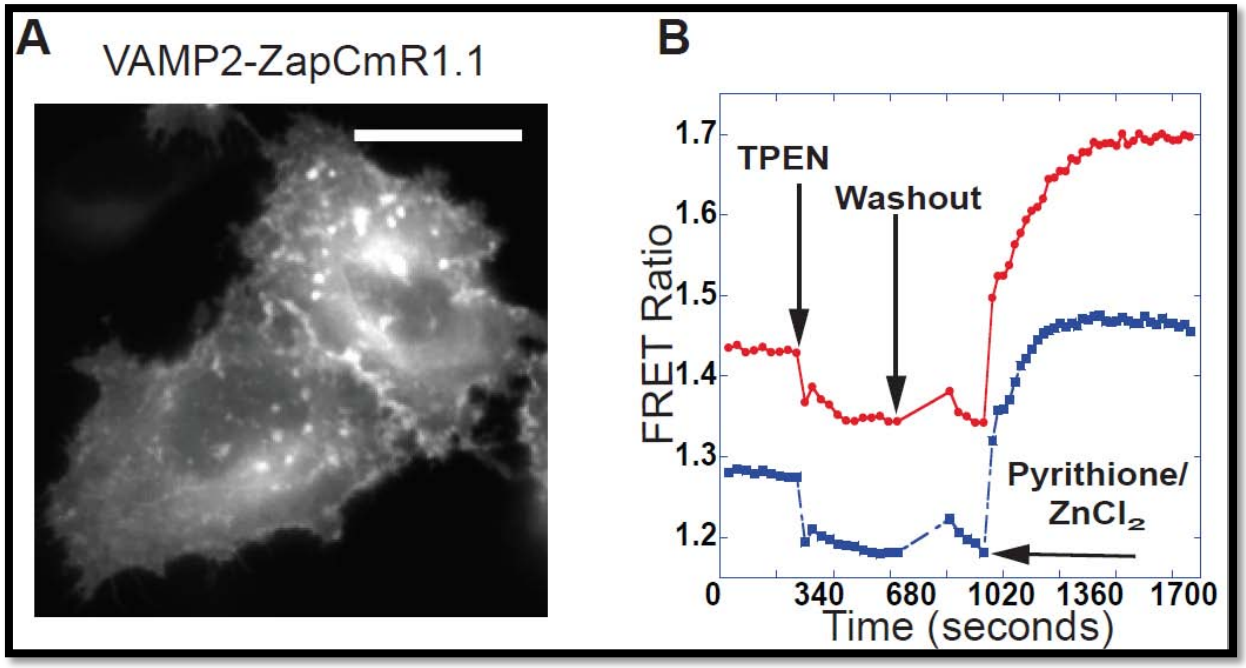

Figure 5.4. Calibration of VAMP2-ZapCmR1.1 in HeLa cells. A) HeLa cell line transfected with VAMP2-ZapCmR1.1 localized to vesicles. B) Two region of interest of vesicle Zn^{2+} measured using VAMP2-ZapCmR1.1. To calibrate the sensor, a region of interest is followed for 300 seconds followed by the addition of 150 μM TPEN to chelate Zn^{2+}. Once the minimum FRET ratio is established TPEN is washed out and subsequently 100 μM Zn^{2+} with 2 μM Pyrithione is added to saturate the sensor and obtain a maximum FRET ratio. Scale Bar = 20 μm.

The dynamic range of a sensor provides a measure of the sensitivity is defined as R_{Zn}/R_{TPEN}. VAMP2-ZapCmR1.1 exhibited a dynamic range of about 1.6 fold, similar to some of our CFP-YFP sensors (*25*). The percent saturation is a measure of how much Zn^{2+} is bound to a sensor under resting conditions and provides a relative measure of Zn^{2+} levels. ZapCmR1.1

in cells exhibited a percent saturation of about 30% in the vesicles observed. Although we have not performed *in vitro* characterization to determine the K_d' of the sensor we estimate to be in the high pM range because the percent saturation is similar to that of our CFP-YFP sensor (*25*). Although this is an estimate based on calibration of the sensor in the cytoplasm to the K_d' is likely to change as a function of pH. In previous studies that determined the K_d' under different pHs the binding affinity the Zn^{2+} binding domain weakens at low pH (*26, 27*). Our preliminary data of VAMP2-ZapCmR1.1 sensor demonstrate that the sensor has a good signal-to-noise ratio, responds to our calibration, and its fluorescence does not seem to be affected by the low pH of the vesicle. In previous study that used a genetically encoded FRET sensor fused to VAMP2 to look at Zn^{2+} in vesicles did not show any response (*28*). A possible explanation could be that under acidic conditions the yellow FP quenched therefore no FRET ratio change was observed upon *in vivo* calibration or the binding domain was not sensitive to the amount of free Zn^{2+} in the vesicle. We believe that this sensor represents an important landmark in being able to quantify Zn^{2+} in an acidic compartment as well as use it with other CFP-YFP sensors and be able to dissect Zn^{2+} signaling in vesicles.

5.5 Discussion

While there is a growing repertoire of tools to monitor free Zn^{2+} in different cellular locations, there are still no ratiometric sensors, explicitly targeted to vesicles to quantify the amount of Zn^{2+} present in vesicles. Yet growing evidence suggests that not only do vesicles represent one of the major storehouses of Zn^{2+} in cells, but also that vesicular Zn^{2+} plays important roles in cellular processes. For example in the brain the absence of vesicular zinc has profound implications for neurotransmission and cortical plasticity (*29*). In addition, in the pancreas, dysruption of vesicular Zn^{2+} is known to cause type 2 diabetes (*30*). Although there exists a pool of Zn^{2+} in prostate cells do date nothing is known about it or if it implicated in disease progression. In this work we created the first functional, ratiometric sensor genetically targeted to vesicles. ZapCmR1.1 was tagged using VAMP2, resulting in robust localization to

vesicles in HeLa cells. Our preliminary data suggest the vesicular localized sensor is fluorescent and response to perturbations of cellular Zn^{2+}.

Until the development of our sensor, the most widely available probe to visualize vesicular Zn^{2+} was FluoZin3. This small molecule probe lacks a specific targeting signal, and therefore while it typically highlights pools of vesicular Zn^{2+}, staining is highly variable and results in illumination of both vesicles and the cytosol. Such heterogeneity makes it difficult to track the vesicular pool. Even so, this dye has been widely used in hippocampal neuron and pancreatic β-cells. In hippocampal neurons it has been used to detect the release of Zn^{2+} from synaptic vesicles (*31, 32*) which is estimated to be approximately 100 μM (*33*). Another study done on hippocampal vesicles observed Zn^{2+} to be around 1-10 μM (*34*). These previous studies demonstrate the variability in trying to quantify vesicular Zn^{2+} in neurons using a small molecule fluorescent dye. In addition to neurons, FluoZin3 has been used in pancreatic β-cells to monitor Zn^{2+} secretion from vesicles. Gee and coworkers (*35*) found that vesicular Zn^{2+} in pancreatic β-cells is estimated to be 600 nM. In addition to the challenges mentioned above with respect to variability in dye localization, an additional concern is that FluoZin3 was derived from a Ca^{2+} dyes and is still sensitive to this divalent ion (*36*). Another problem, particularly with respect to quantification, is that the intracellular concentration of FluoZin3 can reach hundreds of micromolar, thus overwhelming the Zn^{2+} buffering capacity of the cell and leading to perturbations of cellular Zn^{2+} levels.

The development of VAMP2-ZapCmR1.1 FRET sensor will provide insight into the pool of Zn^{2+} in vesicles and how it differs from cell to cell. In order to continue investigating and quantifying this Zn^{2+} we need to perform extensive *in vitro* characterization of this sensor. ZapCmR1.1 protein needs to be purified to determine the disassociation constant as a function of pH. This will allow us to quantify free Zn^{2+} in vesicles. Once this occurs we can move to cells and determine the pool of Zn^{2+} in vesicles in a number of cells with the ultimate goal in

identifying the underlying causes of disease that may be due to dysregulation of this metal in vesicles.

5.6 References

1. Rajesh, R. V., Balasubramanian, A. S., and Boopathy, R. (2009) Evidence for presence of Zn+2-binding site in acetylcholinesterase, *Biochimie 91*, 526-532.
2. Mocchegiani, E., Muzzioli, M., Cipriano, C., and Giacconi, R. (1998) Zinc, T-cell pathways, aging: role of metallothioneins, *Mech Ageing Dev 106*, 183-204.
3. Pavletich, N. P., and Pabo, C. O. (1991) Zinc finger-DNA recognition: crystal structure of a Zif268-DNA complex at 2.1 A, *Science 252*, 809-817.
4. Laity, J. H., and Andrews, G. K. (2007) Understanding the mechanisms of zinc-sensing by metal-response element binding transcription factor-1 (MTF-1), *Arch Biochem Biophys 463*, 201-210.
5. Outten, C. E., and O'Halloran, T. V. (2001) Femtomolar sensitivity of metalloregulatory proteins controlling zinc homeostasis, *Science 292*, 2488-2492.
6. Eide, D. J. (2006) Zinc transporters and the cellular trafficking of zinc, *Biochim Biophys Acta 1763*, 711-722.
7. Franklin, R. B., and Costello, L. C. (2007) Zinc as an anti-tumor agent in prostate cancer and in other cancers, *Arch Biochem Biophys 463*, 211-217.
8. Sorensen, M. B., Stoltenberg, M., Juhl, S., Danscher, G., and Ernst, E. (1997) Ultrastructural localization of zinc ions in the rat prostate: an autometallographic study, *Prostate 31*, 125-130.
9. Zalewski, P. D., Millard, S. H., Forbes, I. J., Kapaniris, O., Slavotinek, A., Betts, W. H., Ward, A. D., Lincoln, S. F., and Mahadevan, I. (1994) Video image analysis of labile zinc in viable pancreatic islet cells using a specific fluorescent probe for zinc, *J Histochem Cytochem 42*, 877-884.

10. Colvin, R. A., Fontaine, C. P., Laskowski, M., and Thomas, D. (2003) Zn2+ transporters and Zn2+ homeostasis in neurons, *Eur J Pharmacol 479*, 171-185.

11. Frederickson, C. J., Koh, J. Y., and Bush, A. I. (2005) The neurobiology of zinc in health and disease, *Nat Rev Neurosci 6*, 449-462.

12. Chimienti, F., Devergnas, S., Favier, A., and Seve, M. (2004) Identification and cloning of a beta-cell-specific zinc transporter, ZnT-8, localized into insulin secretory granules, *Diabetes 53*, 2330-2337.

13. Kelleher, S. L., McCormick, N. H., Velasquez, V., and Lopez, V. (2011) Zinc in specialized secretory tissues: roles in the pancreas, prostate, and mammary gland, *Adv Nutr 2*, 101-111.

14. Besser, L., Chorin, E., Sekler, I., Silverman, W. F., Atkin, S., Russell, J. T., and Hershfinkel, M. (2009) Synaptically released zinc triggers metabotropic signaling via a zinc-sensing receptor in the hippocampus, *J Neurosci 29*, 2890-2901.

15. Yamasaki, S., Sakata-Sogawa, K., Hasegawa, A., Suzuki, T., Kabu, K., Sato, E., Kurosaki, T., Yamashita, S., Tokunaga, M., Nishida, K., and Hirano, T. (2007) Zinc is a novel intracellular second messenger, *J Cell Biol 177*, 637-645.

16. Gee, K. R., Zhou, Z. L., Ton-That, D., Sensi, S. L., and Weiss, J. H. (2002) Measuring zinc in living cells. A new generation of sensitive and selective fluorescent probes, *Cell Calcium 31*, 245-251.

17. Ding, Y., Ai, H. W., Hoi, H., and Campbell, R. E. (2011) Forster resonance energy transfer-based biosensors for multiparameter ratiometric imaging of Ca2+ dynamics and caspase-3 activity in single cells, *Anal Chem 83*, 9687-9693.

18. Heikal, A. A., Hess, S. T., Baird, G. S., Tsien, R. Y., and Webb, W. W. (2000) Molecular spectroscopy and dynamics of intrinsically fluorescent proteins: coral red (dsRed) and yellow (Citrine), *Proc Natl Acad Sci U S A 97*, 11996-12001.

19. Wachter, R. M., Elsliger, M. A., Kallio, K., Hanson, G. T., and Remington, S. J. (1998) Structural basis of spectral shifts in the yellow-emission variants of green fluorescent protein, *Structure 6*, 1267-1277.

20. Sachse, M., Ramm, G., Strous, G., and Klumperman, J. (2002) Endosomes: multipurpose designs for integrating housekeeping and specialized tasks, *Histochem Cell Biol 117*, 91-104.

21. Saftig, P., and Klumperman, J. (2009) Lysosome biogenesis and lysosomal membrane proteins: trafficking meets function, *Nat Rev Mol Cell Biol 10*, 623-635.

22. Lam, A. J., St-Pierre, F., Gong, Y., Marshall, J. D., Cranfill, P. J., Baird, M. A., McKeown, M. R., Wiedenmann, J., Davidson, M. W., Schnitzer, M. J., Tsien, R. Y., and Lin, M. Z. (2012) Improving FRET dynamic range with bright green and red fluorescent proteins, *Nat Methods 9*, 1005-1012.

23. Bonanomi, D., Benfenati, F., and Valtorta, F. (2006) Protein sorting in the synaptic vesicle life cycle, *Prog Neurobiol 80*, 177-217.

24. Bonanomi, D., Rusconi, L., Colombo, C. A., Benfenati, F., and Valtorta, F. (2007) Synaptophysin I selectively specifies the exocytic pathway of synaptobrevin 2/VAMP2, *Biochem J 404*, 525-534.

25. Qin, Y., Dittmer, P. J., Park, J. G., Jansen, K. B., and Palmer, A. E. (2011) Measuring steady-state and dynamic endoplasmic reticulum and Golgi Zn2+ with genetically encoded sensors, *Proc Natl Acad Sci U S A 108*, 7351-7356.

26. Hitomi, Y., Outten, C. E., and O'Halloran, T. V. (2001) Extreme zinc-binding thermodynamics of the metal sensor/regulator protein, ZntR, *J Am Chem Soc 123*, 8614-8615.

27. Lyons, T. J., Nersissian, A., Huang, H., Yeom, H., Nishida, C. R., Graden, J. A., Gralla, E. B., and Valentine, J. S. (2000) The metal binding properties of the zinc site of yeast

copper-zinc superoxide dismutase: implications for amyotrophic lateral sclerosis, *J Biol Inorg Chem 5*, 189-203.

28. Vinkenborg, J. L., Nicolson, T. J., Bellomo, E. A., Koay, M. S., Rutter, G. A., and Merkx, M. (2009) Genetically encoded FRET sensors to monitor intracellular Zn2+ homeostasis, *Nat Methods 6*, 737-740.

29. Nakashima, A. S., Butt, R. H., and Dyck, R. H. (2011) Alterations in protein and gene expression within the barrel cortices of ZnT3 knockout mice: Experience-independent and dependent changes, *Neurochem Int 59*, 860-870.

30. Rutter, G. A. (2010) Think zinc: New roles for zinc in the control of insulin secretion, *Islets 2*, 49-50.

31. Kay, A. R. (2003) Evidence for chelatable zinc in the extracellular space of the hippocampus, but little evidence for synaptic release of Zn, *J Neurosci 23*, 6847-6855.

32. Qian, J., and Noebels, J. L. (2006) Exocytosis of vesicular zinc reveals persistent depression of neurotransmitter release during metabotropic glutamate receptor long-term depression at the hippocampal CA3-CA1 synapse, *J Neurosci 26*, 6089-6095.

33. Pan, E., Zhang, X. A., Huang, Z., Krezel, A., Zhao, M., Tinberg, C. E., Lippard, S. J., and McNamara, J. O. (2011) Vesicular zinc promotes presynaptic and inhibits postsynaptic long-term potentiation of mossy fiber-CA3 synapse, *Neuron 71*, 1116-1126.

34. Frederickson, C. J., Giblin, L. J., 3rd, Balaji, R. V., Masalha, R., Zeng, Y., Lopez, E. V., Koh, J. Y., Chorin, U., Besser, L., Hershfinkel, M., Li, Y., Thompson, R. B., and Krezel, A. (2006) Synaptic release of zinc from brain slices: factors governing release, imaging, and accurate calculation of concentration, *J Neurosci Methods 154*, 19-29.

35. Gee, K. R., Zhou, Z. L., Qian, W. J., and Kennedy, R. (2002) Detection and imaging of zinc secretion from pancreatic beta-cells using a new fluorescent zinc indicator, *J Am Chem Soc 124*, 776-778.

36. Bastian, C., and Li, Y. V. (2007) Fluorescence imaging study of extracellular zinc at the hippocampal mossy fiber synapse, *Neurosci Lett 419*, 119-124.

Chapter VI

Conclusions and Future Directions

6.1 Zinc Dysregulation

Throughout this thesis I have detailed the importance of Zn^{2+} in cells and how proteins such as transporters regulate this metal. I have focused on prostate cancer and found that prostate cancer cell lines are characterized by substantial dysregulation of cellular Zn^{2+}. This includes depletion of total Zn^{2+}, redistribution of free Zn^{2+} amongst intracellular stores, as well as alterations in the expression and regulation of Zn^{2+} transporters.

This has been a major landmark for us as I have developed the most comprehensive picture to date of the distribution of free Zn^{2+} among intracellular organelles and how this distribution may be altered by disease. But I still need to perform more work in these cell lines. During our experiments I tried to quantify the free Zn^{2+} in the Golgi apparatus but our sensor appears to be fully saturated under resting conditions, suggesting that there are significantly higher levels of Zn^{2+} in the Golgi of prostate cells than in the model HeLa cell line used to validate the Golgi sensor. The fact that the sensor is saturated precludes us from being able to quantify Zn^{2+} in the Golgi with this sensor. It also suggests that prostate cells are fundamentally different from HeLa cells in that the Golgi may represent a major Zn^{2+} store. As a first step toward addressing this issue, I cloned in the lower affinity ZapCY2 (*1*) into the Golgi construct. However, the current Golgi-targeting sequence doesn't yield robust Golgi localization of ZapCY2 in prostate cell lines. Instead, typical observations reveal the sensor is primarily mislocalized to the ER. Therefore our next steps are to try using a different Golgi targeting signal sequence, change the fluorescent proteins to variants that don't dimerize in oxidizing compartments such as the secretory pathway (oxCerulean and oxVenus), and to test other low affinity Zn^{2+} binding motifs (it is surprising that ZapCY1 targets better than ZapCY2). Once I obtain a sensor with robust localization, the sensor will be calibrated in the Golgi using methodology previously established in our lab. Quantifying the free Zn^{2+} content in the Golgi of RWPE1 normal cell line and all three prostate cancer cell will be exciting and an important piece of the puzzle of how Zn^{2+} is dysregulated in prostate cancer. In mice, Golgi Zn^{2+} has been implicated in prostate

cancer disease progression due a null mutation in the ZnT7 transporter which is responsible for the accumulation of Zn^{2+} in this compartment (*2*). In addition to quantifying the free Zn^{2+} in the Golgi it will interesting to sequence the ZnT7 Zn^{2+} transporter of all four cell line to determine if there are any differences.

Another key compartment is to profile whether there are any changes in vesicular Zn^{2+} in these prostate cells. As mentioned in Chapter V, as part of this thesis work I developed the first functional ratiometric sensor explicitly targeted to vesicular compartments. Before using this sensor to quantify vesicular Zn^{2+}, the sensor itself needs to be better characterized. In particular, future experiments will be necessary to determine the disassociation constant of the sensor as a function of pH, and ideally I would like to determine the dissociation constant *in situ* as well. Once this characterization occurs I can move into cells and quantify the free Zn^{2+} in vesicles of the normal and cancerous prostate cell lines.

Another future direction is to determine how Zn^{2+} dyshomeostasis influences cellular functions. One of the cellular functions that I hypothesize might be affected is the rate of apoptosis. It has been shown that too much or little Zn^{2+} causes the cell to undergo apoptosis and that the intracellular pool of chelatable Zn^{2+} plays a critical role in this event as well (*3-6*). Elevated Zn^{2+} in the cytosol has been shown to inhibit caspases (*7*), thus inhibiting the apoptotic pathway. To test whether the elevated cysotolic Zn^{2+} observed in the prostate cells makes these cells less sensitive to apoptotic stimuli, I will measure the proportion of cells undergoing apoptosis using a FACS-based assay under non-stimulated and stimulated conditions. If I observe a difference, I will test whether a low dose of a Zn^{2+}-chelator alters the propensity of the cells to undergo apoptosis. The Zn^{2+} chelator was characterized in a previous study in our laboratory by Dr. Yan Qin and she found that PAC-1 and S-PAC-1 chelated low levels of Zn^{2+} and activated procaspase-3 activity to induce apoptosis (*8*).

6.2 Zinc Transporter Expression

To begin to address why Zn^{2+} homeostasis is altered in prostate cancer cells, I measured the levels of key Zn^{2+} regulatory proteins, the ZIP transporters which control Zn^{2+} entry into the cytosol from the extracellular space or from intracellular organelles, and the ZnT transporters which control Zn^{2+} efflux from the cytosol, either across the plasma membrane or across the membranes of intracellular organelles. Our results suggest that the mRNA and protein levels are often differentially regulated (i.e. elevated mRNA but decreased protein levels in a given cell line), indicating the importance of measuring both when building a map of the dysregulation of transporters associated with disease. I observed, more often than not, that the mRNA expression did not correlate with the protein expression and our results have barely scratched the surface on Zn^{2+} dysregulation. In order to better understand how (and whether) free Zn^{2+} levels are regulated by transporters, I need to quantify all 24 known transporters as well as the most common isoforms of the primary Zn^{2+} buffer, metallothionein.

To rigorously assess whether transporter expression indeed controls the observed Zn^{2+} levels requires manipulation of transporter expression levels and measurement of the resulting free Zn^{2+} in compartments across the cell because changes of Zn^{2+} in one compartment could lead to compensatory changes in other compartments For example, I could partially knock down ZnT1 in prostate cancer cell lines and measure whether the levels of Zn^{2+} in the cytosol increase in prostate cancer cell lines by ICP-MS (total Zn^{2+}) or using FRET-based sensors (free Zn^{2+}). These experiments will map the expression of all 24 Zn^{2+} transporters in normal compared to cancerous cell lines to ascertain if there are systematic differences which are responsible for the low levels of Zn^{2+} in prostate cancer cells.

6.3 Conclusion

Prostate cancer will affect 1 in 6 men in our lifetime (*9*). At this time the prognostic tools that physicians use are flawed. One key component that a physician looks at during a regular examination is prostate specific antigen, but it is known to become elevated if the prostate is inflamed. This gives false-positive results which lead to invasive and painful biopsies. Over the

last decade researchers have looked at Zn^{2+} dysregulation in prostate cancer and have found in both cell lines and tissue biopsies that Zn^{2+} levels correlate with malignancy. However, we have very little understanding of how and why Zn^{2+} is altered in prostate cancer. If the changes in Zn^{2+} homeostasis can be precisely defined and if we determine that specific signatures of dysregulation (decreased total Zn^{2+}, altered transporter expression, etc) give rise to and precede the onset of malignancy and metastasis, then Zn^{2+} dysregulation could potentially be used as a diagnostic biomarker of disease. While we are still a long way off from establishing this, this thesis represents the first step to define the full extent of Zn^{2+} regulation at the cellular level.

6.4 References

1. Qin, Y., Dittmer, P. J., Park, J. G., Jansen, K. B., and Palmer, A. E. (2011) Measuring steady-state and dynamic endoplasmic reticulum and Golgi Zn2+ with genetically encoded sensors, *Proc Natl Acad Sci U S A 108*, 7351-7356.
2. Tepaamorndech, S., Huang, L., and Kirschke, C. P. (2011) A null-mutation in the Znt7 gene accelerates prostate tumor formation in a transgenic adenocarcinoma mouse prostate model, *Cancer Lett 308*, 33-42.
3. Sunderman, F. W., Jr. (1995) The influence of zinc on apoptosis, *Ann Clin Lab Sci 25*, 134-142.
4. Adamo, A. M., Zago, M. P., Mackenzie, G. G., Aimo, L., Keen, C. L., Keenan, A., and Oteiza, P. I. (2010) The role of zinc in the modulation of neuronal proliferation and apoptosis, *Neurotox Res 17*, 1-14.
5. Thambiayya, K., Wasserloos, K., Kagan, V. E., Stoyanovsky, D., and Pitt, B. R. (2012) A critical role for increased labile zinc in reducing sensitivity of cultured sheep pulmonary artery endothelial cells to LPS-induced apoptosis, *Am J Physiol Lung Cell Mol Physiol 302*, L1287-1295.

6. Thambiayya, K., Wasserloos, K. J., Huang, Z., Kagan, V. E., St Croix, C. M., and Pitt, B. R. (2011) LPS-induced decrease in intracellular labile zinc, [Zn]i, contributes to apoptosis in cultured sheep pulmonary artery endothelial cells, *Am J Physiol Lung Cell Mol Physiol 300*, L624-632.
7. Franklin, R. B., and Costello, L. C. (2009) The important role of the apoptotic effects of zinc in the development of cancers, *J Cell Biochem 106*, 750-757.
8. West, D. C., Qin, Y., Peterson, Q. P., Thomas, D. L., Palchaudhuri, R., Morrison, K. C., Lucas, P. W., Palmer, A. E., Fan, T. M., and Hergenrother, P. J. (2012) Differential effects of procaspase-3 activating compounds in the induction of cancer cell death, *Mol Pharm 9*, 1425-1434.
9. Troyer, D. A., Mubiru, J., Leach, R. J., and Naylor, S. L. (2004) Promise and challenge: Markers of prostate cancer detection, diagnosis and prognosis, *Dis Markers 20*, 117-128.

Bibliography:

Auld, D. S. (2001) Zinc coordination sphere in biochemical zinc sites, *Biometals 14*, 271-313.

Frederickson, C. J., Koh, J. Y., and Bush, A. I. (2005) The neurobiology of zinc in health and disease, *Nat Rev Neurosci 6*, 449-462.

Nies, D. H. (2007) Biochemistry. How cells control zinc homeostasis, *Science 317*, 1695-1696.

Andreini, C., Banci, L., Bertini, I., and Rosato, A. (2006) Counting the zinc-proteins encoded in the human genome, *J Proteome Res 5*, 196-201.

Maret, W., and Sandstead, H. H. (2006) Zinc requirements and the risks and benefits of zinc supplementation, *J Trace Elem Med Biol 20*, 3-18.

Rajesh, R. V., Balasubramanian, A. S., and Boopathy, R. (2009) Evidence for presence of Zn+2-binding site in acetylcholinesterase, *Biochimie 91*, 526-532.

Mocchegiani, E., Muzzioli, M., Cipriano, C., and Giacconi, R. (1998) Zinc, T-cell pathways, aging: role of metallothioneins, *Mech Ageing Dev 106*, 183-204.

Pavletich, N. P., and Pabo, C. O. (1991) Zinc finger-DNA recognition: crystal structure of a Zif268-DNA complex at 2.1 A, *Science 252*, 809-817.

Laity, J. H., and Andrews, G. K. (2007) Understanding the mechanisms of zinc-sensing by metal-response element binding transcription factor-1 (MTF-1), *Arch Biochem Biophys 463*, 201-210.

O'Green, H., Frietze, S., and Rarnham, P. J. (2010) Using ChIP-seq technology to identify targets of zinc finger transcription factors, *Methods Mol Biol 649*, 437-455.

Freedman, L. P., and Luisi, B. F. (1993) On the mechanism of DNA binding by nuclear hormone receptors: a structural and functional perspective, *J Cell Biochem 51*, 140-150.

Levenson, C. W., and Morris, D. (2011) Zinc and neurogenesis: making new neurons from development to adulthood, *Adv Nutr 2*, 96-100.

Eide, D. J. (2006) Zinc transporters and the cellular trafficking of zinc, *Biochim Biophys Acta 1763*, 711-722.

Outten, C. E., and O'Halloran, T. V. (2001) Femtomolar sensitivity of metalloregulatory proteins controlling zinc homeostasis, *Science 292*, 2488-2492.

Palmiter, R. D., and Findley, S. D. (1995) Cloning and functional characterization of a mammalian zinc transporter that confers resistance to zinc, *EMBO J 14*, 639-649.

Krezel, A., and Maret, W. (2008) Thionein/metallothionein control Zn(II) availability and the activity of enzymes, *J Biol Inorg Chem 13*, 401-409.

Thirumoorthy, N., Shyam Sunder, A., Manisenthil Kumar, K., Senthil Kumar, M., Ganesh, G., and Chatterjee, M. (2011) A review of metallothionein isoforms and their role in pathophysiology, *World J Surg Oncol 9*, 54.

Qin, Y., Dittmer, P. J., Park, J. G., Jansen, K. B., and Palmer, A. E. (2011) Measuring steady-state and dynamic endoplasmic reticulum and Golgi Zn2+ with genetically encoded sensors, *Proc Natl Acad Sci U S A 108*, 7351-7356.

Vinkenborg, J. L., Nicolson, T. J., Bellomo, E. A., Koay, M. S., Rutter, G. A., and Merkx, M. (2009) Genetically encoded FRET sensors to monitor intracellular Zn2+ homeostasis, *Nat Methods 6*, 737-740.

Park, J. G., Qin, Y., Galati, D. F., and Palmer, A. E. (2012) New Sensors for Quantitative Measurement of Mitochondrial Zn(2+), *ACS Chem Biol*.

Inoue, K., Takano, H., Shimada, A., and Satoh, M. (2009) Metallothionein as an anti-inflammatory mediator, *Mediators Inflamm 2009*, 101659.

Maret, W. (2009) Molecular aspects of human cellular zinc homeostasis: redox control of zinc potentials and zinc signals, *Biometals 22*, 149-157.

Barbato, J. C., Catanescu, O., Murray, K., DiBello, P. M., and Jacobsen, D. W. (2007) Targeting of metallothionein by L-homocysteine: a novel mechanism for disruption of zinc and redox homeostasis, *Arterioscler Thromb Vasc Biol 27*, 49-54.

Stitt, M. S., Wasserloos, K. J., Tang, X., Liu, X., Pitt, B. R., and St Croix, C. M. (2006) Nitric oxide-induced nuclear translocation of the metal responsive transcription factor, MTF-1 is mediated by zinc release from metallothionein, *Vascul Pharmacol 44*, 149-155.

Lichten, L. A., and Cousins, R. J. (2009) Mammalian zinc transporters: nutritional and physiologic regulation, *Annu Rev Nutr 29*, 153-176.

Guerinot, M. L. (2000) The ZIP family of metal transporters, *Biochim Biophys Acta 1465*, 190-198.

Delhaize, E., Kataoka, T., Hebb, D. M., White, R. G., and Ryan, P. R. (2003) Genes encoding proteins of the cation diffusion facilitator family that confer manganese tolerance, *Plant Cell 15*, 1131-1142.

Franklin, R. B., and Costello, L. C. (2007) Zinc as an anti-tumor agent in prostate cancer and in other cancers, *Arch Biochem Biophys 463*, 211-217.

Sorensen, M. B., Stoltenberg, M., Juhl, S., Danscher, G., and Ernst, E. (1997) Ultrastructural localization of zinc ions in the rat prostate: an autometallographic study, *Prostate 31*, 125-130.

Palmiter, R. D., Cole, T. B., and Findley, S. D. (1996) ZnT-2, a mammalian protein that confers resistance to zinc by facilitating vesicular sequestration, *EMBO J 15*, 1784-1791.

Perez-Clausell, J., and Danscher, G. (1985) Intravesicular localization of zinc in rat telencephalic boutons. A histochemical study, *Brain Res 337*, 91-98.

Henshall, S. M., Afar, D. E., Rasiah, K. K., Horvath, L. G., Gish, K., Caras, I., Ramakrishnan, V., Wong, M., Jeffry, U., Kench, J. G., Quinn, D. I., Turner, J. J., Delprado, W., Lee, C. S., Golovsky, D., Brenner, P. C., O'Neill, G. F., Kooner, R., Stricker, P. D., Grygiel, J. J., Mack, D. H., and Sutherland, R. L. (2003) Expression of the zinc transporter ZnT4 is decreased in the progression from early prostate disease to invasive prostate cancer, *Oncogene 22*, 6005-6012.

Kambe, T., Narita, H., Yamaguchi-Iwai, Y., Hirose, J., Amano, T., Sugiura, N., Sasaki, R., Mori, K., Iwanaga, T., and Nagao, M. (2002) Cloning and characterization of a novel mammalian zinc transporter, zinc transporter 5, abundantly expressed in pancreatic beta cells, *J Biol Chem 277*, 19049-19055.

Kirschke, C. P., and Huang, L. (2003) ZnT7, a novel mammalian zinc transporter, accumulates zinc in the Golgi apparatus, *J Biol Chem 278*, 4096-4102.

Sim, D. L., and Chow, V. T. (1999) The novel human HUEL (C4orf1) gene maps to chromosome 4p12-p13 and encodes a nuclear protein containing the nuclear receptor interaction motif, *Genomics 59*, 224-233.

3Seve, M., Chimienti, F., Devergnas, S., and Favier, A. (2004) In silico identification and expression of SLC30 family genes: an expressed sequence tag data mining strategy for the characterization of zinc transporters' tissue expression, *BMC Genomics 5*, 32.

Gaither, L. A., and Eide, D. J. (2001) The human ZIP1 transporter mediates zinc uptake in human K562 erythroleukemia cells, *J Biol Chem 276*, 22258-22264.

Dufner-Beattie, J., Langmade, S. J., Wang, F., Eide, D., and Andrews, G. K. (2003) Structure, function, and regulation of a subfamily of mouse zinc transporter genes, *J Biol Chem 278*, 50142-50150.

Wang, K., Zhou, B., Kuo, Y. M., Zemansky, J., and Gitschier, J. (2002) A novel member of a zinc transporter family is defective in acrodermatitis enteropathica, *Am J Hum Genet 71*, 66-73.

Taylor, K. M., and Nicholson, R. I. (2003) The LZT proteins; the LIV-1 subfamily of zinc transporters, *Biochim Biophys Acta 1611*, 16-30.

Huang, L., Kirschke, C. P., Zhang, Y., and Yu, Y. Y. (2005) The ZIP7 gene (Slc39a7) encodes a zinc transporter involved in zinc homeostasis of the Golgi apparatus, *J Biol Chem 280*, 15456-15463.

Ryu, M. S., Lichten, L. A., Liuzzi, J. P., and Cousins, R. J. (2008) Zinc transporters ZnT1 (Slc30a1), Zip8 (Slc39a8), and Zip10 (Slc39a10) in mouse red blood cells are differentially regulated during erythroid development and by dietary zinc deficiency, *J Nutr 138*, 2076-2083.

Kagara, N., Tanaka, N., Noguchi, S., and Hirano, T. (2007) Zinc and its transporter ZIP10 are involved in invasive behavior of breast cancer cells, *Cancer Sci 98*, 692-697.

Giunta, C., Randolph, A., and Steinmann, B. (2005) Mutation analysis of the PLOD1 gene: an efficient multistep approach to the molecular diagnosis of the kyphoscoliotic type of Ehlers-Danlos syndrome (EDS VIA), *Mol Genet Metab 86*, 269-276.

Nemeth, E., Rivera, S., Gabayan, V., Keller, C., Taudorf, S., Pedersen, B. K., and Ganz, T. (2004) IL-6 mediates hypoferremia of inflammation by inducing the synthesis of the iron regulatory hormone hepcidin, *J Clin Invest 113*, 1271-1276.

Franklin, R. B., Milon, B., Feng, P., and Costello, L. C. (2005) Zinc and zinc transporters in normal prostate and the pathogenesis of prostate cancer, *Front Biosci 10*, 2230-2239.

Huang, L., Kirschke, C. P., and Zhang, Y. (2006) Decreased intracellular zinc in human tumorigenic prostate epithelial cells: a possible role in prostate cancer progression, *Cancer Cell Int 6*, 10.

Sakai, I., Harada, K., Hara, I., Eto, H., and Miyake, H. (2005) A comparison of the biological features between prostate cancers arising in the transition and peripheral zones, *BJU Int 96*, 528-532.

Costello, L. C., and Franklin, R. B. (2006) The clinical relevance of the metabolism of prostate cancer; zinc and tumor suppression: connecting the dots, *Mol Cancer 5*, 17.

Albrecht, A. L., Somji, S., Sens, M. A., Sens, D. A., and Garrett, S. H. (2008) Zinc transporter mRNA expression in the RWPE-1 human prostate epithelial cell line, *Biometals 21*, 405-416.

Costello, L. C., Franklin, R. B., Feng, P., Tan, M., and Bagasra, O. (2005) Zinc and prostate cancer: a critical scientific, medical, and public interest issue (United States), *Cancer Causes Control 16*, 901-915.

Franklin, R. B., Feng, P., Milon, B., Desouki, M. M., Singh, K. K., Kajdacsy-Balla, A., Bagasra, O., and Costello, L. C. (2005) hZIP1 zinc uptake transporter down regulation and zinc depletion in prostate cancer, *Mol Cancer 4*, 32.

Iguchi, K., Otsuka, T., Usui, S., Ishii, K., Onishi, T., Sugimura, Y., and Hirano, K. (2004) Zinc and metallothionein levels and expression of zinc transporters in androgen-independent subline of LNCaP cells, *J Androl 25*, 154-161.

Christudoss, P., Selvakumar, R., Fleming, J. J., and Gopalakrishnan, G. (2011) Zinc status of patients with benign prostatic hyperplasia and prostate carcinoma, *Indian J Urol 27*, 14-18.

Desouki, M. M., Geradts, J., Milon, B., Franklin, R. B., and Costello, L. C. (2007) hZip2 and hZip3 zinc transporters are down regulated in human prostate adenocarcinomatous glands, *Mol Cancer 6*, 37.

Feng, P., Li, T. L., Guan, Z. X., Franklin, R. B., and Costello, L. C. (2002) Direct effect of zinc on mitochondrial apoptogenesis in prostate cells, *Prostate 52*, 311-318.

Gomez, Y., Arocha, F., Espinoza, F., Fernandez, D., Vasquez, A., and Granadillo, V. (2007) [Zinc levels in prostatic fluid of patients with prostate pathologies], *Invest Clin 48*, 287-294.

Kelleher, S. L., McCormick, N. H., Velasquez, V., and Lopez, V. (2011) Zinc in specialized secretory tissues: roles in the pancreas, prostate, and mammary gland, *Adv Nutr 2*, 101-111.

Costello, L. C., Franklin, R. B., Zou, J., Feng, P., Bok, R., Mark, G. S., and Kurhanewicz, J. (2011) Human prostate cancer ZIP1/zinc/citrate genetic/metabolic relationship in the TRAMP prostate cancer animal model, *Cancer Biol Ther 12*.

Feng, P., Li, T. L., Guan, Z. X., Franklin, R. B., and Costello, L. C. (2003) Effect of zinc on prostatic tumorigenicity in nude mice, *Ann N Y Acad Sci 1010*, 316-320.

Prasad, A. S., Mukhtar, H., Beck, F. W., Adhami, V. M., Siddiqui, I. A., Din, M., Hafeez, B. B., and Kucuk, O. (2010) Dietary zinc and prostate cancer in the TRAMP mouse model, *J Med Food 13*, 70-76.

Tepaamorndech, S., Huang, L., and Kirschke, C. P. (2011) A null-mutation in the Znt7 gene accelerates prostate tumor formation in a transgenic adenocarcinoma mouse prostate model, *Cancer Lett 308*, 33-42.

Korenchuk, S., Lehr, J. E., L, M. C., Lee, Y. G., Whitney, S., Vessella, R., Lin, D. L., and Pienta, K. J. (2001) VCaP, a cell-based model system of human prostate cancer, *In Vivo 15*, 163-168.

Lee, Y. G., Korenchuk, S., Lehr, J., Whitney, S., Vessela, R., and Pienta, K. J. (2001) Establishment and characterization of a new human prostatic cancer cell line: DuCaP, *In Vivo 15*, 157-162.

van Bokhoven, A., Caires, A., Maria, M. D., Schulte, A. P., Lucia, M. S., Nordeen, S. K., Miller, G. J., and Varella-Garcia, M. (2003) Spectral karyotype (SKY) analysis of human prostate carcinoma cell lines, *Prostate 57*, 226-244.

van Bokhoven, A., Varella-Garcia, M., Korch, C., Johannes, W. U., Smith, E. E., Miller, H. L., Nordeen, S. K., Miller, G. J., and Lucia, M. S. (2003) Molecular characterization of human prostate carcinoma cell lines, *Prostate 57*, 205-225.

Horoszewicz, J. S., Leong, S. S., Kawinski, E., Karr, J. P., Rosenthal, H., Chu, T. M., Mirand, E. A., and Murphy, G. P. (1983) LNCaP model of human prostatic carcinoma, *Cancer Res 43*, 1809-1818.

Bello, D., Webber, M. M., Kleinman, H. K., Wartinger, D. D., and Rhim, J. S. (1997) Androgen responsive adult human prostatic epithelial cell lines immortalized by human papillomavirus 18, *Carcinogenesis 18*, 1215-1223.

Sobel, R. E., and Sadar, M. D. (2005) Cell lines used in prostate cancer research: a compendium of old and new lines--part 2, *J Urol 173*, 360-372.

Sobel, R. E., and Sadar, M. D. (2005) Cell lines used in prostate cancer research: a compendium of old and new lines--part 1, *J Urol 173*, 342-359.

Costello, L. C., Liu, Y., Zou, J., and Franklin, R. B. (1999) Evidence for a zinc uptake transporter in human prostate cancer cells which is regulated by prolactin and testosterone, *J Biol Chem 274*, 17499-17504.

Franklin, R. B., Ma, J., Zou, J., Guan, Z., Kukoyi, B. I., Feng, P., and Costello, L. C. (2003) Human ZIP1 is a major zinc uptake transporter for the accumulation of zinc in prostate cells, *J Inorg Biochem 96*, 435-442.

Hasumi, M., Suzuki, K., Matsui, H., Koike, H., Ito, K., and Yamanaka, H. (2003) Regulation of metallothionein and zinc transporter expression in human prostate cancer cells and tissues, *Cancer Lett 200*, 187-195.

Iguchi, K., Otsuka, T., Usui, S., Sugimura, Y., and Hirano, K. (2006) Correlation between ZIP2 messenger RNA expression and zinc level in rat lateral prostate, *Biol Trace Elem Res 112*, 159-167.

Kirschke, C. P., and Huang, L. (2008) Expression of the ZNT (SLC30) family members in the epithelium of the mouse prostate during sexual maturation, *J Mol Histol 39*, 359-370.

Mickey, D. D., Stone, K. R., Wunderli, H., Mickey, G. H., Vollmer, R. T., and Paulson, D. F. (1977) Heterotransplantation of a human prostatic adenocarcinoma cell line in nude mice, *Cancer Res 37*, 4049-4058.

Stone, K. R., Mickey, D. D., Wunderli, H., Mickey, G. H., and Paulson, D. F. (1978) Isolation of a human prostate carcinoma cell line (DU 145), *Int J Cancer 21*, 274-281.

Kaighn, M. E., Narayan, K. S., Ohnuki, Y., Lechner, J. F., and Jones, L. W. (1979) Establishment and characterization of a human prostatic carcinoma cell line (PC-3), *Invest Urol 17*, 16-23.

Zhau, H. Y., Chang, S. M., Chen, B. Q., Wang, Y., Zhang, H., Kao, C., Sang, Q. A., Pathak, S. J., and Chung, L. W. (1996) Androgen-repressed phenotype in human prostate cancer, *Proc Natl Acad Sci U S A 93*, 15152-15157.

Carney, D. N., Gazdar, A. F., Bepler, G., Guccion, J. G., Marangos, P. J., Moody, T. W., Zweig, M. H., and Minna, J. D. (1985) Establishment and identification of small cell lung cancer cell lines having classic and variant features, *Cancer Res 45*, 2913-2923.

Johnson, B. E., Whang-Peng, J., Naylor, S. L., Zbar, B., Brauch, H., Lee, E., Simmons, A., Russell, E., Nam, M. H., and Gazdar, A. F. (1989) Retention of chromosome 3 in extrapulmonary small cell cancer shown by molecular and cytogenetic studies, *J Natl Cancer Inst 81*, 1223-1228.

Plymate, S. R., Loop, S. M., Hoop, R. C., Wiren, K. M., Ostenson, R., Hryb, D. J., and Rosner, W. (1991) Effects of sex hormone binding globulin (SHBG) on human prostatic carcinoma, *J Steroid Biochem Mol Biol 40*, 833-839.

Mehta, P. P., Lokeshwar, B. L., Schiller, P. C., Bendix, M. V., Ostenson, R. C., Howard, G. A., and Roos, B. A. (1996) Gap-junctional communication in normal and neoplastic prostate epithelial cells and its regulation by cAMP, *Mol Carcinog 15*, 18-32.

Klein, K. A., Reiter, R. E., Redula, J., Moradi, H., Zhu, X. L., Brothman, A. R., Lamb, D. J., Marcelli, M., Belldegrun, A., Witte, O. N., and Sawyers, C. L. (1997) Progression of metastatic human prostate cancer to androgen independence in immunodeficient SCID mice, *Nat Med 3*, 402-408.

Navone, N. M., Olive, M., Ozen, M., Davis, R., Troncoso, P., Tu, S. M., Johnston, D., Pollack, A., Pathak, S., von Eschenbach, A. C., and Logothetis, C. J. (1997) Establishment of two human prostate cancer cell lines derived from a single bone metastasis, *Clin Cancer Res 3*, 2493-2500.

Achanzar, W. E., Diwan, B. A., Liu, J., Quader, S. T., Webber, M. M., and Waalkes, M. P. (2001) Cadmium-induced malignant transformation of human prostate epithelial cells, *Cancer Res 61*, 455-458.

Dittmer, P. J., Miranda, J. G., Gorski, J. A., and Palmer, A. E. (2009) Genetically encoded sensors to elucidate spatial distribution of cellular zinc, *J Biol Chem 284*, 16289-16297.

Palmer, A. E., Qin, Y., Park, J. G., and McCombs, J. E. (2011) Design and application of genetically encoded biosensors, *Trends Biotechnol 29*, 144-152.

Miyawaki, A., Llopis, J., Heim, R., McCaffery, J. M., Adams, J. A., Ikura, M., and Tsien, R. Y. (1997) Fluorescent indicators for Ca2+ based on green fluorescent proteins and calmodulin, *Nature 388*, 882-887.

Palmer, A. E., and Tsien, R. Y. (2006) Measuring calcium signaling using genetically targetable fluorescent indicators, *Nat Protoc 1*, 1057-1065.

Palmer, A. E., Giacomello, M., Kortemme, T., Hires, S. A., Lev-Ram, V., Baker, D., and Tsien, R. Y. (2006) Ca2+ indicators based on computationally redesigned calmodulin-peptide pairs, *Chem Biol 13*, 521-530.

Kao, J. P. (1994) Practical aspects of measuring [Ca2+] with fluorescent indicators, *Methods Cell Biol 40*, 155-181.

Chang, C. J., Nolan, E. M., Jaworski, J., Burdette, S. C., Sheng, M., and Lippard, S. J. (2004) Bright fluorescent chemosensor platforms for imaging endogenous pools of neuronal zinc, *Chem Biol 11*, 203-210.

Gee, K. R., Zhou, Z. L., Qian, W. J., and Kennedy, R. (2002) Detection and imaging of zinc secretion from pancreatic beta-cells using a new fluorescent zinc indicator, *J Am Chem Soc 124*, 776-778.

Taki, M., Wolford, J. L., and O'Halloran, T. V. (2004) Emission ratiometric imaging of intracellular zinc: design of a benzoxazole fluorescent sensor and its application in two-photon microscopy, *J Am Chem Soc 126*, 712-713.

Nolan, E. M., and Lippard, S. J. (2004) The zinspy family of fluorescent zinc sensors: syntheses and spectroscopic investigations, *Inorg Chem 43*, 8310-8317.

Nolan, E. M., Ryu, J. W., Jaworski, J., Feazell, R. P., Sheng, M., and Lippard, S. J. (2006) Zinspy sensors with enhanced dynamic range for imaging neuronal cell zinc uptake and mobilization, *J Am Chem Soc 128*, 15517-15528.

Nolan, E. M., Jaworski, J., Okamoto, K., Hayashi, Y., Sheng, M., and Lippard, S. J. (2005) QZ1 and QZ2: rapid, reversible quinoline-derivatized fluoresceins for sensing biological Zn(II), *J Am Chem Soc 127*, 16812-16823.

Domaille, D. W., Que, E. L., and Chang, C. J. (2008) Synthetic fluorescent sensors for studying the cell biology of metals, *Nat Chem Biol 4*, 168-175.

Kawaai, K., Hisatsune, C., Kuroda, Y., Mizutani, A., Tashiro, T., and Mikoshiba, K. (2009) 80K-H interacts with inositol 1,4,5-trisphosphate (IP3) receptors and regulates IP3-induced calcium release activity, *J Biol Chem 284*, 372-380.

MacDonald, R. S. (2000) The role of zinc in growth and cell proliferation, *J Nutr 130*, 1500S-1508S.

Tan, S., Guschin, D., Davalos, A., Lee, Y. L., Snowden, A. W., Jouvenot, Y., Zhang, H. S., Howes, K., McNamara, A. R., Lai, A., Ullman, C., Reynolds, L., Moore, M., Isalan, M., Berg, L. P., Campos, B., Qi, H., Spratt, S. K., Case, C. C., Pabo, C. O., Campisi, J., and Gregory, P. D. (2003) Zinc-finger protein-targeted gene regulation: genomewide single-gene specificity, *Proc Natl Acad Sci U S A 100*, 11997-12002.

Sunderman, F. W., Jr. (1995) The influence of zinc on apoptosis, *Ann Clin Lab Sci 25*, 134-142.

Honscheid, A., Rink, L., and Haase, H. (2009) T-lymphocytes: a target for stimulatory and inhibitory effects of zinc ions, *Endocr Metab Immune Disord Drug Targets 9*, 132-144.

Zalewski, P. D., Millard, S. H., Forbes, I. J., Kapaniris, O., Slavotinek, A., Betts, W. H., Ward, A. D., Lincoln, S. F., and Mahadevan, I. (1994) Video image analysis of labile zinc in viable pancreatic islet cells using a specific fluorescent probe for zinc, *J Histochem Cytochem 42*, 877-884.

Zhang, Y., Bharadwaj, U., Logsdon, C. D., Chen, C., Yao, Q., and Li, M. (2010) ZIP4 regulates pancreatic cancer cell growth by activating IL-6/STAT3 pathway through zinc finger transcription factor CREB, *Clin Cancer Res 16*, 1423-1430.

Karan, D., Thrasher, J. B., and Lubaroff, D. (2008) Prostate cancer: genes, environment, immunity and the use of immunotherapy, *Prostate Cancer Prostatic Dis 11*, 230-236.

Troyer, D. A., Mubiru, J., Leach, R. J., and Naylor, S. L. (2004) Promise and challenge: Markers of prostate cancer detection, diagnosis and prognosis, *Dis Markers 20*, 117-128.

Ding, Y., Ai, H. W., Hoi, H., and Campbell, R. E. (2011) Forster resonance energy transfer-based biosensors for multiparameter ratiometric imaging of Ca2+ dynamics and caspase-3 activity in single cells, *Anal Chem 83*, 9687-9693.

Costello, L. C., and Franklin, R. B. (1998) Novel role of zinc in the regulation of prostate citrate metabolism and its implications in prostate cancer, *Prostate 35*, 285-296.

Feustel, A., and Wennrich, R. (1984) Determination of the distribution of zinc and cadmium in cellular fractions of BPH, normal prostate and prostatic cancers of different histologies by atomic and laser absorption spectrometry in tissue slices, *Urol Res 12*, 253-256.

Rosoff, B. (1981) Studies of zinc in normal and neoplastic prostatic tissues, *Prog Clin Biol Res 75A*, 447-457.

Grynkiewicz, G., Poenie, M., and Tsien, R. Y. (1985) A new generation of Ca2+ indicators with greatly improved fluorescence properties, *J Biol Chem 260*, 3440-3450.

Ammann, A. A. (2007) Inductively coupled plasma mass spectrometry (ICP MS): a versatile tool, *J Mass Spectrom 42*, 419-427.

Moor, C., Devos, W., Guecheva, M., and Kobler, J. (2000) Inductively coupled plasma mass spectrometry: a versatile tool for a variety of different tasks, *Fresenius J Anal Chem 366*, 159-164.

Fahrni, C. J. (2007) Biological applications of X-ray fluorescence microscopy: exploring the subcellular topography and speciation of transition metals, *Curr Opin Chem Biol 11*, 121-127.

Dasgupta, S., Srinidhi, S., and Vishwanatha, J. K. (2012) Oncogenic activation in prostate cancer progression and metastasis: Molecular insights and future challenges, *J Carcinog 11*, 4.

Ye, L., Kynaston, H. G., and Jiang, W. G. (2007) Bone metastasis in prostate cancer: molecular and cellular mechanisms (Review), *Int J Mol Med 20*, 103-111.

Cooper, C. R., Chay, C. H., Gendernalik, J. D., Lee, H. L., Bhatia, J., Taichman, R. S., McCauley, L. K., Keller, E. T., and Pienta, K. J. (2003) Stromal factors involved in prostate carcinoma metastasis to bone, *Cancer 97*, 739-747.

Raubenheimer, E. J., and Noffke, C. E. (2006) Pathogenesis of bone metastasis: a review, *J Oral Pathol Med 35*, 129-135.

Etzioni, R., Penson, D. F., Legler, J. M., di Tommaso, D., Boer, R., Gann, P. H., and Feuer, E. J. (2002) Overdiagnosis due to prostate-specific antigen screening: lessons from U.S. prostate cancer incidence trends, *J Natl Cancer Inst 94*, 981-990.

Costello, L. C., and Franklin, R. B. (2011) Zinc is decreased in prostate cancer: an established relationship of prostate cancer!, *J Biol Inorg Chem 16*, 3-8.

Liang, J. Y., Liu, Y. Y., Zou, J., Franklin, R. B., Costello, L. C., and Feng, P. (1999) Inhibitory effect of zinc on human prostatic carcinoma cell growth, *Prostate 40*, 200-207.

Coyle, P., Philcox, J. C., Carey, L. C., and Rofe, A. M. (2002) Metallothionein: the multipurpose protein, *Cell Mol Life Sci 59*, 627-647.

Zalewski, P. D., Forbes, I. J., and Betts, W. H. (1993) Correlation of apoptosis with change in intracellular labile Zn(II) using zinquin [(2-methyl-8-p-toluenesulphonamido-6-quinolyloxy)acetic acid], a new specific fluorescent probe for Zn(II), *Biochem J 296 (Pt 2)*, 403-408.

Zalewski, P. D., Forbes, I. J., and Giannakis, C. (1991) Physiological role for zinc in prevention of apoptosis (gene-directed death), *Biochem Int 24*, 1093-1101.

Cousins, R. J. (1998) A role of zinc in the regulation of gene expression, *Proc Nutr Soc 57*, 307-311.

Falchuk, K. H. (1998) The molecular basis for the role of zinc in developmental biology, *Mol Cell Biochem 188*, 41-48.

Finkel, T., and Hwang, P. M. (2009) The Krebs cycle meets the cell cycle: mitochondria and the G1-S transition, *Proc Natl Acad Sci U S A 106*, 11825-11826.

Costello, L. C., Liu, Y., Franklin, R. B., and Kennedy, M. C. (1997) Zinc inhibition of mitochondrial aconitase and its importance in citrate metabolism of prostate epithelial cells, *J Biol Chem 272*, 28875-28881.

Liang, D., Yang, M., Guo, B., Cao, J., Yang, L., Guo, X., Li, Y., and Gao, Z. (2012) Zinc inhibits H(2)O(2)-induced MC3T3-E1 cells apoptosis via MAPK and PI3K/AKT pathways, *Biol Trace Elem Res 148*, 420-429.

Thornton, J. K., Taylor, K. M., Ford, D., and Valentine, R. A. (2011) Differential subcellular localization of the splice variants of the zinc transporter ZnT5 is dictated by the different C-terminal regions, *PLoS One 6*, e23878.

Diehl, J. A., Fuchs, S. Y., and Koumenis, C. (2011) The cell biology of the unfolded protein response, *Gastroenterology 141*, 38-41, 41 e31-32.

Grootjans, J., Hodin, C. M., de Haan, J. J., Derikx, J. P., Rouschop, K. M., Verheyen, F. K., van Dam, R. M., Dejong, C. H., Buurman, W. A., and Lenaerts, K. (2011) Level of activation of the unfolded protein response correlates with Paneth cell apoptosis in human small intestine exposed to ischemia/reperfusion, *Gastroenterology 140*, 529-539 e523.

Kaser, A., Lee, A. H., Franke, A., Glickman, J. N., Zeissig, S., Tilg, H., Nieuwenhuis, E. E., Higgins, D. E., Schreiber, S., Glimcher, L. H., and Blumberg, R. S. (2008) XBP1 links ER stress to intestinal inflammation and confers genetic risk for human inflammatory bowel disease, *Cell 134*, 743-756.

Kaser, A., Tomczak, M., and Blumberg, R. S. (2011) "ER stress(ed out)!": Paneth cells and ischemia-reperfusion injury of the small intestine, *Gastroenterology 140*, 393-396.

Ellis, C. D., Wang, F., MacDiarmid, C. W., Clark, S., Lyons, T., and Eide, D. J. (2004) Zinc and the Msc2 zinc transporter protein are required for endoplasmic reticulum function, *J Cell Biol 166*, 325-335.

Chen, Q. G., Zhang, Z., Yang, Q., Shan, G. Y., Yu, X. Y., and Kong, C. Z. (2011) The role of zinc transporter ZIP4 in prostate carcinoma, *Urol Oncol*.

Zaichick, V., Sviridova, T. V., and Zaichick, S. V. (1997) Zinc in the human prostate gland: normal, hyperplastic and cancerous, *Int Urol Nephrol 29*, 565-574.

Hennigar, S. R., and Kelleher, S. L. (2012) Zinc networks: the cell-specific compartmentalization of zinc for specialized functions, *Biol Chem 393*, 565-578.

Gaither, L. A., and Eide, D. J. (2000) Functional expression of the human hZIP2 zinc transporter, *J Biol Chem 275*, 5560-5564.

Iguchi, K., Usui, S., Inoue, T., Sugimura, Y., Tatematsu, M., and Hirano, K. (2002) High-level expression of zinc transporter-2 in the rat lateral and dorsal prostate, *J Androl 23*, 819-824.

Song, Y., Elias, V., Wong, C. P., Scrimgeour, A. G., and Ho, E. (2010) Zinc transporter expression profiles in the rat prostate following alterations in dietary zinc, *Biometals 23*, 51-58.

Valkenburg, K. C., and Williams, B. O. (2011) Mouse models of prostate cancer, *Prostate Cancer 2011*, 895238.

Peehl, D. M. (2005) Primary cell cultures as models of prostate cancer development, *Endocr Relat Cancer 12*, 19-47.

Webber, M. M., Bello, D., and Quader, S. (1997) Immortalized and tumorigenic adult human prostatic epithelial cell lines: characteristics and applications Part 2. Tumorigenic cell lines, *Prostate 30*, 58-64.

Webber, M. M., Bello, D., and Quader, S. (1997) Immortalized and tumorigenic adult human prostatic epithelial cell lines: characteristics and applications. Part 3. Oncogenes, suppressor genes, and applications, *Prostate 30*, 136-142.

Goidin, D., Mamessier, A., Staquet, M. J., Schmitt, D., and Berthier-Vergnes, O. (2001) Ribosomal 18S RNA prevails over glyceraldehyde-3-phosphate dehydrogenase and beta-actin genes as internal standard for quantitative comparison of mRNA levels in invasive and noninvasive human melanoma cell subpopulations, *Anal Biochem 295*, 17-21.

Schmittgen, T. D., and Zakrajsek, B. A. (2000) Effect of experimental treatment on housekeeping gene expression: validation by real-time, quantitative RT-PCR, *J Biochem Biophys Methods 46*, 69-81.

Ohl, F., Jung, M., Xu, C., Stephan, C., Rabien, A., Burkhardt, M., Nitsche, A., Kristiansen, G., Loening, S. A., Radonic, A., and Jung, K. (2005) Gene expression studies in prostate cancer tissue: which reference gene should be selected for normalization?, *J Mol Med (Berl) 83*, 1014-1024.

Eide, D. J. (2004) The SLC39 family of metal ion transporters, *Pflugers Arch 447*, 796-800.

Lopez, V., and Kelleher, S. L. (2009) Zinc transporter-2 (ZnT2) variants are localized to distinct subcellular compartments and functionally transport zinc, *Biochem J 422*, 43-52.

Kelleher, S. L., and Lonnerdal, B. (2003) Zn transporter levels and localization change throughout lactation in rat mammary gland and are regulated by Zn in mammary cells, *J Nutr 133*, 3378-3385.

Iguchi, K., Morihara, N., Usui, S., Hayama, M., Sugimura, Y., and Hirano, K. (2011) Castration- and aging-induced changes in the expression of zinc transporter and metallothionein in rat prostate, *J Androl 32*, 144-150.

Huang, L., and Gitschier, J. (1997) A novel gene involved in zinc transport is deficient in the lethal milk mouse, *Nat Genet 17*, 292-297.

Bozeman, C. B., Carver, B. S., Eastham, J. A., and Venable, D. D. (2002) Treatment of chronic prostatitis lowers serum prostate specific antigen, *J Urol 167*, 1723-1726.

Emberton, M., Andriole, G. L., de la Rosette, J., Djavan, B., Hoefner, K., Vela Navarrete, R., Nordling, J., Roehrborn, C., Schulman, C., Teillac, P., Tubaro, A., and Nickel, J. C. (2003) Benign prostatic hyperplasia: a progressive disease of aging men, *Urology 61*, 267-273.

Polascik, T. J., Oesterling, J. E., and Partin, A. W. (1999) Prostate specific antigen: a decade of discovery--what we have learned and where we are going, *J Urol 162*, 293-306.

Bradford, T. J., Tomlins, S. A., Wang, X., and Chinnaiyan, A. M. (2006) Molecular markers of prostate cancer, *Urol Oncol 24*, 538-551.

Stamey, T. A., Caldwell, M., McNeal, J. E., Nolley, R., Hemenez, M., and Downs, J. (2004) The prostate specific antigen era in the United States is over for prostate cancer: what happened in the last 20 years?, *J Urol 172*, 1297-1301.

Cortesi, M., Fridman, E., Volkov, A., Shilstein, S., Chechik, R., Breskin, A., Vartsky, D., Raviv, G., and Ramon, J. New prospective for non-invasive detection, grading, size evaluation, and tumor location of prostate cancer, *Prostate 70*, 1701-1708.

Franklin, R. B., and Costello, L. C. (2009) The important role of the apoptotic effects of zinc in the development of cancers, *J Cell Biochem 106*, 750-757.

Ghosh, S. K., Kim, P., Zhang, X. A., Yun, S. H., Moore, A., Lippard, S. J., and Medarova, Z. A novel imaging approach for early detection of prostate cancer based on endogenous zinc sensing, *Cancer Res 70*, 6119-6127.

Weaver, B. P., Dufner-Beattie, J., Kambe, T., and Andrews, G. K. (2007) Novel zinc-responsive post-transcriptional mechanisms reciprocally regulate expression of the mouse Slc39a4 and Slc39a5 zinc transporters (Zip4 and Zip5), *Biol Chem 388*, 1301-1312.

Giedroc, D. P., Chen, X., and Apuy, J. L. (2001) Metal response element (MRE)-binding transcription factor-1 (MTF-1): structure, function, and regulation, *Antioxid Redox Signal 3*, 577-596.

Giedroc, D. P., Chen, X., Pennella, M. A., and LiWang, A. C. (2001) Conformational heterogeneity in the C-terminal zinc fingers of human MTF-1: an NMR and zinc-binding study, *J Biol Chem 276*, 42322-42332.

Shaner, N. C., Steinbach, P. A., and Tsien, R. Y. (2005) A guide to choosing fluorescent proteins, *Nat Methods 2*, 905-909.

Newman, R. H., Fosbrink, M. D., and Zhang, J. (2011) Genetically encodable fluorescent biosensors for tracking signaling dynamics in living cells, *Chem Rev 111*, 3614-3666.

VanEngelenburg, S. B., and Palmer, A. E. (2008) Fluorescent biosensors of protein function, *Curr Opin Chem Biol 12*, 60-65.

Carlson, H. J., and Campbell, R. E. (2009) Genetically encoded FRET-based biosensors for multiparameter fluorescence imaging, *Curr Opin Biotechnol 20*, 19-27.

Ai, H. W., Hazelwood, K. L., Davidson, M. W., and Campbell, R. E. (2008) Fluorescent protein FRET pairs for ratiometric imaging of dual biosensors, *Nat Methods 5*, 401-403.

Ai, H. W., Henderson, J. N., Remington, S. J., and Campbell, R. E. (2006) Directed evolution of a monomeric, bright and photostable version of Clavularia cyan fluorescent protein: structural characterization and applications in fluorescence imaging, *Biochem J 400*, 531-540.

Miyawaki, A., Griesbeck, O., Heim, R., and Tsien, R. Y. (1999) Dynamic and quantitative Ca2+ measurements using improved cameleons, *Proc Natl Acad Sci U S A 96*, 2135-2140.

Davidson, M. W., and Campbell, R. E. (2009) Engineered fluorescent proteins: innovations and applications, *Nat Methods 6*, 713-717.

Grant, D. M., Zhang, W., McGhee, E. J., Bunney, T. D., Talbot, C. B., Kumar, S., Munro, I., Dunsby, C., Neil, M. A., Katan, M., and French, P. M. (2008) Multiplexed FRET to image multiple signaling events in live cells, *Biophys J 95*, L69-71.

Ni, Q., Ganesan, A., Aye-Han, N. N., Gao, X., Allen, M. D., Levchenko, A., and Zhang, J. (2011) Signaling diversity of PKA achieved via a Ca2+-cAMP-PKA oscillatory circuit, *Nat Chem Biol 7*, 34-40.

Niino, Y., Hotta, K., and Oka, K. (2009) Simultaneous live cell imaging using dual FRET sensors with a single excitation light, *PLoS One 4*, e6036.

Ouyang, M., Huang, H., Shaner, N. C., Remacle, A. G., Shiryaev, S. A., Strongin, A. Y., Tsien, R. Y., and Wang, Y. (2010) Simultaneous visualization of protumorigenic Src and MT1-MMP activities with fluorescence resonance energy transfer, *Cancer Res 70*, 2204-2212.

Piljic, A., and Schultz, C. (2008) Simultaneous recording of multiple cellular events by FRET, *ACS Chem Biol 3*, 156-160.

Zapata-Hommer, O., and Griesbeck, O. (2003) Efficiently folding and circularly permuted variants of the Sapphire mutant of GFP, *BMC Biotechnol 3*, 5.

Lam, A., St-Pierre, F., Gong, Y., Marshall, J. D., Cranfill, P. J., Baird, M. A., McKeown, M. R., Wiedenmann, J., Davidson, M. W., Schnitzer, M., Tsien, R. Y., Lin, M. Z. (2012) Improved dynamic range of genetically encoded FRET sensors with bright new green and red fluorescent proteins., *Nat Methods*.

Karasawa, S., Araki, T., Nagai, T., Mizuno, H., and Miyawaki, A. (2004) Cyan-emitting and orange-emitting fluorescent proteins as a donor/acceptor pair for fluorescence resonance energy transfer, *Biochem J 381*, 307-312.

Shaner, N. C., Lin, M. Z., McKeown, M. R., Steinbach, P. A., Hazelwood, K. L., Davidson, M. W., and Tsien, R. Y. (2008) Improving the photostability of bright monomeric orange and red fluorescent proteins, *Nat Methods 5*, 545-551.

Merzlyak, E. M., Goedhart, J., Shcherbo, D., Bulina, M. E., Shcheglov, A. S., Fradkov, A. F., Gaintzeva, A., Lukyanov, K. A., Lukyanov, S., Gadella, T. W., and Chudakov, D. M. (2007) Bright monomeric red fluorescent protein with an extended fluorescence lifetime, *Nat Methods 4*, 555-557.

Shaner, N. C., Campbell, R. E., Steinbach, P. A., Giepmans, B. N., Palmer, A. E., and Tsien, R. Y. (2004) Improved monomeric red, orange and yellow fluorescent proteins derived from Discosoma sp. red fluorescent protein, *Nat Biotechnol 22*, 1567-1572.

Shcherbo, D., Merzlyak, E. M., Chepurnykh, T. V., Fradkov, A. F., Ermakova, G. V., Solovieva, E. A., Lukyanov, K. A., Bogdanova, E. A., Zaraisky, A. G., Lukyanov, S., and Chudakov, D. M. (2007) Bright far-red fluorescent protein for whole-body imaging, *Nat Methods 4*, 741-746.

Andreini, C., Banci, L., Bertini, I., and Rosato, A. (2006) Zinc through the three domains of life, *J Proteome Res 5*, 3173-3178.

Tsujikawa, K., Imai, T., Kakutani, M., Kayamori, Y., Mimura, T., Otaki, N., Kimura, M., Fukuyama, R., and Shimizu, N. (1991) Localization of metallothionein in nuclei of growing primary cultured adult rat hepatocytes, *FEBS Lett 283*, 239-242.

Spahl, D. U., Berendji-Grun, D., Suschek, C. V., Kolb-Bachofen, V., and Kroncke, K. D. (2003) Regulation of zinc homeostasis by inducible NO synthase-derived NO: nuclear metallothionein translocation and intranuclear Zn2+ release, *Proc Natl Acad Sci U S A 100*, 13952-13957.

Gandhi, M. S., Deshmukh, P. A., Kamalov, G., Zhao, T., Zhao, W., Whaley, J. T., Tichy, J. R., Bhattacharya, S. K., Ahokas, R. A., Sun, Y., Gerling, I. C., and Weber, K. T. (2008) Causes and consequences of zinc dyshomeostasis in rats with chronic aldosteronism, *J Cardiovasc Pharmacol 52*, 245-252.

Gibson, R. S., Hess, S. Y., Hotz, C., and Brown, K. H. (2008) Indicators of zinc status at the population level: a review of the evidence, *Br J Nutr 99 Suppl 3*, S14-23.

Stoecker, B. J., Abebe, Y., Hubbs-Tait, L., Kennedy, T. S., Gibson, R. S., Arbide, I., Teshome, A., Westcott, J., Krebs, N. F., and Hambidge, K. M. (2009) Zinc status and cognitive function of pregnant women in Southern Ethiopia, *Eur J Clin Nutr 63*, 916-918.

Sorensen, M. B., Stoltenberg, M., Danscher, G., and Ernst, E. (1999) Chelation of intracellular zinc ions affects human sperm cell motility, *Mol Hum Reprod 5*, 338-341.

Takeda, A. (2012) Zinc signaling in the hippocampus and its relation to pathogenesis of depression, *J Trace Elem Med Biol 26*, 80-84.

Yoshida, K., Kawano, N., Yoshiike, M., Yoshida, M., Iwamoto, T., and Morisawa, M. (2008) Physiological roles of semenogelin I and zinc in sperm motility and semen coagulation on ejaculation in humans, *Mol Hum Reprod 14*, 151-156.

Kim, A. M., Vogt, S., O'Halloran, T. V., and Woodruff, T. K. (2010) Zinc availability regulates exit from meiosis in maturing mammalian oocytes, *Nat Chem Biol 6*, 674-681.

Du, S., McLaughlin, B., Pal, S., and Aizenman, E. (2002) In vitro neurotoxicity of methylisothiazolinone, a commonly used industrial and household biocide, proceeds via a zinc and extracellular signal-regulated kinase mitogen-activated protein kinase-dependent pathway, *J Neurosci 22*, 7408-7416.

Perry, D. K., Smyth, M. J., Stennicke, H. R., Salvesen, G. S., Duriez, P., Poirier, G. G., and Hannun, Y. A. (1997) Zinc is a potent inhibitor of the apoptotic protease, caspase-3. A novel target for zinc in the inhibition of apoptosis, *J Biol Chem 272*, 18530-18533.

West, D. C., Qin, Y., Peterson, Q. P., Thomas, D. L., Palchaudhuri, R., Morrison, K. C., Lucas, P. W., Palmer, A. E., Fan, T. M., and Hergenrother, P. J. (2012) Differential effects of procaspase-3 activating compounds in the induction of cancer cell death, *Mol Pharm 9*, 1425-1434.

Andreini, C., Bertini, I., and Rosato, A. (2009) Metalloproteomes: a bioinformatic approach, *Acc Chem Res 42*, 1471-1479.

Colvin, R. A., Fontaine, C. P., Laskowski, M., and Thomas, D. (2003) Zn2+ transporters and Zn2+ homeostasis in neurons, *Eur J Pharmacol 479*, 171-185.

Chimienti, F., Devergnas, S., Favier, A., and Seve, M. (2004) Identification and cloning of a beta-cell-specific zinc transporter, ZnT-8, localized into insulin secretory granules, *Diabetes 53*, 2330-2337.

Besser, L., Chorin, E., Sekler, I., Silverman, W. F., Atkin, S., Russell, J. T., and Hershfinkel, M. (2009) Synaptically released zinc triggers metabotropic signaling via a zinc-sensing receptor in the hippocampus, *J Neurosci 29*, 2890-2901.

Yamasaki, S., Sakata-Sogawa, K., Hasegawa, A., Suzuki, T., Kabu, K., Sato, E., Kurosaki, T., Yamashita, S., Tokunaga, M., Nishida, K., and Hirano, T. (2007) Zinc is a novel intracellular second messenger, *J Cell Biol 177*, 637-645.

Gee, K. R., Zhou, Z. L., Ton-That, D., Sensi, S. L., and Weiss, J. H. (2002) Measuring zinc in living cells. A new generation of sensitive and selective fluorescent probes, *Cell Calcium 31*, 245-251.

Heikal, A. A., Hess, S. T., Baird, G. S., Tsien, R. Y., and Webb, W. W. (2000) Molecular spectroscopy and dynamics of intrinsically fluorescent proteins: coral red (dsRed) and yellow (Citrine), *Proc Natl Acad Sci U S A 97*, 11996-12001.

Wachter, R. M., Elsliger, M. A., Kallio, K., Hanson, G. T., and Remington, S. J. (1998) Structural basis of spectral shifts in the yellow-emission variants of green fluorescent protein, *Structure 6*, 1267-1277.

Sachse, M., Ramm, G., Strous, G., and Klumperman, J. (2002) Endosomes: multipurpose designs for integrating housekeeping and specialized tasks, *Histochem Cell Biol 117*, 91-104.

Saftig, P., and Klumperman, J. (2009) Lysosome biogenesis and lysosomal membrane proteins: trafficking meets function, *Nat Rev Mol Cell Biol 10*, 623-635.

Lam, A. J., St-Pierre, F., Gong, Y., Marshall, J. D., Cranfill, P. J., Baird, M. A., McKeown, M. R., Wiedenmann, J., Davidson, M. W., Schnitzer, M. J., Tsien, R. Y., and Lin, M. Z. (2012) Improving FRET dynamic range with bright green and red fluorescent proteins, *Nat Methods 9*, 1005-1012.

Bonanomi, D., Benfenati, F., and Valtorta, F. (2006) Protein sorting in the synaptic vesicle life cycle, *Prog Neurobiol 80*, 177-217.

Bonanomi, D., Rusconi, L., Colombo, C. A., Benfenati, F., and Valtorta, F. (2007) Synaptophysin I selectively specifies the exocytic pathway of synaptobrevin 2/VAMP2, *Biochem J 404*, 525-534.

Hitomi, Y., Outten, C. E., and O'Halloran, T. V. (2001) Extreme zinc-binding thermodynamics of the metal sensor/regulator protein, ZntR, *J Am Chem Soc 123*, 8614-8615.

Lyons, T. J., Nersissian, A., Huang, H., Yeom, H., Nishida, C. R., Graden, J. A., Gralla, E. B., and Valentine, J. S. (2000) The metal binding properties of the zinc site of yeast copper-zinc superoxide dismutase: implications for amyotrophic lateral sclerosis, *J Biol Inorg Chem 5*, 189-203.

Nakashima, A. S., Butt, R. H., and Dyck, R. H. (2011) Alterations in protein and gene expression within the barrel cortices of ZnT3 knockout mice: Experience-independent and dependent changes, *Neurochem Int 59*, 860-870.

Rutter, G. A. (2010) Think zinc: New roles for zinc in the control of insulin secretion, *Islets 2*, 49-50.

Kay, A. R. (2003) Evidence for chelatable zinc in the extracellular space of the hippocampus, but little evidence for synaptic release of Zn, *J Neurosci 23*, 6847-6855.

Qian, J., and Noebels, J. L. (2006) Exocytosis of vesicular zinc reveals persistent depression of neurotransmitter release during metabotropic glutamate receptor long-term depression at the hippocampal CA3-CA1 synapse, *J Neurosci 26*, 6089-6095.

Pan, E., Zhang, X. A., Huang, Z., Krezel, A., Zhao, M., Tinberg, C. E., Lippard, S. J., and McNamara, J. O. (2011) Vesicular zinc promotes presynaptic and inhibits postsynaptic long-term potentiation of mossy fiber-CA3 synapse, *Neuron 71*, 1116-1126.

Frederickson, C. J., Giblin, L. J., 3rd, Balaji, R. V., Masalha, R., Zeng, Y., Lopez, E. V., Koh, J. Y., Chorin, U., Besser, L., Hershfinkel, M., Li, Y., Thompson, R. B., and Krezel, A. (2006) Synaptic release of zinc from brain slices: factors governing release, imaging, and accurate calculation of concentration, *J Neurosci Methods 154*, 19-29.

Bastian, C., and Li, Y. V. (2007) Fluorescence imaging study of extracellular zinc at the hippocampal mossy fiber synapse, *Neurosci Lett 419*, 119-124.

Adamo, A. M., Zago, M. P., Mackenzie, G. G., Aimo, L., Keen, C. L., Keenan, A., and Oteiza, P. I. (2010) The role of zinc in the modulation of neuronal proliferation and apoptosis, *Neurotox Res 17*, 1-14.

Thambiayya, K., Wasserloos, K., Kagan, V. E., Stoyanovsky, D., and Pitt, B. R. (2012) A critical role for increased labile zinc in reducing sensitivity of cultured sheep pulmonary artery endothelial cells to LPS-induced apoptosis, *Am J Physiol Lung Cell Mol Physiol 302*, L1287-1295.

Thambiayya, K., Wasserloos, K. J., Huang, Z., Kagan, V. E., St Croix, C. M., and Pitt, B. R. (2011) LPS-induced decrease in intracellular labile zinc, [Zn]i, contributes to apoptosis in cultured sheep pulmonary artery endothelial cells, *Am J Physiol Lung Cell Mol Physiol 300*, L624-632.